STRUCTURAL AND ANALYTICAL STUDIES

BY

TANDEM MASS SPECTROMETRY

A Thesis submitted by

TRACEY MADDEN

for the degree of Doctor of Philosophy

in the University of London

Faculty of Science

Department of Pharmaceutical Chemistry

The School of Pharmacy

University of London

CONTENTS

LIST OF FIGURES

LIST OF TABLES

LIST OF ABBREVIATIONS

[A]	intensity of A
a	shielding radius
AE	appearance energy
B	magnetic field strength
CAD	collisionally activated dissociation
CI	chemical ionisation
CID	collisionally induced dissociation
CIDI	collision induced dissociative ionisation
d	internuclear distance
D(M_n^+)	dissociation energy of M_n^+
DADI	direct analysis of daughter ions
E	electrostatic potential
e	electron charge (1.602×10^{-19}C)
eV	electron volt (1.602×10^{-19}J)
EI	electron impact
ESA	electrostatic analyser
FAB	fast atom bombardment
FD	field desorption
FFR	field free region (nFFR = n^{th} FFR)
FI	field ionisation
FIK	field ionisation kinetics
h	Planck's constant (6.626×10^{-34}Js)
I	instantaneous intensity
I_o	initial intensity
IE(A)	ionisation energy of A

KER	kinetic energy release
$\mathbf{l_p}$	path length
M	molecule
$\mathbf{M^+}$	even electron ion
$\mathbf{M^{+\cdot}}$	odd electron ion (radical)
MIKES	mass-analysed ion kinetic energy spectrum
m/z	mass to charge ratio
N	target density
NIBS	neutralised ion beam spectroscopy
NRMS	neutralisation-reionisation mass spectrometry
$\mathbf{Q_N}$	energy defect
QET	quasi equilibrium theory
RE(A)	recombination energy of A
T	kinetic energy release
$\mathbf{T_{½}}$	KER calculated at 50% of the maximum peak intensity
$\mathbf{T^e}$	contribution to T from ε^e_o
$\mathbf{T^§}$	contribution to T from $\varepsilon^§$
$\mathbf{t_F}$	time of flight
$\mathbf{V_{ACC}}$	acceleration voltage
$\mathbf{V_C}$	cell voltage
$\mathbf{V_D}$	deflector voltage
v	velocity
$\mathbf{W_H}$	width of a peak at H% of its maximum intensity
Z	nuclear charge (number of protons)
$\mathbf{z_A}$	total electronic charge (z_A=z.e)
$\varepsilon^§$	non-fixed energy of the activated complex

ε^{e}_{0}	reverse activation energy
ε_{0}	minimum energy for the formation of a primary fragment ion
σ_{S}	scattering cross section
σ_{N}	neutralisation cross section
σ_{I}	ionisation cross section
σ_{CE}	charge exchange cross section
σ_{CID}	collision induced dissociation cross section

ABSTRACT

This thesis describes the use of several such tandem mass spectrometrical techniques, the majority including controlled collisions with a target gas to effect dissociation or charge exchange.

A range of MS/MS techniques was utilized in the study of the fragmentation of $[M-CO]^{+\cdot}$ ions from various positional isomers of the hydroxyquinoline molecular ion, and $[M-CS]^{+\cdot}$ ions from various positional isomers of the mercaptoquinoline molecular ion. CID/MIKES spectra give evidence in favour of the $[M-CO]^{+\cdot}$ and $[M-CS]^{+\cdot}$ ions from the 2-, 3- and 4-isomers adopting an indole-like structure. Deuterium labelling experiments with the $[M-CO]^{+\cdot}$ and $[M-CS]^{+\cdot}$ ions showed the uniqueness of the two 2-isomers, which unlike the other positional isomers, gave no evidence of hydrogen scrambling. It has already been shown through the study of the metastable peak corresponding to the loss of CO from the molecular ion that 2-hydroxyquinioline is tautomeric with quinolin-(1H)-one. This type of study was extended to structurally related ions that also lost CO, revealing other instances of tautomerism and competitive routes for loss of CO from a single ion.

A comparative study using various MS/MS techniques was carried out on the acetamide ion, comparing its structure with $C_2H_5NO^{+\cdot}$ ions formed from N-ethylacetamide

and n-butyramide by a McLafferty rearrangement.

A similar study was made of t-butylbenzene, various techniques being used to investigate its fragmentation pattern and the structure of the ions formed.

It has been reported that the analysis of mass spectral data from peptides is greatly aided by close examination of low mass peaks, particularly those due to immonium ions and other closely associated ions. Tandem mass spectrometry was used to study the effects of small changes in the peptide sequence on the relative abundances of these low mass ions.

ACKNOWLEDGEMENTS

I should like to thank my colleagues at The School of Pharmacy, University of London, particularly those who worked in the Mass Spectrometry Laboratory during the period 1987-1990. In particular my thanks go to my supervisor Dr M.A. Baldwin for giving me the opportunity to research in mass spectrometry and his help and encouragement throughout. Also, my thanks to D.M Carter, J. Hill (University College, London), S.A. Howell, Dr G.J. Langley (University of Southampton) and K.J. Welham for time, patience and technical assistance, and many others at the School of Pharmacy whose help and support I could not have done without.

I gratefully acknowledge financial support from VG Analytical, Manchester and the Science and Engineering Research Council, through the award of a CASE studentship.

"The essential requirements of a high vacuum system are a rotary pump, diffusion pump and a leak."

Undergraduate student, in answer to an applied physics exam question.
(SNIPPETS, IoP, 1988)

CHAPTER 1 : INTRODUCTION

1.1 TANDEM MASS SPECTROMETRY

The basic concept of tandem mass spectrometry [1,2] (MS/MS) is the subdivision of the mass spectrometer into a linear series of two or more analytical 'stages', working in tandem, rather like the linking of mass spectrometry and chromatography.

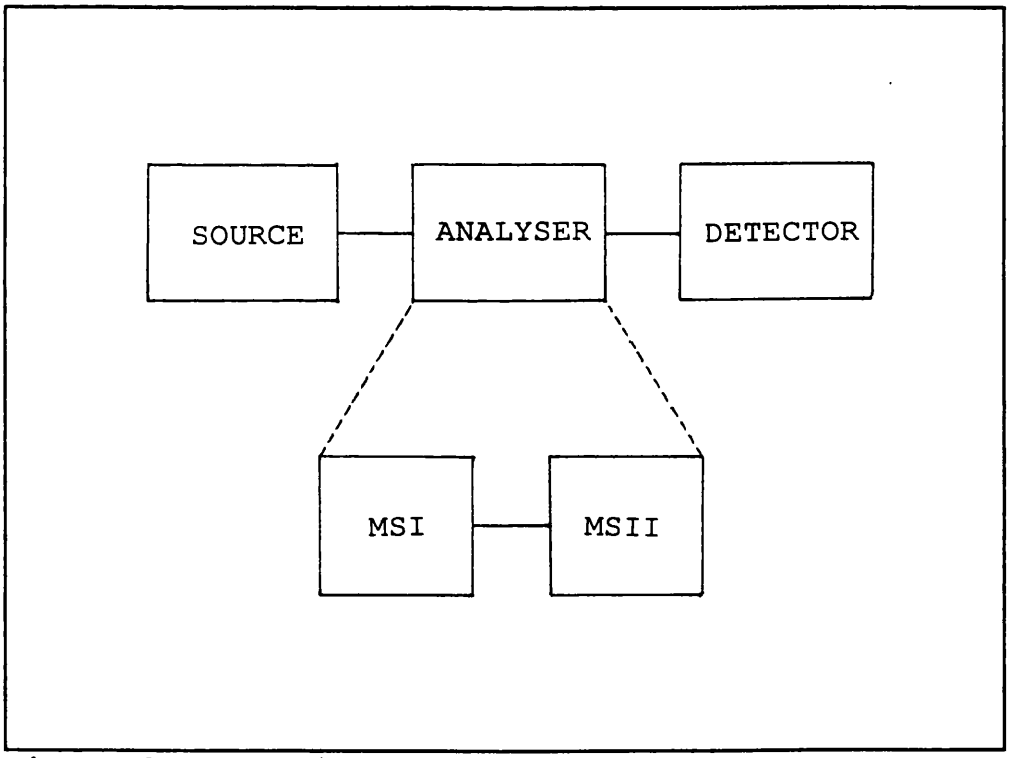

Figure 1 Schematic of a 'Tandem' Mass Spectrometer

Each stage can act as a gate to pass a preselected ion, or an analyser to scan the product. The region in between

the analysers can be used as a reaction region (Fig 1).

One application of tandem mass spectrometry is in the area of mixture analysis [3,4]. MS/MS has been compared favourably to GC/MS. The comparison is valid when the first analyser, MSI, is used to select a component from the mixture, and MSII to scan the product or 'daughter' ions - a 'daughter ion scan'. As well as some compounds being amenable to spectrometric rather than chromatographic separation, MS/MS offers a great reduction in analysis time (the components being available simultaneously rather than sequentially) and an increase in sensitivity, due to the dilution of the analyte in the chromatographic separation [5,6].

Tandem mass spectrometry allows the investigation into the generic relationship between the ions in a spectrum [5]. A single ion is selected by MSI, allowed to dissociate and its product ions scanned by MSII. Alternatively, a single ion is selected by MSII and MSI is scanned to reveal its precursors - a 'parent ion scan'. In this way a detailed picture can be drawn up concerning the fragmentation of a molecule.

The feature that marks MS/MS out from GC/MS or LC/MS is the possibility of manipulating the ion beam between the analytical stages. This usually takes the form of a collision between the ion beam and a laser beam, electrons or a neutral gas. The resulting spectra can often be used to characterise the sample in terms of its

ionic structure [7].

Tandem mass spectrometry has also been found useful in such areas as trace analysis [5], where its value is measured not so much in terms of its sensitivity, but rather its selectivity. It has been shown [8] that as the number of discrete analytical stages increases, though both the absolute levels of signal and noise decrease, the noise decreases at a faster rate, hence there is an increase in signal to noise ratio.

Where there are more than two discrete analysers (MSIII etc) there is the possibility of performing multiple stage scans (eg granddaughter ion scans).

REFERENCES : Chapter 1 Introduction

1. F.W. McLafferty (Ed.), Tandem Mass Spectrometry, Wiley, 1983
2. K.L. Busch, G.L. Glish and S.A. McLuckey, Mass Spectrometry/Mass Spectrometry : Techniques and Applications of Tandem Mass Spectrometry, VCH, 1988
3. R.G. Cooks, Amer. Lab., 111-123, 1978
4. R.W. Kondrat and R.G. Cooks, Anal. Chem., 50, 81A-92A, 1978
5. J. Johnson and R.A Yost, Anal. Chem., 57, 758A-768A, 1985
6. R.G. Cooks and G.L. Glish, Chem. Eng. News, 59, 40-52, 1981
7. R.A. Yost and D.D. Fetterolf, Mass Spectrom. Rev., 2, 1-45, 1983
8. R.G.Cooks, K.L.Busch, J. Chem. Educ., 59, 1982, 926-33

CHAPTER 2 : THEORY

2.1 MASS SPECTROMETRY

A mass spectrometer consists of three main components : an ion source, an analyser which discriminates between ions on the basis of their mass, or some parameter which ultimately relates to their mass, and a detector to register the number of ions, or intensity at each particular mass (Fig 2). There may also be some form of data recording (eg chart recorder, computer) and a plot of intensity against mass is termed a 'mass spectrum'.

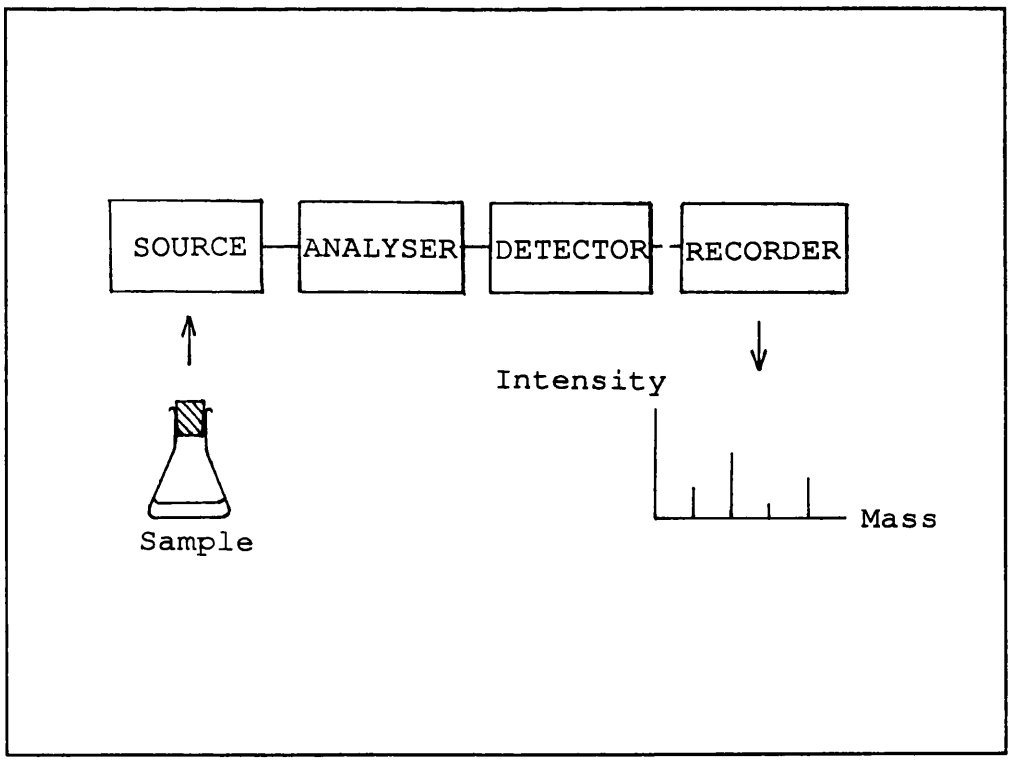

Figure 2 Schematic of a Mass Spectrometer

Ionising the particles makes it possible to use magnetic and electrostatic fields to bring about their separation (see Section 3.2). This is carried out under high vacuum to minimise collisions between the ion beam and residual gas molecules. The ionisation process may be carried out in a number of ways, for instance, collisions with electrons, bombardment with ions or atoms, thermal evaporation of a sample from a metallic surface or through irradiation with UV light. The ionisation method will to a large extent reflect the physical and chemical nature of the sample (see Section 3.1).

The first mass spectrometer had only a single analyser, a magnet, which separated ions on the basis of their mass to charge ratio (m/z) [1]. The mass spectrum was detected and recorded on a photographic plate. This gave an indication of the ions formed within the mass spectrometer.

This procedure (with an updated detection system) is adequate for many applications. If the sample molecule under investigation survives the ionisation process intact, a 'molecular ion' or 'pseudo molecular ion' (see Section 2.1) is formed. Its mass measurement gives the molecular mass of the sample. If the molecule should acquire sufficient energy it may fragment, thus other lower mass ions will appear in the spectrum. The mass and intensity of these fragments can help to characterise the molecular ion in terms of its structure.

Having more than one analyser allows a finer discrimination between ions of similar mass - better 'mass resolution'. This also allows more accurate measurement of the mass of an ion for the determination of its elemental structure. An accurate mass measurement to within ~1ppm (part per million) allows unambiguous assignment of the molecular formular for low to middle mass organic compounds (< 500 daltons).

2.2 FORMATION OF THE MOLECULAR ION

The best established method of forming ions from organic molecules in the mass spectrometer is a process known as 'electron impact' (see Section 3.1.1). The electrons are produced by a heated filament and have energies determined by the pd between the filament and the chamber. They interact with the sample molecules by inelastic collisions and transfer a range of energies. When only a small amount of energy is transferred to the molecule by an electron it will be excited but not ionized

$$M + e \rightarrow M^* + e$$

the kinetic energy lost by the electron being equal to that gained by the molecule M^*. Increasing the energy transferred by the electrons past a threshold value, the 'ionisation potential', leads to ionisation

$$M + e \rightarrow M^{+\cdot} + 2e$$

Most organic molecules contain an even number of electrons, so ionisation by this method produces an odd-electron ion (a radical). The abundance of $M^{+\cdot}$ in the mass spectrum will depend on its stability with respect to decomposition within the time scale of the mass spectrometry experiment, the ions generally spending ~1

microsecond in the ion source and 1-100 microseconds in flight. The stability of $\mathbf{M}^{+\cdot}$ may also mirror the stability of **M** if they have comparable structures. This will itself depend on its structure (degree of saturation, bonding etc), and also the amount of energy transfered to the neutral molecule above the ionisation potential [2] (see Section 2.4).

2.2.1 Vertical and Adiabatic Ionisation Energies

When an ion is formed with the minimum energy, keeping all the nuclei within $\mathbf{M}^{+\cdot}$ at the positions they were in **M**, the ionisation process is said to be 'vertical', the energy necessary being the 'vertical ionisation energy'. To produce a molecular ion in its ground state requires the 'adiabatic ionisation energy'. These two energies may be the same [3].

2.2.2 Ionisation Efficiency Curve

The probability of at least the amount of energy needed to ionise **M** being transferred is a function of the electron energy; a plot of ion current versus electron energy is known as an 'ionisation efficiency curve' (Fig 3). The initial part of the plot is curved due to the

spread of electron energies from the filament. Following this is a linear portion where the ion current is very sensitive to the electron energy. At approximately 60eV the ion current is at its maximum. Increasing the energy still further the ion current usually decreases slightly and enters a plateau region [4].

2.2.3 Appearance Energy

For any fragment ion formed within the electron impact there is a characteristic electron energy below which the species is not seen. This is known as the 'appearance energy' AE, of that ion.

The minimum energy needed to form M_2^+ by the process

$$M_1^{+\cdot} \dashrightarrow M_2^+ + M_3^\cdot$$

is ε_0, where

$$\varepsilon_0 = AE(M_2^+) - IE(M_1)$$

For M_2^+ to be detected in the mass spectrometer it must be formed within a certain time within the source. Hence the measured energy, ε_0', will be greater than the true value, ε_0, by an amount known as the 'kinetic shift' or 'k shift' (Fig 4). This additional energy is necessary to

raise the rate constant of the reaction sufficiently for M_2^+ to be detected [4,6].

$$\varepsilon_0'(\text{detected}) = \varepsilon_0(\text{true}) + \text{'k shift'}$$

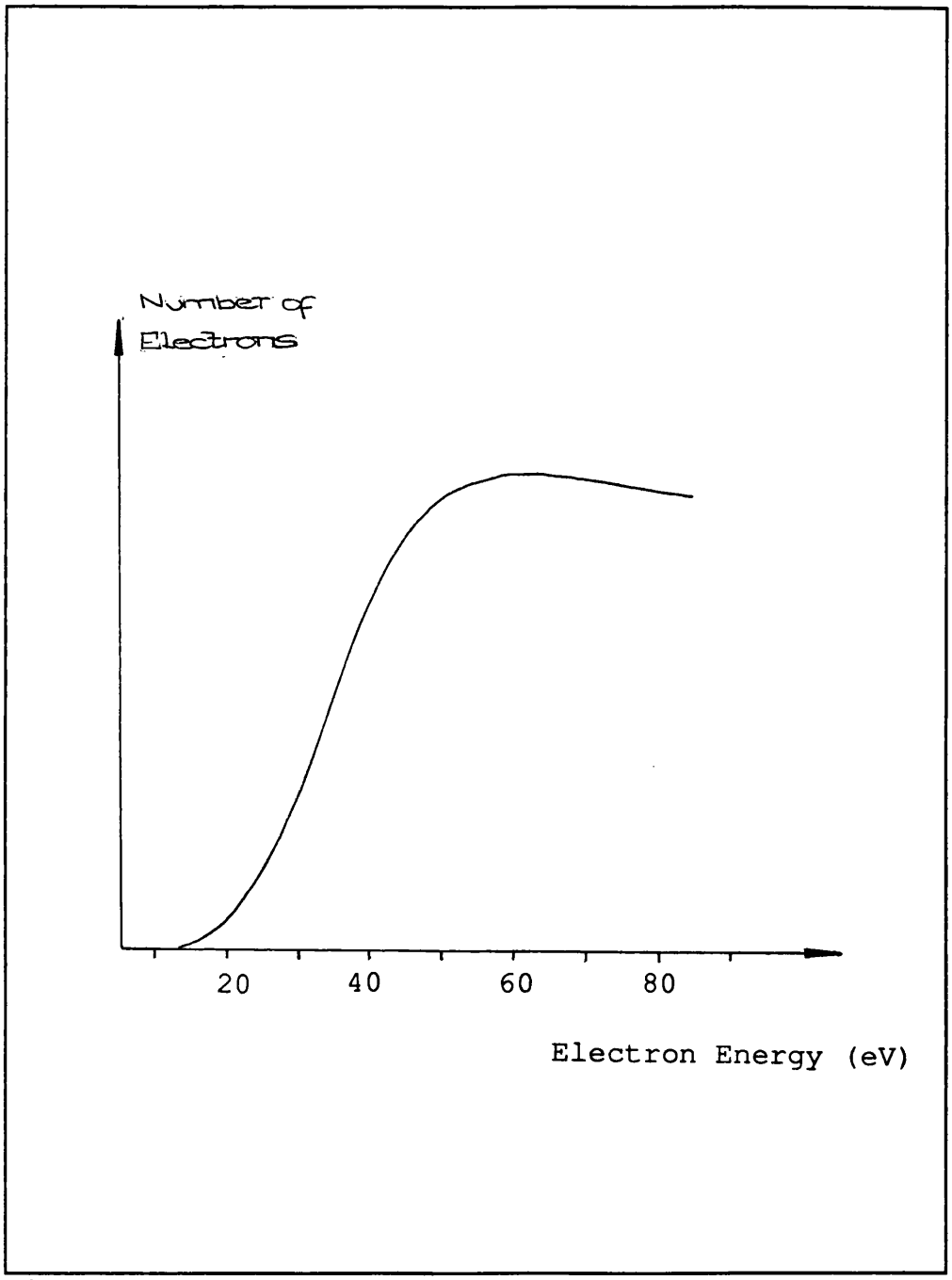

Figure 3 Ionisation Efficiency Curve

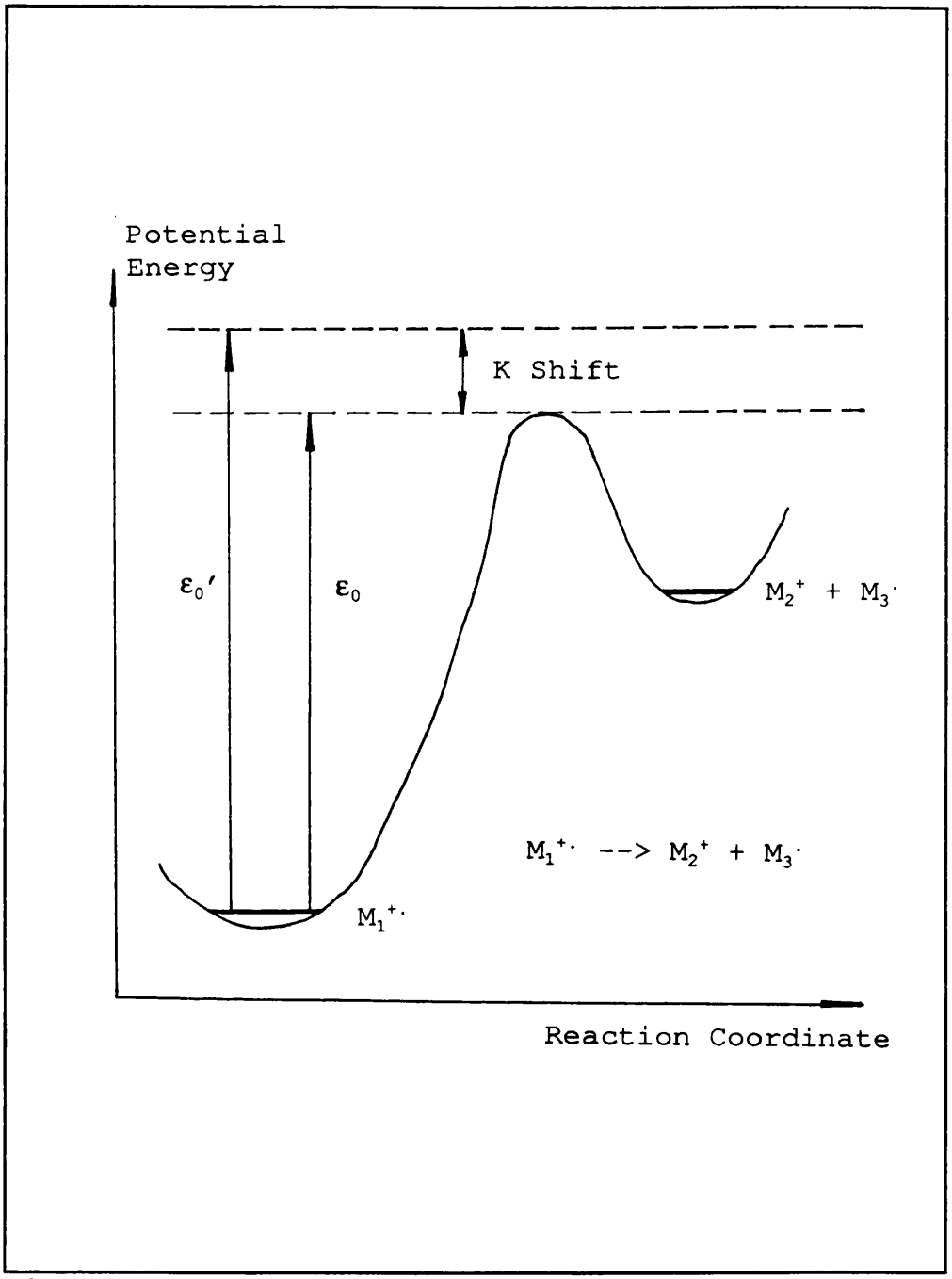

Figure 4 Relationship between appearance energy, kinetic shift and ε_0

2.3 QUASI EQUILIBRIUM THEORY

Although the decomposition of diatomic molecules is well understood, such a model of behaviour is not valid for polyatomic systems, failing to predict metastable ions or kinetic energy release on fragmentation, for instance.

In response to this, Rosenstock et al [6] developed the Quasi Equilibrium Theory, QET, based on the Absolute Rate Theory of Eyring et al [7].

The basic assumptions of QET are these:

a) the time required for the dissociation of the molecular ion is far greater than the time for the interaction leading to its formation and excitation,

b) the rate of dissociation is slow compared with the rate of redistribution of the excitation energy over all the degrees of freedom

c) fragments are formed by a series of competing and consecutive unimolecular processes

d) ions generated in a mass spectrometer represent 'isolated systems' in a state of 'internal equilibrium' [3].

This theory was originally developed to predict complete mass spectra which it is generally unable to do, but its value lies in its ability to provide a theoretical framework for understanding fragmentation processes.

QET assumes that dissociation occurs after several

oscillations (the shortest oscillation would be of the order of 10^{-14}s) so that the ion loses all memory of how it was energised. For this reason dissociation becomes independent of the mode of energisation, which has important consequences for collision processes [3].

2.4 FRAGMENTATION

The molecular ions $M^{+\cdot}$ are formed with a range of internal energies. Those with little internal energy will be relatively stable tending not to react further and being collected intact at the detector. Those with more internal energy may have sufficient to undergo other reactions.

In the one step fragmentation of $ABC^{+\cdot}$

$$ABC^{+\cdot} \rightarrow AB^{+} + C^{\cdot}$$

AB^{+} and $C^{\cdot}$ are 'primary' fragments. These relate directly to the structure of the parent ion. If these products are formed in an excited state they may have the energy to react further

$$AB^{+} \rightarrow A^{+} + B$$

giving the 'secondary' fragments A^{+} and **B**. These may also dissociate and so on, until the products formed have insufficient energy for further reaction. For these fragments to be observed in the mass spectrum they have to occur within the appropriate time scale for the geometry of that instrument.

2.4.1 Stevenson's Rule

For hydrocarbons, the fragmentation of an ion tends to leave the charge on the fragment with the lowest ionisation energy.

In the fragmentation of $M_1^{+\cdot}$

$$M_1^{+\cdot} \longrightarrow M_2^{+} + M_3^{\cdot}$$
$$\longrightarrow M_2^{\cdot} + M_3^{+}$$

the appearance energy (see Section 2.2.3) of M_2^+, $AE(M_2^+)$, is lower than that of M_3^+ (Fig 5) so the former reaction will take precedence. $AE(M_n^+)$ is given by

$$AE(M_n^+) = IE(M_n^+) + D(M_n^+)$$

where $D(M_n^+)$ is the dissociation energy of M_n^+ [3,5].

As the excess internal energy in $M_1^{+\cdot}$ increases beyond that needed for the reaction to proceed, the rate of reaction increases.

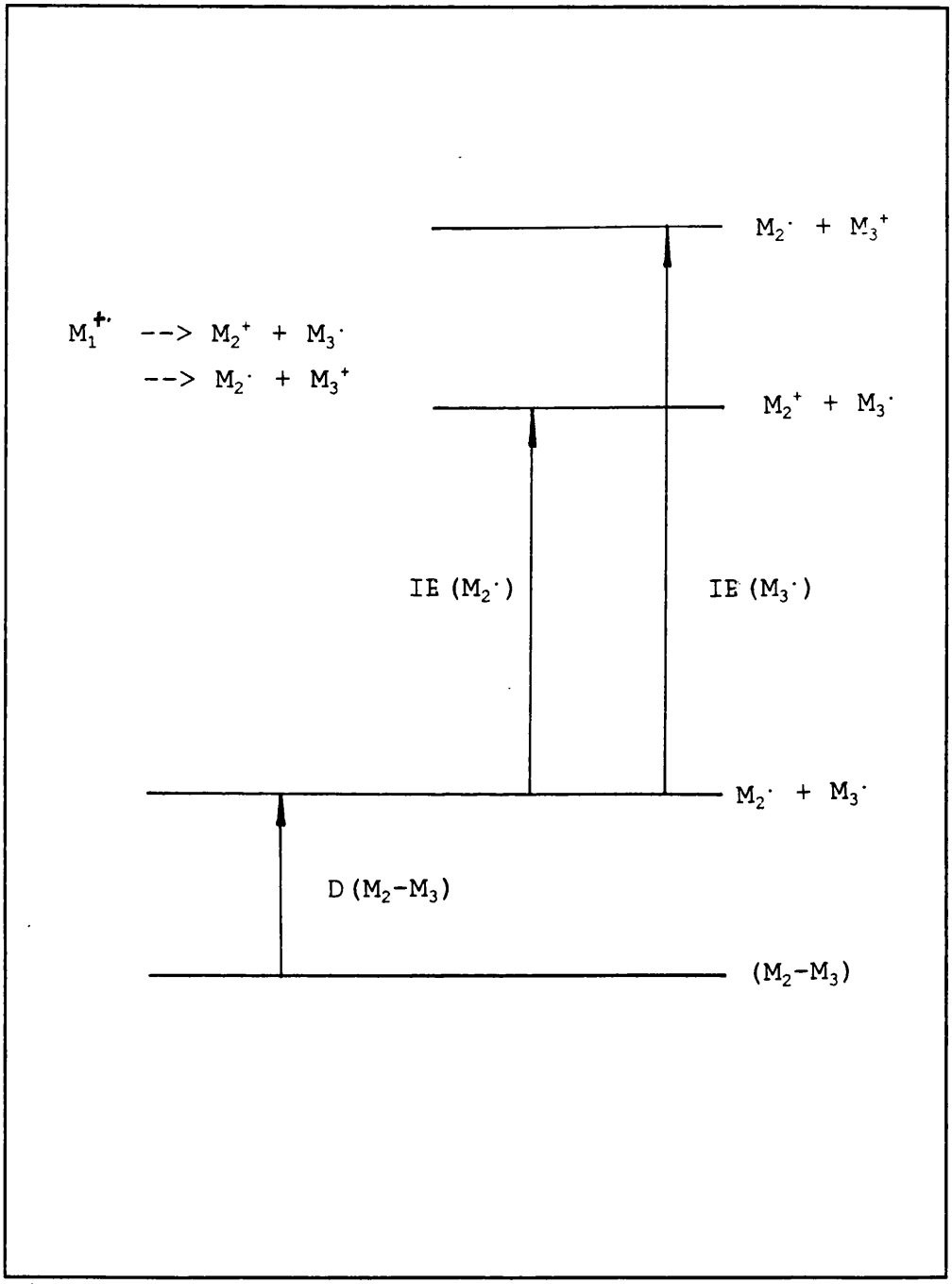

Figure 5 Illustration of Stevenson's rule in relation to the fragmentation of $M_1^{+\cdot}$

2.5 REARRANGEMENT

The fragmentation of an ion may be accompanied by or in competition with the transfer or rearrangement of atoms or groups of atoms

$$ABC^{+\cdot} \rightarrow AC^{+} + B^{\cdot}$$

Rearrangement reactions tend to yield highly stable ionic and neutral products. These products can be very abundant because although rearrangements are entropically unfavourable (the precursor has to be in a certain conformation before the reaction can take place) the associated activation energies are low. Specific rearrangements usually involve the formation of a structure which has a competitive fragmentation pathway.

'Skeletal rearrangements' refer to those involving the basic molecular structure. 'Random rearrangements' occur especially in hydrocarbons, where a series of transfers of the hydrogen (usually) or carbon atoms leaves them with no specific site on the precursor, but statistically distributed over several sites. When this occurs the hydrogen or carbon atom is said to be 'scrambled' (no preference for any specific site) or 'partially scrambled' (some degree of preference). Ions that undergo random rearrangements are usually associated with very low activation energy reactions [2].

2.6 ION STABILITY

The time taken for an ion formed in the source to travel to the detector, t_F, will depend on the instrument geometry, its mass (**M**), the number of charges (z) and the accelerating voltage (V_{ACC}) [2].

$$t_F \propto [M/(zeV_{ACC})]^{\frac{1}{2}}$$

Ions are formed with a range of lifetimes, hence they will fragment at various regions in the mass spectrometer: either in the ion source itself, within the field regions or in the field free regions. Some ions will have a lifetime outside the time of flight through the instrument so will be detected intact : these are termed 'stable '. Ions with the shortest lifetimes that decompose before the acceleration region are termed 'unstable'. Those that fragment between these two regions are termed 'metastable'.

2.6.1 Stable Ions

The time of flight through a two sector instrument is typically 10^{-5} to 10^{-4} s [2], so these ions have a t_F of at least this value. The number of stable ions that are formed will depend on how much excess energy is put into

the molecule at ionisation (see section 3.1).

2.6.2 Unstable Ions

Such ions have a lifetime of the order of 10^{-6} s or less and their decomposition continues until a stable or metastable product is formed [2]. Like stable ions, the population of unstable ions depends upon the excess energy of the ions originally formed.

2.6.3 Metastable Ions

If an ion decomposes within one of the field regions it will not be detected. However, if decomposition occurs within one of the field free regions, it may give rise to a detectable 'metastable peak' [2,8], their occurrence being first reported in 1945 [9].

In normal spectra, the metastable fragmentation of $\mathbf{M}_1^+$ to form an ion of mass $\mathbf{M}_2$ in the 1FFR will be recorded as a peak at mass $\mathbf{M}^*$, where

$$\mathbf{M}^* = \mathbf{M}_2^2/\mathbf{M}_1$$

$\mathbf{M}^*$ often being non integral. Hence the metastable peak indicates not only the mass of the daughter ion but that

of the precursor. Even if a metastable transition does take place, the corresponding peak at $\mathbf{M}^*$ may not be seen in a normal spectrum, for instance if the transition is too slow to take place in the 1FFR (it may involve a prior rearrangement of $\mathbf{M}_1^+$) or the fragment $\mathbf{M}_2^+$ undergoes a dissociation itself before reaching the detector.

Metastable peaks are characteristically broad compared with other peaks in the ordinary mass spectrum. This is due to a fraction of the fragmenting ions' internal energy being converted to kinetic energy on fragmentation [10].

Metastable transitions in the 2FFR can also be followed by scanning the instrument in the MIKES mode (see Section 3.5.2).

2.6.3.1 Kinetic Energy Release

The kinetic energy, **T**, released in the decomposition

$$\mathbf{M}_1^+ \text{ --> } \mathbf{M}_2^+ + \mathbf{M}_3$$

can be made up of two components [2]:

i) $\mathbf{T}^{\S}$ the contribution from $\varepsilon^{\S}$, the excess energy of the activated complex, which is available for partitioning between the internal energies of the products and the

translational energy of their separation, and

ii) $\mathbf{T}^e$ the contribution from ε^e_0, the reverse activation energy, which is partitioned between internal and translational energy (Fig 6).

Hence the kinetic energy release (KER) is given by

$$\mathbf{T} = \mathbf{T}^{\S} + \mathbf{T}^e$$

The ions that the mass spectrometer detects as metastable are those that fragment within a very narrow time interval, so the values of $\varepsilon^{\S}$ are closely determined by instrumental conditions. Because of this, whether or not ε^e_0 makes a major contribution to **T**, the KER will be more sensitive to ion structure than internal energy, unlike parameters such as relative abundance.

Thus the comparison of KER values can be structurally diagnostic. Substantially different values for KER from two ions decomposing via the same pathway, suggests different initial structures, similar KER value suggest similar structures. However, it is not impossible for structurally unrelated ions to decompose via the same pathway and give the same KER [2,3].

When the same ion is generated via two pathways, one by direct ionisation the other following a fragmentation step, the latter will usually be associated with a

slightly higher KER (a much smaller difference than if the initial structures were distinct).

Changes in the electron energy or source temperature will have little effect on the measured KER because of the restrictions on $\varepsilon^{\S}$ [2,3].

The value of **T** is usually small, typically 0.02 eV, but can rise to 2eV or more [11]. The average kinetic energy released upon decomposition can be calculated from the metastable peak width at 22% of the maximum height for an exact gaussian (Fig 7), or the width at ~50% maximum height ($\mathbf{T}_{½}$) for an exact square profile [8].

This value can be corrected for the width of the main beam peak using the equation [12]

$$\mathbf{W}_H(\text{corrected}) = \sqrt{[\mathbf{W}_H^2(\text{metastable}) - \mathbf{W}_H^2(\text{main beam})]}$$

where $\mathbf{W}_H$ is the width of the peak at height H% of its full value. This is an approximation that relies on the metastable and main beam peaks having the same gaussian profile. A full mathematical deconvolution may be used for more complex situations [13] but this approximation is usually adequate [14].

For the dissociation

$$\mathbf{M}_1^+ \text{ --> } \mathbf{M}^+_2 + \mathbf{M}_3$$

$\mathbf{T}_{½}$ can be calculated from

$$T_{½} = (\Delta E)^2 / V_{ACC} \cdot M_1^2 / (M_2 M_3 16)$$

where ΔE is measured from the metastable peak [2].

For other peak shapes the average KER can only be found from a full mathematical analysis of the peak, though the value of $T_{½}$ may be calculated for comparative purposes.

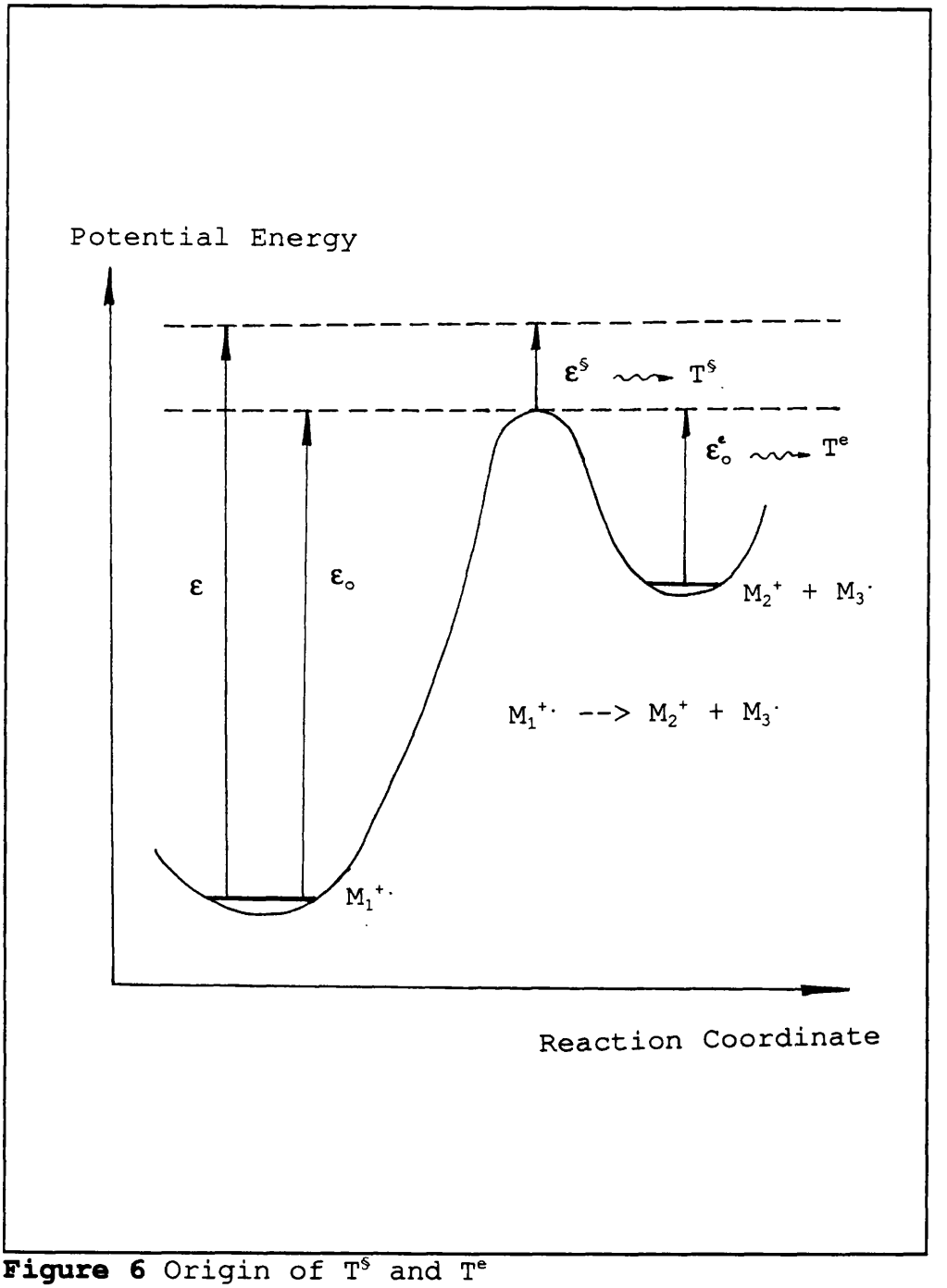

Figure 6 Origin of $T^{\S}$ and T^{e}

2.6.3.2 Metastable Peak Shapes

The majority of metastable peaks are relatively narrow and approximately gaussian, corresponding to a low KER and $T_{½}$ of the order of 80 meV or less [8]. Flat-topped or dished-topped peaks (Fig 8) occur when the KER is much greater, typically a few hundred meV. The dished-top is not a phenomenon associated with the breakdown of the ion, but is rather caused by the instrument itself.

Ions formed through fragmentation in the mass spectrometer will typically have components of velocity in three directions: **x**, **y** and **z**. The length of the focusing slits lie along the **z** direction and the instrument usually has no focusing in this direction. An ion with a considerable velocity component in the z direction will be discriminated against by the finite length of the slit. Such an ion should appear in the centre of the metastable peak, and this discrimination results in a flattening of the peak in the centre, giving a flat-topped or dished profile. This effect is enhanced by short focusing slits and a large distance between the slit and the detector [2].

In some instances, the metastable is neither gaussian, flat or dished but a combination of say a dished peak and a gaussian or two dished peaks: these are known as 'composite' metastable peaks (Fig 9). A composite peak can occur when [8]

a) two isomers decompose to form a common daughter ion,

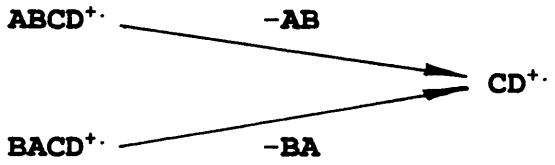

b) a precursor of one isomeric form decomposes to yield two isomeric daughters, or

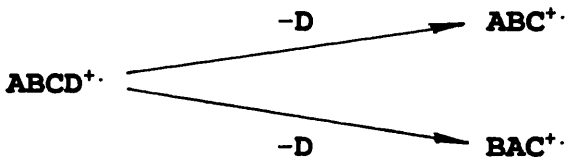

c) a precursor decomposes via two different routes to form daughter ions of the same isomeric form

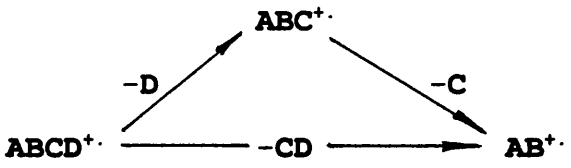

Attributing the occurrence of a composite metastable peak to one of these particular causes may not be a straightforward task [8].

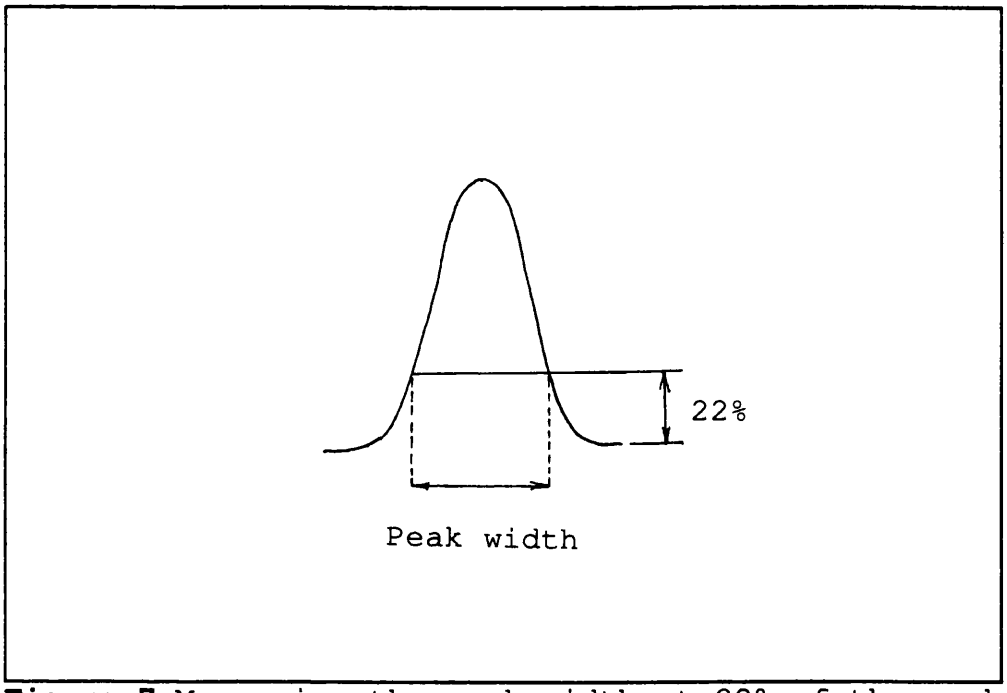

Figure 7 Measuring the peak width at 22% of the peak height

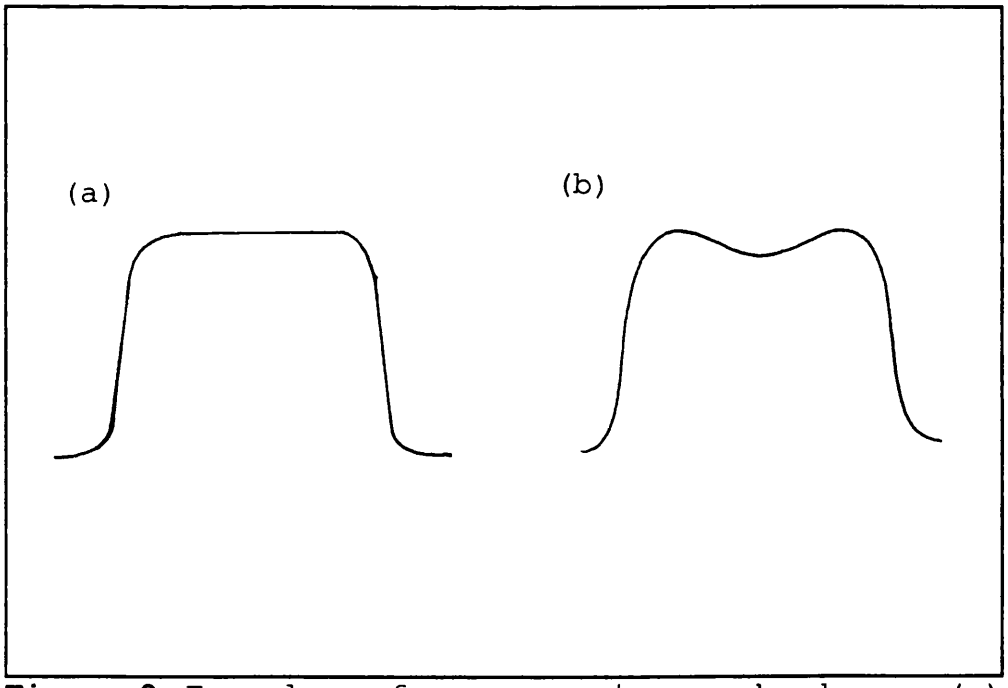

Figure 8 Examples of non-gaussian peak shapes (a) flat-topped (b) dished-topped

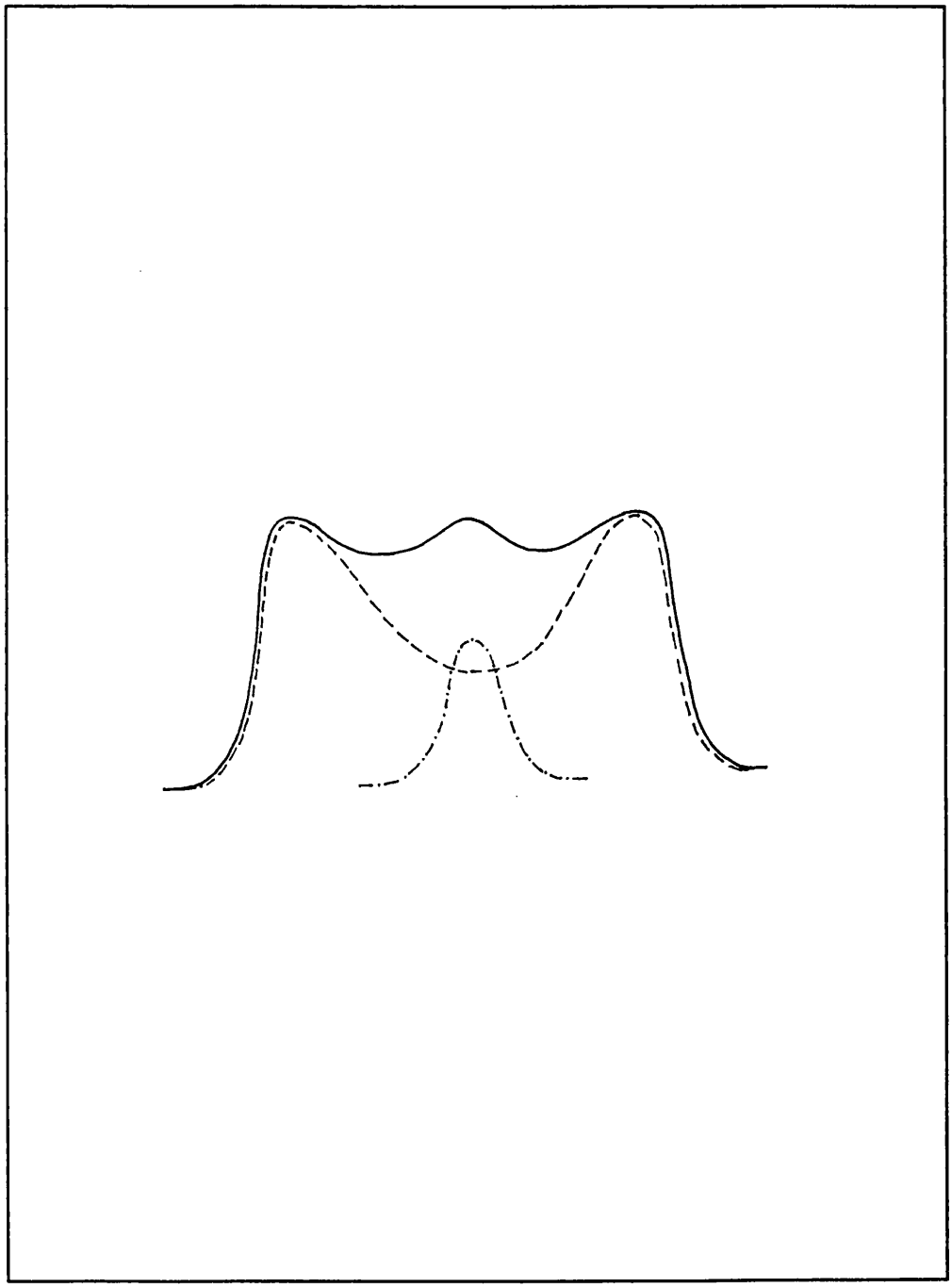

Figure 9 Example of a composite peak

2.7 COLLISIONS

Uncontrolled collisions between the ion beam and residual molecules in the mass spectrometer are unwanted since they ultimately lead to a reduction in the intensity of the ion beam. Much care is taken therefore to ensure that there is a good vacuum within the flight tubes. However, controlled collisions with a 'target' gas within specific regions ie gas or collision cells, or within a quadrupole, can be used to manipulate the ion beam, eg generate neutral species, reverse the charge of the incoming ions or produce controlled fragmentation.

The main processes [15] that can be achieved through colliding ions or neutrals with a target gas or vapour are

a) scattering
b) collisional activation

the second of which can lead to

i) collisionally induced dissociation
ii) charge exchange
iii) charge stripping
iv) charge reversal (charge inversion).

These are competing processes all taking place at the

same time though with differing probabilities.

The scattering referred to here is large angle scattering, that which results in the ion changing its direction so radically that it is lost to the mass spectrometer. Such scattering is always present and has to be kept to a minimum.

The amount of energy gained by an ion on collision with a target atom or molecule, is dependent upon the velocities of the particle involved, their molecular weights and the nearness of the collision. The most probably energy deposited, E_{COLL}, is given by Massey's equation

$$E_{COLL} = (h/a)(2eV/M)^{1/2}$$

where **h** is Planck's constant, **a** is the interaction distance or 'shielding radius', **eV** the translational energy of the ion and **M** the mass of the ion [16]. Small targets will tend to deposit more energy in the ion because of the reduction in **a**.

The probability of a process following from a collision is given in terms of its 'cross section' σ. For instance, the higher the probability of a collision resulting in scattering, the higher the value of the scattering cross section, σ_s. Control over which process predominates is exercised through the selection of the target gas and its pressure. Through careful choice of

these parameters the cross section of the desired process can be enhanced and the others suppressed.

The selective use of one or more of these collision processes leads to a range of different techniques able to yield more information on matters such as molecular structure and stability.

2.7.1 Gas Pressure

It is usually impossible to measure directly the pressure inside the gas cell (the size of the cell often prohibits the presence of a pressure gauge), and measurements of the overall pressure in the source or analyser region are not always useful. An accepted way of recording the collision gas pressure is by relating it to the attenuation of the main ion beam intensity due to the presence of the gas. The percentage attenuation is given by

$$\% \text{ Attn.} = [\text{main beam}]_{gas} \times 100\% \; / \; [\text{main beam}]_{no\ gas}$$

and percentage transmission is thus

$$\% \text{ Transmission} = 100\% - \% \text{ Attenuation}$$

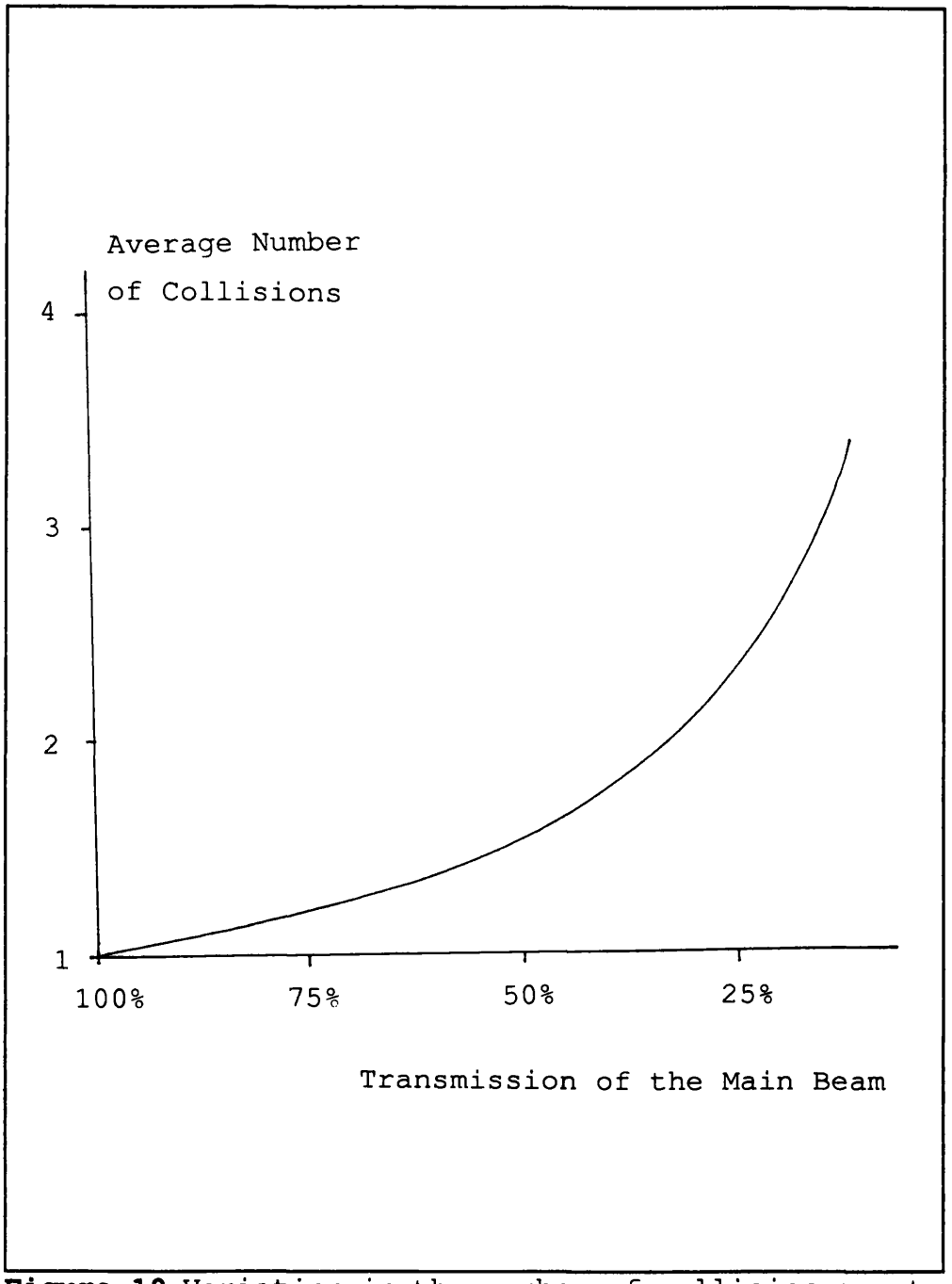

Figure 10 Variation in the number of collision events with pressure

Varying the gas pressure can have a marked effect on the average number of collisions suffered by an one ion or neutral, and it is important to bear this in mind when setting the gas pressure (Fig 10) [17].

2.7.2 Scattering

Large angle scattering is a major cause of reduction in the ion beam intensity, for instance the ion M^+ colliding with a gas molecule **G**

$$M^+ + G \rightarrow M^+_{SCATTERED} + G$$

The simplest picture of a collision is that between two atoms represented by rigid spheres [18]. If the collision is elastic then none of the translational energy of the atoms will be converted into internal energy (Fig 11). Simplifying the model further, one atom may be thought of as being stationary while the other moves with a velocity **v**, equal to the vector sum of the two original velocities.

For rigid spheres, the collision can be said to take place when the distance **d** between the spheres is equal to the sum of the radii. Since the collision is dependent upon **d** not the individual radii, it does not matter if, for convenience, the radius of one of the spheres becomes

a geometric point and the other the sum of the two radii (Fig 12).

The probability of collision between the moving point and stationary sphere can be seen to be dependent upon the size of that sphere, or its cross section. From semi-classical theory, the cross section of collisions between two atoms which results in elastic scattering is given by

$$\sigma_s = \pi a^2 (Z_1 Z_2 e^2 / hv)^2$$

where **a** is the shielding radius (approximately equal to the sum of the two atomic radii), Z_1 and Z_2 are the nuclear charges on the two atoms, **h** is Planck's constant and **v** is the velocity [19].

Although this greatly simplified approach cannot be expected to work for polyatomic systems, it does predict trends which have been verified experimentally.

Large angle scattering in atomic and polyatomic systems is due to Coulombic repulsion between nuclei (hence the nuclear charges are included in the equation). When the particles are close enough for a collision to take place, the nucleus of one particle experiences the force of the other nucleus which it usually exerts on its own electrons. This Coulombic potential determines the ionisation energy (IE) and as the IE increases, σ_s decreases.

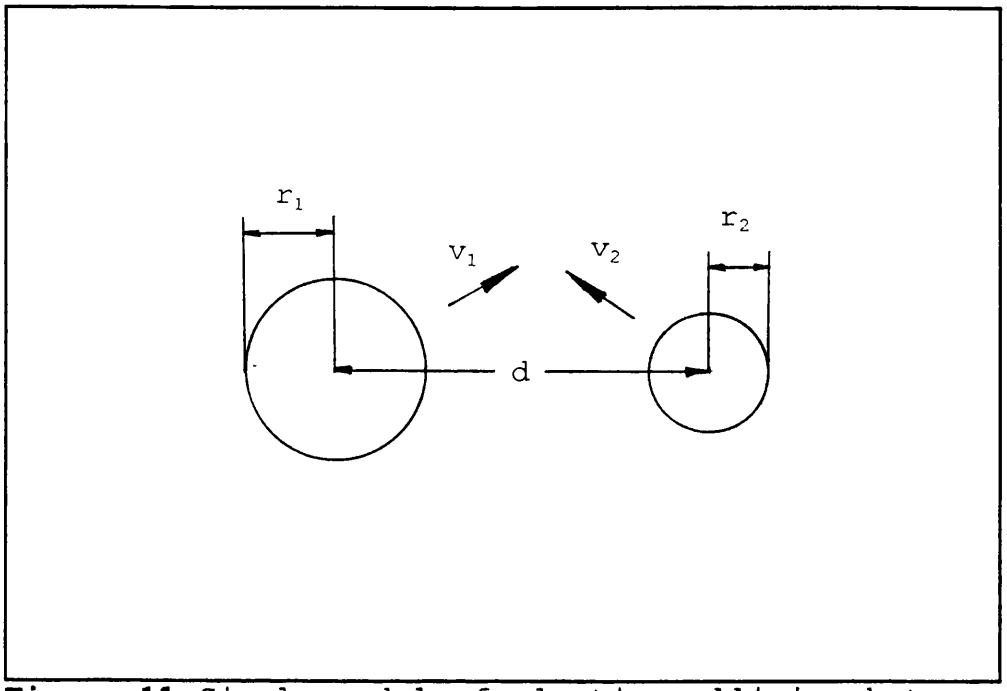

Figure 11 Simple model of elastic collision between two rigid spheres

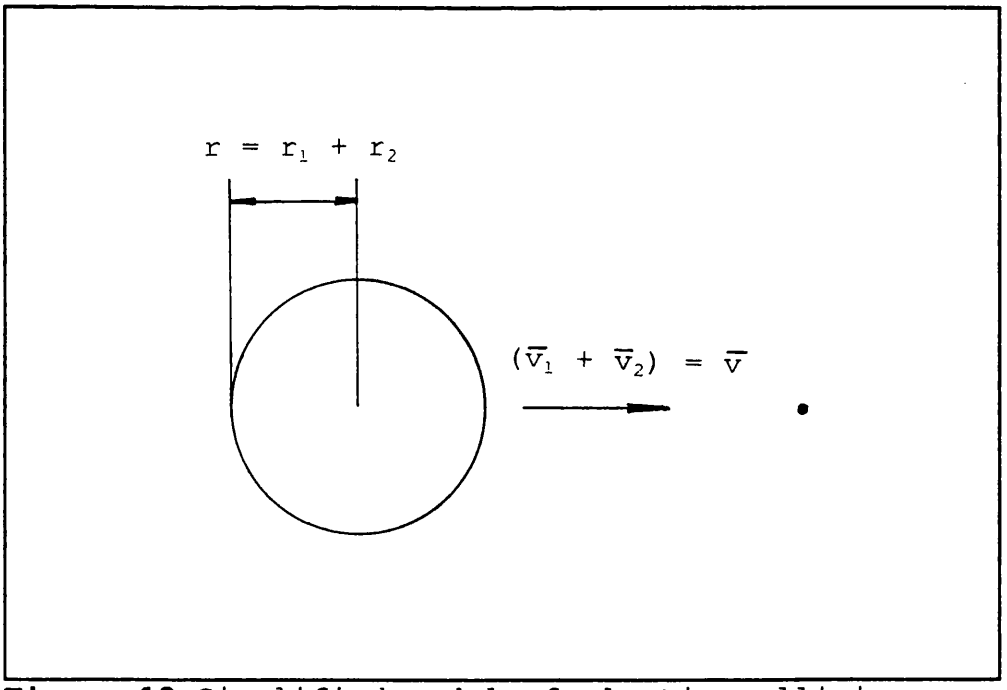

Figure 12 Simplified model of elastic collision

The values for neutralisation cross sections are of the same order of magnitude or greater than those for collision induced dissociation (see Section 2.8.1).

To keep scattering to a minimum the target gas or vapour should be selected to give a low σ_s, ie one with a small molecular size, low molecular mass and high IE. The probability of scattering can also be reduced by decreasing the number of target molecules ie lowering the gas pressure, but this will also reduce the probability of all the other collision processes, wanted or not.

2.7.3 Charge Exchange

2.7.3.1 Neutralisation

After scattering, neutralisation by charge exchange is the most important process for removing ions from the primary ion beam

$$M^+ + G \rightarrow M + G^+$$

If the structure of the neutral is closely related to the structure of its (stable) ionic precursor then stable neutrals will be generated. However if the structure of the neutral is inherently unstable or it is formed with a large amount of internal energy, the neutral will

subsequently rearrange or dissociate.

The internal energy of the neutral will depend on the energy defect Q_N

$$Q_N = IE(G) - RE(M^+)$$

where $RE(M^+)$ is the recombination energy of M^+. For exothermic reactions (Q_N < 0eV) dissociation of the neutral will be a significant process. At resonant or near resonant conditions (Q_N ~ 0eV) the neutrals are formed with little internal energy, and for mono- and diatomic species this has been found to be optimal for charge exchange neutralisation [4].

The cross section for neutralisation σ_N is, to a first approximation [15]

$$\sigma_N \propto 1/[IE(G) - IE(M)]$$

The variation in neutralisation cross section for mono- and diatomic species has been studied extensively [20]. From Massey's adiabatic criterion [16] the translational energy corresponding to the optimum neutralisation cross section can be estimated from

$$v_{MAX} = Q_N a/h$$

where v_{MAX} is the velocity of the incident ion

corresponding to the optimum value of σ_N, Q_N the energy defect, **a** the shielding radius and **h** Planck's constant. Where thermochemical data is not available to calculate Q_N, a target estimated to have a lower IE (eg Xe) is recommended (to avoid forming neutrals with appreciable internal energy) [4].

It is possible to use both metal vapours (eg Hg and Na) [21] and gases [22] as neutralisation agents, though metal vapours have the disadvantage of being comparatively less easy to handle. A study [23] made of the efficiency of various gases and vapours to neutralise molecular acetone, found them to be in the following order of efficiency :

$$Hg > Zn > Xe > Na > CH_3COCH_3 > O_2 > He$$

Ion structure does affect the overall efficiency of neutralisation, but the relative efficiency of the target gases seems to be species independent.

Increasing the target gas pressure will increase the probability of neutralisation but it will also increase the loss due to scattering. Studies have shown that for the highest yield of neutrals through charge exchange, the target gas should be admitted to a pressure that gives 25-35% transmission of the original ion beam [23]. However at this pressure many ions will undergo multiple collisions (Fig 10) giving a more complex result [19].

Therefore the recommended [23] target pressure is that which gives approximately 70% transmission of the main beam or higher, to favour single collision conditions.

2.7.3.2 Ionisation

Ionisation of a neutral species **M** through collision with a target **G** can be achieved in two main ways, either through charge exchange

$$M + G \rightarrow M^+ + G^-$$

or through electron detachment

$$M + G \rightarrow M^+ + G + e^-$$

with most evidence in favour of electron detachment as the general process [4].

An extensive study [24] of the efficiency of ionising CH_3COCH_3, CH_3Cl and $.CH_2NH_2$ neutrals by various targets, gave the following relative efficiencies :

Neutral:	Target:
CH_3COCH_3	$Cl_2 > O_2 > NO > NO_2 > N_2 > He > CH_4 > SF_6 > Xe$
CH_3Cl	$NO_2 > O_2 > NO > Cl_2 > N_2 > CH_4 > Xe > He > SF_6$
$.CH_2NH_2$	$Cl_2 > NO > NO_2 > O_2 > Xe > N_2 > CH_4 > SF_6 > He$

Table 1: Relative efficiencies of three targets for neutralisation

The target gases subdivide into two groups, 'hard' and 'soft'. The hard targets were He, CH_4, SF_6 and Xe, giving low ionisation efficiencies and a high degree of fragmentation. Soft targets O_2, NO, Cl_2 and NO_2 gave much higher ionisation efficiencies and much less fragmentation. The type of gas chosen depends upon the application : fragmentation can be useful for structural determination while less fragmentation is required for the determination of molecular weight. For ionisation with a low degree of fragmentation O_2 is a popular choice, but NO_2 has been found to yield better results for fast neutrals with a low IE.

Soft targets accept an electron in the ionisation process, whereas with a hard target the process goes by

the dissociation equation, which probably has the higher energy requirement of the two [24].

The amount of energy deposited in the molecule during ionisation, is dependent upon the energy defect Q_N of the reaction. Therefore, by selecting a target with an appropriate IE it should be possible to control the amount of energy deposited in the ion. Generally, ionisation processes tend to have a large energy defect (typically > 100kV) so the optimum translational energy for ionisation will often be higher that the optimum for neutralisation [4]. Increasing the accelerating voltage from 3 to 10 keV has little effect on the value of σ_I [24], however it does decrease losses due to scattering.

When the IE of the neutral is higher than that of the target, ionisation of the target

$$M + G \rightarrow M + G^+ + e^-$$

becomes a significant process., and thus the efficiency of ionising **M** will decrease.

Ionisation efficiency can be increased by increasing the target gas pressure, but this also increases losses due to scattering and multiple collision effects. Studies have shown that for ionisation the optimum target pressure corresponds to approximately 30% transmission of the main beam, but as with neutralisation, a lower gas pressure has to be used [24].

2.8 COLLISIONAL TECHNIQUES IN MASS SPECTROMETRY

The possible outcomes of ion-molecule collisions eg. fragmentation, have been outlined (see Section 2.7) together with their dependence on gas type and pressure. The inclusion of special collision gas cells in the field free regions of the mass spectrometer has made possible the utilisation of collision processes in a range of tandem techniques for structural and analytical studies.

2.8.1 Collision Induced Dissociation

Metastable decomposition has long been used to investigate the structure of the parent ion. However since ions which decompose this way have a signif_icant energy content, they may have undergone rearrangement before decomposition. Also there may be few structurally significant fragment peaks, either because of the stability of the ion or because a soft ionisation technique was used.

Collisionally induced dissociation CID (or collisionally activated dissociation CAD) is a two step process - excitation of the selected species through its collision with a target gas

$$M^+ + G \rightarrow M^{+*} + G$$

followed by its dissociation.

$$M^{+*} \rightarrow M_2^+ + M_3$$

Collisions that are effective at inducing CID are those that involve an interaction between the ion nucleus and the electrons in the target [2].

There are two main excitation processes- vertical electronic excitation and adiabatic vibrational excitation. Electronic excitation [25] tends to dominate at high collision energies (ie greater than 1kV) with small target species (eg He). Part of the kinetic energy of the ion is converted directly into internal energy [2] and because of the high translational energy of the ion, the law of conservation of momentum requires that negligible translational energy is transfered to the target [3]. Hence the kinetic energy lost by the ion is of the same magnitude as its gain in internal energy. This loss of kinetic energy **Q**, leads to the fragment peak due to collision induced dissociation appearing at a lower energy than the same fragment peak from a unimolecular decomposition. The position of the peak in the MIKES spectrum gives **Q'**, an approximation to **Q** . Any spread in **Q** will usually have less effect on the width of the peak than the kinetic energy release **T** [2].

Just as in the case of metastable peaks, a portion of the non-fixed energy $\varepsilon^{\S}$ of the collisionally activated

ion will be released as kinetic energy T^s. The total kinetic energy released **T**, (where $T = T^e + T^s$) can be deduced from the peak width just as with a metastable peak.

From studies on the collisional dissociation of ions it is believed that the decomposition process obeys the quasi equilibrium theory, QET [3]. The electronic excitation of the ion is rapidly converted to vibrational excitation which, within picoseconds, distributes itself statistically over the whole ion. The excited ion subsequently dissociates at a rate much slower than the energy redistribution, the excess energy not needed to overcome the dissociation threshold being released as translational energy of the fragment ions and neutrals.

To be useful analytically, the collisionally induced peaks should reflect only the structure of the parent ion not its formation or internal energy before the collision took place. Experiment shows that this is indeed true in all but a few instances, such as when the collisions are of very low critical energy or the parent is of very high mass. Therefore when two molecules give identical CID spectra (equal in peak height ratios and widths) it may be concluded that they are identical in structure.

The intensity of peaks due to unimolecular fragmentation can be considerable in a CID spectrum and may obscure the collision induced peaks. The amount of energy released when an ion fragments offers a method of

distinguishing between unimolecular and collision induced fragmentation. Peaks corresponding to fragments from unimolecular dissociation should show no change in relative abundance or shape as the collision gas pressure is increased (except some slight decrease due to scattering) . Peaks corresponding to CID fragments will increase linearly in intensity with increasing gas pressure.

Unimolecular fragments are dependent upon the electron energy. Such products are believed to originate from a relatively narrow range of internal energies so are sensitive to changes in the electron energy. Processes with higher activation energies (eg those observed as CID fragments) are believed to originate from a much larger range of energies, so are less sensitive to this change [3]. In the analysis of CID spectra unimolecular fragment peaks are discounted. If the spectrum is still found to be dependent on the electron energy, this may suggest that there is a mixture of non-interconverting structures present, formed simultaneously from the precursor through competing mechanisms and having different appearance energies. That the spectrum is independent of the electron energy does not guarantee that there is only one structure present- there may a mixture of interconverting structures or non-interconverting structures with similar appearance energies [3].

The main processes in competition with CID are scattering and charge exchange, so the efficiency of CID can be expressed by [15]

$$\text{CID efficiency} = [\sigma_{CID} / (\sigma_{CID} + \sigma_{CE} + \sigma_S)]\ T_R$$

where σ_{CE} is the cross section for charge exchange and T_R is the relative transmission of daughter ions to precursor ions. Hence the efficiency of CID can be improved by decreasing the probability of scattering and charge exchange (neutralisation, ionisation or charge stripping). Relative CID efficiencies can be found by measuring the pressure (from the ion gauge) against the increase in fragment ion intensity [26].

The cross section for CID is defined by [15]

$$I = I_0 \exp(-\sigma_{CID}.l_p.N)$$

hence

$$\sigma_{CID} = \ln(I_0/I) / (l_p N)$$

where l_p is the path length between collisions, N is the target density and I and I_0 the final and initial beam intensities. So σ_{CID} can be increased by decreasing l_p, achieved by increasing the pressure of the target gas, bearing in mind that this will also increase σ_{CE}, σ_S and

the instances of multiple collisions [27]. The nature of the target gas has been found to have no effect on the relative intensities of the fragments [27] but does influence the overall fragment yield [15].

To determine absolute values of collision cross section from relative values, the target gas pressure has to be known accurately. Also the length of the collision region needs to be known, but as gas leaks out of the collision cell, this will actually be greater than the physical length of the cell itself [11].

The cross section for CID is high since many more stable ions enter the collison region than metastable ions. However transmission of the CID fragments through the mass spectrometer is lower than that of the primary beam due to the kinetic energy release upon dissociation, and scattering which leads to greater beam divergence. The design of the instrument can improve the collisional ionisation efficiency, for instance by confining the collision gas to a small region near the focal point and building in mass analysers with a large acceptance angle [15].

In a CID experiment only stable ions are sampled ie those that lack sufficient internal energy to fragment unimolecularly, and hopefully to rearrange. Hence, ideally CID spectra feature fragments formed through structurally characteristic direct bond cleavages, of ions of well defined structures [28].

2.8.2 Neutralisation-Reionisation Mass Spectrometry

Neutralisation-reionisation mass spectrometry (NRMS), as its name implies, combines the techniques of producing neutral molecules from ions, either through charge exchange or collision induced dissociation, and then (re)ionising them, again through charge exchange or CID. Such experiments have been used as far back as 1976 [29] for studies on the energy states of argon, but the idea saw a resurgence of interest from 1980 [21] onwards, for dealing with a range of different problems. Much has been published on this technique including extensive review articles [30,31].

In a tandem mass spectrometer the neutralisation and (re)ionisation stages are carried out between the two analytical stages (the 2FFR in the VG ZAB-2F). Two gas cells are required, one for each stage, and a deflector plate between them to which a positive or negative voltage may be applied, so that ions from the first cell may be prevented from entering the second cell (Fig 13).

An alternative to using a deflector plate is to float the second gas cell at a voltage V_C (Fig 14). If V_C is greater than the accelerating voltage V_{ACC}, then no ions will enter the second cell. However, this method has its limitations. There is a practical maximum value for V_C above which electrical discharge takes place inside the cell (in one case this has been found to be 5.5 k V

[32]). Hence V_{ACC} may have to be reduced below its optimum value to ensure it does not exceed V_C. Another important problem occurs when gas from the second cell diffuses back along the flight tube (this tends to happen as the gas pressure is increased) and ions emerging from the first cell are able to interact with this gas before they are deflected (Fig 15). A deflector plate requires a voltage of a few hundred volts to deflect all ions away.

The possibility of floating the second gas cell can be used for differentiating between fragmentation after the deflector that takes place within the second cell and outside it. The cell voltage V_C is set between 0 and a few hundred volts. Fragments that are formed just before the cell with the same energy that they would have without the cell voltage, appear at the normal mass position in the mass spectrum. However those fragments formed within the cell emerge with an increased energy dependent upon the value of V_C and thus appear at a higher than normal position on the mass scale. V_C should be selected such that any peaks that are displaced in this manner do not coincide with existing peaks. This technique is useful for differentiating between unimolecular dissociation outside the cell and CID within the cell. (A small proportion of unimolecular dissociations will take place inside the cell but unfortunately the technique of floating the cell this way cannot differentiate between this and CID within the

cell. This however should not be a problem as long as the unimolecular contribution is relatively small.)

Since by using different collision gases, the neutralisation and ionisation stages can be carried out in different ways, NRMS can be adapted to yield different types of information. For instance, if both the collision gases chosen give a high probability of charge exchange over CID, the stability of a selected neutral may be studied (Fig 16). Here the selected ion $\mathbf{M}^{+\cdot}$ should be neutralised with a minimum of fragmentation to **M**, any unreacted ions removed by the deflector and the neutral reionised to $\mathbf{M}^{+\cdot}$. However if the neutral is unstable in the time taken to travel from the point of neutralisation to the point of reionisation (approximately 1 μs [13]) **M** will undergo unimolecular dissociation within this time and will not appear in the NRMS spectrum.

Using a neutralisation gas with a higher cross section for CID can give extra information on the structure of $\mathbf{M}^{+\cdot}$ (Fig 17). In the first gas cell the selected ion is fragmented, the daughter ions usually seen in a CID spectrum are removed by the deflector and the neutral fragments ionised with a minimum of fragmentation. Hence this method gives information which is complementary to the CID spectrum of $\mathbf{M}^{+\cdot}$.

Structural information on the neutral **M** can be found using the combination of soft neutralisation target and hard reionisation target (Fig 18). Here the selected ion

$M^{+\cdot}$ is neutralised with a minimum of fragmentation, unreacted ions removed and the neutral fragmented. This is equivalent to a CID spectrum of the neutral **M**, which may not be the same as the spectrum of the $M^{+\cdot}$ ion since they may not necessarily fragment via the same pathway [23].

If both collision gases used are hard, the resultant spectrum will be all daughter ions of all daughter neutrals from the collision induced dissociation of $M^{+\cdot}$. Obviously, this will be very complex and difficult to analyse, since there will be no way of determining from the spectrum which of the detected ions came from which parent neutral.

Since two collision processes are being used, each with a low yield of ions or neutrals, the overall efficiency of NRMS is low, which usually leads to the use of signal averaging to combat low signal to noise ratios.

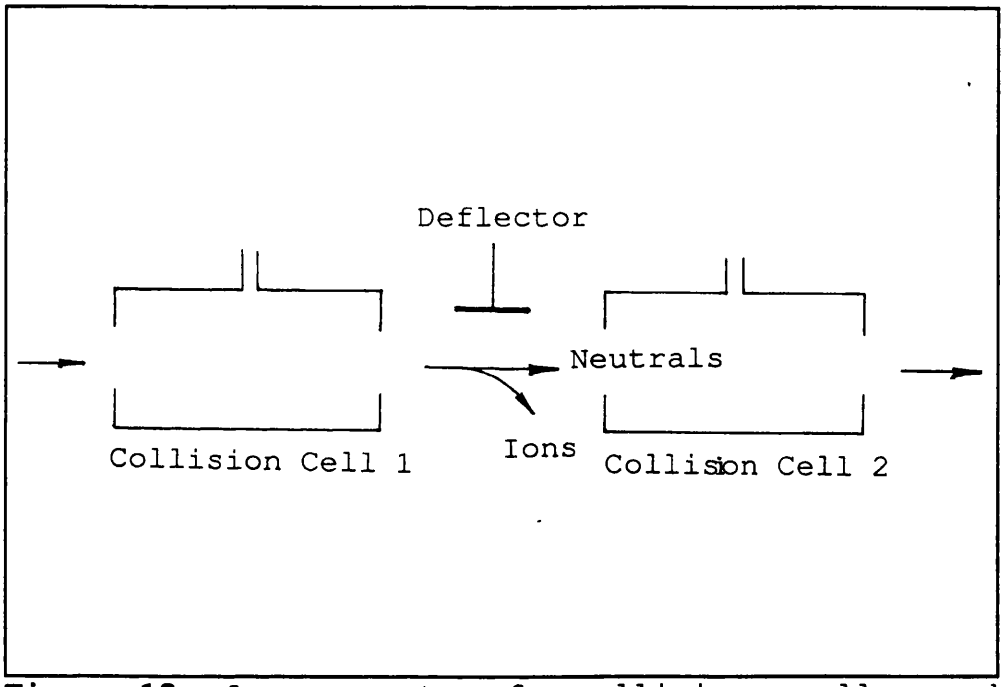

Figure 13 Arrangement of collision cells and deflector plate for NRMS

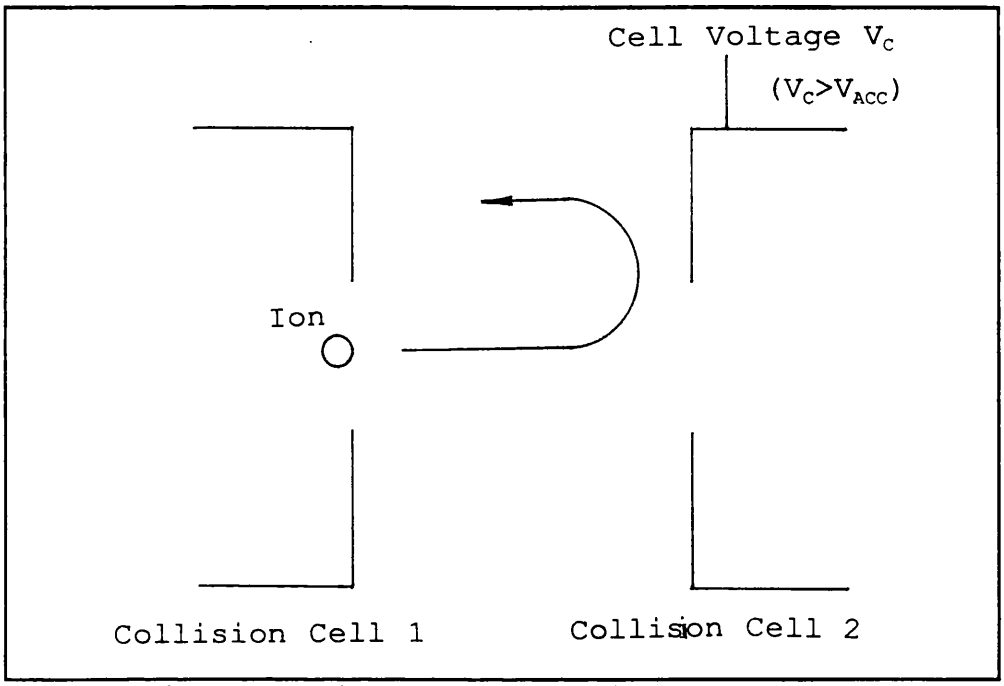

Figure 14 Deflection of ions using a voltage on the second collision cell

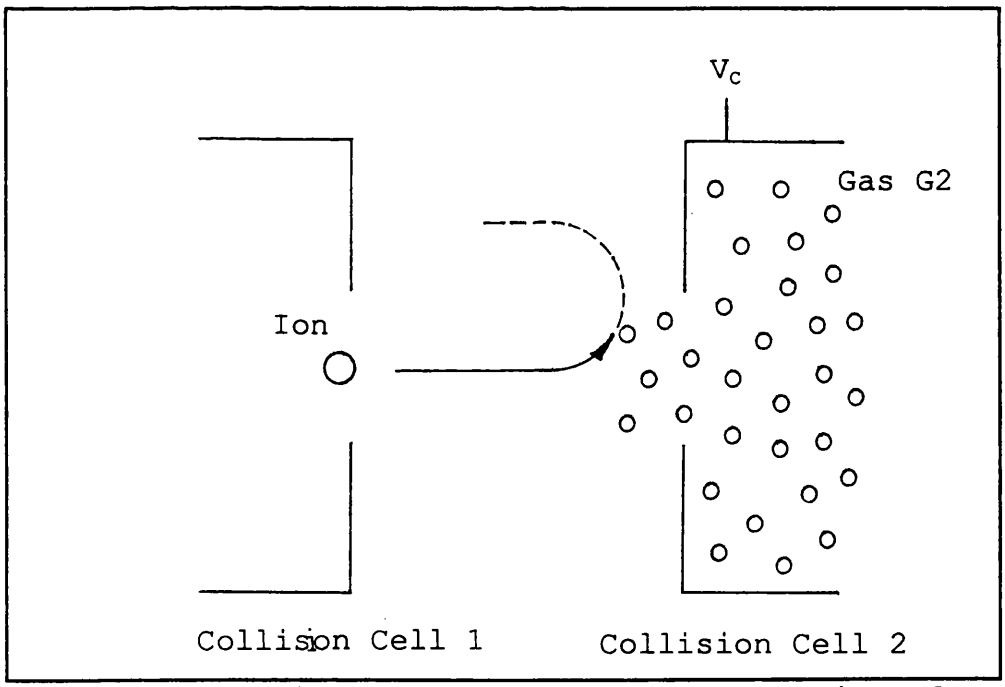

Figure 15 Collision between an ion emerging from collision cell 1 and gas streaming back from collision cell 2

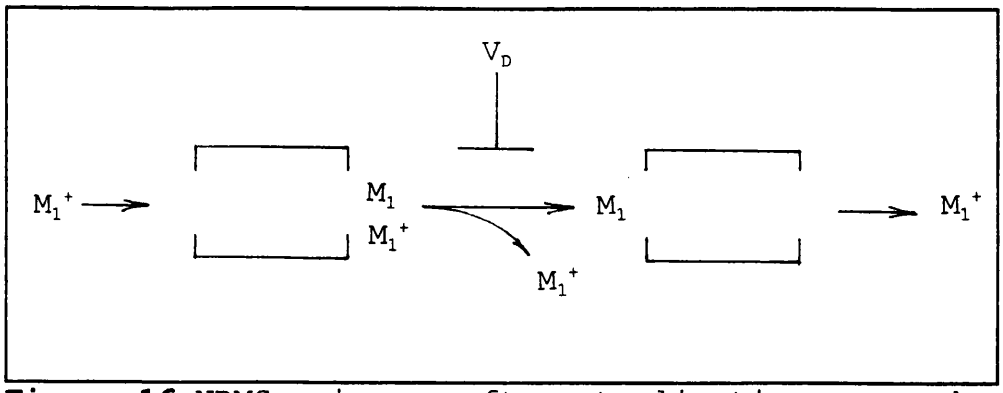

Figure 16 NRMS using a soft neutralisation gas and a soft ionisation gas

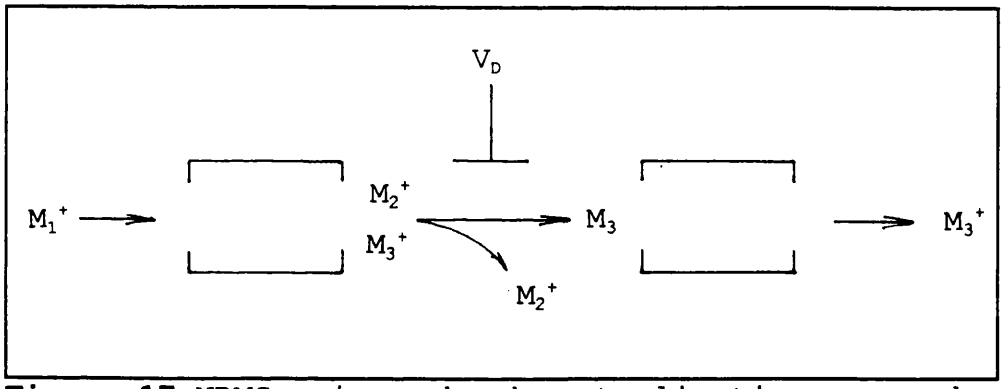

Figure 17 NRMS using a hard neutralisation gas and a soft ionisation gas

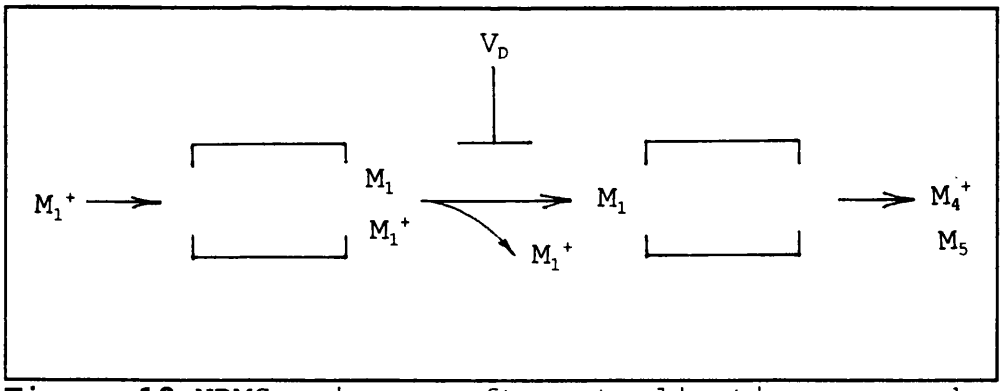

Figure 18 NRMS using a soft neutralisation gas and a hard ionisation gas

2.8.3 Collisionally-Induced Dissociative Ionisation

Collision induced dissociative ionisation (CIDI) is a technique very similar to NRMS, and requires similar instrumentation [11,28]. CIDI allows the investigation into the structure of neutral fragments from unimolecular decomposition through their collision induced dissociation. The metastable parent ions $M^{+\cdot}$ are selected by MSI, some of which then undergo unimolecular fragmentation in the 2FFR. Unfragmented ions and ionic products are removed with the deflector and the neutral beam undergoes collisions with a target gas or vapour in the second collision cell (Fig 19).

Great care must be taken when setting the gas pressure. If it is too high, the neutrals may gain enough energy (through multiple collisions) to isomerise prior to fragmentation, which will result in a loss of structural information. Also it may lead to increased losses due to scattering, and there may be problems with gas leaking out of the gas cell and back along the flight tube, causing fragmentation prior to the deflector.

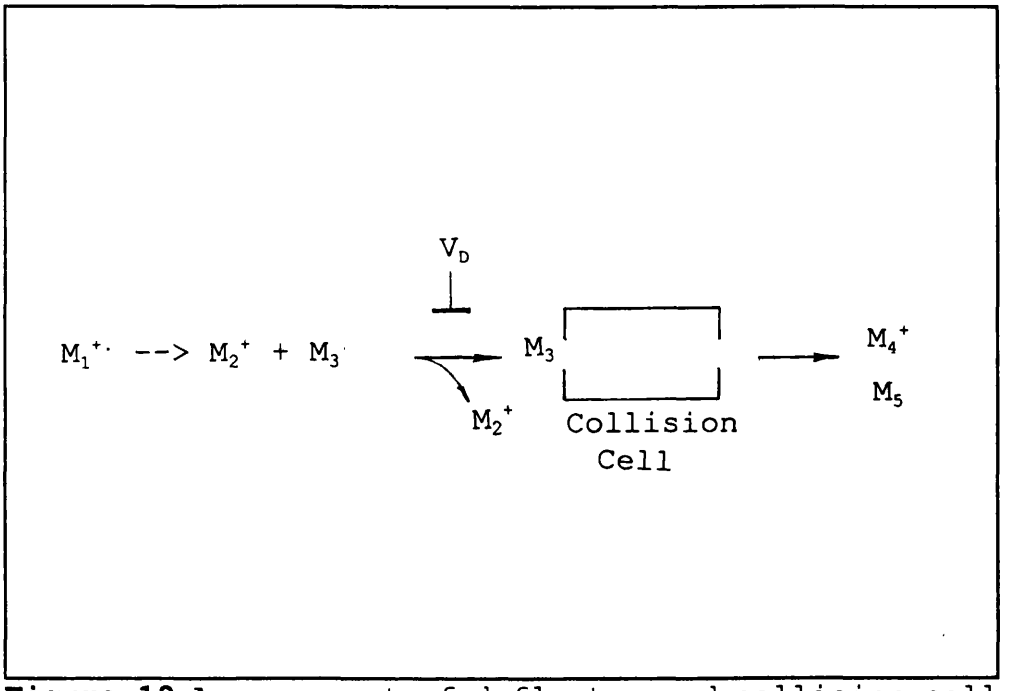

Figure 19 Arrangement of deflector and collision cell for CIDI

2.8.4 Neutralised Ion Beam Spectroscopy

A collisional technique that has been developed for the direct study of neutrals without their prior ionisation is that of neutralised ion beam spectroscopy (NIBS) [33,34]. The precursor ions $M^{+\cdot}$ are selected by the mass spectrometer and than neutralised, usually with a gas or vapour giving a low degree of fragmentation. Unreacted ions and ionic products are removed with the deflector and the neutrals are detected (Fig 20).

The detector itself can be translated in a direction normal to the beam to enable a neutral beam profile (of intensity versus angle) to be plotted. The shape of the neutral beam profile gives information on the stability of the neutralised ion. A neutral that is stable for the time it takes to travel from the neutralisation chamber to the detector gives a sharp profile with a width corresponding to that of the parent ion profile. However if the neutral is not stable for that length of time the neutral beam profile will show broadening due to fragments with velocity components normal to the beam. Apparent lifetimes of metastable species may also be calculated.

A variation on this technique is possible through the addition of a second chamber and deflector after the first, thus enabling the neutral beam to be reionised. This beam is deflected off axis with the second deflector

(to separate it from the neutral beam) and detected as before (Fig 21).

Since the deflection of the beam is inversely proportional to the kinetic energy, and kinetic energy is proportional to mass, a mass spectrum may be produced. The second chamber may be floated to a negative potential to increase mass resolution.

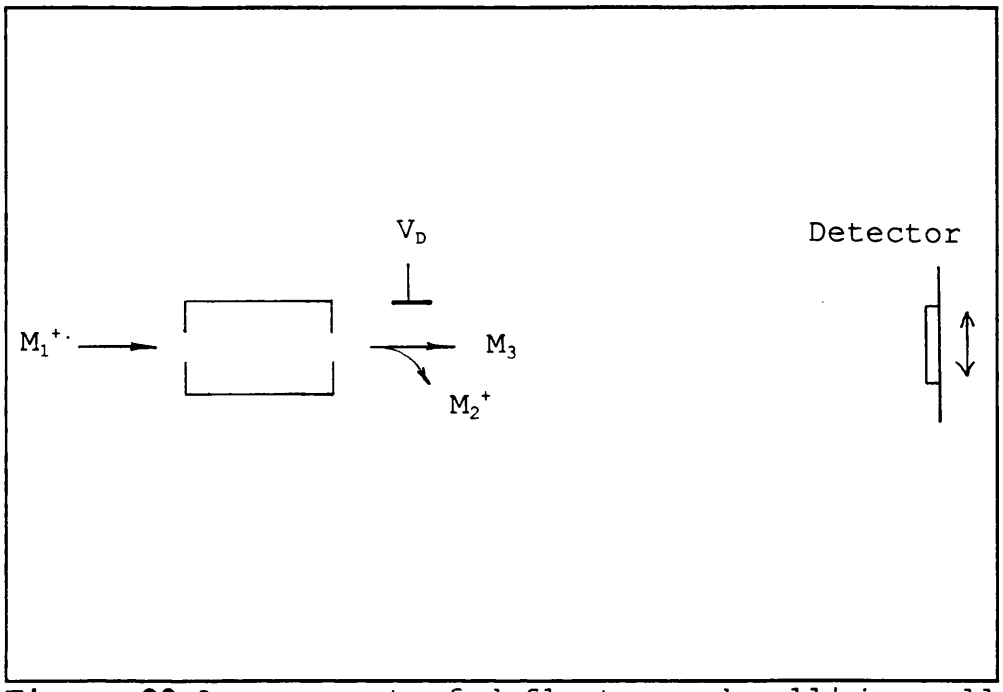

Figure 20 Arrangement of deflector and collision cell for NIBS

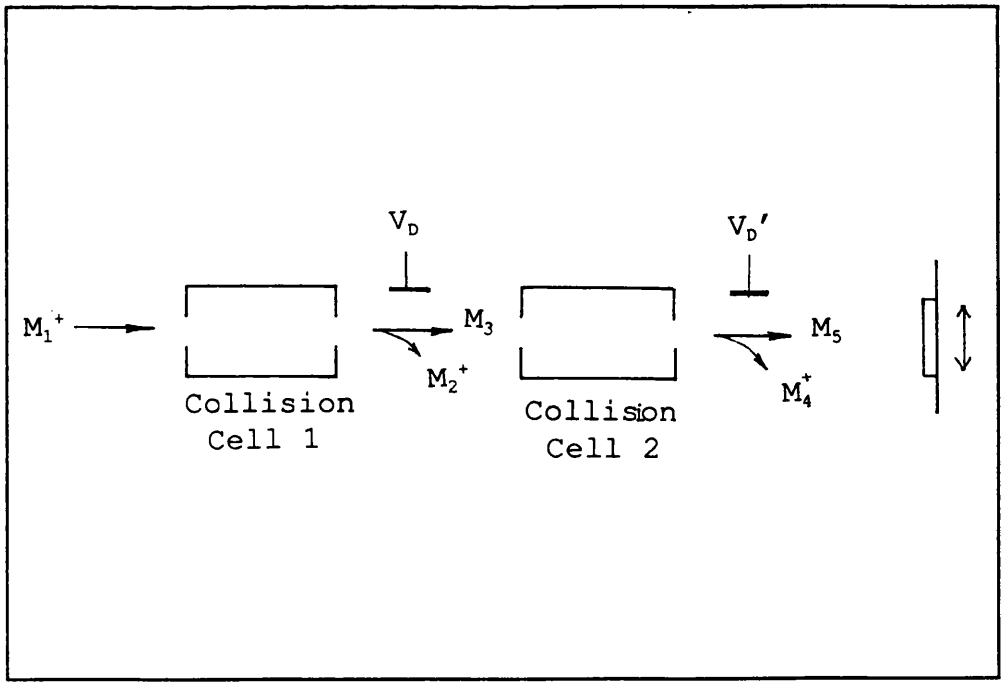

Figure 21 Alternative arrangement for NIBS

2.8.5 Charge Stripping

Charge stripping of a singly charged positive ion can occur by one of two routes, which one depends on the target used.

$$M^+ + G \rightarrow M^{++} + G^-$$

$$M^+ + G \rightarrow M^{++} + G + e$$

Charge stripping was first reported by Beynon [35]. Such peaks often appear in CID spectra and are easily distinguishable by their low intensity, narrow profile and position on the energy scale.

Charge stripping by gas collision is a relatively inefficient process so such peaks typically have an intensity of only a few percent. The narrowness of the peaks relates to the low kinetic energy release on their formation. The doubly ionised ion M^{++} will appear at approximately half the energy at which the singly ionised species appears ie at that corresponding to (0.5 V_{ACC}). However part of its translational energy will be lost in the ionisation step hence M^{++} will appear at an energy slightly below that corresponding to (0.5 V_{ACC}). Since this shift is proportional to the second ionisation energy, charge stripping was used to estimate this parameter. Initially this was done by measuring the difference between the energy corresponding to the peak

maximum of the M^{++} and $_{\wedge}(0.5\ V_{ACC})$ [36] and later the difference between the onsets of the M^{+} and M^{++} peaks [37]. Both methods assume that the peaks are the same shape, whereas in reality measurements from different instruments can differ by as much as 1-2eV [11].

Charge stripping reactions may be observed, in the case of a reverse geometry sector instrument, by doubling the ESA potential. Spectra produced this way (so called '2E spectra' [3]) have been successful in isomer differentiation where CID spectra have shown few or no differences [3].

2.8.6 Charge Inversion (Charge Reversal)

Charge inversion [11,38] was first introduced by Bowie et al [39]. This process can be brought about through collisional charge exchange of positively and negatively charged species, either in a single step

$$M^{+} + G \rightarrow M^{-} + G^{++}$$

$$M^{-} + G \rightarrow M^{+} + G^{--}$$

or by making the ion go through two identical collision processes ie

$$M^+ + G \rightarrow M + G^+$$

$$M + G \rightarrow M^- + G^+$$

$$M^- + G \rightarrow M + G^-$$

$$M + G \rightarrow M^+ + G^-$$

Because the collisional excitation of the singly charged ion is very fast (compared with a molecular vibration), the atoms have insufficient time to change their positions. Hence the charge inversion of **M**+ -> **M**- (or **M**- -> **M**+) in this case is 'vertical' (see Section 2.2.1) and, at least initially, the resultant species has the same structure as its precursor ion [11].

Investigation in to rearrangement following charge inversion [40] showed it to be less extensive than that following EI ionisation.

In a reverse geometry sector instrument, charge inversion reactions may be studied by reversing the polarity of the ESA potential ('-E spectra' for positive to negative inversions [3,41], a positive ESA potential for negative to positive inversions). This technique has also been used successfully in isomer differentiation [3].

REFERENCES : Chapter 2 Theory

1. J.H. Beynon, Mass Spectrometry and its Applications to Organic Chemistry, Elsevier, 1960
2. R.G. Cooks, J.H. Beynon, R.M. Caprioli and G.R. Lester, 'Metastable Ions', Elserier, 1973
3. K.Levsen, 'Progress in Mass Spectrometry Vol.4 : Fundamental Aspects of Organic Mass Spectrometry', McGraw-Hill, 1972
4. R.Davis and M.Frearson, 'Mass Spetrometry', Wiley, 1987
5. D.H. Williams and I. Howe, 'Principles of Organic Mass Spectrometry', McGraw-Hill, 1972
6. H.M. Rosenstock, M.B. Walenstein, A.L. Wahrhaftig and H. Eyring, Proc. Nat. Acad. Sci., 38, 667-, 1952
7. S. Glasstone, K.J. Laider and H. Eyring, 'Theory of Rate Processes', McGraw-Hill, 1941
8. J.L. Holmes and J.H. Terlouw, Org. Mass Spectrom., 15, 383-396, 1980
9. J.A. Hipple and E.U. Condon, Phys. Rev., 68, 54-, 1945
10. J.A. Hipple, R.E. Fox and E.U. Condon, Phys. Rev., 69, 347-, 1945
11. A.A. Mommers, PhD Thesis, University of Utrect, Netherlands, 1985
12. C. Ottinger, Phys. Lett., 17, 269-, 1965
13. M.A. Baldwin, P.J. Derrick and R.P. Morgan, Org.

Mass Spectrom., 11, 440-, 1976

14. J.L. Holmes, J.K. Terlouw, Org. Mass Spectrom., 15, 383-396, 1980

15. K. Levsen and H. Schwarz, Mass Spectrom. Rev., 2, 77-148, 1983

16. H.S.W. Massey, Rep. Prog. Phys., 12, 248-269, 1948

17. K.R. Jennings and R.S. Mason in 'Tandem Mass Spectrometry', Ed. F.W. McLafferty, Wiley, 1983

18. M.R. Weir, J.A. Richards Jr. and T.W. Adair III, 'Physics of The Atom' (4th ed.), Addison-Wesley, 1983

19. P.J. Todd and F.W. McLafferty in Ref 17.

20. C.E.C.A. Hop, PhD Thesis, University of Ottawa, Canada, 1988

21. F.W. McLafferty, P.J. Todd, D.C. Gilvery and M.A. Baldwin, J. Amer. Chem. Soc., 102, 3360, 1980.

22. J.K. Terlouw, W.M. Kieskamp, J.L. Holmes, A.A. Mommers and P.C. Bergers, Int. J. Mass Spectrom. Ion Proc., 64, 254-, 1985

23. P.O. Danis, R. Feng and F.W. McLafferty, Anal. Chem., 58, 348-354, 1986

24. P.O. Danis, R. Feng and F.W. McLafferty, Anal. Chem., 58, 355-358, 1986

25. M.S. Kim, J. Am. Chem. Soc., 100, 3279-, 1984

26. M. Rabrenovic, G.W. Troff, M.S. Kim and J.H. Beynon, Org. Mass Spectrom., 19, 203-, 1984

27. F.W. McLafferty, P.F. Bente III, R. Kornfeld, S. -C.

Tsai and I. Howe, J. Am Chem. Soc., 95, 2120-, 1973

28. B.L.M. van Baar, PhD Thesis, University of Utrect, Netherlands, 1988

29. M. Durup, G. Parlant, J. Appell, J. Durup and J. -B. Ozenne, Chem. Phys., 25, 245-261, 1977

30. J.K. Terlouw and H. Schwarz, Ange. Chem. Int. Ed. Eng., 26, 805-938, 1987

31. C. Wesdemiotis and F.W. McLafferty, Chem. Rev., 87, 485-500, 1987

32. J.L. Holmes and A.A. Mommers, Org. Mass Spectrom., 19, 460-461, 1984

33. A.B. Raskit, D.M. Hudgins, S. Buchau and R.F. Porter, Rapid Comm. Mass Spectrom., 1, 4, 57-59, 1987

34. R. Clair, J.L. Holmes, A.A. Mommers and P.C. Burgers, Org. Mass Spectrom., 20, 207-212, 1985

35. J.H. Beynon, J. Am. Chem. Soc., 94, 1004, 1974

36. R.G. Cooks, T. Ast and J.H. Beynon, Int. J. Mass Spectrom. Ion Phys., 11, 490, 1973

37. M. Rabrenovic, C.J. Proctor, T. Ast, C.G. Herbert, A.G. Brenton and J.H. Beynon, J. Phys. Chem., 87, 3305-, 1983

38. R.W. Kondrat in Ref 17

39. J.H. Bowie and T. Blumenthal, J. Am. Chem. Soc., 97, 2959-, 1975

40. J.H. Bowie, P.Y. White, J.C. Wilson, F.C.V. Larsson, S.O-. Lawesson, J.O. Madsen, C. Nobel and G.

Schroll, Org. Mass Spectrom., 12, 191-, 1977

41. T. Keough, J.H. Beynon and R.G. Cooks, J. Am. Chem. Soc., 95, 1695-, 1973

CHAPTER 3 : INSTRUMENTATION

3.1 IONISATION METHODS

Almost all mass spectrometrical methods require that the sample molecules be ionised before they can be separated and analysed. Though neutralised ion beam spectroscopy (see Section 2.8.4) analyses neutral species, the initial separation is performed on their ionic counterparts.

The positive molecular ion is usually produced in one of two ways: either by electron removal or proton donation. Likewise, the negative molecular ion is produced by electron capture or proton removal. Methods which ionise by electron removal tend to put a substantial amount of energy into the molecule at the same time, causing it to subsequently fragment; these are known as 'hard' ionisation methods. Methods which rely on proton donation are known as 'soft' ionisation methods as much less energy is given to the molecule as a consequence.

The original ionisation method used in mass spectrometry is that of electron impact (EI), and though it is still widely used, a range of new ionisation techniques, such as chemical ionisation and fast atom bombardment, has been developed, for use where EI is inappropriate.

3.1.1 Electron Impact

When an electron passes very near to an atom it can bring about its ionisation, either by the removal of an electron

$$M + e \rightarrow M^+ + 2e$$

or by electron capture

$$M + e \rightarrow M^-$$

Electron capture is approximately one hundred times less probable and usually results in the formation of an energetically unstable ion [1].

The EI source relies on the former method to produce a stream of high energy positive ions. To operate at maximum efficiency ie to generate the greatest number of ionised molecules, the bombarding electrons should have an energy of approximately 60eV, judging by a typical ionisation efficiency curve (see Section 2.2.2). By convention and for reasons of stability and experimental reproducibility, EI spectra are usually produced at 70eV in the plateau region of the curve, without considerable loss of efficiency.

The source itself (Fig 22) comprises an almost sealed ionisation chamber, a tungsten filament, two

electrodes: the repeller plate and the trap, and two permanent magnets. Electrons are generated by heating the filament and are then accelerated through a potential difference V_A between the filament and the ionisation chamber. Here, they travel at constant velocity and energy $z_A V_A$, to be collected at the trap, which is held at a higher voltage than the chamber itself. The permanent magnets help focus and colimate the electron beam, though they may be omitted. Sample vapour bleeds into the ionisation chamber and undergoes collision with the electrons. The ions formed are steered towards a slit by the repeller plate and by field penetration from V_A and they leave the source chamber [2].

The electron energy may be varied (by adjusting V_A) from 5 to 100eV. The trap current or the total emission current is used in a feedback mechanism to control the filament current in such a way as to maintain a constant electron flux and thus a constant rate of ion production [3].

The ionisation energy of most compounds is in the range 8 to 12eV, so collision with 70eV electrons can result in the formation of highly excited ions with sufficient energy to rearrange and/or fragment. For this reason, EI is known as a 'hard' ionisation technique and will often result in a spectrum with a great many fragment peaks. In certain circumstances, no molecular ion will be seen; for unstable compounds the temperature

of the source alone may be sufficient to cause thermal decomposition, or else the molecule or ion may be inherently unstable, even at the ionisation threshold. In instances where the mass of the molecular ion needs to be known or structural detail is important, this may not be the ionisation technique of choice. EI is also inappropriate for involatile samples. For these reasons, a 'soft' ionisation technique such as chemical ionisation, field ionisation, field desorption or fast atom bombardment may be more useful. Both field desorption and fast atom bombardment ionise from the condensed phase and thus can be most appropriate for involatile samples.

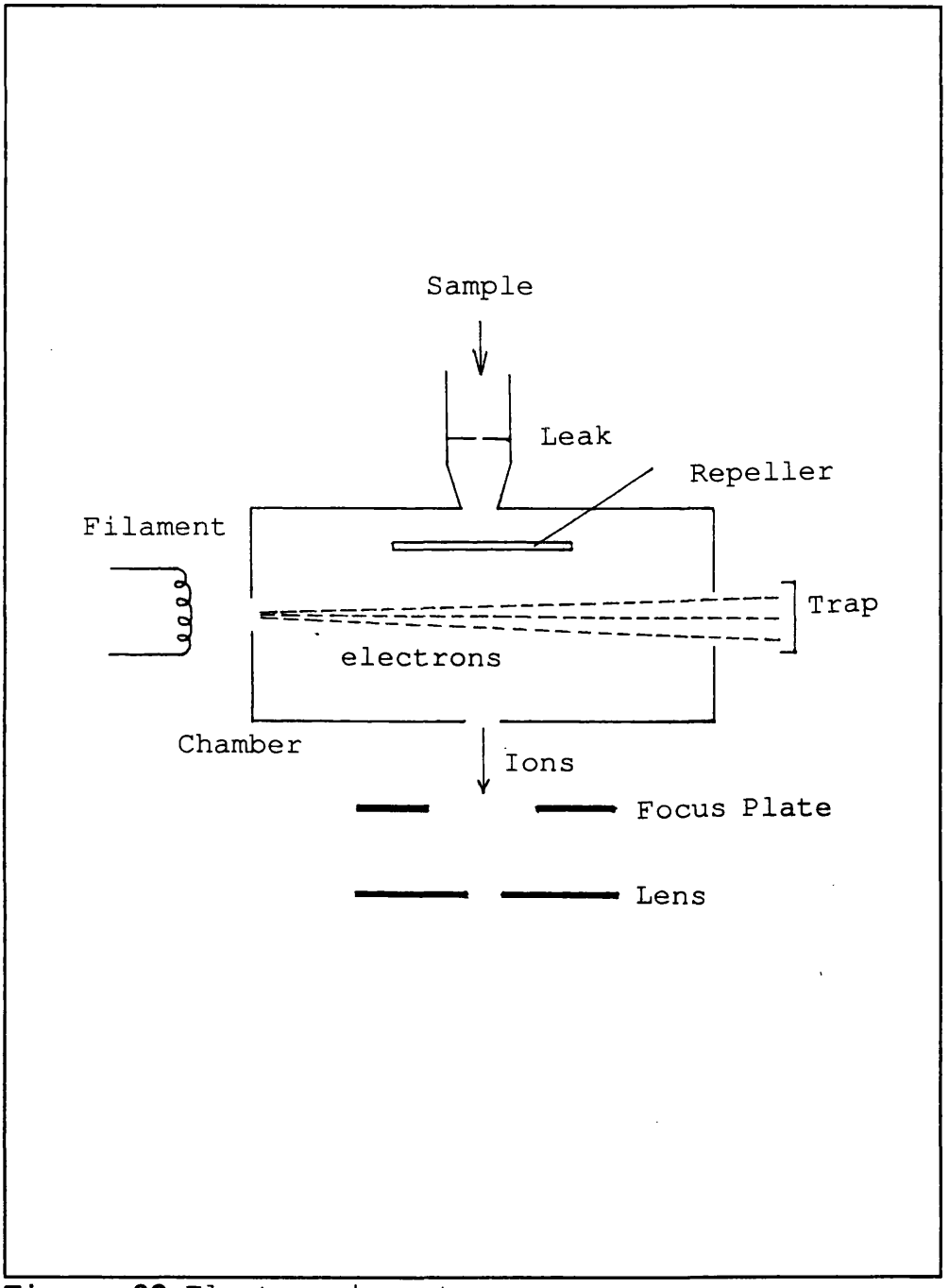

Figure 22 Electron impact source

3.1.2 Fast Atom Bombardment

Molecules with highly polar or ionic groups are not amenable to EI or CI. Also, high mass molecules generally do not survive these ionisation techniques intact. With these problems in mind new ionisation techniques were sought. Fast atom bombardment (FAB) was developed by Barber et al from solid sputtering techniques such as secondary ion mass spectrometry (SIMS).

The primary fast atom beam usually comprises rare gas atoms such as xenon or argon. To produce this beam the gas atoms, **G**, are first ionised and then accelerated to high kinetic energy.

$$G \longrightarrow G^{+\cdot} + e$$

$$G^{+\cdot} \xrightarrow{\text{(energy)}} G^{+\cdot}_{fast}$$

These fast ions then undergo collisions with slow atoms, resonant charge exchange takes place and fast neutrals result.

$$G^{+\cdot}_{fast} + G \longrightarrow G_{fast} + G^{+\cdot}$$

The neutralised species retain much of their original energy. The ions are then removed from the beam by a deflector plate leaving a neutral beam (1,4,5). Studies

have shown however that there is little difference between using an ion or an atom gun (6), although ion beams are more easily controlled and focussed. Also high energy ions (~30keV) give higher sensitivity for high mass compounds.

This atom beam bombards the sample (deposited on a flat metal stage known as a 'probe tip') causing ions, both positive and negative, and neutrals to be sputtered (Fig 23). With the appropriate potential difference between the probe tip and extraction plate, the ions of required polarity are removed and subsequently focused by the lens system.

The optimum angle of incidence Θ, of the primary beam to give maximum yield of secondary particles (Fig 23), is to some extent instrument dependent, though generally ~60° from the perpendicular. The yield is also dependent on the distance between the primary atom source (atom gun) and the probe tip. This probe tip must be made of a material that does not react with the sample or the matrix; stainless steel is a common choice; though gold has been used, its surface has to be covered completely to avoid sputtering of the metal [8,9].

FAB spectra are characterised by intense pseudo molecular ions, usually either $[M+H]^+$ or $[M-H]^-$, and very little coherent fragmentation. Of those fragments that are seen most are even-electron species, and in this way FAB spectra resemble EI and CI spectra.

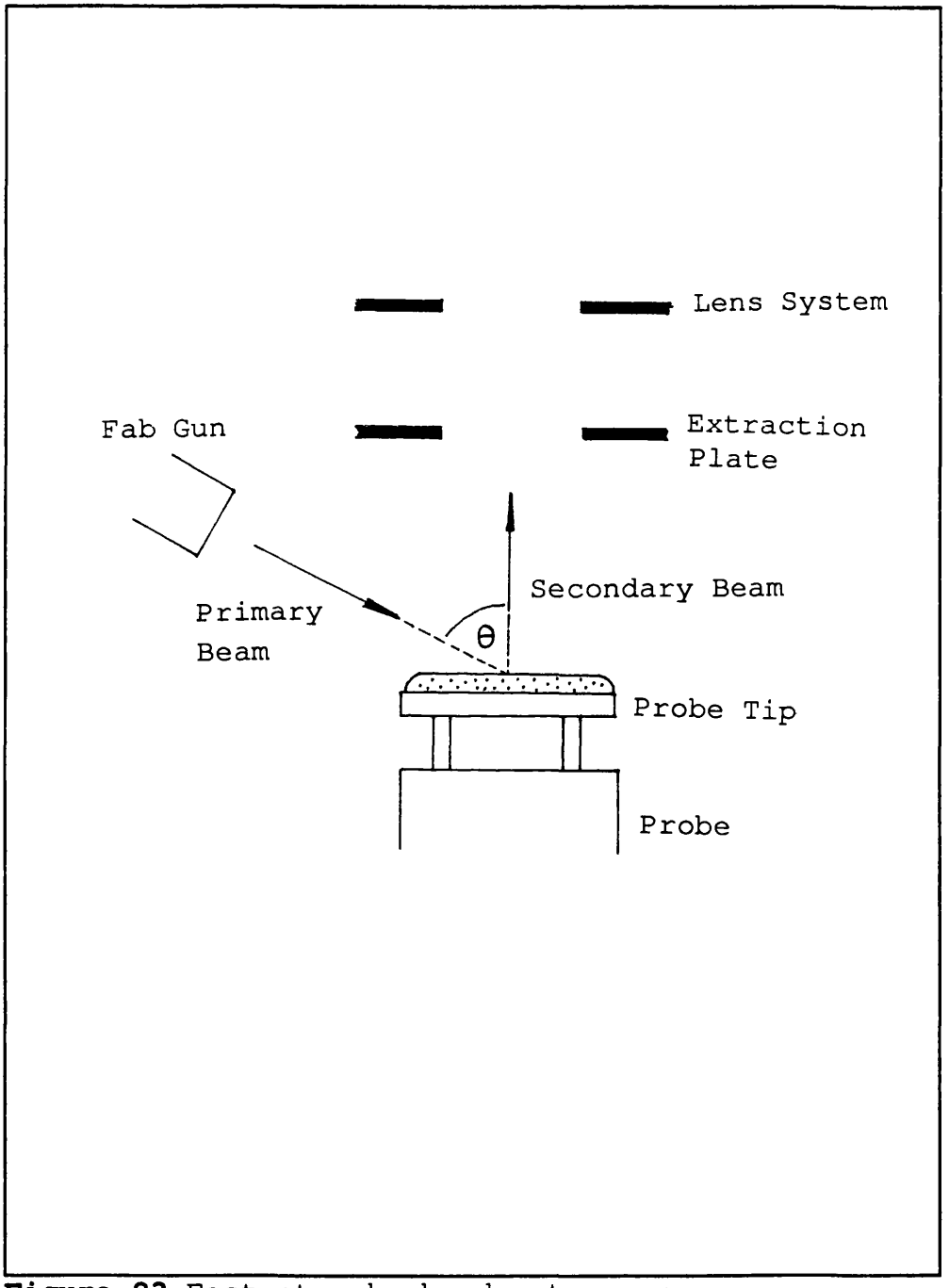

Figure 23 Fast atom bombardment source

Cationated species may also be produced through the addition of ammonium or alkali metal salts, yielding $[M+NH_4]^+$ or $[M+X]^+$ (X= alkali metal). These ions are often more stable than their protonated counterparts. Where the sample molecule is not basic enough to protonate, this may be one way of producing a pseudo molecular ions. Such species may be formed without doping when appropriate impurities are present, and may be helpful in confirming molecular weight information.

In early sputtering experiments the sample was dissolved in a volatile solvent, applied to the probe tip and evaporated to dryness. This resulted in a transient spectrum, lasting only seconds in the worst cases. Low vapour pressure liquids however were found to give long lasting spectra, and adding such a liquid to the sample solution on the probe tip was found to perpetuate the sample spectrum.

Such a liquid used in this way is known as a 'matrix'. The first matrix to be tried successfully was glycerol, and although this is still popular other alternatives are available such as monothioglycerol, polyethyleneglycol (PEG) and m-nitrobenzylalcohol.

The actual mechanism for ionisation in FAB mass spectrometry is still a matter of debate. It is known that sputtering itself is not an efficient way of creating ions, and alternative theories for ionisation fall into two main categories: gas phase, where the ions

observed in the mass spectrum are the result of gas phase reactions between the sputtered ions and neutrals; and liquid phase, where the ions observed are preformed within the matrix solution. Gas phase ionisation has been demonstrated through experiments where the sample is introduced directly as a vapour into the primary atom beam [10,11] and mixed dimer formation when two different analytes are introduced on a split probe tip. Such theories are also supported by evidence of the importance of gas-phase basicities when analysing mixtures [12]. Support for theories of liquid phase ionisation comes from the importance of factors such pH, surface activity, and the role played by the matrix [13]. It is quite likely that there is not one clear mechanism but a combination that may be sample dependent [10].

Studies suggest that the relative contributions to the spectrum of the sample and the matrix depend on their relative surface activity. In the analysis of mixtures, those that have a higher surface activity are found to make a larger contribution to the FAB spectrum, and this suggests that to some extent ions are being sputtered preferentially from the sample surface. It follows therefore that the sample should have a higher surface activity than the matrix, a characteristic feature of molecules with hydrophobic groups. This will ensure a high concentration of sample at the surface of the matrix. Even so there should also be sample dissolved in

the matrix to replenish the surface when the upper molecules are sputtered away. Also there is evidence that not only the surface layer is sputtered but there is some contribution from the bulk [14].

The matrix should be selected according to the nature of the sample. That it is of low volatility is important: the matrix must not be exhausted before adequate data has been collected eg thioglycerol alone is somewhat volatile and shortlived but when mixed with glycerol it retains many of its advantages as a matrix but is much less prone to evaporate. The matrix provides a medium in which sample ion can be formed. It also solvates and separates these ions so lowering the energy needed to desorb them [15]. It has been found that stronger and more persistent spectra result when the sample or sample solution actually dissolves in the matrix rather than just forming a suspension [15]. Whether the matrix should be added to the probe before or after the sample is a matter of conjecture [16,17].

The main disadvantage of having to analyse a sample with a matrix present is that matrix ions are also sputtered and appear in the spectrum. These tend to be low mass ions (glycerol peaks appear at masses [n.92+1] in positive ion spectra and [n.92-1] in negative ion spectra, the intensity diminishing at higher masses) and are more of a problem with low mass samples. However, cluster ions may form beyond the mass of the pseudo

molecular ion, comprising the matrix, the matrix and the sample, or the matrix and alkali metal salt contaminants. These may well serve to confuse the spectrum if they are of a significant intensity.

A sample that runs well by the FAB technique will often give a strong spectrum, with unwanted matrix peaks of insignificant intensity that may be 'subtracted' from the spectrum by the data system. The contribution of the matrix may be decreased further by increasing the concentration of the sample, increasing its surface activity or by use of tandem mass spectrometric techniques to effectively screen out unwanted signals (see Section 1.1).

Addition of an acid (eg oxalic, hydrochloric or acetic acid) to a cationic sample can greatly enhance the ion current through ionisation prior to bombardment. A similar effect can be seen with the addition of a suitable base (eg sodium hydroxide, ammonium hydroxide or calcium hydride) to an anionic sample [18].

3.1.3 Chemical Ionisation

Chemical ionisation is a two stage process: firstly a reagent gas (or gas mixture) is ionised by the EI process, then the sample is ionised through collisions with the reagent gas ions.

The reagent gas R, is admitted to the ion source at a pressure of approximately 0.2 to 1 torr. This is usually a conventional EI source which has been made reasonably gas tight by closing off unused entry ports and inserting a narrower source slit.The reagent molecules are bombarded with high energy electrons from the filament and are ionised

$$\mathbf{R} + \mathbf{e}^- \rightarrow \mathbf{R}^{+\cdot} + 2\mathbf{e}^-$$

These ions then go on to collide with neutral reagent molecules

$$\mathbf{R}^{+\cdot} + \mathbf{R} \rightarrow \mathbf{R}{+}\mathrm{H}^+ + \mathbf{R}{-}\mathrm{H}\cdot$$

The sample is admitted to the source at a much lower pressure than the reagent gas (typically 10^{-4} torr) and in this way sample molecules are much less likely to be ionised directly through EI. The ionisation of the sample takes place by proton transfer

$$[\mathbf{R}{+}\mathrm{H}]^+ + \mathbf{M} \rightarrow \mathbf{R} + [\mathbf{M}{+}\mathrm{H}]^+$$

where the species produced, $[\mathbf{M}{+}\mathrm{H}]^+$, is known as a quasi-molecular ion. The outcome of this reaction depends upon the relative proton affinities of the reagent and sample molecules. If the proton affinity of the sample is

greater, then the reaction will proceed as shown above; if however the reagent has a higher proton affinity a $[\mathbf{M}-H]^+$ ion may be formed thus

$$[\mathbf{R}+H]^+ + \mathbf{M} \rightarrow [\mathbf{M}-H]^+ + \mathbf{R} + H_2$$

Although the protonated molecular ion is usually formed, the CI process can give rise to adduct ions. For instance, in the case where methane is used as the reagent

$$CH_4^{+\cdot} \rightarrow CH_3^+ + H^\cdot$$

$$CH_3^+ + CH_4 \rightarrow C_2H_5^+ + H_2$$

$$C_2H_5^+ + \mathbf{M} \rightarrow (\mathbf{M}+C_2H_5)^+$$

The presence of adduct ions need not make the spectrum difficult to interpret, since they are a function of the reagent gas used and so may be predicted.

The ionisation process outlined thus far whereby the reagent ionises the sample through proton donation, is known as Bronsted CI, since the reagent acts as a Bronsted acid. The most common Bronsted reagents are methane

$$CH_4 + e^- \rightarrow CH_4^{+\cdot} + 2e^-$$

$$CH_4^{+\cdot} + CH_4 \rightarrow CH_5^+ + CH_3^\cdot$$

ammonia

$$NH_3 + e^- \rightarrow NH_3^{+\cdot} + 2e^-$$

$$NH_3^{+\cdot} + NH_3 \rightarrow NH_4^+ + NH_2^\cdot$$

and isobutane

$$(CH_3)_3CH + e^- \rightarrow CH_3CH^+CH_3 + CH_3^\cdot + 2e^-$$

$$CH_3CH^+CH_3 + (CH_3)_3CH \rightarrow CH_3CH_2CH_3 + (CH_3)_3C^+$$

although almost any volatile organic molecule may be used.

Alternatively, charge exchange CI can be achieved using a one electron oxidising agent such as $Ar^{+\cdot}$ or $N_2^{+\cdot}$. The reagent molecules are collided with high energy electrons to give a mixture of ions $\mathbf{R}^{+\cdot}$ and metastable neutrals $\mathbf{R}^*$ which ionise the sample molecules

$$\mathbf{R}^{+\cdot} + \mathbf{M} \rightarrow \mathbf{R} + \mathbf{M}^{+\cdot}$$

$$\mathbf{R}^* + \mathbf{M} \rightarrow \mathbf{R} + \mathbf{M}^{+\cdot} + \mathbf{e}^-$$

resulting in a spectrum very similar in appearance to an EI spectrum.

The main advantage of CI over EI is the control that can be exercised over the extent of fragmentation of the sample molecules. This is achieved by selecting a reagent with the appropriate proton affinity (in the case of

Bronsted CI) or ionization energy (in the case of charge exchange CI). Further more, $[M+H]^+$ is an even-electron ion and as such may have different fragmentation pathways available to it than the corresponding odd-electron ion.

Negative ion CI is also possible through electron capture using a Bronsted reagent [1,18,19]. A reagent gas such as methane is often used for negative CI. By operating at lower pressure in the ion chamber (~0.1 torr) the methane thermolyses the electrons and increases the probability of electron capture.

3.1.4 Field Ionisation

Field ionisation [1,20] is a completely different technique to EI and CI. Within the source there is an anode and cathode, held at a potential difference of up to 10kV and sufficiently close to give a potential gradient of at least $10^8 Vcm^{-1}$ close to the surface of the anode (Fig 24). The sample is vaporised within the source and when a molecule enters the intense electric field an electron is removed. The ions so formed are attracted towards the cathode, enter a focusing region where they may be retarded (ions formed by FI will have energies of approximately 10kV which may be incompatible with the mass spectrometer) and focused at the source slit.

The anode is sometimes referred to as the 'emitter'

and may be a sharp wire, edge or tip. The efficiency of the emitter may be increased by a process known as 'whiskering', whereby carbon filaments or microneedles are grown on to the surface. This has the effect of increasing the surface area of the emitter and also providing areas of high charge density (charge concentrating at sharp edges and points).

Ions formed through FI have much less energy than those formed by EI but there is usually some fragmentation which may be structurally informative. Usually the molecular ion is formed, though the quasi-molecular ion $[M+H]^{+\cdot}$ may be formed instead or in addition. This uncertainty is a disadvantage of FI for giving molecular weight information.

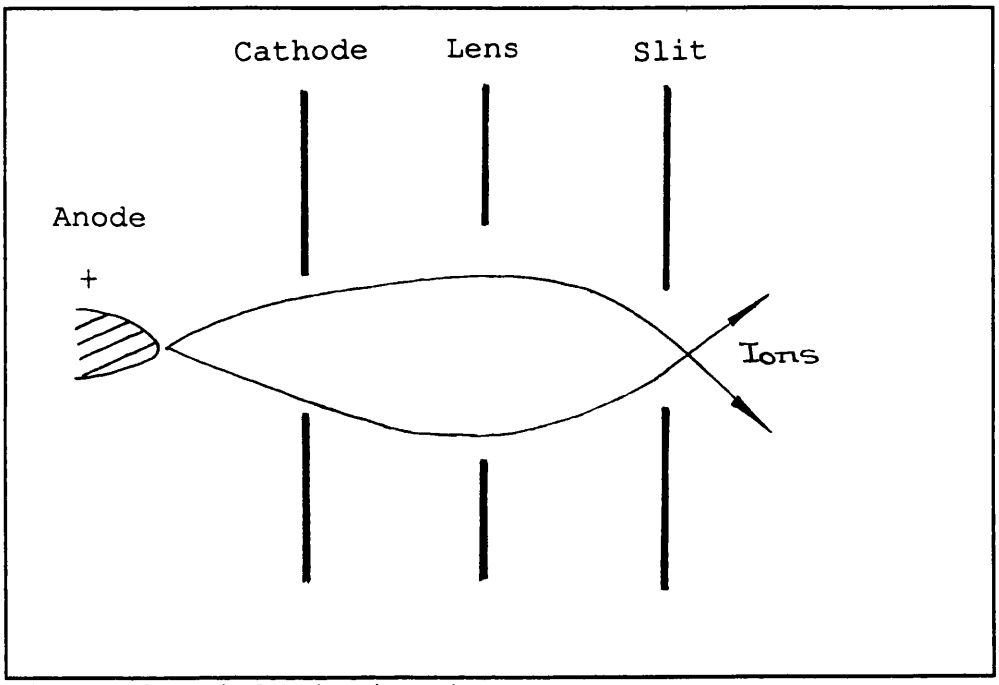

Figure 24 Field ionisation source

3.1.5 Field Desorption

Field Desorption (FD) [20] is carried out in much the same way as field ionisation except that the sample is applied directly to the emitter as a solution, and hence FD is particularly useful for involatile samples. The emitter is heated, sample ions are desorbed and travel towards the cathode. The emitter is prepared by heating in a reduced pressure atmosphere of benzonitrile whilst applying a high potential to the emitter. Needles are grown giving a large surface area and local areas of high charge density.

Field desorption is the softest of all the ionisation techniques producing molecular ions or quasi-molecular ions with virtually no fragmentation. A disadvantage of this technique is that the ion current may be very short lived, giving little time for instrument tuning, hence the sample may be run under less than optimum conditions. Furthurmore the emitters are time consuming to prepare in a reproducible fashion. Nevertheless, FD has enjoyed a resurgence of interest in recent years and has been used to advantage in the analysis of industrial polymers.

3.2 ANALYSERS

An analyser in a mass spectrometer is any device which brings about separation of ions on the basis of mass, mass to charge ratio, energy, velocity or momentum. The first mass spectrometers employed permanent magnets, later to be replaced by electromagnets whose magnetic field strength could be controlled. Electrostatic analysers were introduced to improve focusing, and later the quadrupole mass analyser was developed. 'Sector' instruments comprise any combination of magnetic and electrostatic sectors, whereas 'hybrid' instruments combine sectors and quadrupoles.

3.2.1 Magnetic Sectors

Ions of mass m, electronic charge z_A ($z_A = ze$ where z is the number of charges), accelerated through voltage V_{ACC} have kinetic energy given by

$$V_{ACC} z_A = mv^2/2$$

All masses have the same energy $V_{ACC} z_A$ and their momenta is given by

$$mv = (2V_{ACC} z_A m)^{1/2}$$

On entering the magnetic field **B** the ions travel in circular path radius **r** and experience a force (mv^2/r) where

$$mv^2/r = Bz_Av$$

Substitution gives

$$m/z_A = r^2B^2/(2V_{ACC})$$

By varying the magnetic field **B** and keeping the accelerating voltage V_{ACC} constant, ions of different mass to charge ratio **(m/z)** are brought to focus at the collector slit or detector after the magnet (Fig 25). Alternatively, **B** may be kept constant and V_{ACC} scanned [2,3,21].

The radius **r** may also be regarded as a variable if the ions are detected with a photoplate or a diode array detector.

3.2.2 Electrostatic Analysers

The electrostatic analyser (ESA) comprises two curved plates (arcs of a circle) the outer plate positive with respect to the inner plate for positive ion mass spectrometry (Fig 26). Ions of mass **m**, velocity **v**,

accelerated through a voltage V_{ACC}, will have kinetic energy given by

$$z_A V_{ACC} = mv^2/2$$

On entering the electric field **E**, ions of energy ($z_A V_{ACC}$) will follow a circular path of radius **R** where

$$mv^2/R = z_A E$$

$$mv^2 = 2z_A V_{ACC}$$

where $R = 2V_{ACC}/E$. These ions can then be selected by means of a focusing slit.

The ESA discriminates on the basis of energy not mass or charge, and it can be used as a means of focusing a divergent, mono-energetic ion beam [2,3,21]. The combination of an ESA and a magnetic sector can compensate for divergences in both angle and energy, to give a so called 'double focussing' mass spectrometer.

3.2.3 Quadrupole Mass Analysers

The quadrupole [20] is a true mass analyser, unlike the magnetic and electrostatic sectors which discriminate on the basis of momentum and energy respectively. It

comprises a set of four metal rods (optimally of hyperbolic cross section) in a square array. The two diagonally opposite pairs of rods are connected electrically to ac and dc supplies. For one pair the dc component is positive (+**U**), for the other it is negative (-**U**), and the ac voltages (**Vcoswt**) are out of phase by π (Fig 27).

Low energy ions (~20 eV) enter the rod assembly and travel a helical path under the influence of the electrical field. Depending on the values of **U** and **V** only one mass will follow a stable path and emerge from the analyser.

The mass resolution is variable depending upon the ratio of ac and dc voltages. The peak width is constant throughout the mass range and the quadrupole is described as having 'unit resolution' when adjacent masses are just resolved.

When no dc voltage is applied there is no mass resolution and ions are transmitted with high efficiency through the quadrupole. This the basis of the ac only quadrupole, which may be used as a reaction cell in combination with other analysers.

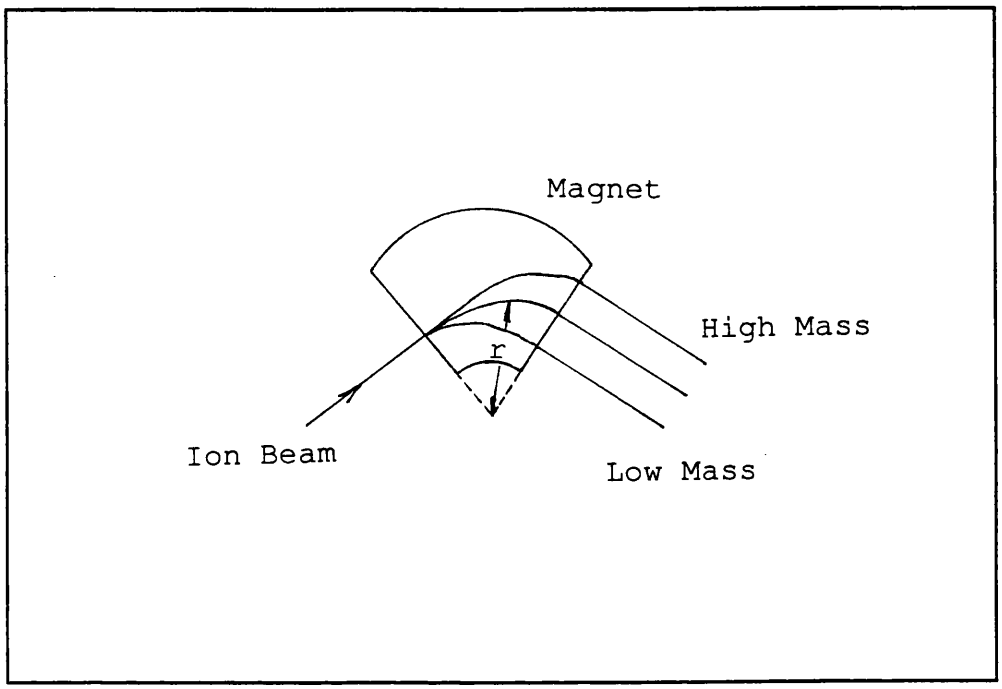

Figure 25 Magnetic sector

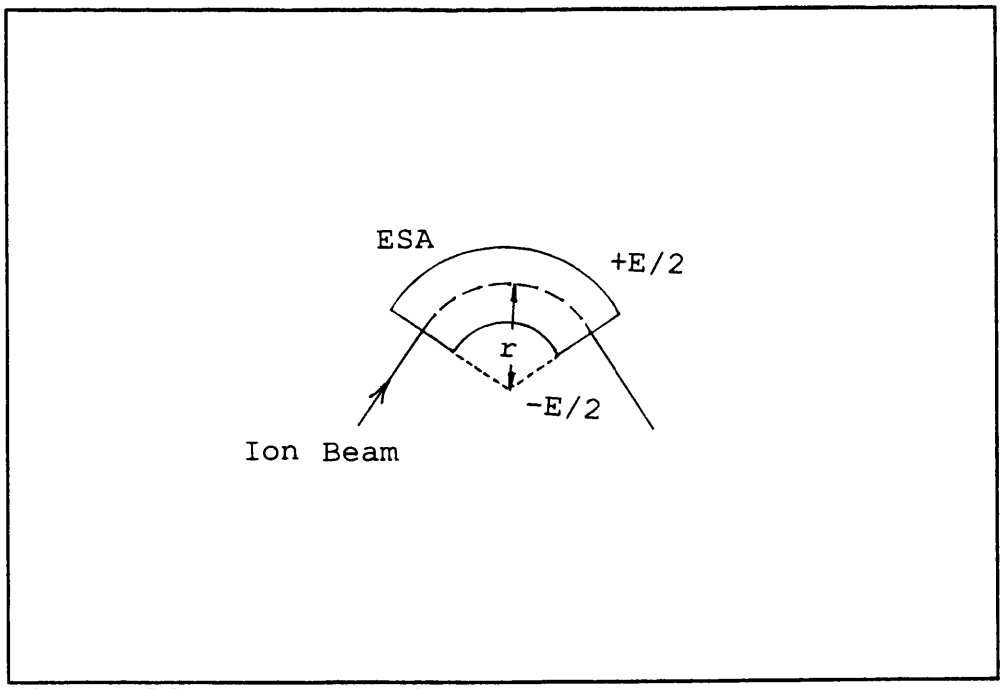

Figure 26 Electrostatic sector

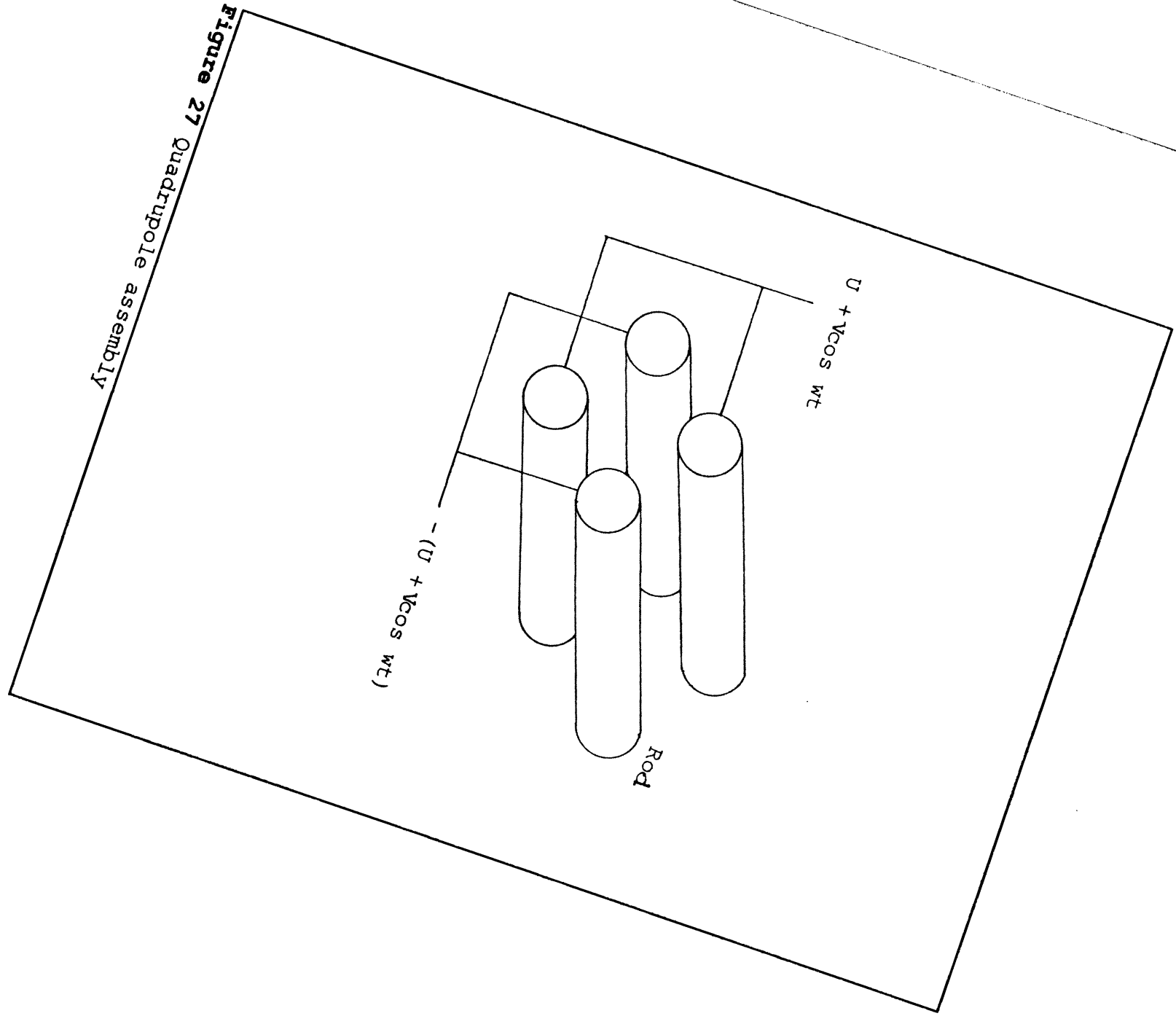

Figure 27 Quadrupole assembly

3.3 DETECTORS

There are several types of detector that can be used in the mass spectrometer.

3.3.1 Focal Plane Detection

The earliest type of detector was the photographic plate which gave a series of lines corresponding to the points at which the ions impinged and exposed the plate. The relative positions of the lines gave the m/z values and the extent of exposure gave some measure of the relative intensities. This type of detector is only useful when the ions of different m/z values are focused at different positions on the z plane, for instance in an instrument with Mattauch-Hertzog geometry.

A modern development is the use of diode arrays for focal plane detection which allows the simutaneous detection of up to 50% of the mass range, greatly enhancing sensitivity.

3.3.2 Faraday cup (Faraday cage)

A Faraday cup comprises an open metal box connected to earth via a resistor. When an ion hits the Faraday

cup, the charge is neutralised, current flows through the resistor and is amplified and detected. This type of detector is relatively insensitive and so more useful for measuring high ion currents (Fig 28). It may also be fitted with a suppressor electrode and permanent magnets to reduce the effects of secondary electrons formed when ions strike the detector surface [22]. It may be useful for calibration purposes as it allows absolute ion current measurement.

3.3.3 Electron Multiplier

Probably the most popular detector used today is the electron multiplier. It works on the principal of secondary electron emission and consists of a series of electrodes known as 'dynodes' which are good secondary emitters. The ion beam hits the first dynode releasing a shower of electrons, which impact on the second dynode and so on to produce a greatly amplified signal at the final dynode, the collector (Fig 29) [22].

Alternatively the multiplier may have a continuous dynode as in the 'channeltron'.

3.3.4 Photomultiplier

The photomultiplier works on much the same principle as the electron multiplier except in the initial stages. The ion beam triggers a scintillation crystal (scintillator) to release photons, causing electron release from a photocathode to initiate the electron cascade as before (Fig 30) [22].

3.3.5 Scintillation detector

This detector comprises a phosphor screen and a scintillation counter. When the ions hit the screen photons are released and detected [22].

The Daly detector based on this principle was designed to optimise the study of metastable ion fragmentations.

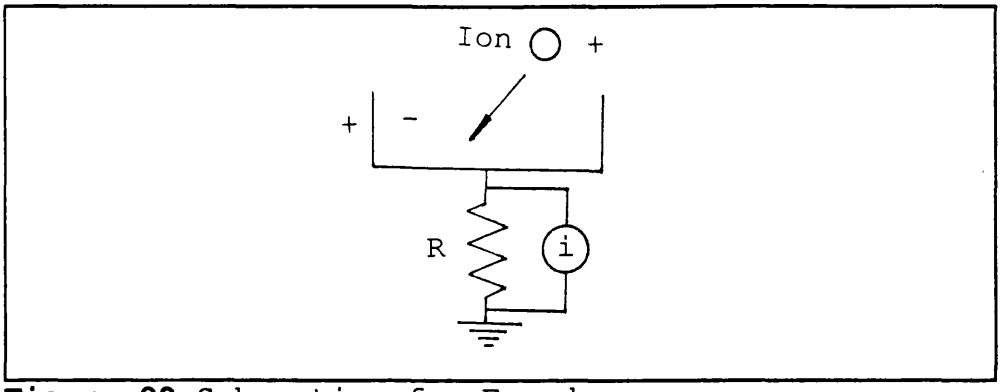

Figure 28 Schematic of a Faraday cup

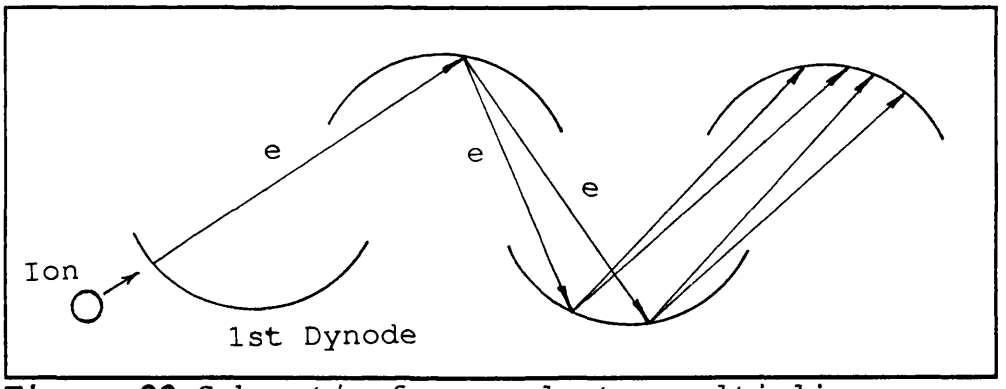

Figure 29 Schematic for an electronmultiplier

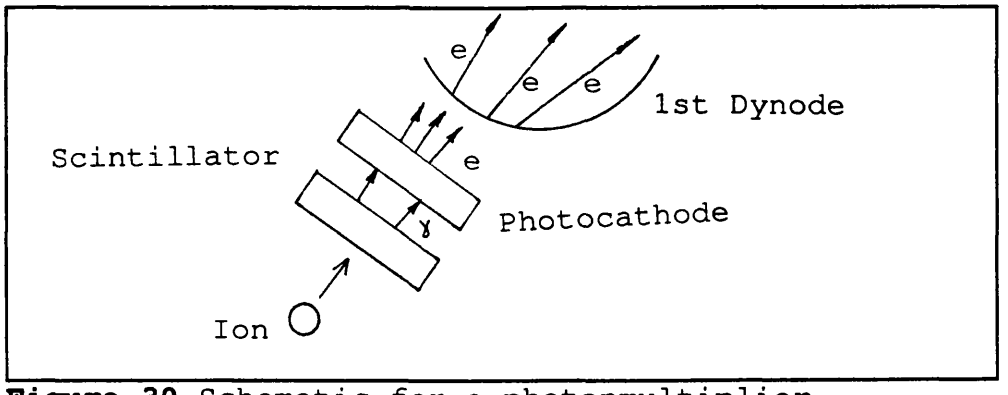

Figure 30 Schematic for a photonmultiplier

3.4 INSTRUMENTAL GEOMETRY

It is possible to perform tandem mass spectrometrical experiments on a variety of instruments, from the basic two sector double-focusing mass spectrometer, through the triple sector and hybrid instruments to the four sector mass spectrometer (Table 2) [23,24]. There are few restrictions on the suitability of an instrument geometry for this type of analysis: a minimum of two analysers will be required, MSI and MSII, and a collision region (a collision cell or rf only quadrupole) in the appropriate FFR if collision experiments are to be performed. Metastable dissociations may still be followed in FFRs where there is no collision region present. With certain types of scan it may be more appropriate for the mass spectrometer to be scanned under computer control.

True tandem experiments can be said to involve MSI and MSII being decoupled and operated as separate 'mass spectrometers'. There are also 'linked scan' experiments which involve MSI and MSII being scanned in concert (see Section 3.5.1). For certain instrument configurations, eg EB, where the ESA alone is used as MSI, parent and daughter ion scans can only be performed using a linked scan. This is because the ESA is an energy analyser, and all ions emerge from the acceleration region with same energy regardless of their mass. Constant neutral loss

scans are always performed by linking the scans of MSI and MSII.

The main disadvantage of have only single sectors as MSI and MSII is their limited resolution. An ESA with high energy resolution when used as MSII can offer only poor mass resolution. A magnetic sector will generally provide higher mass resolution than a quadrupole as MSI, but poorer resolution as MSII. This is because the quadrupole is a mass analyser and its resolution will be unaffected by the kinetic energy released in dissociations between MSI and MSII. Quadrupoles offer unit resolution over their entire mass range. Linked scans offer better resolution than alternative equivalent scans on the same instrument.

Instruments with more than two analysers (eg EBE, BEQ) offer the possibility of multiple stage analysis (eg granddaughter ion scans) or increased resolution in MSI or MSII. Having two sectors operate as MSI means that isobaric ions may be separated from mixtures introduced into or formed within the source. Two sectors operating as MSII enables isobaric daughter ions to be distinguished. In the triple quadrupole mass spectrometer, the second quadrupole is used as a collision region and to focus the ion beam.

A four sector instrument offers both high resolution of both parent and daughter ions.

Geometry	MSI	MSII	Dissociation Region		
			Parent Ion Scan	Daughter Ion Scan	CNL Scan
BE	B	E	1FFR 2FFR	1FFR 2FFR	1FFR 2FFR
EB	E	B	1FFR 2FFR	1FFR	1FFR
BQ	B	Q	2FFR	2FFR	2FFR
QB	Q	B	2FFR	2FFR	2FFR
Q_1Q_2	Q_1	Q_2	2FFR	2FFR	2FFR
$Q_1Q_2Q_3$	Q_1	Q_3	Q_2	Q_2	Q_2
E_1BE_2	E_1B	E_2	1FFR 2FFR	1FFR 2FFR	1FFR 2FFR
B_1EB_2	B_1E	B_2	1FFR 2FFR	1FFR 2FFR	1FFR 2FFR
BEQ	BE	Q	2FFR	2FFR	2FFR
B_1EB_2	B_1	EB_2	1FFR 2FFR	1FFR 2FFR	1FFR 2FFR
E_1BE_2	E_1	BE_2	1FFR 2FFR	1FFR	1FFR
$E_1B_1E_2B_2$	E_1B_1	E_2B_2	1FFR 2FFR	1FFR 2FFR	1FFR 2FFR
$B_1E_1B_2E_2$	B_1E_2	B_2E_2	1FFR 2FFR	1FFR 2FFR	1FFR 2FFR
$B_1E_1E_2B_2$	B_1E_1	E_1B_1	1FFR 2FFR	1FFR 2FFR	1FFR 2FFR
$E_1B_1B_2E_2$	E_1B_1	B_2E_2	1FFR 2FFR	1FFR 2FFR	1FFR 2FFR

Table 2 : Possible geometries for tandem mass spectrometry (and the FFR where dissociation can be observed)

3.5 SCANNING REGIMES

A number of different scanning regimes are available with a double focusing instrument. These enable specific reactions in any of the field free regions of a multi-sectored or hybrid instrument to be monitored. To follow reactions in the 1FFR and 2FFR of a reverse geometry two sector instrument, the most useful scanning modes are linked scanning and the MIKES scan.

3.5.1 Linked Scanning

To follow dissociations in the 1FFR of a double focusing instrument, either of forward or reverse geometry, so called 'linked scans' may be used. Here the magnetic field **B** and the electrostatic field **E** are scanned at some constant ratio of their values, either to examine daughter ions from a specified parent, precursor ions of a specified daughter ion, or dissociations where a specific neutral molecule has been lost.

It is also possible to use these scans to follow reactions in a 1FFR collision cell.

3.5.1.1 Daughter Ion Scan (B/E)

This type of scan is used to study daughter ions lost from a chosen precursor ion M_1^+.

Assuming that the velocity of both the precursor ion and daughter ion, M_2^+, is v, their energies are given by

$$\text{energy } (M_1^+) = \tfrac{1}{2}M_1v^2 = eV_{ACC}$$

$$\begin{aligned}\text{energy } (M_2^+) = \tfrac{1}{2}M_2v^2 &= (M_2/M_1)\ \tfrac{1}{2}M_1v^2 \\ &= (M_2/M_1)\ eV_{ACC} \\ &= (M_2/M_1)\ [\text{energy } (M_1^+)]\end{aligned}$$

and their momenta are given by

$$\text{momentum } (M_1^+) = M_1v = (2eV_{ACC}M_1)^{1/2}$$

$$\begin{aligned}\text{momentum } (M_2^+) = M_2v &= M_2(2eV_{ACC}/M_1)^{1/2} \\ &= (M_2/M_1)\ (2eV_{ACC}M_1)^{1/2} \\ &= (M_2/M_1)\ [\text{momentum } (M_1^+)]\end{aligned}$$

Thus to transmit any fragment ion, B and E should be varied such that B/E is constant, and the accelerating voltage held at V_{ACC}.

The resolving power is affected by the energy released during the formation of M_2, but resolution of the order of several hundred is typical [21].

3.5.1.2 Parent Ion Scan (B^2/E)

This scan enables the study of parent ions of a selected daughter ion M_2^+.

For the formation of M_2^+ from the precursor M_1^+ in the 1FFR, the energy of M_2^+ is given by

$$\text{energy } (M_2^+) = (M_2/M_1)\ eV_{ACC}$$

and its momentum is given by

$$\text{momentum } (M_2^+) = (2eV_{ACC}M_2)^{1/2}$$
$$= (M_1/\sqrt{M_2})\ (2eV_{ACC})^{1/2}$$

The precursors of M_2^+ will be transmitted if the magnetic field is scanned such that the ratio of B values is kept equal to the ratio of the momenta of M_2^+ and M_1^+,

$$((2eV_{ACC})^{1/2}M_1)\ /\ ((2eV_{ACC}M_1)^{1/2}M_2^{1/2}) = (M_1/M_2)^{1/2}$$

and the electric field is scanned such as to keep its values equal to the ratio of the energies of M_1^+ and M_2^+

$$(M_2/M_1)\,eV_{ACC}/eV_{ACC} = M_2/M_1$$

Hence B and E are scanned such that B^2/E is constant, with the accelerating voltage held at V_{ACC} [21].

3.5.1.3 Constant Neutral Loss Scan

This type of scan allows the study of all ions M_2^+ formed in the 1FFR with a complementary neutral of specified mass M_3.

In the dissociation of M_1^+, the ionic fragment M_2^+ will be transmitted by the ESA if

$$M_2/M_1 = E_2/E_1 = E' = 1 - (M_3/M_1)$$

and will be transmitted by the magnetic sector if

$$M^* = M_2^2/M_1 = M_2E_1 = (M_1-M_3)E'$$
$$= (M_3/((1-E')-M_3))E'$$
$$= M_2E'^2/(1-E')$$

$$M^*/e = M_3E'^2/((1-E')e) = R^2B_2^2/2V_1$$
$$B_2^2(1-E')E'^2 = (2V_1e/R^2)M_3$$

where R is the radius of the magnet and B_2 is the value of magnetic field necessary to transmit ion M_2^+.

If $B^2(1-E')E'^2$ is kept constant when B and E are scanned, only those ions M_2^+ will be transmitted when its formation is accompanied by the loss of M_3 [21].

3.5.2 MIKES Scan

The mass-analysed ion kinetic energy spectrum scan is appropriate only in a double focusing instrument of reverse geometry or one comprising two stages, the first of which may be used to analyse mass and the second kinetic energy. It allows the investigation of daughter ions formed in the FFR between the two sectors or stages, and relies on the principle that when an ion fragments its energy is partitioned between the fragments in proportion to their mass.

$$M_1^+ \dashrightarrow M_2^+ + M_3$$

$$\text{kinetic energy} = E = Mv^2/2$$

$$E_1/E_2 = (M_1v_1^2) / (M_2v_2^2)$$

and since $v_1 = v_2$

$$E_1/E_2 = M_1/M_2$$

The first stage (magnetic sector or magnetic sector and ESA) is used to select the parent mass M_1. The second stage (ESA or magnet sector and ESA) then scans across the energy range from zero to the energy of the parent ion. Since the energy of the daughter ions E_2 is related to the parent energy E_1 by the above equation the mass of

the daughter ions M_2 may be calculated.

This type of scan can not only be used to follow unimolecular dissociations but any kind of collision reaction taking place in this FFR.

The main disadvantage of this type of scan when performed on a two sector instrument, is that of poor resolution, since the precursor ion is defined only by the magnet and the daughter ions are resolved only by the ESA. This can lead to problems when not only the desired precursor is selected but also its isotope peaks. Three and four sector instruments can avoid this by using two sectors to focus the parent ion, and using two sectors to resolve the daughter ion peaks can improve the quality of the spectrum.

3.6 VG ZAB-2F

All experiments were performed on a modified VG Analytical VG ZAB-2F. This is a two sector instrument, with a magnet and electrostatic analyser, of reverse geometry.

The source is interchangeable allowing different ionisation methods to be used (eg EI, CI, FAB). For EI and CI the sample may be introduced in one of two ways, either injected through the heated septum or on a direct insertion probe, which may be externally heated or water cooled. The EI source has a heater connected to it, which may be controlled by a programmable unit. It was found that source temperatures of up to ~200°C could be obtained relying on the heat of the filament alone.

In between the source and the magnet, the magnet and the ESA, and the ESA and the detector are three field free regions (FFR) (Fig 31). In the 1FFR is a gas cell allowing collision experiments to be carried out. To follow such experiments it is necessary to use linked scanning (see Section 3.5.1).

In the 2FFR there are two gas cells with a deflection plate in between them (Fig 32). Each of the cells has a separate gas supply with regulator valves enabling the flow of gas into the cell to be controlled. There are no pressure gauges for the cells themselves but some idea of the overall pressure on that region can be

found from the analyser pressure gauge. The deflector plate has an external power supply which can be set to a few kV positive or negative. Also the second of the two gas cells can be floated either positive or negative using a second power supply.

There are two detector units, one in the 2FFR after the gas cells, the other after the 3FFR. Both are situated off axis, the first so that it may be used only when required, the second to avoid the detection of neutrals: ions of the required polarity are directed towards one of the detectors by means of a deflector (Fig 33).

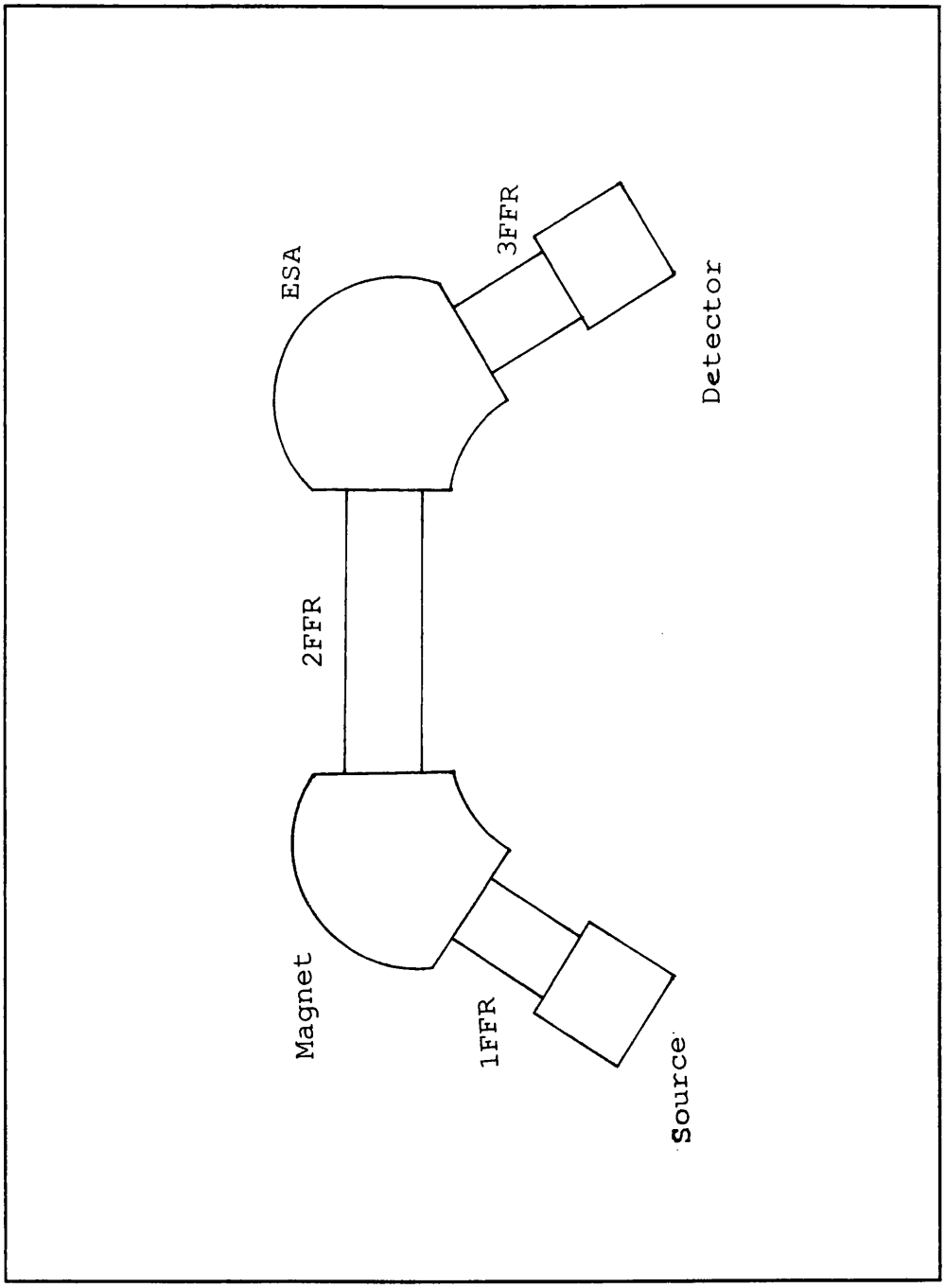

Figure 31 Schematic of the VG ZAB-2F

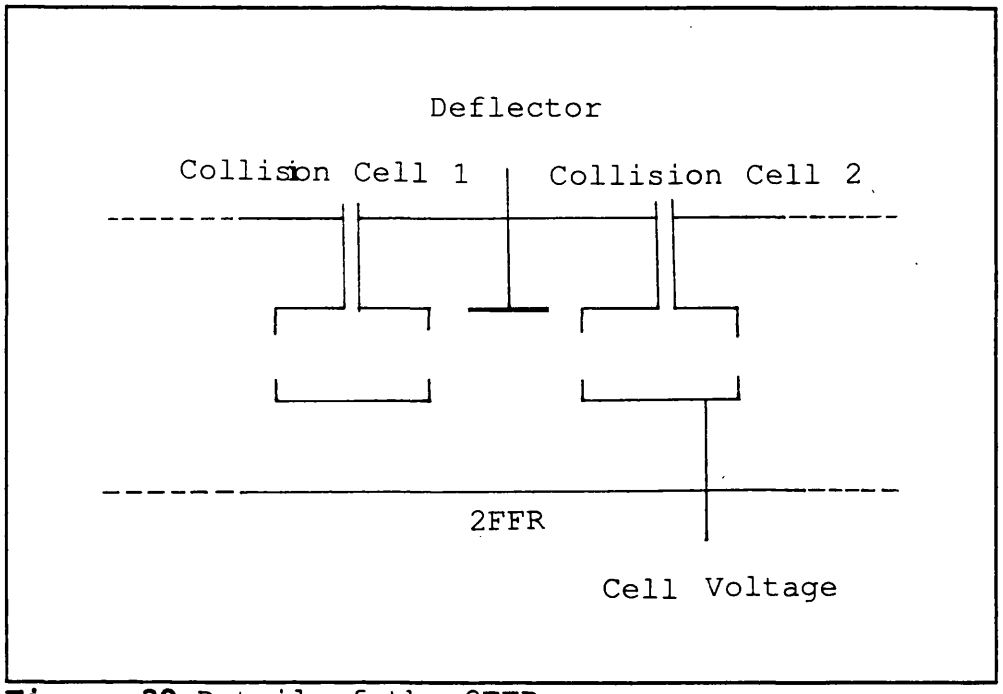

Figure 32 Detail of the 2FFR

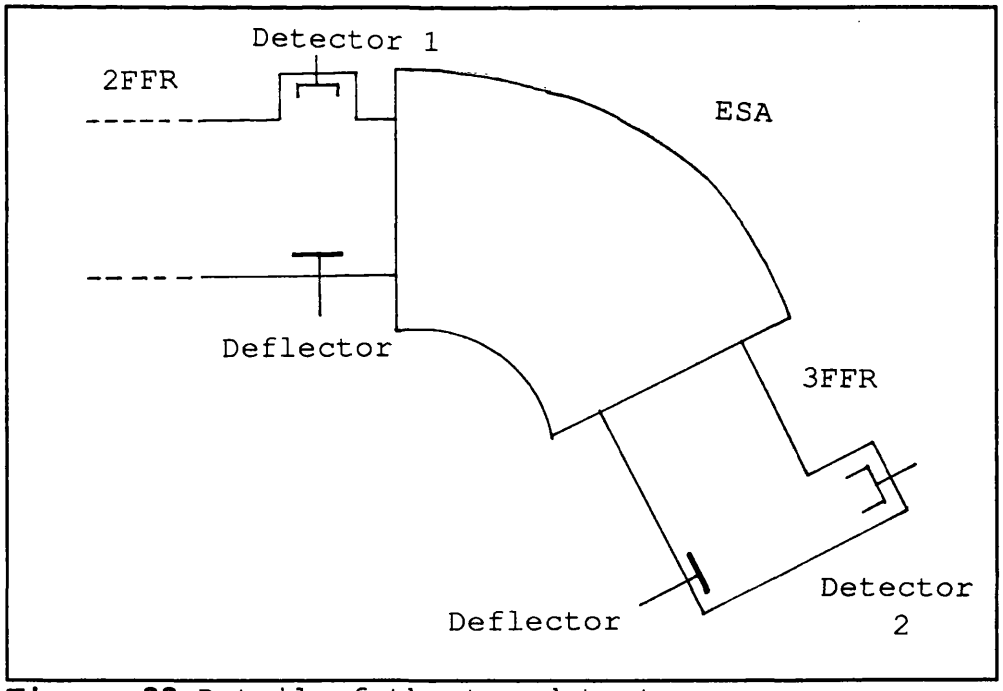

Figure 33 Detail of the two detectors

3.6.1 Cell Voltage

The application of a voltage V_C to a gas cell in the second collision cell in the 2FFR, where $V_C<V_{ACC}$, has been found to improve sensitivity and resolution of fragments formed within this region.

Aniline was used as an example compound with which to investigate the effect of V_C on the spectrum. The sample was obtained from a commercial source and used without further purification. Approximately 2µl was introduced via the heated sample inlet, ionised by 70eV electrons and the ions accelerated through 6kV. The source temperature was maintained at approximately 200°C.

The instrument was operated in a MIKES mode that is selecting the parent ion, in this case the molecular ion, with the magnet and scanning the ESA voltage down from the value corresponding to the energy of the parent (nominally 6keV in this case). Daughter ion scans were recorded using the UV oscillograph on UV sensitive paper. Each scan was repeated several times to examine the reproducibility of the data.

The data in Table 3 shows the variation in intensity of daughter ion peaks at m/z 12 and m/z 15, formed from the molecular ion of aniline, as the voltage applied to the second collision cell in the 2FFR is decreased. Each intensity measurement is the average of five separate measurements, the error is given by the standard

deviation.

It can be seen that in this case the optimum value of V_C lies in the range 1-3kV when V_{ACC}=6kV. It is likely that the increase in sensitivity and resolution through applying V_C is due a focusing action on the ion beam.

Cell Voltage V_C (V)	[m/z 12]	[m/z 15]
5.6	107±7	37±2
5.4	102±1	34±2
5.0	106±5	37±3
4.5	108±6	36±1
4.0	115±3	39±2
3.0	122±3	48±1
2.0	124±2	62±2
0.8	69±4	11±1
0.6	43±2	4±1
0.4	35±2	2
0.2	22±3	
0	23±3	

Table 3: Variation with cell voltage V_C of the intensity (arbitrary units) of daughter ions m/z 12 and m/z 15 in the MIKES spectrum of the molecular ion of aniline. (Intensity measurements are the average of five single measurements.)

3.6.2 Deflector Voltage

The deflection plate between the two gas cells in the 2FFR serves to remove ions emerging from the first cell from the main beam when a voltage V_D is applied.

Aniline was used as an example compound with which to investigate the effect of increasing the value of V_D on the spectrum, and finding the value of V_D adequate to deflect all the ions from the main beam. The sample was obtained from a commercial source and used without further purification. Approximately 2µl was introduced via the heated sample inlet, ionised by 70eV electrons and the ions accelerated through 6kV. The source temperature was maintained at approximately 200°C.

The instrument was operated in a MIKES mode that is selecting the parent ion, in this case the molecular ion, with the magnet and scanning the ESA voltage down from the value corresponding to the energy of the parent (nominally 8keV in this case). Daughter ion scans were recorded using the UV oscillograph on UV sensitive paper. Each scan was repeated several times to examine the reproducibility of the data.

The data in Table 4 shows the variation in intensity of the daughter ion m/z 27 from the molecular ion of aniline as the value of V_D was increased. It can be seen that with the deflector voltage set at 200V almost all the ions were removed from the main beam between the cells. For all subsequent experiments where this

deflector plate was used, V_D was set at 1kV to ensure that all ions were deflected away.

Deflector Voltage V_D (V)	[m/z 27]
0	100%
100	77%
150	1%
200	0.7%

Table 4 : Attenuation of the daughter ion signal in the MIKES spectrum of the molecular ion of aniline as the deflector voltage V_D on the deflector between the collision cells in the 2FFR is increased. Intensity is measured in arbitrary units and normalised to the intensity of m/z 27 where V_D=0.

3.7 Data Aquisition and Recording

There are two systems available for data acquisition from the VG ZAB-2F: a UV oscilloscope and a VG 11-250J data system.

3.7.1 UV Oscilloscope

The UV oscilloscope is based on a moving coil galvanometer. Changes in the input signal - the amplified output signal from the mass spectrometer detector - cause a wire to twist. A mirror attached to this wire is attached also moves, deflecting the beam of light from a UV arc lamp which is reflected from the mirror. Such a system is extremely sensitive and has a fast response time.

The model used here (SE Labs (EMI) Ltd, SE 6150 Mk II) has been adapted to record simultaneously two traces of the input signal at magnifications x1 and x10. With normal magnet scans a simple mass scale also recorded, with a mark at each mass unit and a distinctive mark at each multiple of one hundred mass units. Spectra of modest mass range can be calibrated from this scale. For scans which require an energy scale (eg CID/MIKES or NRMS) no scale is given and the spectra must be calibrated manually, either by comparison with the oscilloscope display or by noting the initial and final

energy values of the spectrum recorded.

The UV oscillograph serves only as a recorder, the scan parameters such as scan speed and mass or energy range being set manually on the instrument. Recording can be initiated either by a signal from the instrument when the scan begins or using a manual 'Record' button on the oscillograph. In both cases the recording will halt when the scan is complete. Alternatively, set recording times of 1 or 2s may be selected, which are activated manually or by the instrument; 'Cont' will give a continuous recording until halted manually. The chart speed can be varied from 0.2 to 1000 mms^{-1}.

Gain and response time are controlled manually from the FA3 amplifier. The setting of 'Amps Full Scale' (AFS), variable from 10^{-4} to 10^{-9}A, determines the magnification of the recorded spectrum. The gain on the output signal from the FA3 amplifier fed to the oscillograph can be varied by factors of x1, x2 and x5. Response time is variable from 0.03 to 3000ms and must be balanced with the scan speed. For normal operation with AFS set to 10^{-6} or 10^{-7}A, a response time of 0.3ms is suitable. However for weaker signals AFS must be increased which amplifies not only the wanted signal but the unwanted noise. Because the noise is typically of a much higher frequency it may be filtered out by increasing the response time of the amplifier, say to a value in the region of 10-100 ms. However to ensure there

is no distortion of the signal the scan speed should be kept low.

The UV oscilloscope provides a simple and reliable method of recording mass spectral data. The oscilloscope is relatively inexpensive though UV sensitive paper can be costly over time. Under normal light conditions the recording will fade after a few days. A stabilising lacquer can be applied to the paper which will preserve the trace for a few weeks, and chemical processing or stroring inlight free conditions is necessary for archiving.

The main disadvantage of this method is the inflexibility in data handling and analysis after acquisition.

3.7.2 Data System

The VG ZAB-2F is equipped with a VG 11-250J data system. This not only acquires and stores mass spectral data but also sets up instrumental parameters and initiates scans.

Each scan has its associated parameters set out in a so called 'systems page', this includes details of the instrument such as its geometry, accelerating voltage V_{ACC}, ionisation mode, resolution and gas types (for CI). The scan is fully described in terms of:

a) type of scan ie which sectors or quadrupoles are to be scanned

b) upper and lower mass or energy

c) linear or exponential scan

d) scan up or down

e) scan time

f) interscan time

g) run duration (time or number of scans)

h) continuum or multi channel analyser mode

i) zero level

these are parameters which the operator sets prior to data acquisition, the data system ignoring the corresponding parameter values set manually on the instrument.

The FA3 amplifier is still set manually even when under data system control. The gain is set so as to give a signal which is sufficiently intense without saturation occurring (a nominal 10V). The response time is usually set at 0.1ms, and the zero level is adjusted to correspond with the zero level of the data system.

Selecting 'Continuum' gives discrete spectra whereas 'MCA' (multi channel analysis) continuously sums the spectra into a single file. Rejecting both these options means that the data will be stored and displayed in histogram form.

Though the data system allow scan times ranging from

a fraction of a second to several minutes, the value selected should to some extent reflect the nature of the instrument, for instance in the case of a magnetic sector instrument, there are practical limits on the maximum scan speed due to hysteresis. A long scan time (slow scan speed) may be inappropriate where the ion current is rising or falling, which will give a false impression of the relative intensities of the peaks in the spectrum.

Where an analyser is tuned to some constant value throughout the scan, such as the magnetic sector of a double focusing instrument of reverse geometry during a MIKES scan, this value is input and the analyser tuned automatically (with the option of fine tuning by the operator). Such data is automatically plotted against an energy scale but can be given a mass or time scale without the need for a calibration file. Calibration is carried out by the data system on the basis of a linear scan beginning at the precursor ion. This means that there is little flexibility in the selected energy range (which must begin at that corresponding to $_{\Lambda}V_{ACC}$). Any nonlinearity in the scan will invalidate the allotted mass scale; this has been seen to be the case at the low mass end of MIKE spectra, and for this reason the masses were always independendently verified off line. The data system recognises the peak corresponding to the precursor ion only when it is the most intense peak in the spectrum. When this is not the case, or there is another peak of

comparable intensity, this can be wrongly assigned the precursor ion mass, thus the masses of the other peaks in the spectrum will also be incorrect.

A great advantage of the data system over the UV oscillograph is in its flexibility in data handling. A number of discrete scans may be averaged into a new file, spectra may be smoothed to remove high frequency noise or noise spikes and it is also possible to 'subtract' background interference when stored on a separate file. Data files are first stored on a hard disk but may also be archived on tape.

REFERENCES : Chapter 3 Instrumentation

1. R. Davis and M. Frearson, 'Mass Spectrometry', Wiley, 1987
2. M.E. Rose and R.A.W. Johnson, 'Mass Spectrometry for Chemists and Biochemists', Cambridge University Press, 1982
3. R.G. Cooks, J.H. Beynon, R.M. Caprioli and G.R. Lester, 'Metastable Ions', Elservier, 1973
4. M. Barber, R.S. Bordoli, R.D. Sedgwick and A.N. Tyler, J. Chem. Soc. Chem. Commun., 325-327, 1981
5. M. Barber, R.S. Bordoli, G.J. Elliot, R.D. Sedgwick and A.N. Tyler, Anal. Chem., 54, 645A-657A, 1982
6. A.L. Burlingame, T.A. Baille and P.J. Derrick, Anal. Chem., 58, 165R-211R, 1986
7. S.A. Martin, C.E. Costello and K. Biemann, Anal. Chem., 54, 2362-2368, 1982
8. A.M. Buko and B.A. Fraser, Biomed. Mass Spectrom., 10, 577-585, 1985
9. A.M. Buko and L.R. Phillips and B.A. Fraser, Biomed. Mass Spectrom., 10, 408-416, 1983
10. Q,-W. Huang, G.-L Wu and H.-T. Tang, Int. J. Mass Spectrom. Ion Processes, 70, 145-152, 1986
11. G. Bojesen and J. Moller, Int. J. Mass Spectrom. Ion Processes, 68, 239-248, 1986
12. J. Sunner, A. Morales and P. Kebarle, Anal. Chem., 59, 1378-1383, 1987

13. M.P. Lacey and T. Keough, Rapid Commun. Mass Spectrom., 3, 46-50, 1989

14. S.S. Wong, F.W. Rollgen, I. Manz and M. Przybylski, Biomed. Mass Spectrom., 12, 43-46, 1985

15. C. Fenslau and R.J. Cotter, Chem. Rev., 87, 501-512, 1987

16. S.A. Martin, C.E. Costello and K. Biemann, Anal. Chem., 54, 2362-2368, 1982

17. S. Naylor, A.F. Findeis, B.W. Gibson and D.H. Williams, J. Am. Chem. Soc., 108, 6359-6363, 1986

18. D.F. Hunt in Ref 'Tandem Mass Spectrometry', Ed. F.W. McLafferty, Wiley, 1983

19. D.H. Williams in 'Principles of Organic Mass Spectrometry', McGraw-Hill, 1972

20. H.D. Beckey, 'Principles of Field Ionisation and Field Desorbtion', Pergamon Press, 1977

21. K.R. Jennings and R.S. Mason in Ref. 19

22. E.C.Young, 'The New Penguin Dictionary of Electronics', Penguin, 1979

23. F.W McLafferty, Science, 214, 280-287, 1981

24. R.G. Cooks and G.L Glish, Chem. Eng. News., 59, 40-52, 1981

CHAPTER 4 : EXPERIMENTAL

4.1 HYDROXYQUINOLINE ISOMERS

4.1.1 Metastable Peak Shapes

4.1.1.1 Introduction

It has been noted that the shape of metastable peaks can be highly informative (see Section 2.6.3.2), the width of the peak giving an indication of the KER upon its formation. CO loss from 1,4-naphthoquinone illustrates the case of a fragmentation giving a low KER, the metastable peak being a narrow gaussian with $T_{\frac{1}{4}}$ 88 meV; this is typical of a carbonyl-containing aromatic compound. CO loss from 2-naphthol however is a case of a high KER, the metastable peak being broad and dished with $T_{\frac{1}{4}}$ 820 meV, typical of a phenolic compound [1].

Composite metastable peaks can occur due to a number of different reasons (see Section 2.6.3.2). Earlier work in this laboratory showed that 2-hydroxyquinoline is an example of a compound which gives a composite metastable peak, the only positional isomer of hydroxyquinoline to do so for the loss of CO (Fig 34). The peak is composed of a broad dished component $T_{\frac{1}{2}}$ 800 meV, and a narrow gaussian component $T_{\frac{1}{2}}$ 80 meV by comparison with 2-naphthol and 1,4-naphthoquinone. These were identified as

CO loss from the 2-hydroxyquinoline tautomer and CO loss from the quinoline-2(1H)-one form respectively [1]. Thus the shape of the metastable peak has shown both of these tautomers to exist to a significant extent in the gas phase. The other positional isomers give broad dished metastable peaks for CO loss indicating that they exist only in the hydroxy forms.

In this current work, the loss of CO from hydroxy substituted bicyclic nitrogen-containing heterocyclics related to the hydroxyquinolines has been studied, with the hope of understanding better the behaviour of 2-hydroxyquinoline. Quinoline N-oxide also gives metastable loss of CO and was included in this study.

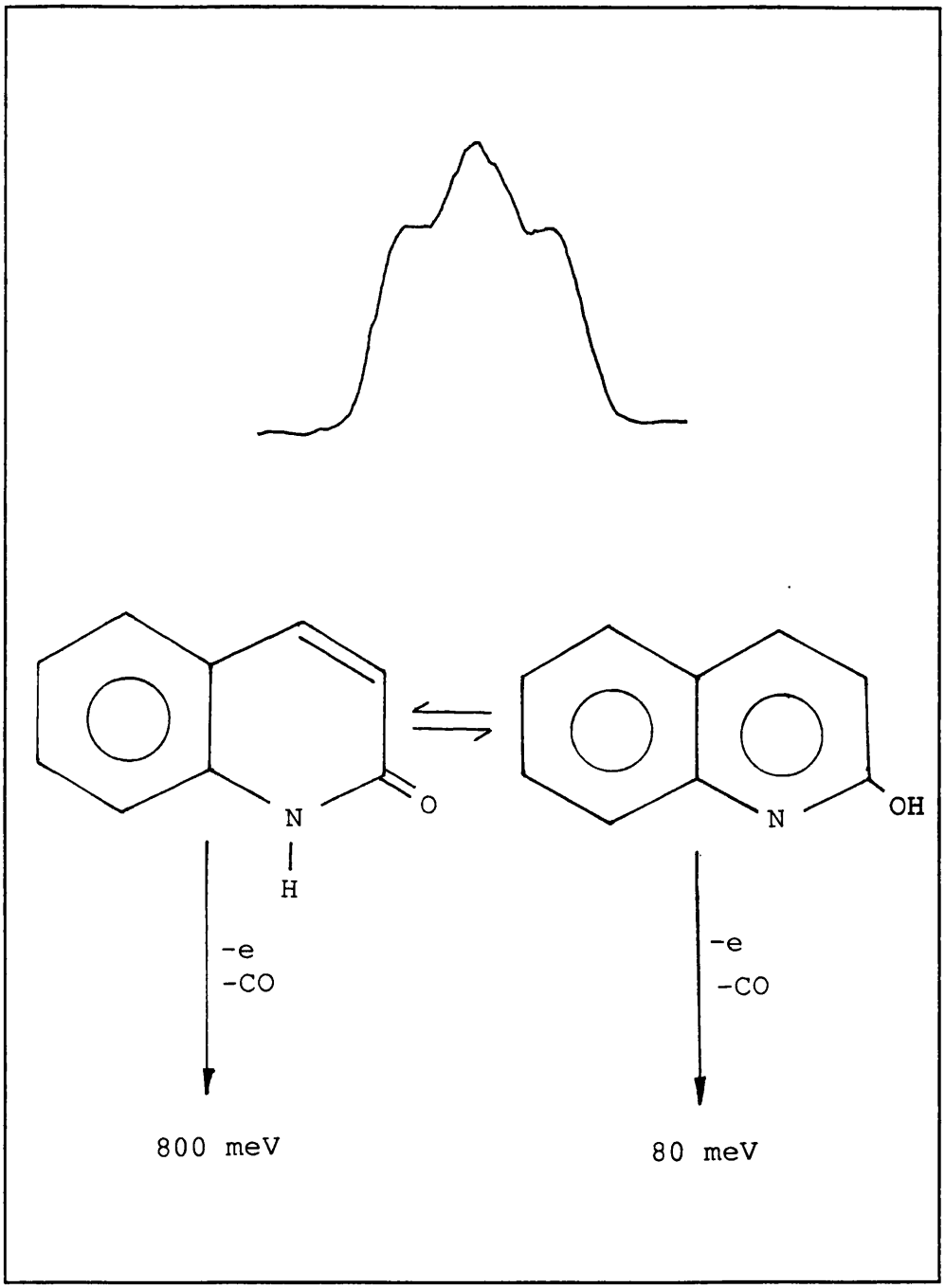

Figure 34 Comopsite peak for unimolecular CO loss from 2-hydroxyquinoline = quinoline-2H(1H)-one

4.1.1.2 Experimental

The following compounds were studied

4-hydroxyquinazoline

2-hydroxyquinoxalinol

and quinoline N-oxide

which were of commercial origin and used without further purification. In each case they were introduced using the direct insertion probe, ionised with 70eV electrons and the ions accelerated through 8kV. The source temperature was maintained at ~200°C.

Metastable peaks were observed through operating the instrument in a MIKES mode, selecting the parent ion with the magnet and scanning the ESA down from the energy of the parent (nominally 8kV).

High energy CID spectra were obtained by scanning the instrument in the same manner, with helium admitted into the second collision cell in the 2FFR, at a pressure sufficient to attenuate the main beam intensity by 30%.

Data was recorded using a UV oscilloscope and UV sensitive paper. Each scan was recorded several times to examine the reproducibility of the data.

4.1.1.3 Results and Discussion

The unimolecular MIKE spectra are illustrated in

Figs 35-37. The spectrum for 4-hydroxyquinazoline shows significant HCN loss while the $[M-CO]^{+\cdot}$ peak is a complex gaussian with $T_{½}$ ~200 meV for the broader component. The complex nature of the metastable peak could suggest that more than one tautomer of the parent exists in the gas phase. However, although the broader component may relate to CO loss from the hydroxy form, the KER is notably lower than that for CO loss from 2-hydroxyquinoline, and would be considered to be exceptionally low for this process (Fig 35).

2-hydroxyquinoxalinol appears to exist only in the hydroxy form as this gives only a dished peak of $T_{½}$~400 meV with no narrow component (Fig 36). It is interesting to compare this result with those of 2-hydroxyquinoline and 4-hydroxyquinazoline, both of which show evidence of tautomerism by their composite metastable peaks. The fact that 2-hydroxyquinoline is the only positional isomer of hydroxyquinoline to tautomerise, shows the critical nature of the position of the hydroxy group on whether this takes place. The relatively small KER for the broader component of the composite metastable peak for 4-hydroxyquinazoline could be due to some effect other than tautomerism. The fact that an OH group in the 2-position will not always cause tautomerism is shown by the failure of 2-hydroxyquinoxalinol to tautomerise.

Quinoline N-oxide is an interesting case as it loses CO to give a composite peak ,the broader component having

$T_{½}$ ~450 meV (Fig 37). Since there are no tautomers of the parent ion there must be either two isomeric product ions or two mechanisms to produce the same product ion. The latter has been proposed [2] on the basis of mass spectral data. Both mechanisms must involve an initial rearrangement as the oxygen atom is not bonded to a carbon atom in the original molecule so there is no straightforward route to CO loss.

Deuterium labelling experiments gave no exchange with D_2O, indicating that as anticipated for quinoline N-oxide, there was no hydroxy group present before ionisation [3]. These reactions suggested that the final structure after the loss of CO could be that of indole. High energy CID experiments were carried out on $[M-CO]^{+\cdot}$ from quinoline N-oxide and $M^{+\cdot}$ from indole. The spectra showed strong similarities giving evidence in favour of the structures being identical (Figs 38,39).

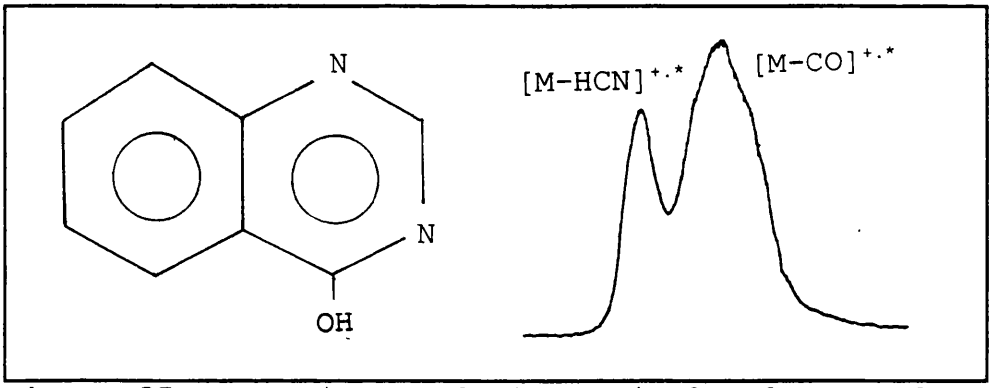

Figure 35 Composite peak for unimolecular CO loss from 4-hydroxyquinazoline

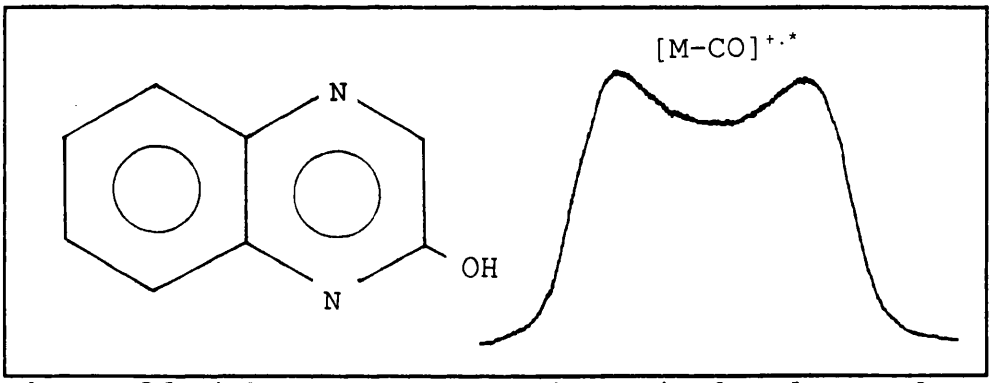

Figure 36 Dished-topped peak for unimolecular CO loss from 2-hydroxyquinoxalinol

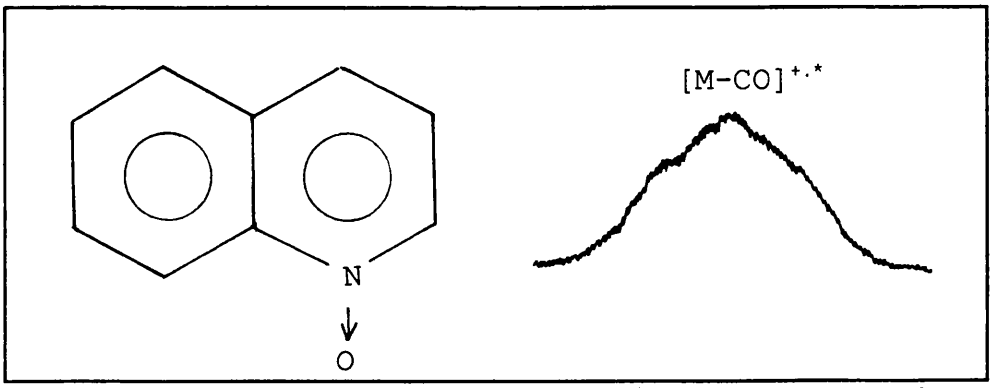

Figure 37 Composite peak for unimolecular CO loss from quinoline N-oxide

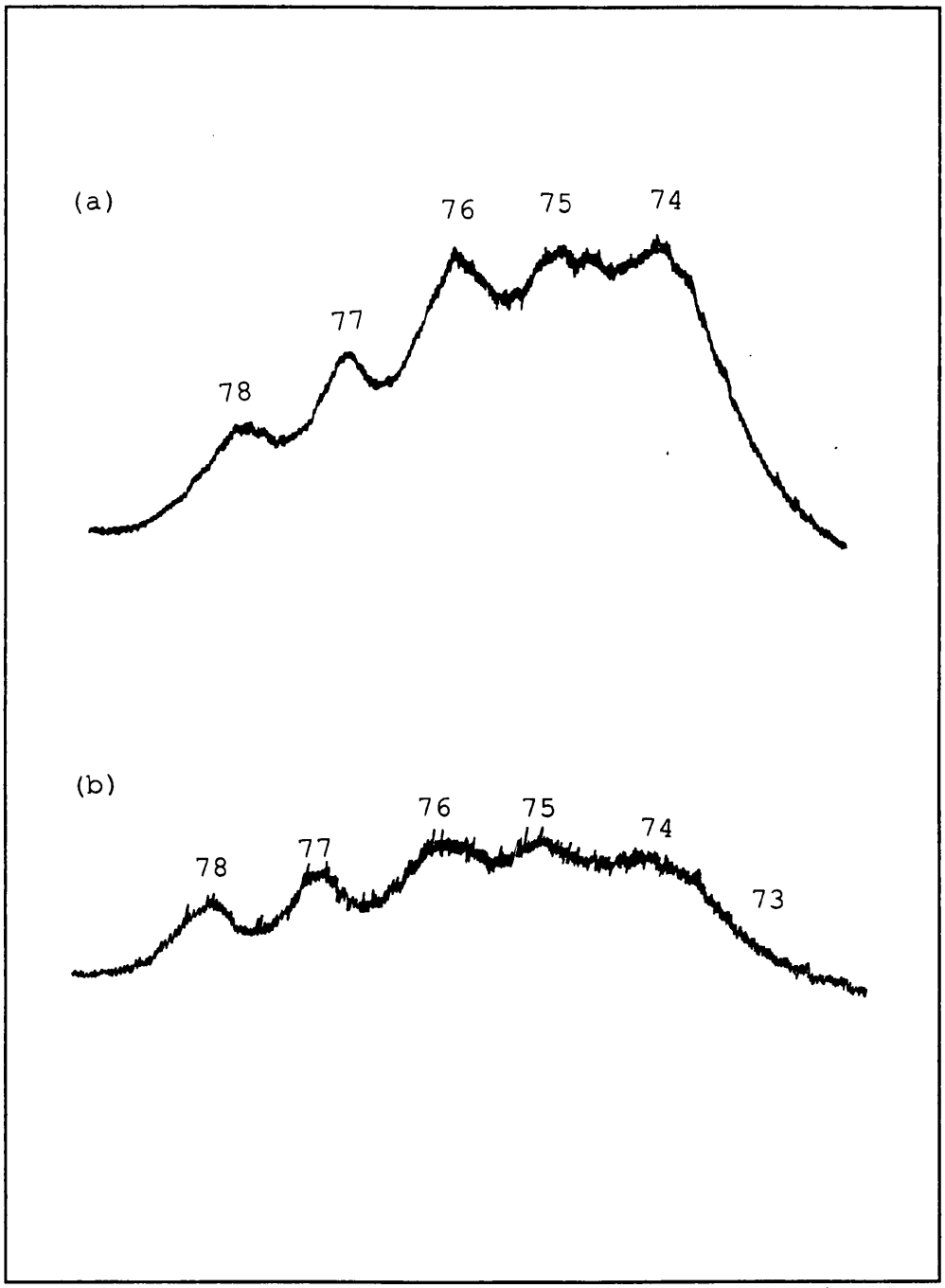

Figure 38 Partial CID spectra of the $[M-CO]^{+\cdot}$ ions from (a) 2-hydroxyquinoline and (b) quinoline N-oxide

4.1.2 High Energy CID Spectra

4.1.2.1 Introduction

It might be assumed that the hydroxyquinoline isomers, losing a common group CO, would all take a common structure. For the 2-, 3- and 4-isomers this structure would be most likely to be that of indole. Therefore a way was sought to characterise the structure of the $[M-CO]^{+\cdot}$ ions for the hydroxyquinolines and find out if indeed they did resemble indole.

The CID technique was chosen in order to produce spectra yielding structural information, and to minimise the contributions from the fragmentation of molecules that had previously undergone rearrangement.

4.1.2.2 Experimental

The following compounds were studied

2-, 3-, 4-, 5- and 8-hydroxyquinoline

2-, 3-, 4- and 8-mercaptoquinoline

and indole

which were obtained through commercial sources and used without further purification. In each case they were introduced using the direct insertion probe, ionised with 70eV electrons and the ions accelerated through 8kV. The

source temperature was maintained at ~200°C.

High energy CID spectra were obtained by scanning the instrument in a MIKES mode, selecting the precursor ion with the magnets and scanning the ESA voltage down from the value corresponding to the energy of the precursor (nominally 8keV). Helium was admitted into the second collision cell in the 2FFR, at a pressure sufficient to attenuate the main beam intensity by 30%. Where it was necessary to differentiate between fragments formed through unimolecular dissociation and those formed through CID, a voltage $\mathbf{V}_c$ was applied to the second collision cell in the 2FFR. By observing the effect that increasing $\mathbf{V}_c$ had on the appearance of the spectrum it was found that a cell voltage of 1.6kV was sufficient in this instance to discriminate between the two kinds of fragments.

Data was recorded using a UV oscilloscope and UV sensitive paper. Each scan was recorded several times to examine the reproducibility of the data.

4.1.2.3 Results and Discussion

Initially it was decided to examine the intensity ratios of m/z 89 to m/z 90 from the CID spectra of the m/z 117 $[M-CO]^{+\cdot}$ ions from the hydroxyquinolines and compare them with the corresponding spectrum of $M^{+\cdot}$ from

indole. These fragment peaks were selected since they were intense in all the CID spectra.

However, there were already strong m/z 89 and 90 peaks in the MIKES spectra of $[M-CO]^{+\cdot}$ due to unimolecular dissociation, therefore the peaks observed in the CID spectra were actually a mixture of unimolecular dissociation products and collisionally induced products. The accepted way of separating these two components is to apply a voltage $\mathbf{V_C}$ to the collision cell. This has the effect of changing the relative energy of the fragment ions formed within the cell, so moving them to a higher energy (or lower, depending on the polarity of $\mathbf{V_C}$) on the spectrum. Those fragments formed outside the cell appear at the same energies as before. However, a proportion of the unimolecular dissociations that take place within the 2FFR take place inside the cell itself. These are also shifted in the spectrum and appear in the same position as the CID peaks. Fortunately, this contribution is often small and may be ignored.

With the cell voltage connected and no gas present, the intensities of m/z 89 and 90 were measured ie unimolecular decompositions in the collision cell (known as $[89]_u$ and $[90]_u$). Then the collision gas was admitted to give 30% attenuation of the main beam, and the intensities of m/z 89 and 90 measured (known as $[89]_{u+c}$ and $[90]_{u+c}$). These values were measured from spectra recorded from UV oscillograph paper and hence only a

certain limited accuracy could be obtained. To reduce the uncertainty in the final ratios, repeated spectra were recorded and average values of $[89]_{u+c}$ and $[90]_{u+c}$ determined (Appendix I).

A table of [89/90] without any correction for the unimolecular contribution ("no correction") is given (Table 5). It can be seen that the ratios of m/z 89 and 90 for the CID of the $[M-CO]^{+\cdot}$ isomers show subtle yet definite differences which are brought out by the averaging process.

It was then found that the small unimolecular contributions to the CID peaks at m/z 89 and 90 were of significant intensity and could not be overlooked. With no gas present and the cell voltage still applied, the peaks representing unimolecular loss of masses 27 and 28 within the gas cell could be measured ie $[89]_u$ and $[90]_u$. However, when the collision gas is present it is not certain that these peaks would have the same intensities since there would be losses due to scattering. No way could be found of directly measuring $[89]_u$ and $[90]_u$ or their change in intensity, if any, when the helium was introduced. Two forms of correction were applied: the first involved subtracting half the measured values of $[89]_u$ and $[90]_u$ from $[89]_{u+c}$ and $[90]_{u+c}$ (as if the introduction of collision gas has reduced the unimolecular contribution within the gas cell by 50%) called "half correction" (Table 6). The second method

involved subtracting the full values of $[89]_u$ and $[90]_u$ from $[89]_{u+c}$ and $[90]_{u+c}$ (as if the introduction of the collision gas had no effect on the unimolecular contribution in the gas cell) called "full correction" (Table 7).

The three sets of data show similarities in trends despite the different correction methods, except in the case of 5-hydroxyquinoline. Some preliminary measurements were made of [89]:[90] for indole $M^{+\cdot}$, but many measurements would have been required to reduce the overall error to a satisfactory level. This line of investigation was not carried any further whilst the method of correction for unimolecular contributions was uncertain.

Compound:	No. of Samples:	Ratio:
2-OHQ	9	1.0±0.01
3-OHQ	11	0.6±0.01
4-OHQ	18	0.9±0.01
5-OHQ	56	0.9±0.01
8-OHQ	2	1.1±0.03
Indole	1	0.9±0.36

Table 5: Ratio of the intensities of m/z 89 to m/z 90 from high energy CID spectra. (No correction made for unimolecular contribution.)

Compound:	No. of Samples:	Ratio:
2-OHQ	9	1. ±0.02
3-OHQ		0. ±0.03
4-OHQ	18	1. ±0.04
5-OHQ		1. ±0.04
8-OHQ	2	1. ±0.1
Indole		

Table 6: Ratio of the intensities of m/z 89 to m/z 90 from high energy CID spectra.('Half correction')
(* large error)

Compound:	No. of Samples:	Ratio:
2-OHQ	9	1.3±0.02
3-OHQ	11	0.9±0.03
4-OHQ	18	1.1±0.04
5-OHQ	56	1.8±0.04
8-OHQ	2	1.5±0.1
Indole	1	1.6 *

Table 7: Ratio of the intensities of m/z 89 to m/z 90 from high energy CID spectra. ('Full correction')
(* large error)

Close examination of the whole CID spectra of the hydroxyquinolines after CO loss, revealed that only the group of peaks from m/z 73 to 79 gave any significant differences between these compounds, the remainder of the spectra being identical, hence attention was focused on this group.

CID spectra of $[M-CO]^{+\cdot}$ at 30% attenuation for 2-, 3-, 4-, 5- and 8-hydroxyquinoline and $M^{+\cdot}$ for indole (Table 8) fell into three groups: the 2-isomer and indole (Fig 39), the 3- and 4-isomers (Fig 40), and the 5- and 8-isomers (Fig 41). Interference from unimolecular decomposition was found to be significant only for the 3- and 4-isomers, leading to an increase in the intensity of m/z 77. By applying a voltage $\mathbf{V_C}$=1.6 kV to the collision cell the unimolecular contribution was effectively separated out, leaving the spectra for the 3- and 4-isomers resembling those of the 2-isomer and indole (Fig 42). The CID spectra for the 5- and 8-isomers were broadly similar to each other, both showing an intense peak at m/z 78. However the intensity of this peak was notably greater in the spectrum of the 5-isomer, even with the application of the cell voltage $\mathbf{V_C}$, so the difference was judged not to be due to interference from unimolecular dissociation (Table 9).

CID spectra were also recorded for 2-, 3-, 4- and 8-mercaptoquinoline after the loss of CS, $[M-CS]^{+\cdot}$, under the same collision conditions that had been used for the

hydroxyquinolines but without the cell voltage V_c applied (Table 10). Comparing these spectra (Figs 45-47) with those for the corresponding positional isomers of $[M-CO]^{+\cdot}$ for the hydroxyquinolines revealed a strong similarity.

In summary, the CID spectra gave firm evidence in support of the theory that the $[M-CO]^{+\cdot}$ ions from 2-, 3- and 4-hydroxyquinoline have an indole structure. The data further suggests that the $[M-CS]^{+\cdot}$ ions from 2-, 3- and 4-mercaptoquinoline also form indole. The similarity of CID spectra for the 5- and 8-isomers suggests a similarity in structure (which may be expected from the similarity of the $M^{+\cdot}$ ions in each case) but they nevertheless seem to retain their individuality, as the spectra are not identical. Possible structures for $[M-CO]^{+\cdot}$ from 5- and 8-hydroxyquinoline would probably take the form of an intact pyrido ring fused to a cyclopentadieno ring (Fig 48). Since these suggested structures may interconvert, it may be that one positional isomer yields proportionally more of one structure than the other resulting in dissimilarity in the spectra.

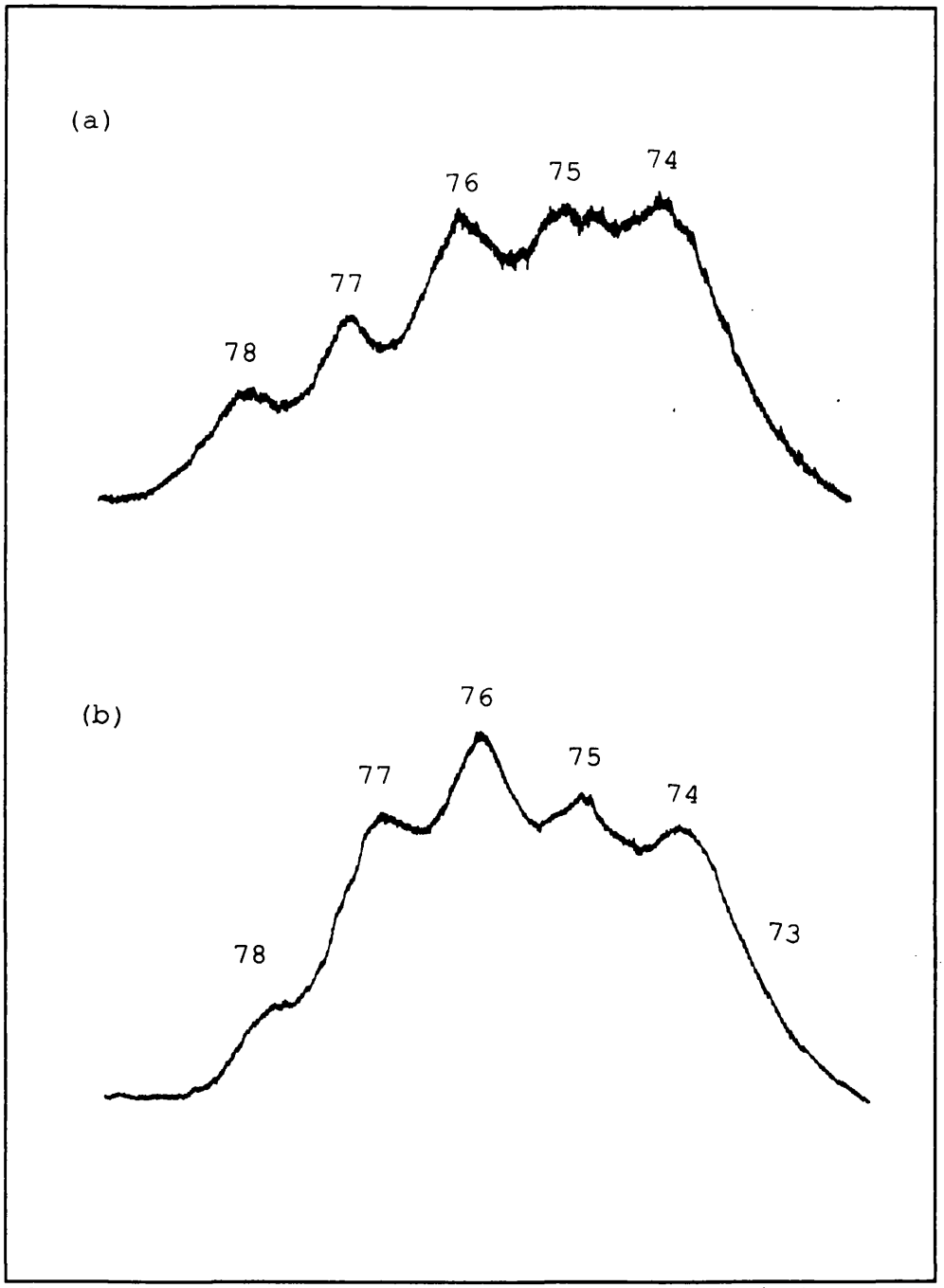

Figure 39 Partial CID spectra of the $[M-CO]^{+\cdot}$ ion from (a) 2-hydroxyquinoline and (b) the $M^{+\cdot}$ ion from indole (V_C=0)

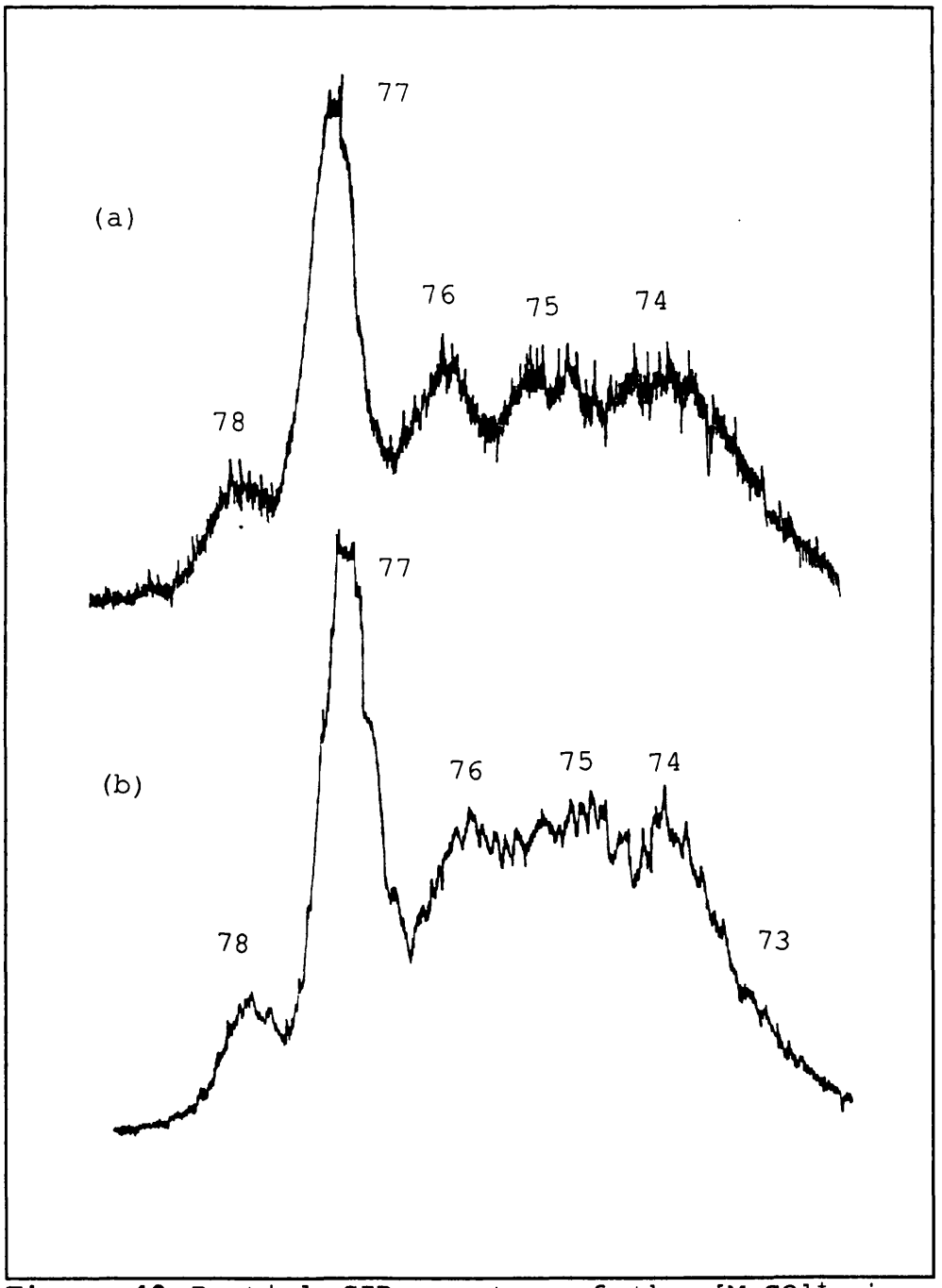

Figure 40 Partial CID spectra of the $[M-CO]^{+\cdot}$ ions from (a) 3- and (b) 4-hydroxyquinoline (V_c=0)

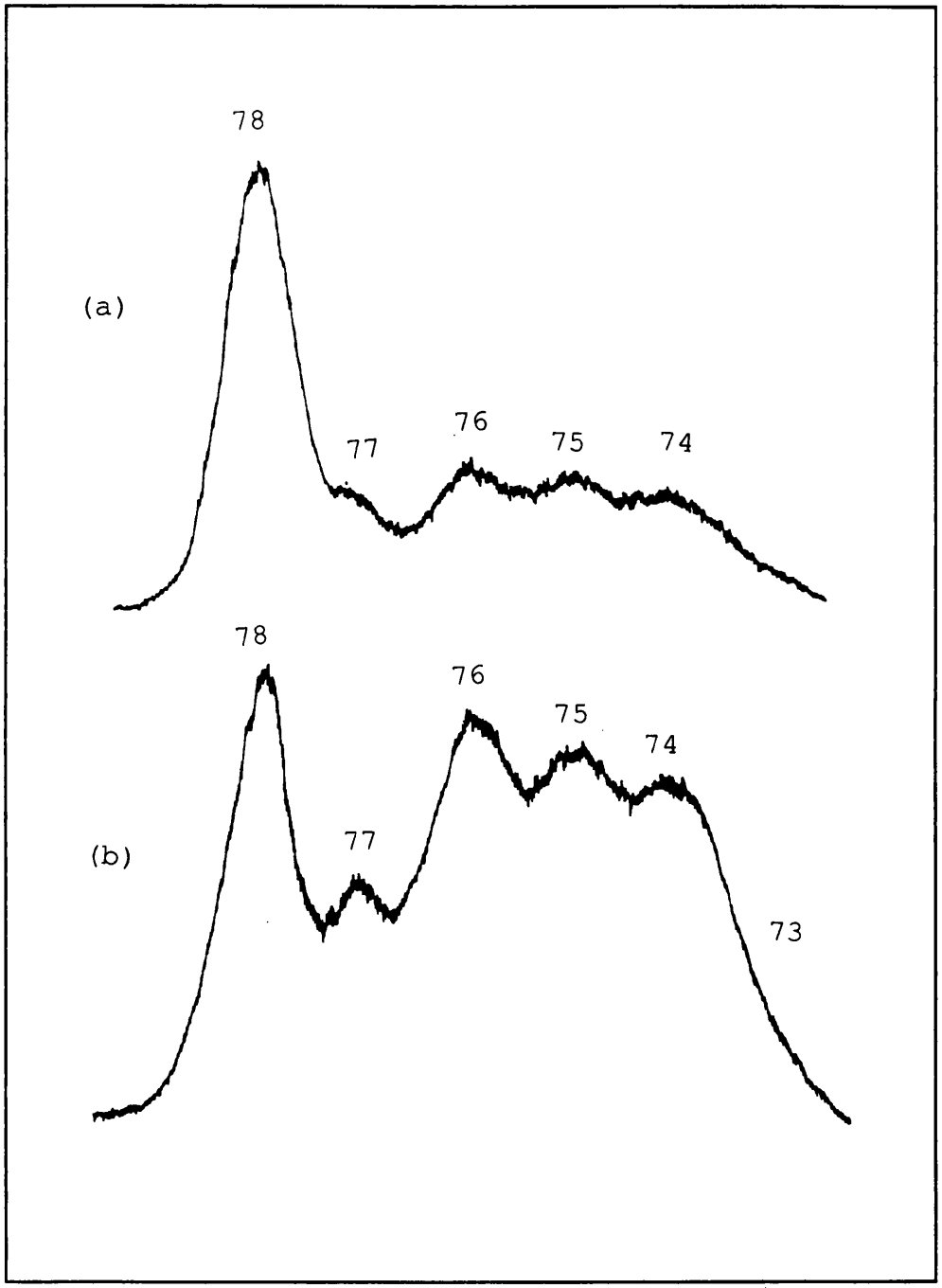

Figure 41 Partial CID spectra of the $[M-CO]^{+\cdot}$ ion from (a) 5- and (b) 8-hydroxyquinoline (V_C=0)

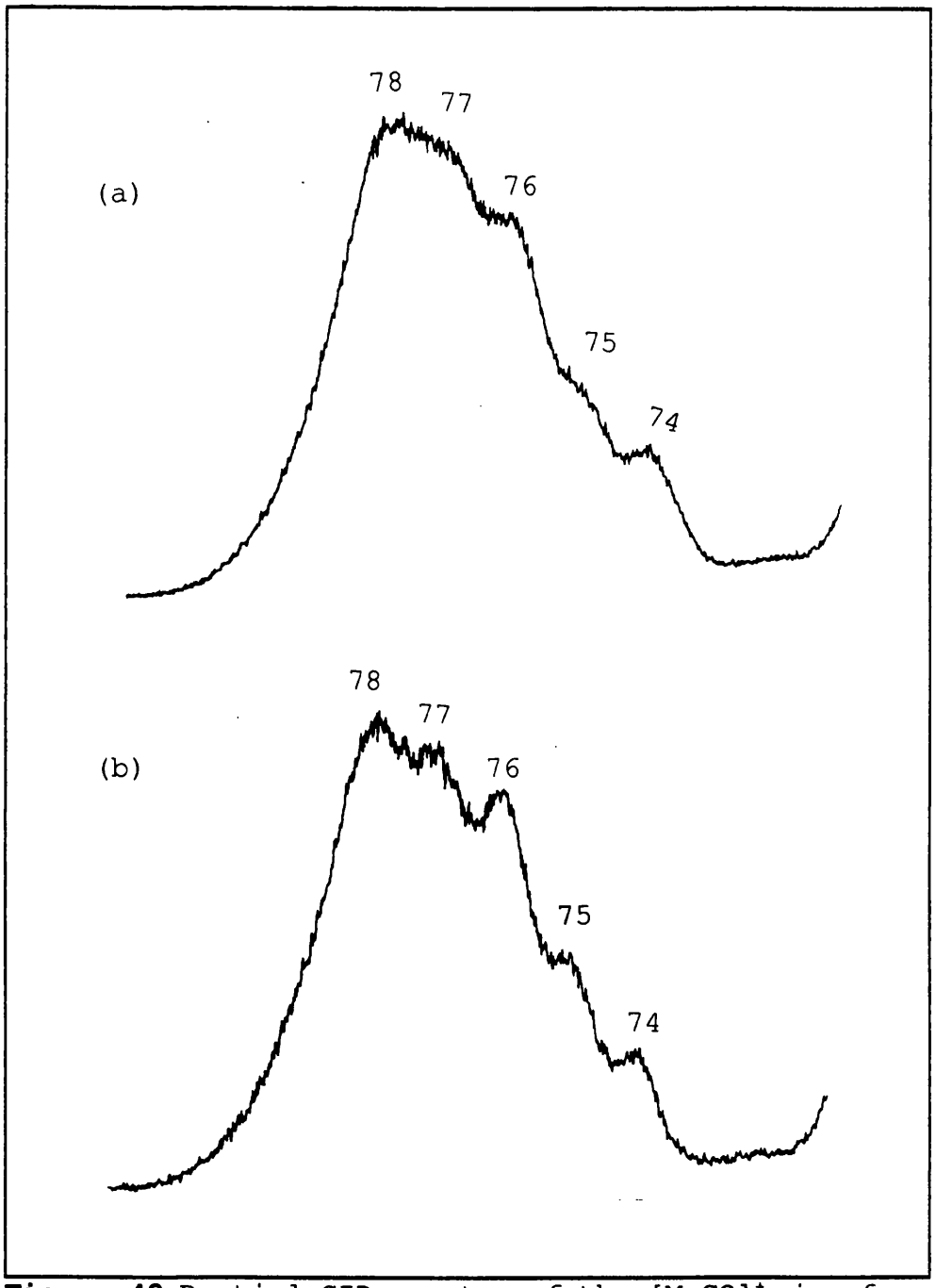

Figure 42 Partial CID spectra of the $[M-CO]^{+\cdot}$ ion from (a) 2-hydroxyquinoline and (b) the $M^{+\cdot}$ ion from indole (V_c = 1.6kV)

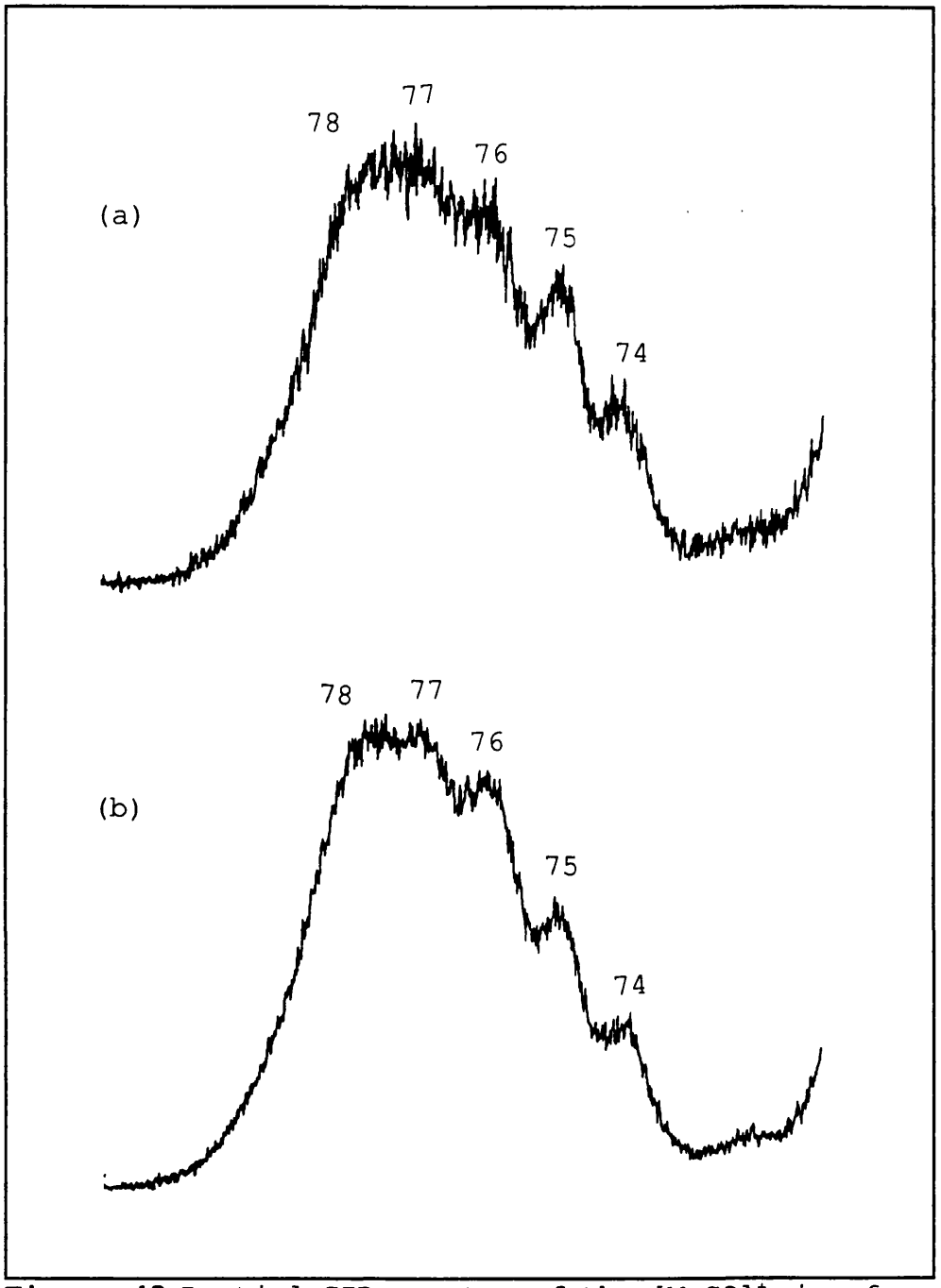

Figure 43 Partial CID spectra of the $[M-CO]^{+\cdot}$ ion from (a) 3- and (b) 4-hydroxyquinoline (V_c = 1.6kV)

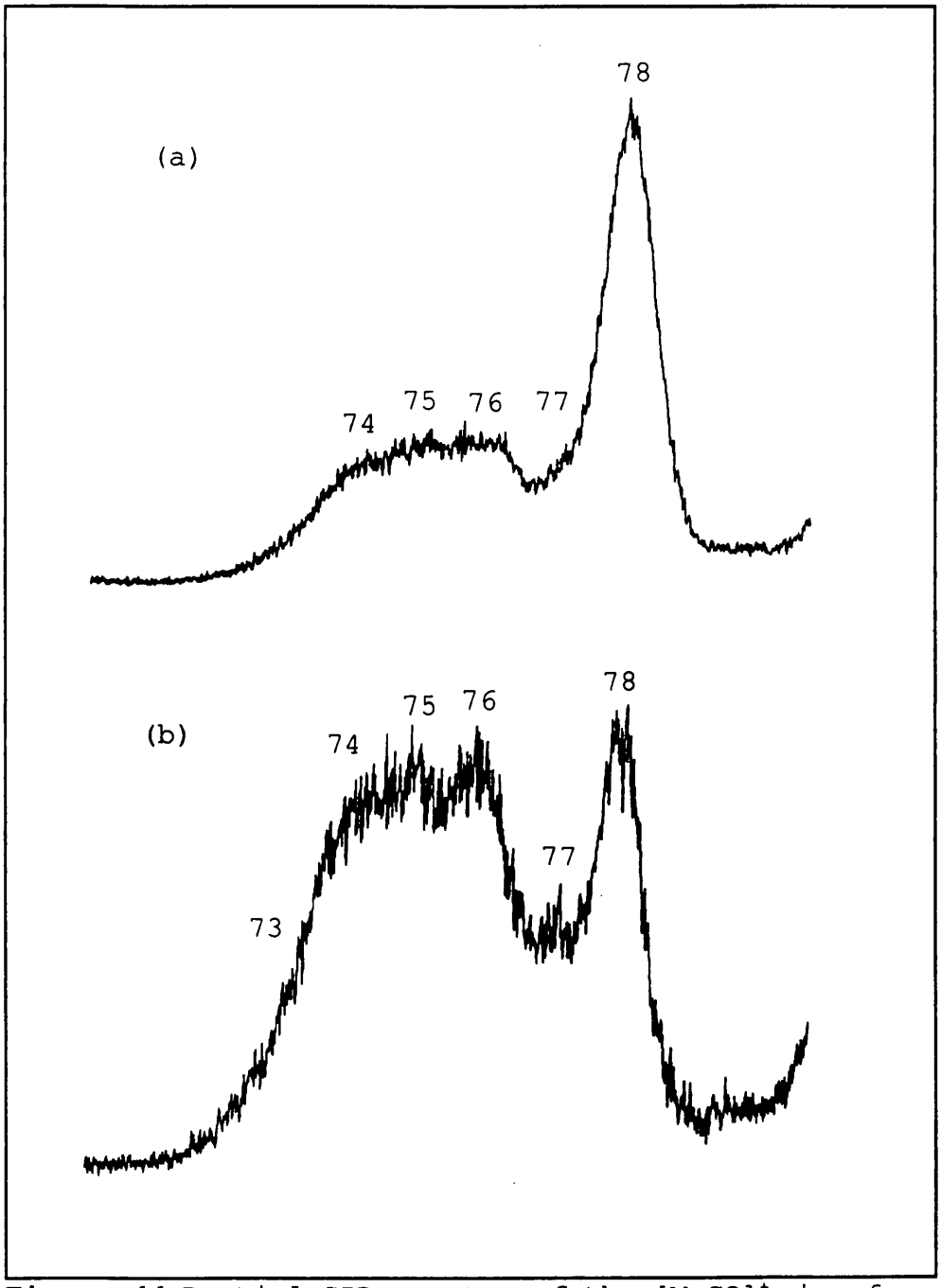

Figure 44 Partial CID spectra of the $[M-CO]^{+\cdot}$ ion from (a) 5- and (b) 8-hydroxyquinoline (V_c = 1.6kV)

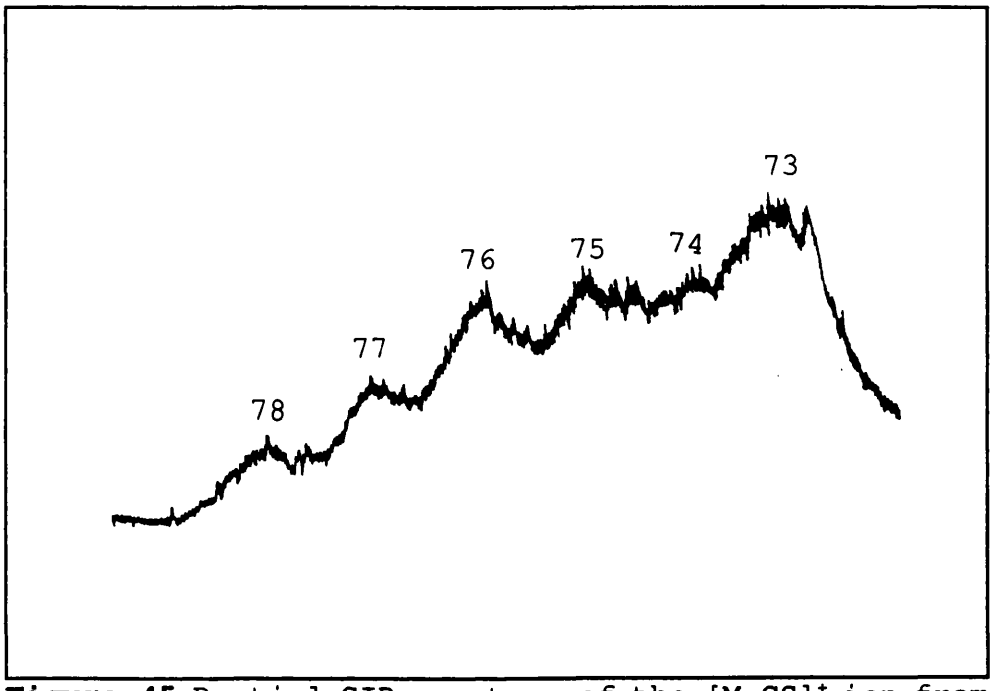

Figure 45 Partial CID spectrum of the $[M-CS]^+$ ion from (a) 2-mercaptoquinoline (V_c=0)

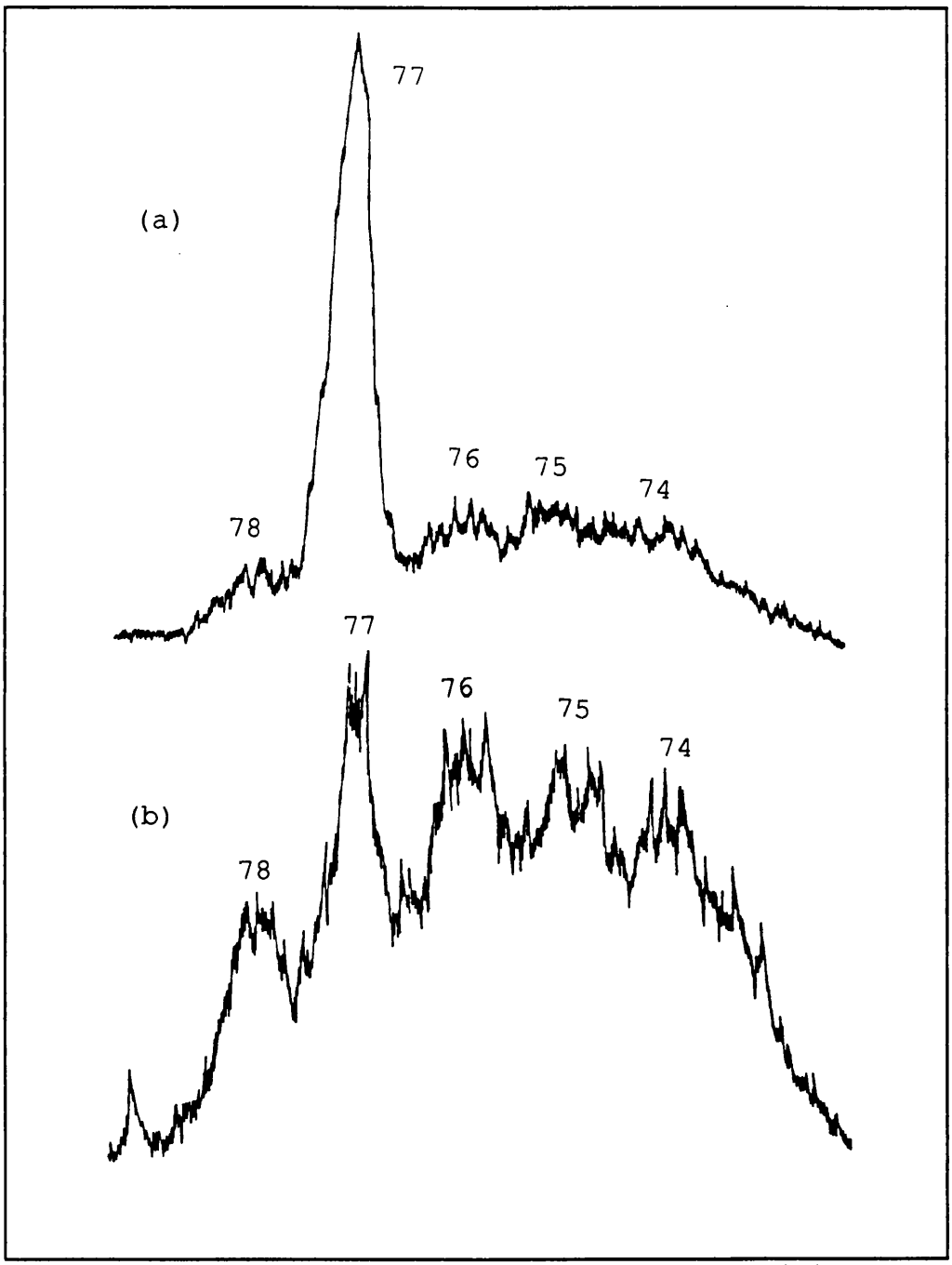

Figure 46 Partial CID spectrum of the $[M-CS]^+$ ion from (a) 3- and (b) 4-mercaptoquinoline (V_C=0)

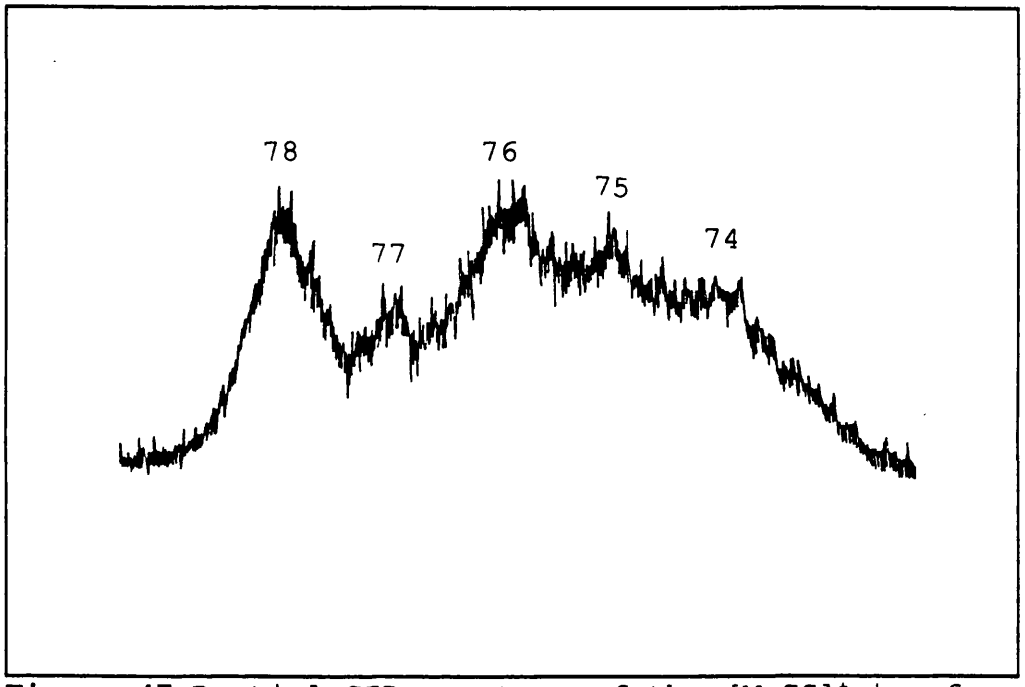

Figure 47 Partial CID spectrum of the $[M-CS]^+$ ion from (a) 8-mercaptoquinoline (V_c=0)

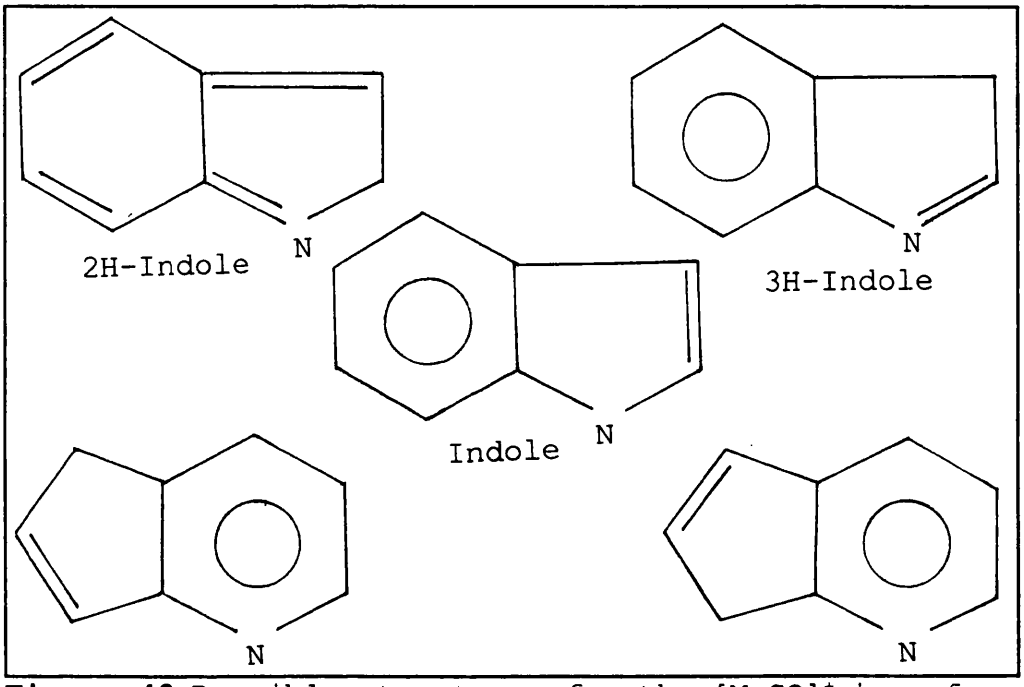

Figure 48 Possible structures for the $[M-CO]^+$ ions from the hydroxyquinoline isomers

Compound:	[78]	[77]	[76]	[75]	[74]
2-OHQ	36±5	62±6	97±7	98±6	100
3-OHQ	24±6	100	49±3	49±3	48±3
4-OHQ	23±2	100	54±3	56±3	55±3
5-OHQ	100	26±3	32±3	30±3	25±3
8-OHQ	100	54±3	57±4	83±5	77±4
Indole	26±4	78±5	100	83±6	75±5

Table 8: Relative intensities of m/z 74 to 78 in the high energy CID spectra of the $[M-CO]^{+\cdot}$ ions from 2-, 3-, 4-, 5- and 8-hydroxyquinoline (OHQ) and the $M^{+\cdot}$ ion from indole. Intensities are normalised to the largest peak in the group. V_c=0

Compound:	[78]	[77]	[76]	[75]	[74]
2-OHQ	30±5	43±5	79±6	94±6	100
3-OHQ	4±5	7±6	87±7	100	98±6
4-OHQ	36±4	59±5	89±6	99±5	100
5-OHQ	100	27±5	30±4	30±4	28±4
8-OHQ	100	59±5	94±6	94±6	89±6
Indole	25±2	48±5	84±6	94±6	100

Table 9: Relative intensities of m/z 74 to 78 in the high energy CID spectra of the $[M-CO]^{+\cdot}$ ions from 2-, 3-, 4-, 5- and 8-hydroxyquinoline and the $M^{+\cdot}$ ion from indole. Intensities are normalised to the largest peak in the group. V_c=1.6kV

Compound:	[78]	[77]	[76]	[75]	[74]
2-SHQ	24±5	44±6	72±7	78±7	100
3-SHQ	14±2	100	24±2	22±3	21±2
4-SHQ	53±4	100	89±4	83±5	71±4
8-SHQ	98±8	61±7	100	88±8	71±8

Table 10: Relative intensities of m/z 74 to 78 in the high energy CID spectra of the $[M-CS]^{+\cdot}$ ions from 2-, 3-, 4- and 8-mercaptoquinoline. Intensities are normalised to the largest peak in the group. $\mathbf{V}_C$=0

4.1.3 Deuterium Labelling

4.1.3.1 Introduction

When a labelled molecule fragments, the label will be located on either

(a) the ionic fragment

$$[D\text{-}AB\text{-}H]^{+\cdot} \rightarrow [D\text{-}A]^{+\cdot} + [B\text{-}H]$$

or (b) the neutral fragment.

$$[H\text{-}AB\text{-}D]^{+\cdot} \rightarrow [H\text{-}A]^{+\cdot} + [B\text{-}D]$$

Comparing the expected results from the labelled molecule with those for the unlabelled molecule

$$[H\text{-}AB\text{-}H]^{+\cdot} \rightarrow [H\text{-}A]^{+\cdot} + [B\text{-}H]$$

may reveal the extent of H/D randomisation associated with a particular reaction.

Isotopic labelling experiments were carried out to determine whether or not hydrogen migration took place in the $[M\text{-}CO]^{+\cdot}$ ions of the hydroxyquinolines and the $[M\text{-}CS]^{+\cdot}$ ions of the mercaptoquinolines.

4.1.3.2 Experimental

The following compounds were studied

2-, 3-, 4-, 5- and 8-hydroxyquinoline

2- and 8-mercaptoquinoline

which were of commercial origin and used without further purification. In each case the sample was introduced using the direct insertion probe, ionised with 70eV electrons and the ions accelerated through 8kV. The source temperature was maintained at ~200°C.

Data was recorded using a UV oscilloscope and UV sensitive paper. Each scan was recorded several times to examine the reproducibility of the data.

Deuterium exchange was achieved by introducing 1-2 μl of D_2O through the heated sample inlet as the sample was introduced via the direct insertion probe. In the case of the hydroxyquinolines, the daughters of the labelled molecular ion (labelled with one deuterium) after the loss of CO, $[M_D\text{-}CO]^{+\cdot}$, were examined and compared with the corresponding results for the unlabelled precursors, $[M_H\text{-}CO]^{+\cdot}$. A similar comparison was carried out with labelled and unlabelled mercaptoquinoline after the loss of CS, $[M_D\text{-}CS]^{+\cdot}$ and $[M_H\text{-}CS]^{+\cdot}$ respectively.

High energy CID spectra were obtained by scanning the instrument in a MIKES mode, selecting the labelled precursor ion with the magnet and scanning the ESA voltage dowm from the value corresponding to the energy of the precursor (nominally 8keV). Helium was admitted

into the second collision cell in the 2FFR, at a pressure sufficient to attenuate the main beam intensity by 30%.

4.1.3.3 Results and Discussion

The spectra from the labelled compounds are illustrated in Figs 49-52 for the region m/z 74-78. They fall into two categories: firstly there are those that resemble the corresponding spectra for the unlabelled sample except that the daughter ion peaks are increased by one mass unit, but they retain the same relative intensities (Fig 53). Secondly, there are those that give a more complex spectrum made up of two sets of daughter ion peaks superimposed, one set identical in position to the peaks from the unlabelled experiment, summed with a second set shifted by one mass unit (Fig 54). This indicates extensive hydrogen migration is taking place.

Of those compounds examined only the two 2-isomers fell into the first category, the rest giving evidence of hydrogen migration.

The behaviour of the 2-isomers implies that after the initial CO loss, the deuterium atom moves to another site on the ion which is retained in the subsequent m/z 74-78 ion group. Therefore the CID fragmentation processes do not bring about H/D randomisation for these isomers.

Although the mechanism of these reactions are not

elucidated by these results, they confirm the unique character of the $[M-CO]^{+\cdot}$ and $[M-CS]^{+\cdot}$ ions from the 2-isomers.

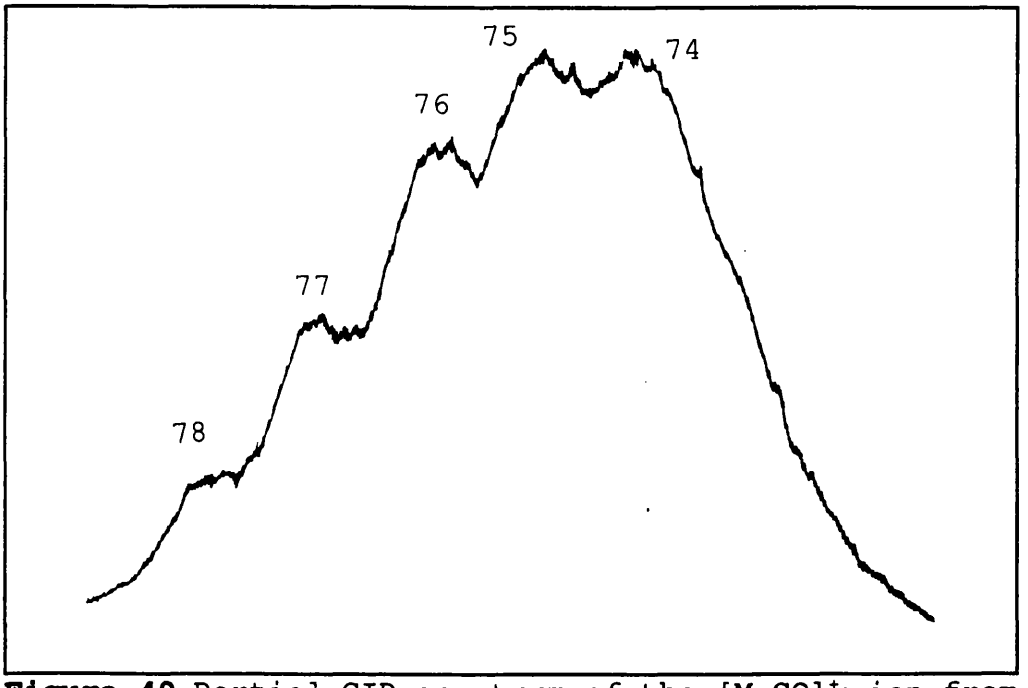

Figure 49 Partial CID spectrum of the $[M_D\text{-}CO]^{+\cdot}$ ion from (a) 2-hydroxyquinoline

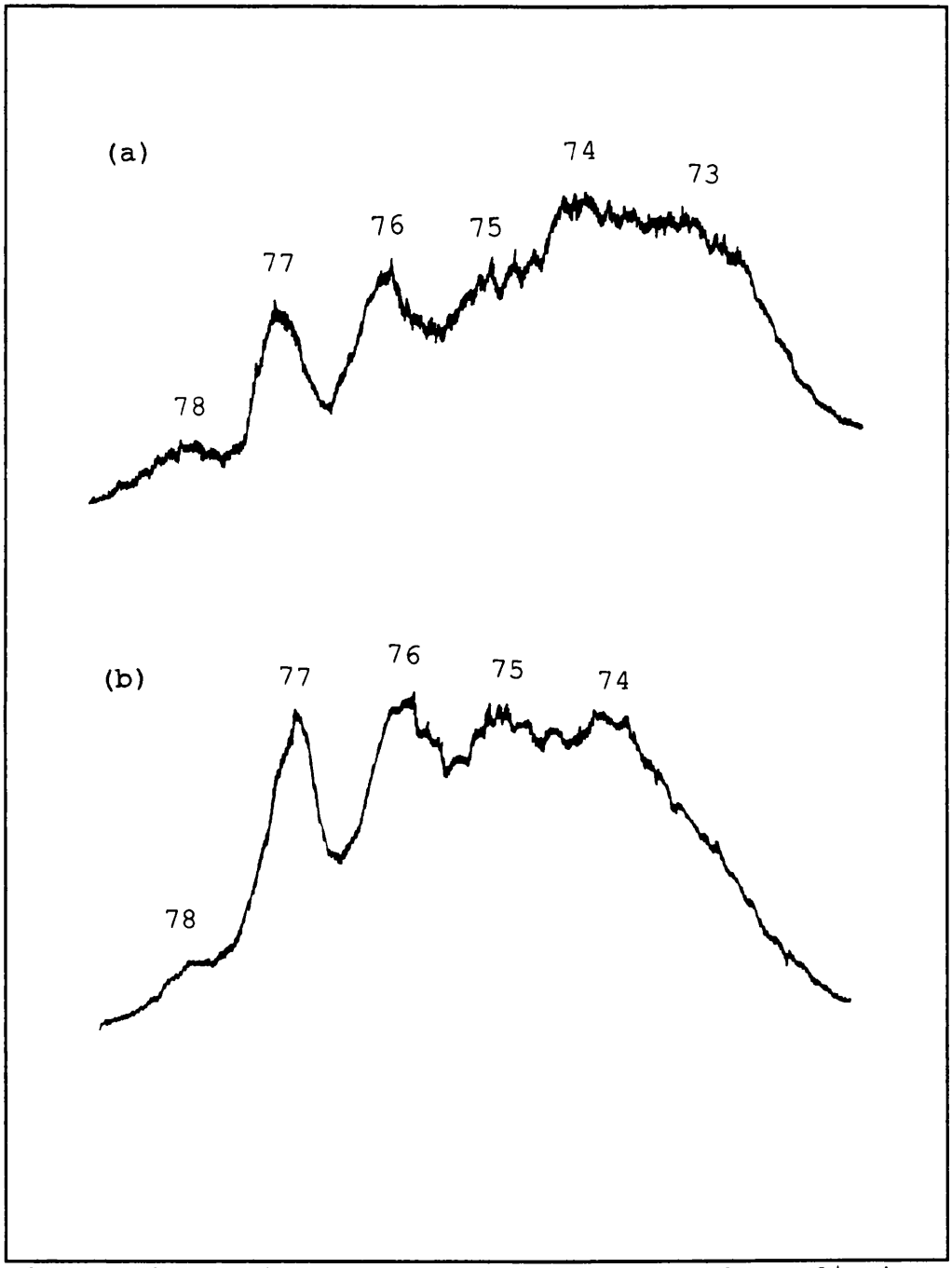

Figure 50 Partial CID spectrum of the $[M_b\text{-}CO]^{+\cdot}$ ions from (a) 3- and (b) 4-hydroxyquinoline

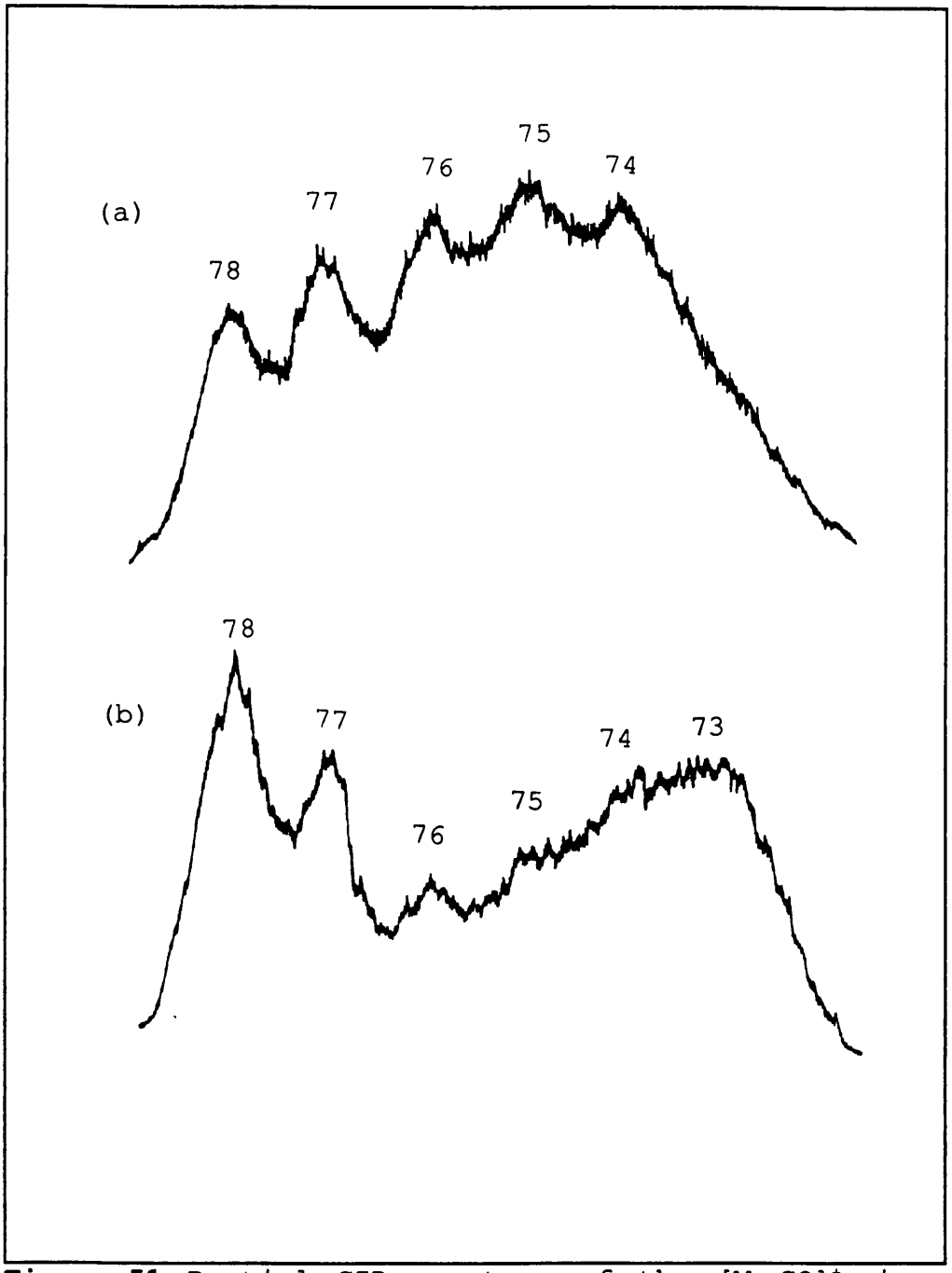

Figure 51 Partial CID spectrum of the $[M_b\text{-}CO]^{+\cdot}$ ions from (a) 5- and (b) 8-hydroxyquinoline

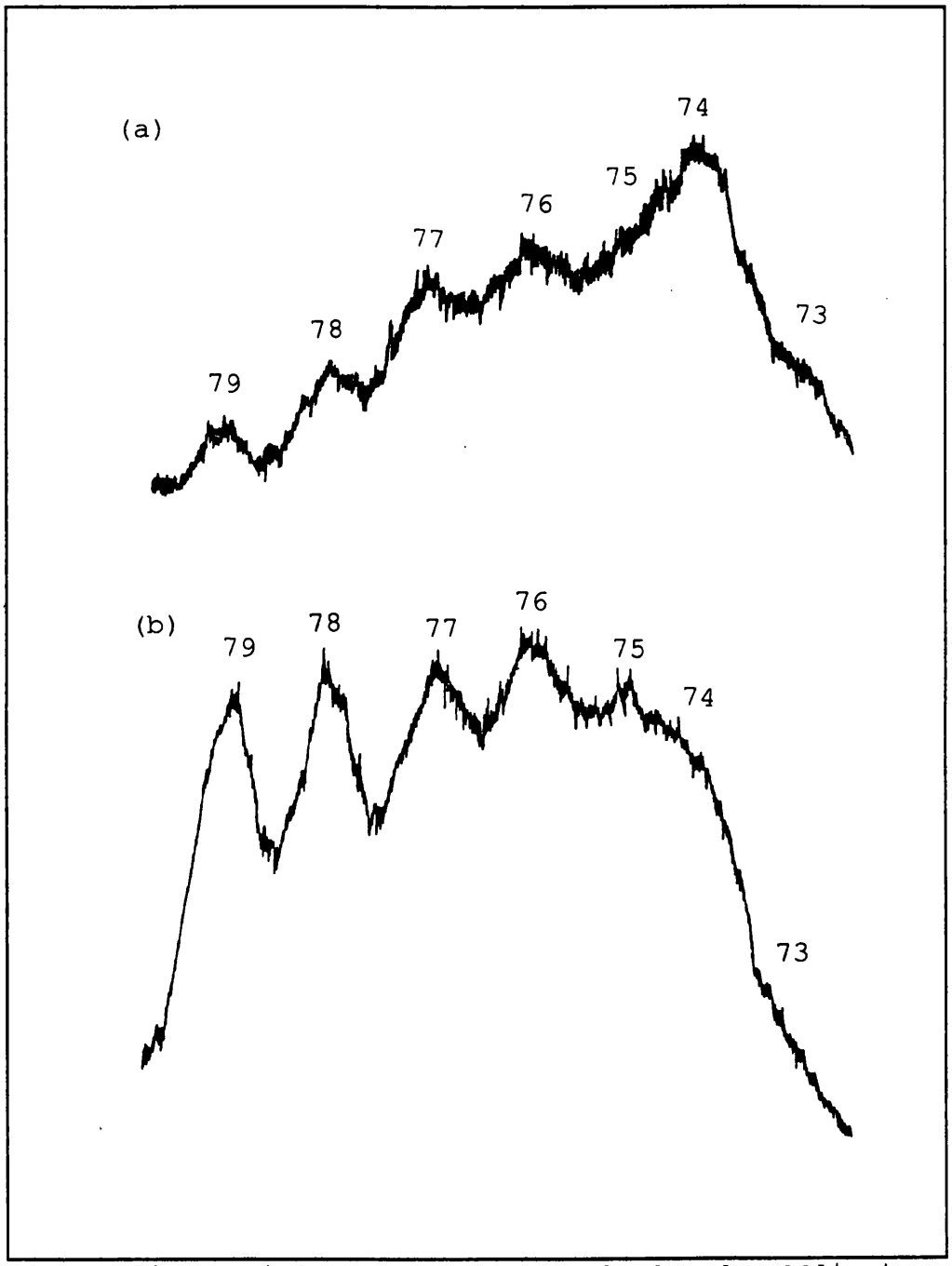

Figure 52 Partial CID spectrum of the $[M_D\text{-CS}]^{+\cdot}$ ions from (a) 2- and (b) 8-mercaptoquinoline

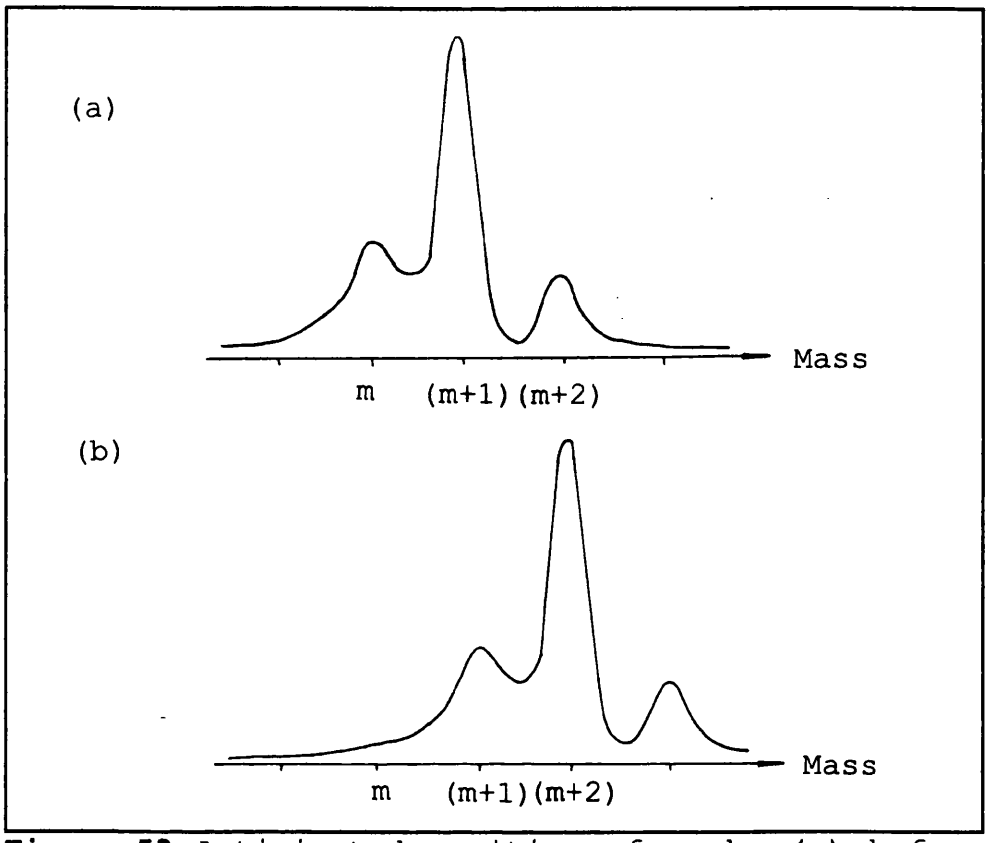

Figure 53 Anticipated position of peaks (a) before and (b) after deuterium labelling, when no H/D scrambling takes place

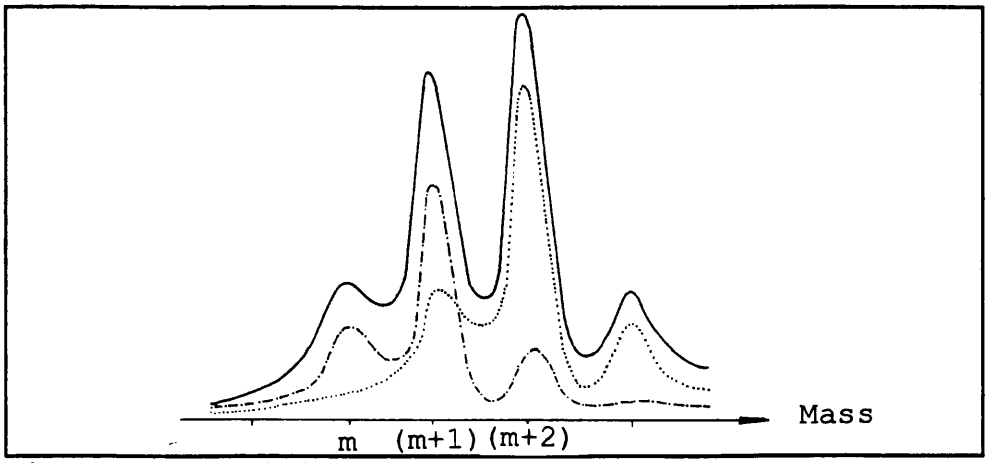

Figure 54 Anticipated appearance of spectra when H/D scrambling takes place

4.2 ISOMER DIFFERENTIATION BY NRMS

4.2.1 Introduction

Examples are given elsewhere in this thesis (see Sections 4.3 and 4.4) of the use of NRMS in structural determination. A study was therefore undertaken to examine the utility of NRMS in the field of isomer differentiation.

4.2.2 Experimental

The samples examined were

a) methyl iso-propylketone and methyl n-propylketone

b) o-, m-, p-methylphenol

c) o-, m-, p-aminophenol

d) o-, m-, p-cyanophenol

e) o-, m-, p-tolunitrile

f) 1-, 2-naphthonitrile

g) 2-, 3- ,4-hydroxypridine

h) o-tolunitrile, benzylcyanide

All the samples were obtained through commercial sources and were used without further purification. In each case approximately 5µl of the sample was introduced through the heated septum inlet, ionised with 70eV

electrons and the ions accelerated through 8 kV. The source temperature was maintained at ~200°C.

Although every effort was made to record this data using the available data system, it was found that with these particularly weak spectra computer acquisition and averaging did not enhance the data and the data were more prone to the problems of noise. Using a high response time (in the order of 100-300 ms) and slow scan speed (several minutes) NRMS spectra were recorded using the UV oscillograph and UV sensitive paper. Each scan was repeated several times to ensure its reproducibility.

NRMS spectra were obtained by scanning the instrument in the manner used for MIKES, selecting the precursor ion with the magnet and scanning the ESA down from the energy of the precursor (nominally 8kV). The neutralisation gas $\mathbf{G}_1$ was admitted to the first cell in the 2FFR at a pressure sufficient to cause a x% attenuation of the main beam intensity, '$\mathbf{G}_1$(x)' ; the reionisation gas $\mathbf{G}_2$ was admitted to the second cell in the 2FFR again at a pressure giving y% attenuation of the main beam intensity '$\mathbf{G}_2$(y)'. The experimental conditions for the spectrum could then be described by '$\mathbf{G}_1$(x)/$\mathbf{G}_2$(y)'.

The deflector plate between the two gas cells was set at 1kV which had been found adequate to prevent any residual ions from the first cell entering the second collision cell.

4.2.3 Results and Discussion

The majority of samples that were examined were aromatic in structure, the isomers usually differing by the position of one group on the ring.

a) methyl iso-propylketone and methyl n-propylketone

The two spectra (Fig 55,56) have the same groups of peaks but with differences in the relative intensities of the peaks within several of the groups. The spectrum for methyl iso-propyl ketone shows an intense peak at m/z 71 (loss of CH_3) probably due to decomposition of the isopropyl group in addition to the anticipated α cleavage at the carbonyl; there is also a stronger peak at m/z 15. This spectrum also shows a stronger peak at m/z 43, reflecting the greater tendency for cleavage at the branch site. The peak probably contains a component due to the more stable $(CH_3)_2CH$- fragment ion as well as the acetyl ion. The spectrum for methyl n-propyl ketone has a more intense peak at m/z 28, it seems likely that C_2H_4 would be more easily formed from this structure.

b) o-, m-, p-methylphenol

Examination of these spectra (Fig 57-59) showed no differences.

c) o-, m-, p-aminophenol

From the complete spectra (Fig 60-62) two groups of peaks showed differences between the three isomers, these being m/z 24-28 and m/z 36-41, in particular the ratios of [m/z 27]:[m/z 28] and [m/z 37]:[m/z 38]. It can be seen that these ratios are subtly different for each isomer (Fig 63).

d) o-, m-, p-cyanophenol

The spectra again showed only a subtle difference, in this case the ratios of [m/z 37]:[m/z38]:[m/z 39] (Fig 64).

e) o-, m-, p-tolunitrile

These spectra (Fig 65-67) appear identical in all respects.

f) 1-, 2-naphthonitrile

No significant differences could be seen between these two spectra (Figs 68,69).

g) 2-, 3- ,4-hydroxypridine

Differences were seen between the three spectra (Fig 70-72) in respect to the peak groups m/z 25-28 and m/z 38-40. The 2- and 3-isomers differed in the relative intensities of the peaks at m/z 25-30, and the 3- and 4-isomers differed in their ratios of [m/z 38]:[m/z 39]:[m/z 40].

h) o-tolunitrile, benzylcyanide

The two spectra (Fig 65,73) were essentially the same, differing in the relative intensities of the peaks in group m/z 74-77.

The common feature of the comparisons of the aromatic species, all of which involve a change in position of a functional group around the ring, was the small or negligable differences seen between the spectra. In all cases the spectra were recorded several times to confirm the data and where differences have been described these have been confirmed as significant. Those positional isomers that gave apparently identical NRMS spectra, b), e) and f), may reveal very minor differences on even more careful study but this seems unlikely.

The disadvantage of studying such aromatic compounds is that they experience much more complex reactions, making it extremely difficult to rationalise the differences seen. Contrast this data with that in a) for two simple aliphatic ketones, where the differences in the NRMS spectra can be rationalised in terms of known structural differences. This is in broad agreement with the experience from other mass spectrometric techniques in that the positional isomers of aromatic compounds are notoriously difficult to differentiate. On ionisation they rapidly isomerise to give common structures or mixtures of interconverting structures. By contrast,

aliphatic ions retain much of their original character and can be readily distinguished in most cases.

It should be stressed that this a preliminary study and this work has yet to be compared with isomer differentiation by alternative methods such as high energy CID.

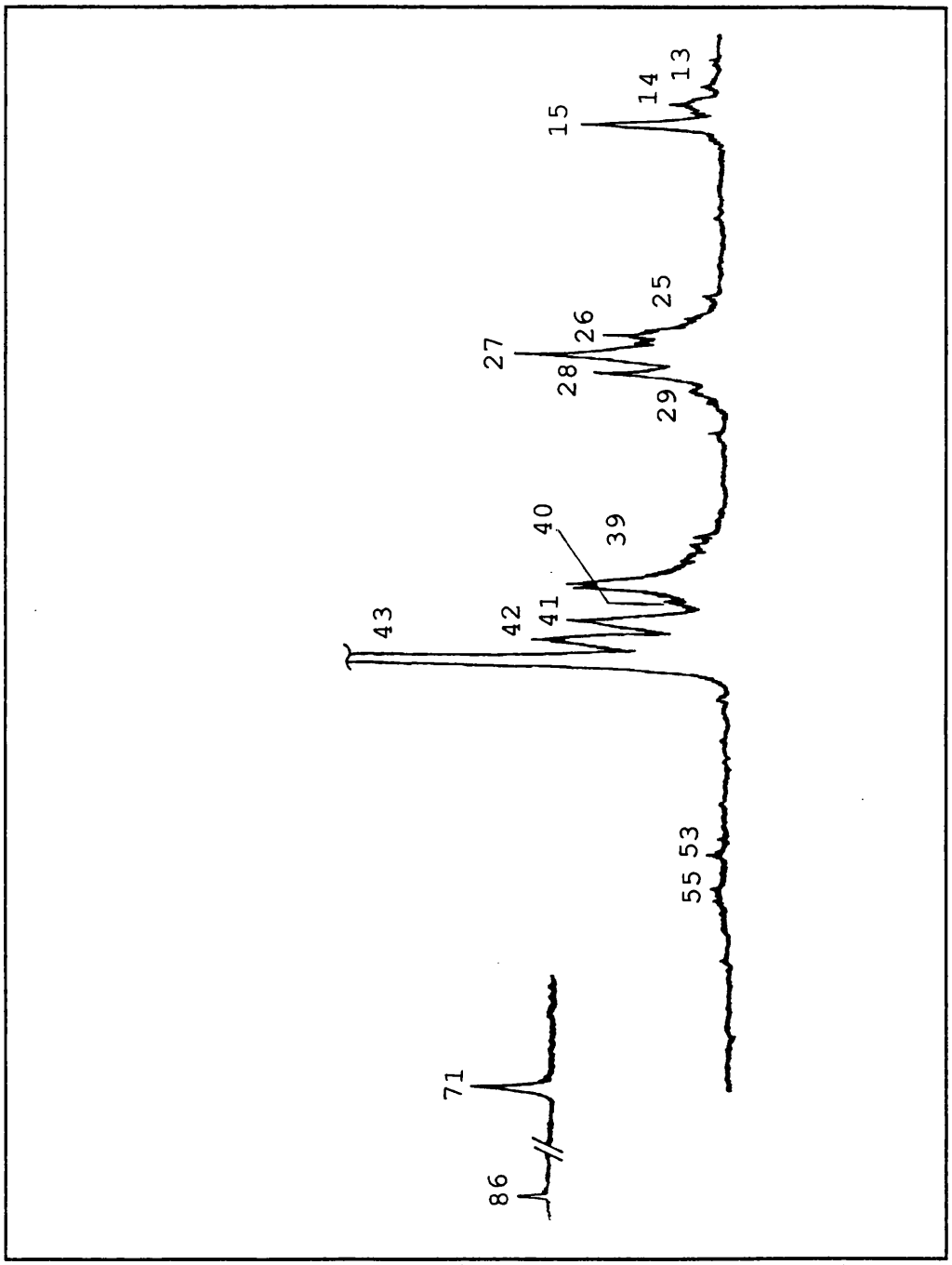

Figure 55 NRMS ($Xe(10)/O_2(10)$) spectrum of the molecular ion of methyl iso-propyl ketone

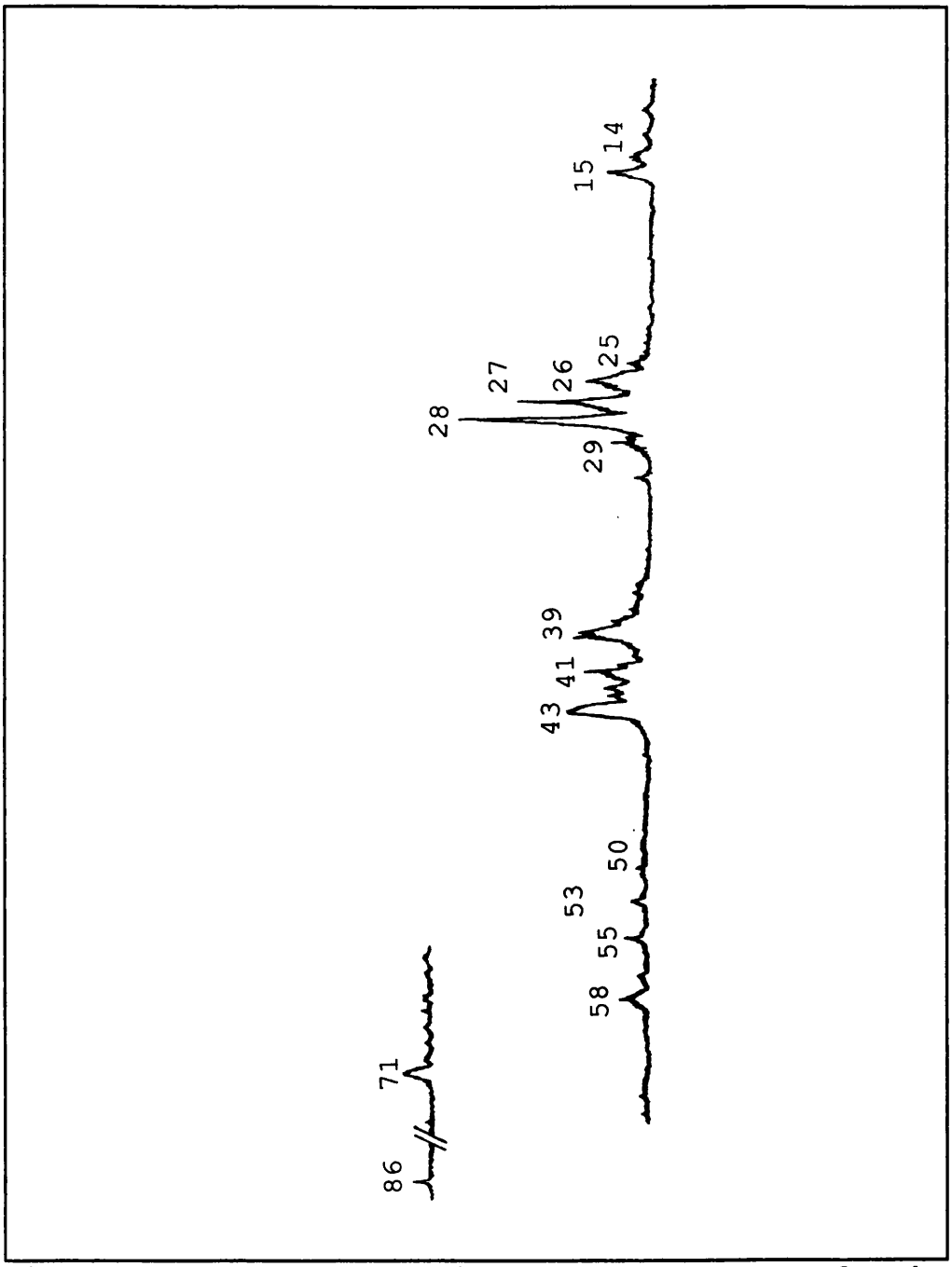

Figure 56 NRMS ($Xe(10)/O_2(10)$) spectrum of the molecular ion of methyl n-propyl ketone

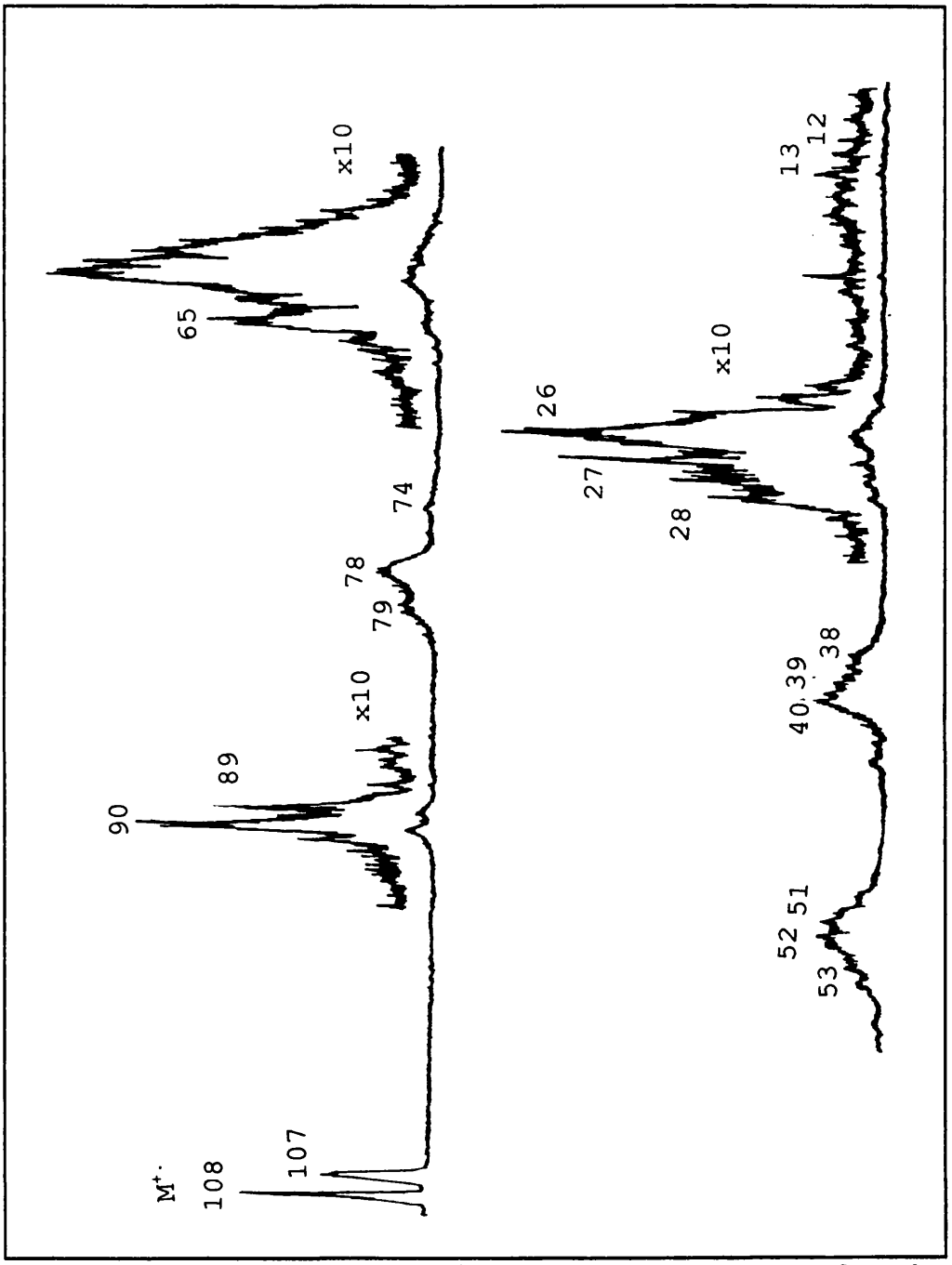

Figure 57 NRMS (Xe(10)/O_2(10)) spectrum of the molecular ion of o-methylphenol

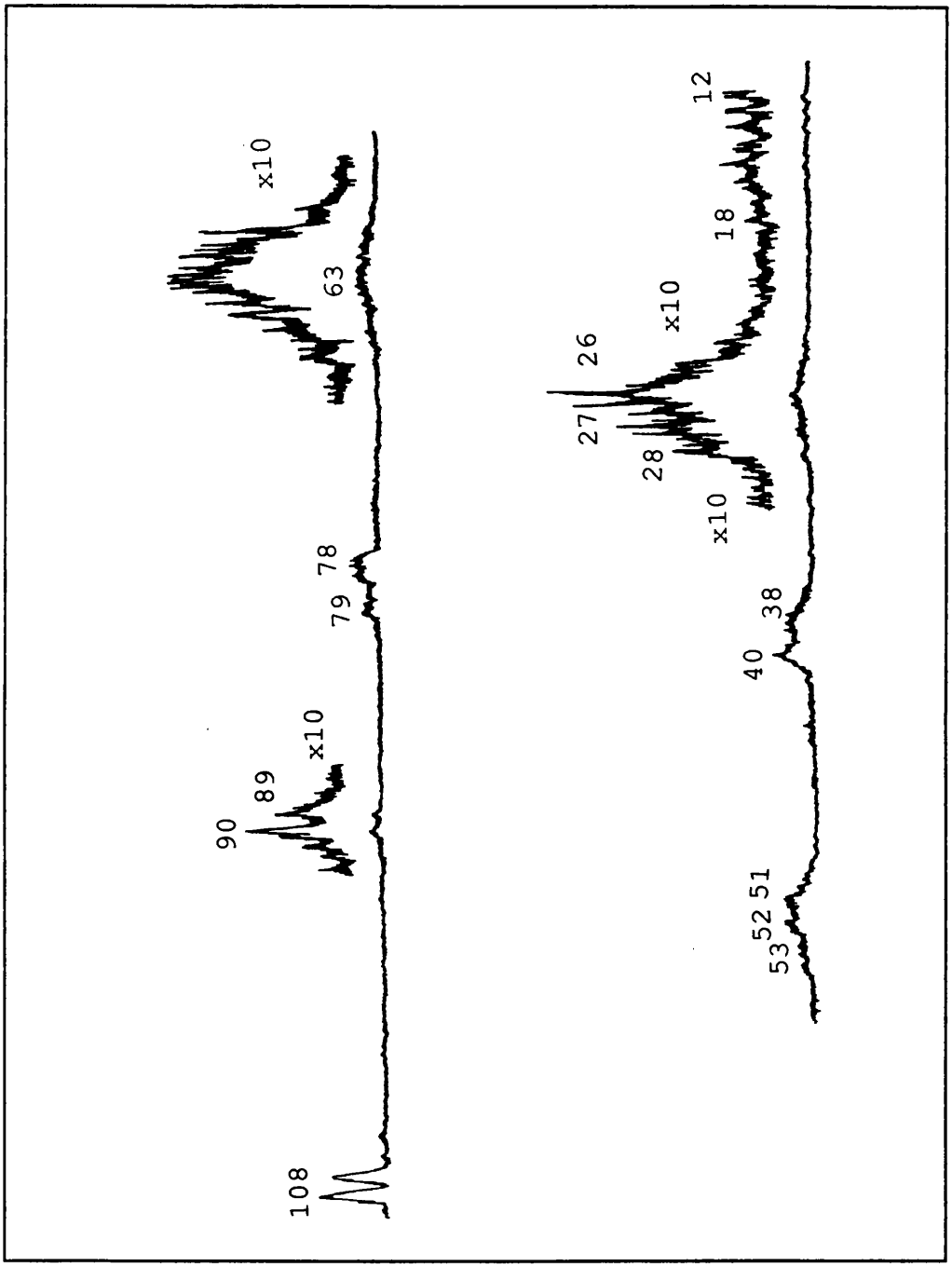

Figure 58 NRMS (Xe(10)/O_2(10)) spectrum of the molecular ion of m-methylphenol

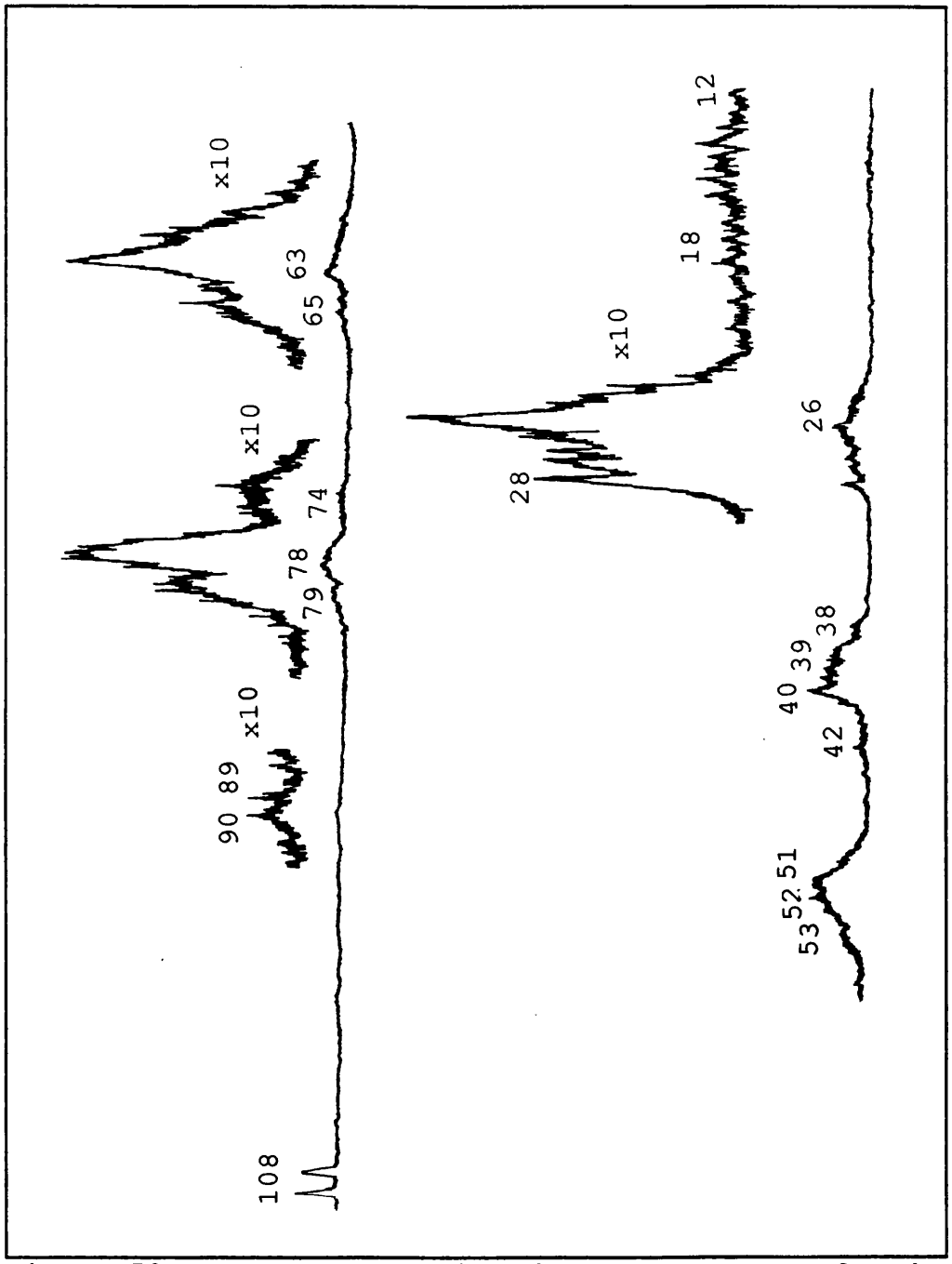

Figure 59 NRMS ($Xe(10)/O_2(10)$) spectrum of the molecular ion of p-methylphenol

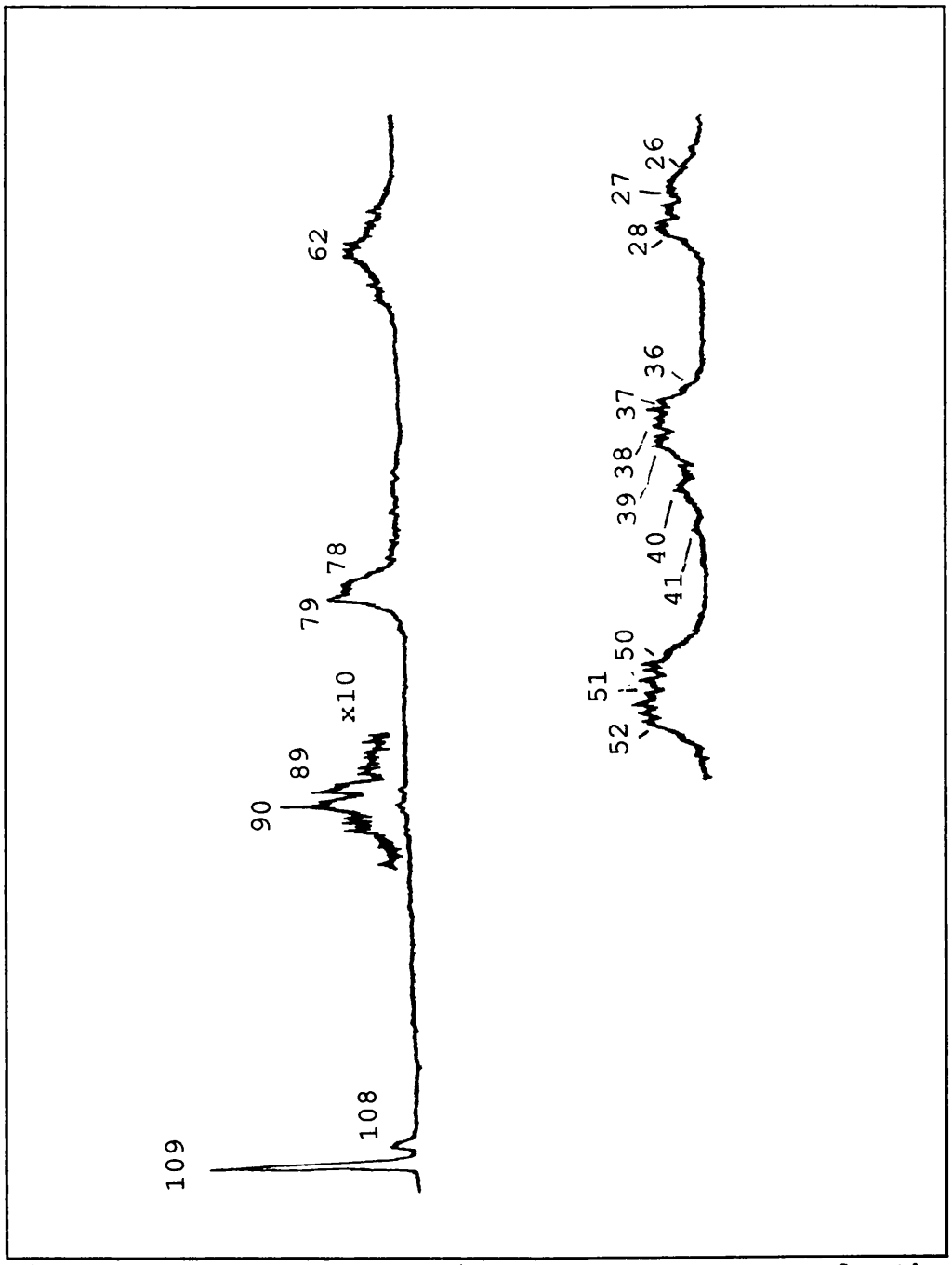

Figure 60 NRMS (Xe(10)/O_2(10)) spectrum of the molecular ion of o-aminophenol

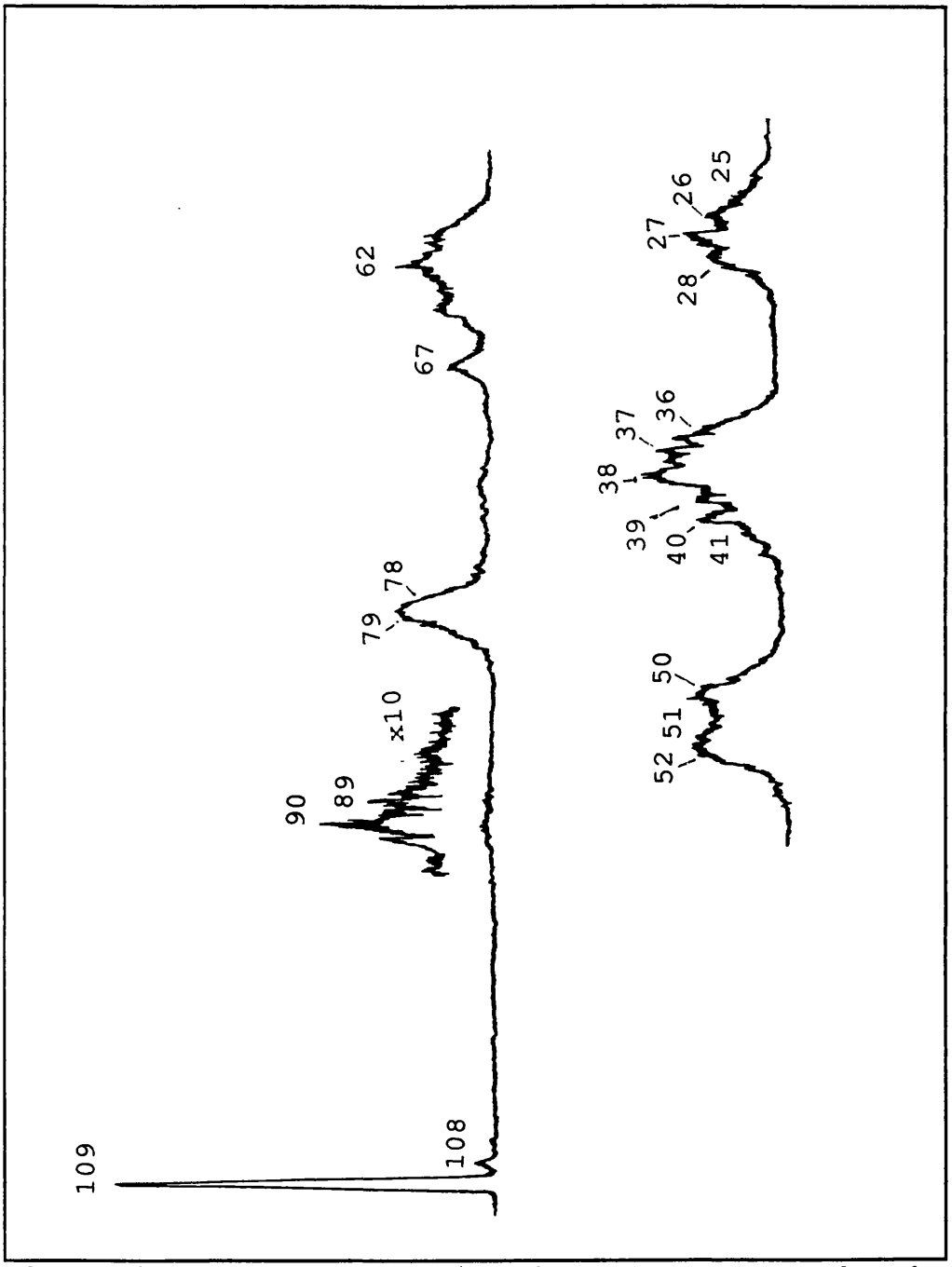

Figure 61 NRMS (Xe(10)/O_2(10)) spectrum of the molecular ion of m-aminophenol

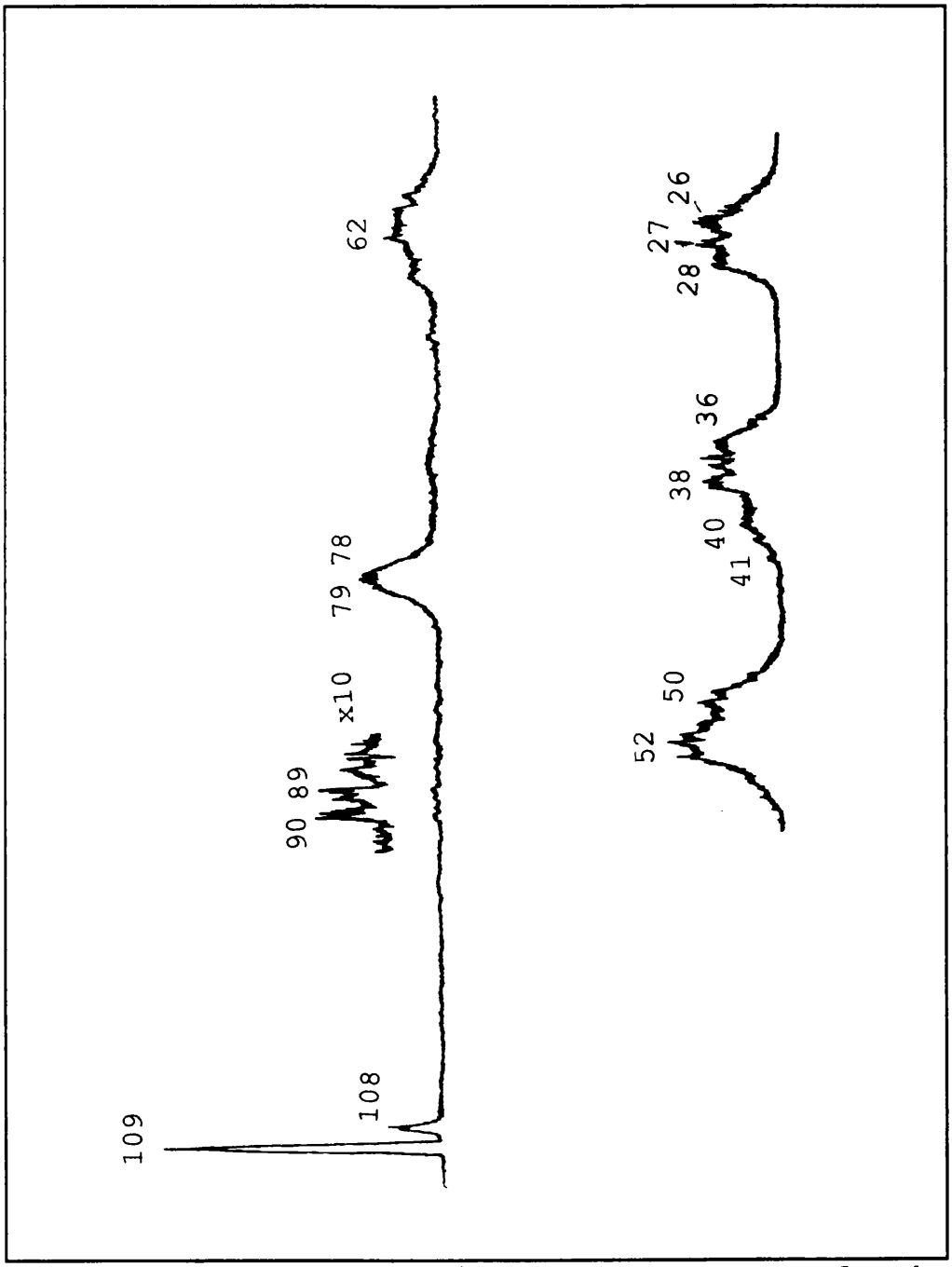

Figure 62 NRMS (Xe(10)/O_2(10)) spectrum of the molecular ion of p-aminophenol

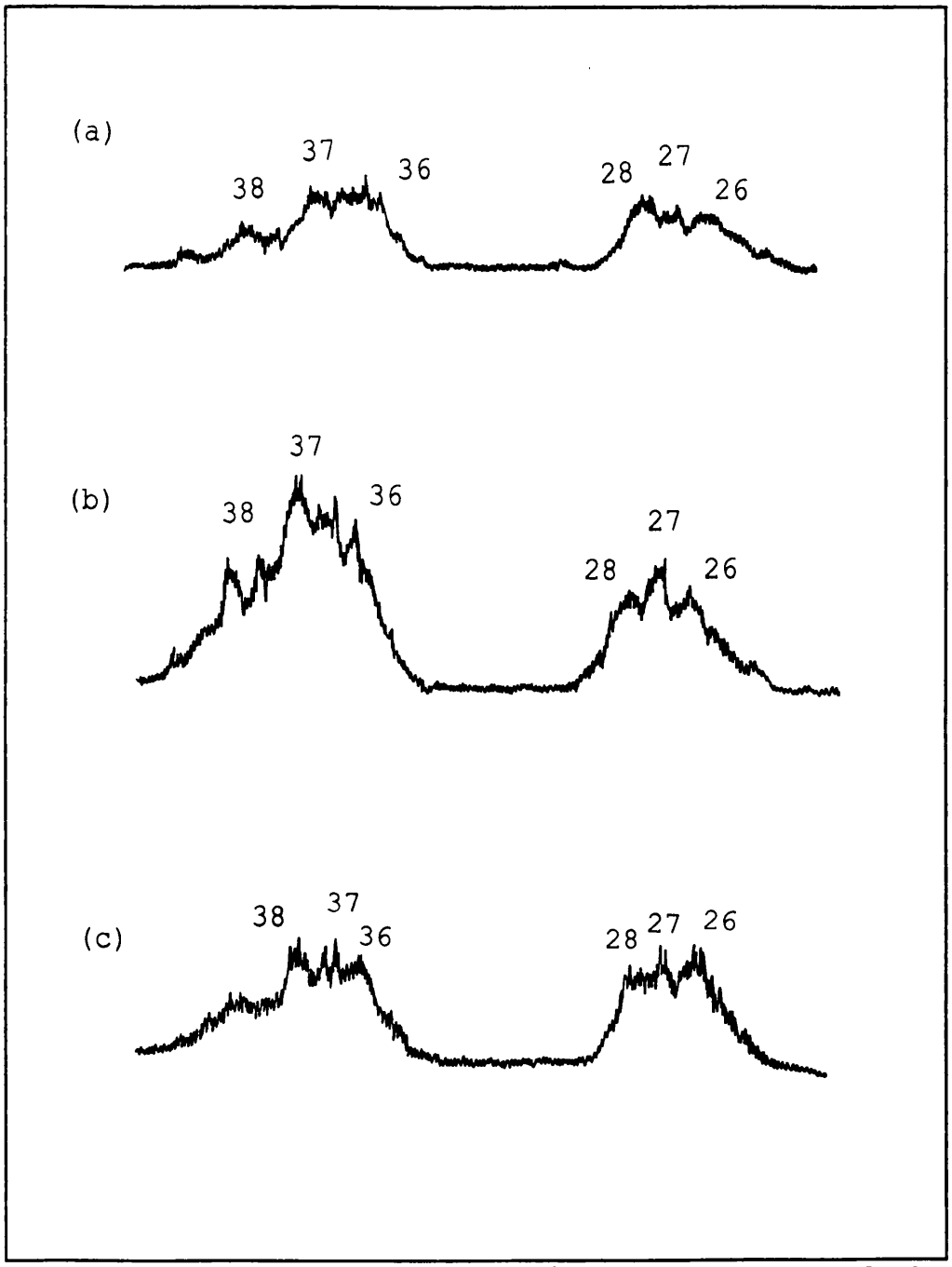

Figure 63 Partial NRMS ($Xe(10)/O_2(10)$) spectra of the molecular ions of (a) o- (b) m- and (c) p-aminophenol

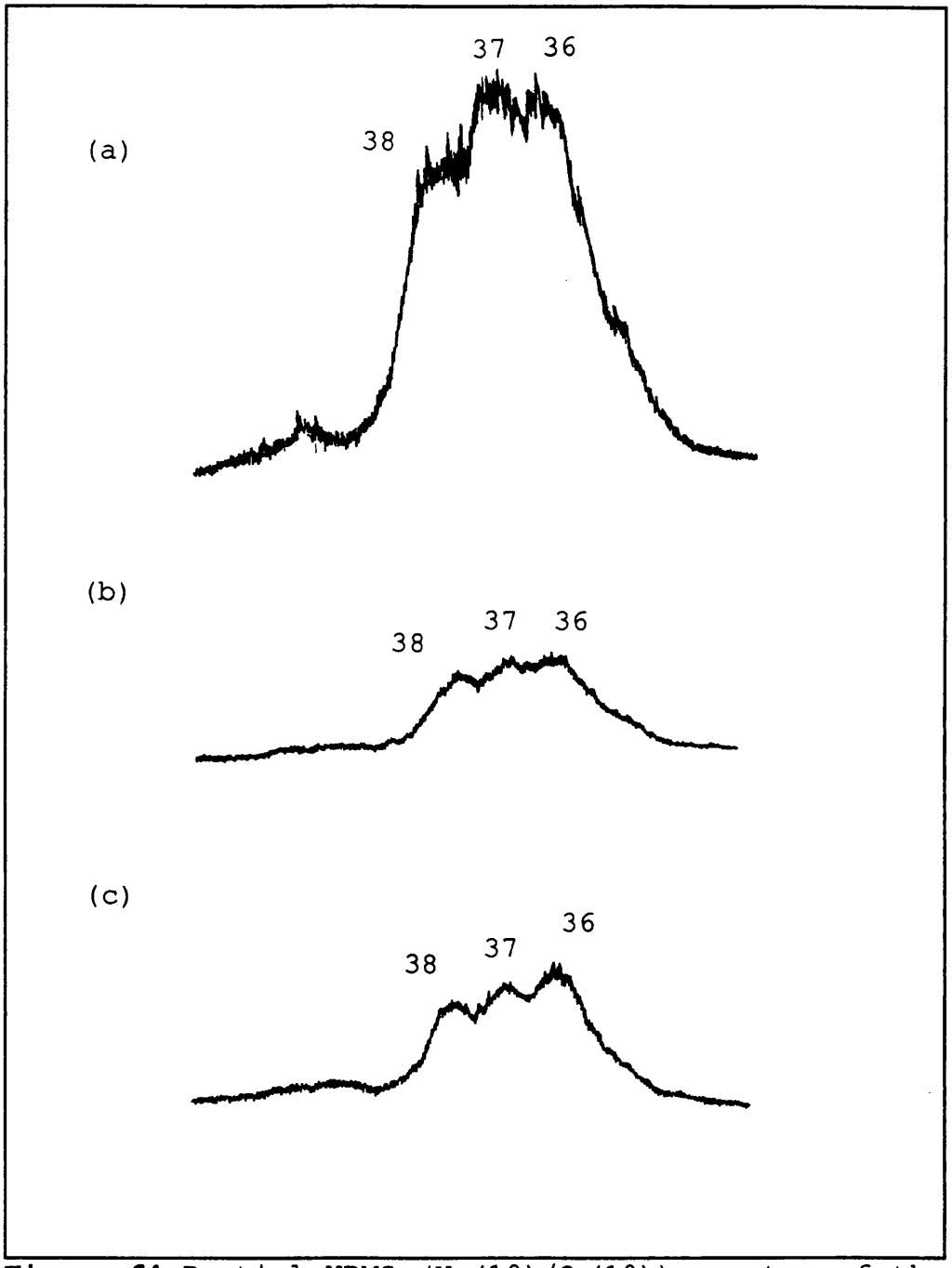

Figure 64 Partial NRMS ($Xe(10)/O_2(10)$) spectra of the molecular ions of (a) o- (b) m- and (c) p-cyanophenol

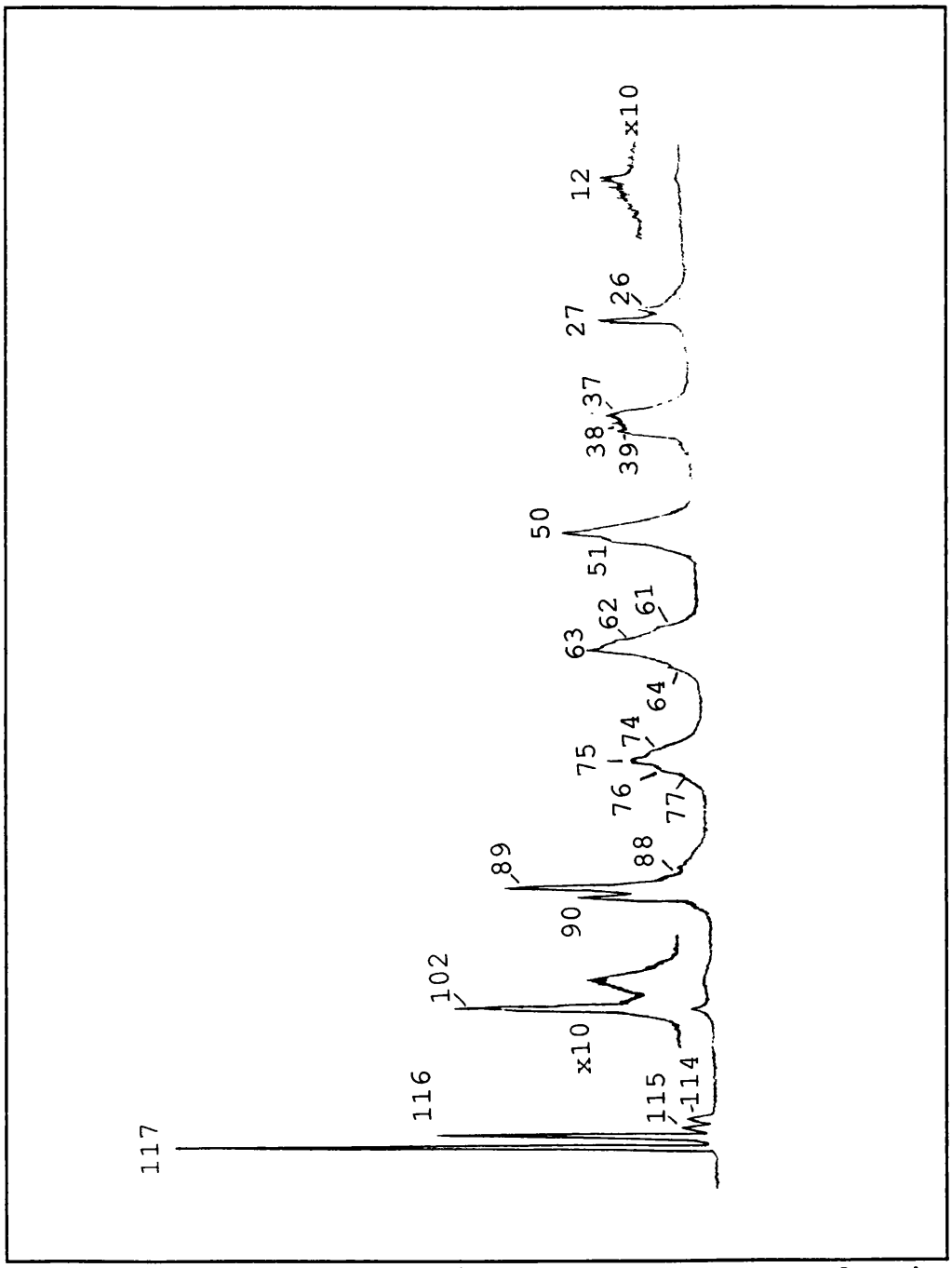

Figure 65 NRMS (Xe(10)/O_2(10)) spectrum of the molecular ion of o-tolunitrile

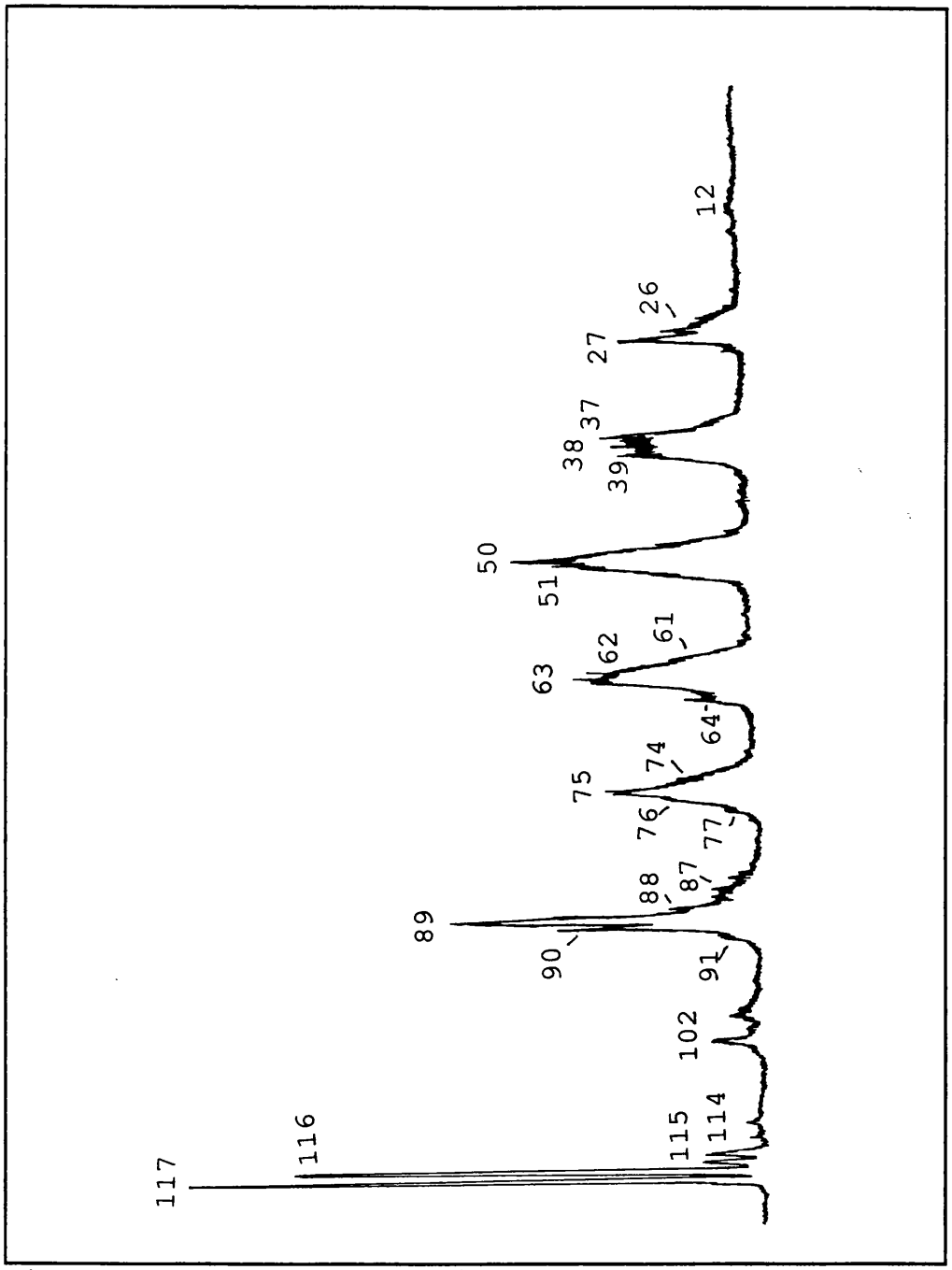

Figure 66 NRMS ($Xe(10)/O_2(10)$) spectrum of the molecular ion of m-tolunitrile

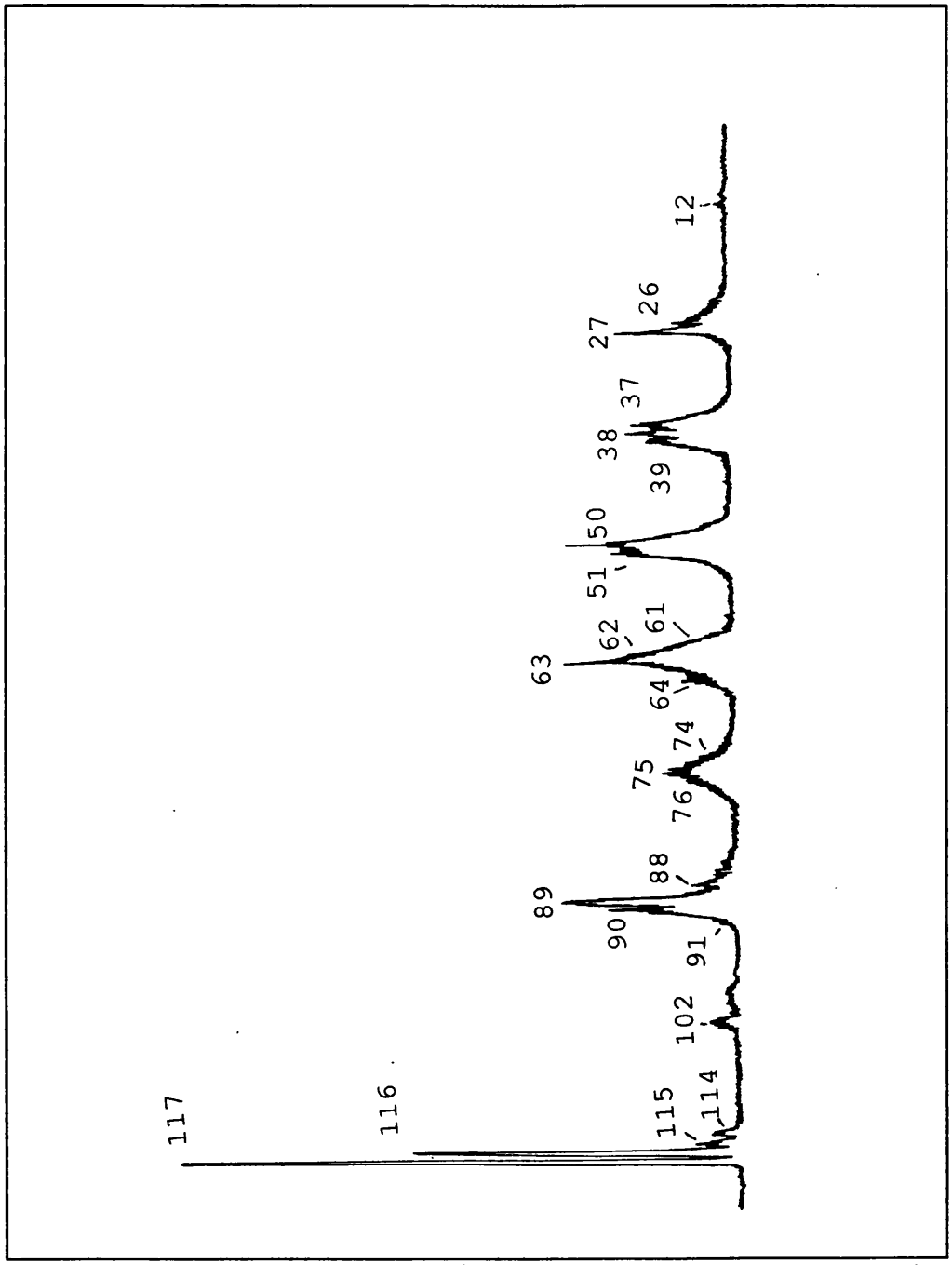

Figure 67 NRMS ($Xe(10)/O_2(10)$) spectrum of the molecular ion of p-tolunitrile

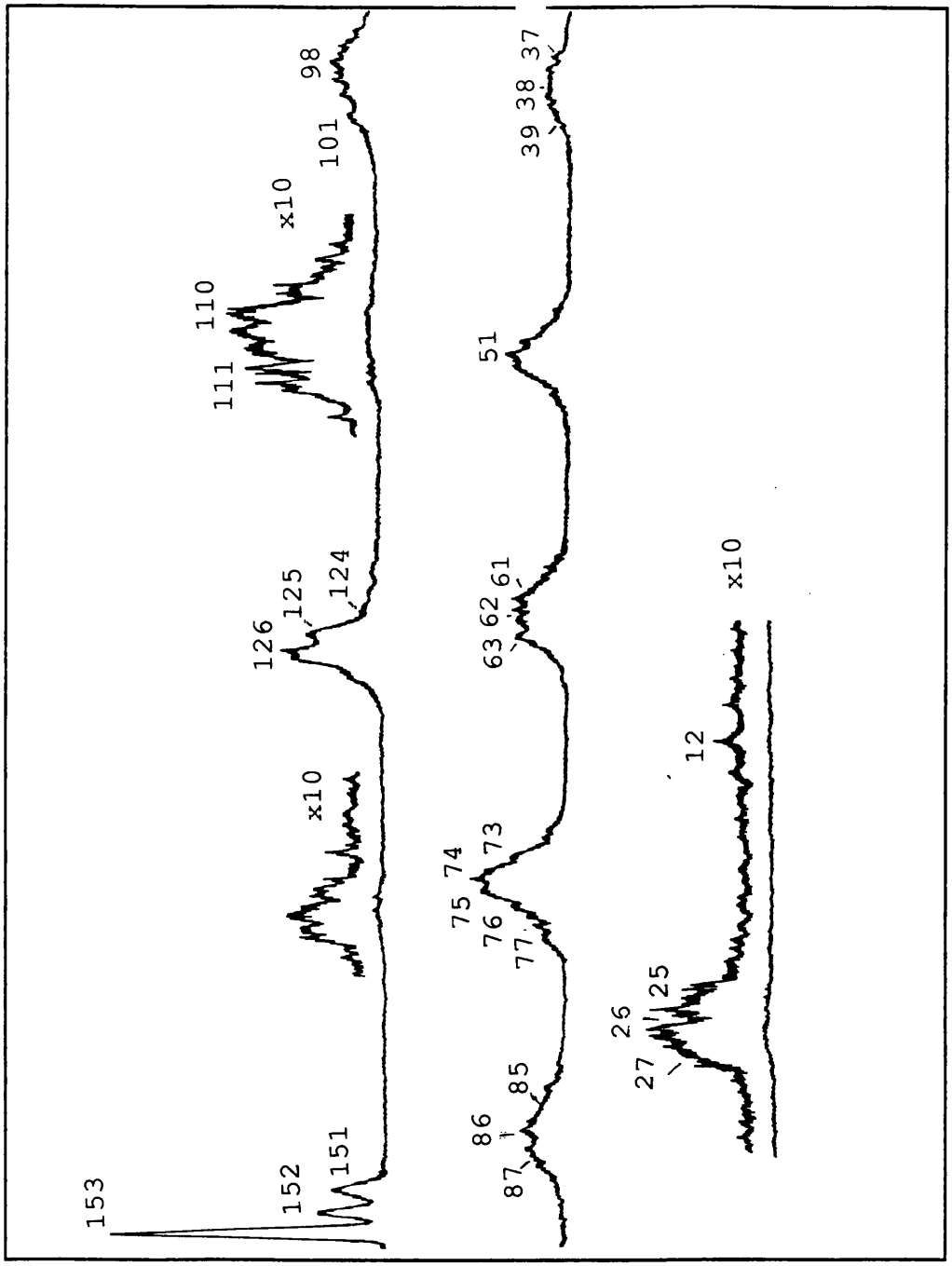

Figure 68 NRMS (Xe(10)/O_2(10)) spectrum of the molecular ion of 1-naphthonitrile

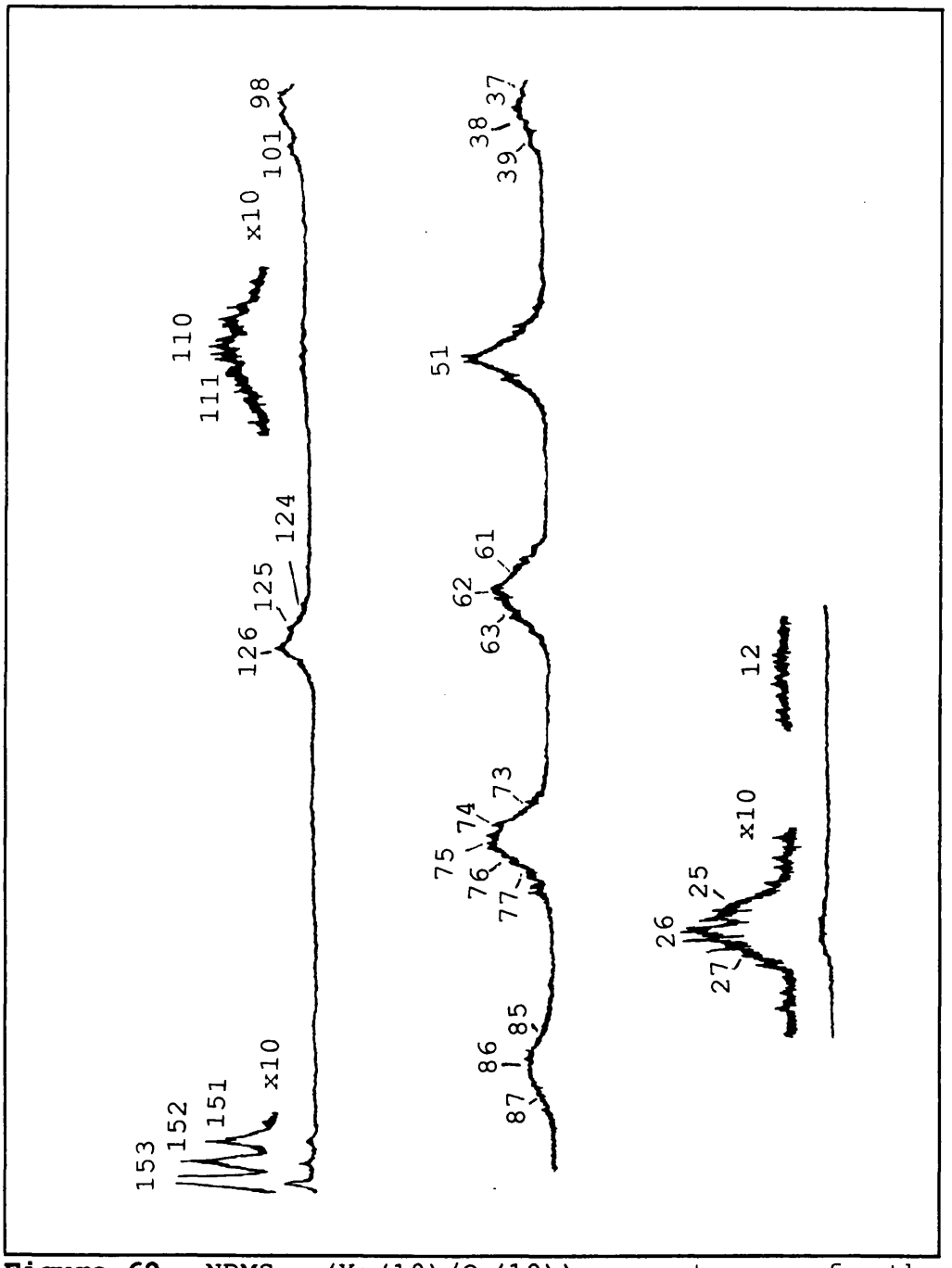

Figure 69 NRMS (Xe(10)/O_2(10)) spectrum of the molecular ion of 2-naphthonitrile

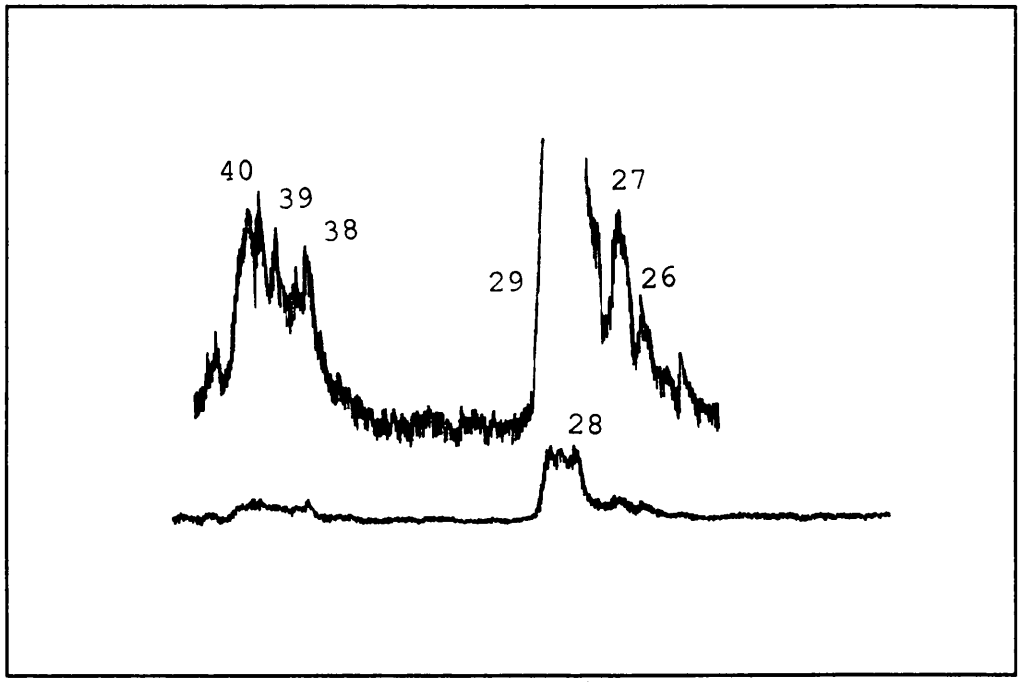

Figure 70 Partial NRMS (Xe(10)/O_2(10)) spectrum of the molecular ion of 2-hydroxypyridine

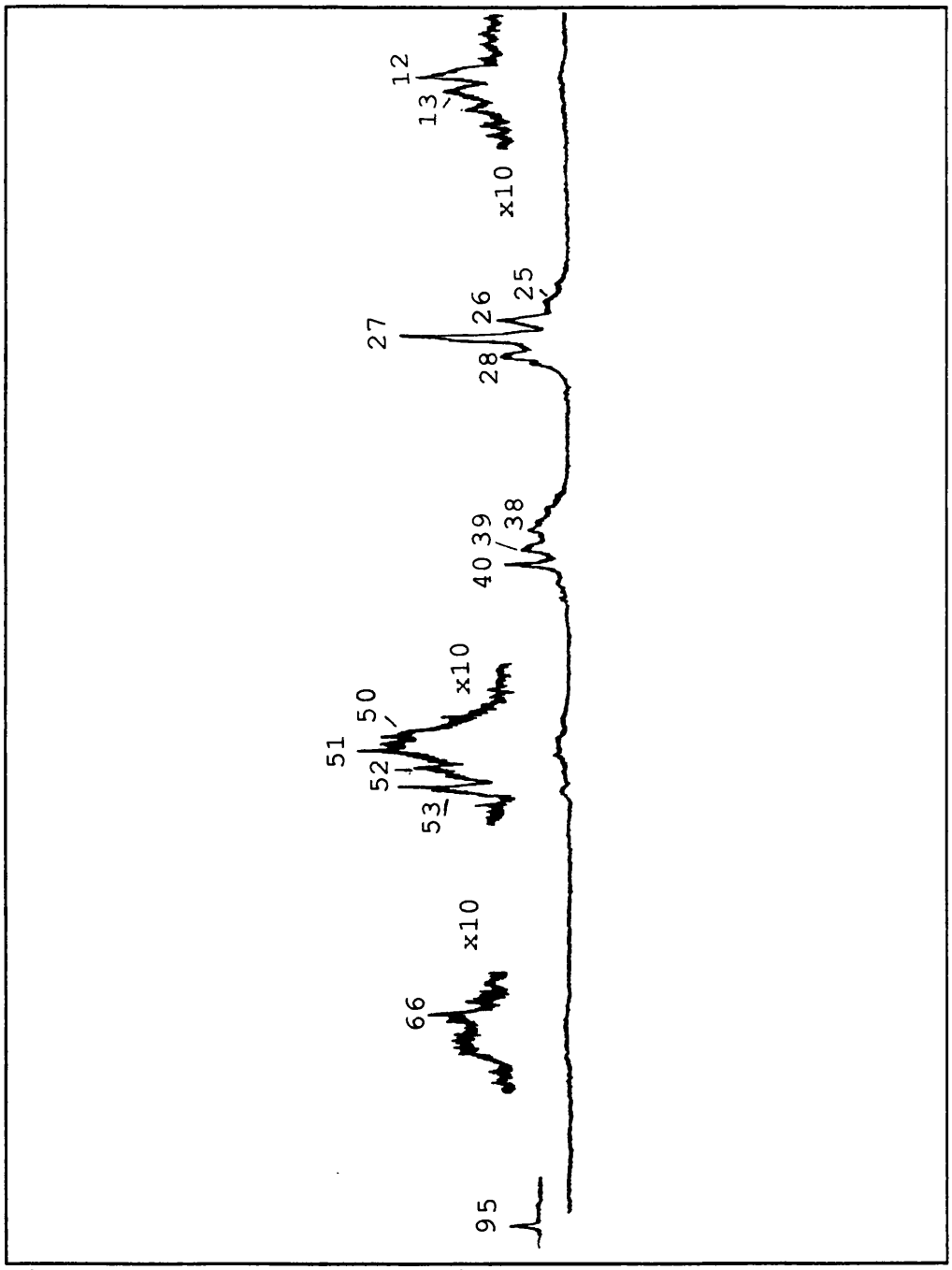

Figure 71 NRMS ($Xe(10)/O_2(10)$) spectrum of the molecular ion of 3-hydroxypyridine

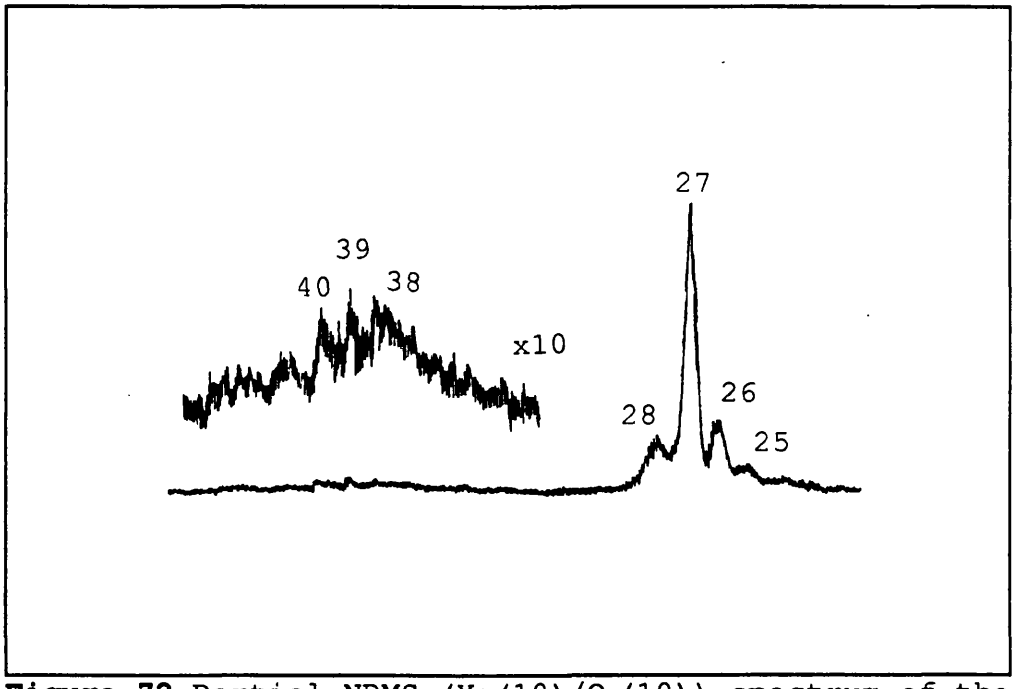

Figure 72 Partial NRMS ($Xe(10)/O_2(10)$) spectrum of the molecular ion of 4-hydroxypyridine

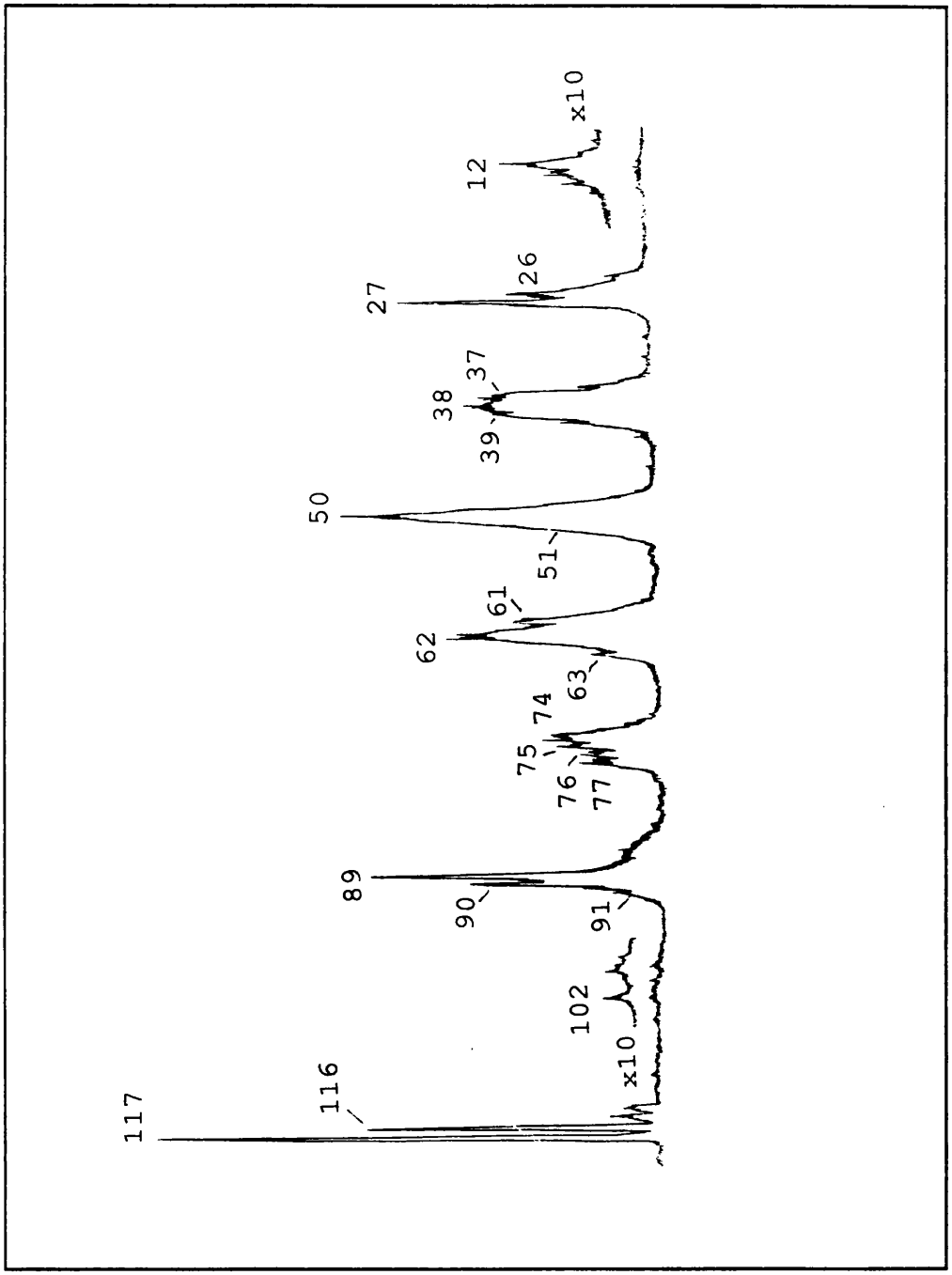

Figure 73 NRMS ($Xe(10)/O_2(10)$) spectrum of the molecular ion of benzylcyanide

4.3 FRAGMENTATION OF TERTIARY BUTYLBENZENE

4.3.1 Introduction

A range of tamdem mass spectrometrical techniques was used in the study of the fragmentation pattern of t.butylbenzene, identifying some of the major ionic and neutral components.

4.3.2 Establishing the Major Fragments of t-butyl benzene

High energy CID/MIKES spectra and neutralisation-reionisation spectra were used to establish the major fragmentaion route of t-butyl benzene.

4.3.2.1 Experimental

The tertiary butyl benzene used was obtained from a commercial source and used without furthur purification. Approximately 5µl of the sample was introduced through the heated septum inlet, ionised with 70eV electrons and accelerated through 8 kV. The source temperature was maintained at ~200°C.

All data except that for NRMS was acquired by the data system in multichannel analyser (MCA) mode and

averaged over several scans. The NRMS data was acquired over a single scan using a UV oscillograph. Each scan was repeated several times to examine the reproducibility of the data.

4.3.2.1.1 CID/MIKES

CID/MIKE spectra were obtained by admitting helium into the second of the collision cells in the 2FFR, at a pressure sufficient to attenuate the main beam intensity by 30%. The precursor ion was selected by the magnet and the ESA voltage scanned down from the value corresponding to the energy of the precurser ion (nominally 8keV).

4.3.2.1.2 B/E and B^2/E Linked Scans

B/E and B^2/E linked scans gave daughter ion and parent ion scans for fragmentations taking place in the 1FFR. Both the magnet and ESA were scanned together at a constant ratio under data system control.

4.3.2.1.3 NRMS

NRMS spectra were also obtained by scanning the

instrument in the manner used for MIKES. The neutralisation gas He was admitted to the first cell in the 2FFR at a pressure sufficient to cause a 10% attenuation of the main beam intensity, 'He(10)' ; the reionisation, oxygen, was admitted to the second cell in the 2FFR again at a pressure giving 10% attenuation of the main beam intensity 'O_2(10)'. The deflector plate between the two gas cells was set at 1kV which had been found adequate to prevent any residual ions from the first cell entering the second collision cell.

4.3.2.2 Results and Discussion

Linked scans of the molecular ion of t.butylbenzene and its major fragments (Fig 74), gave the following fragmentation pattern:

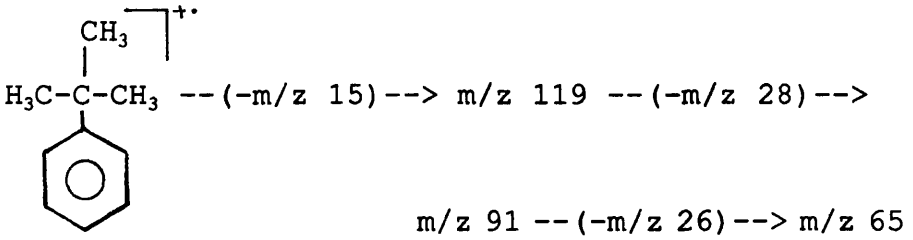

NRMS spectra (He(10)/O_2(10)) were used to examine the neutral fragments formed when these ionic fragments were generated (Figs 75-77). These confirmed the successive

losses of neutrals of mass 15, 28 and 26 daltons as shown.

The loss of a neutral mass 15 from the molecular ion is readily accounted for by the loss of one of the three methyl groups

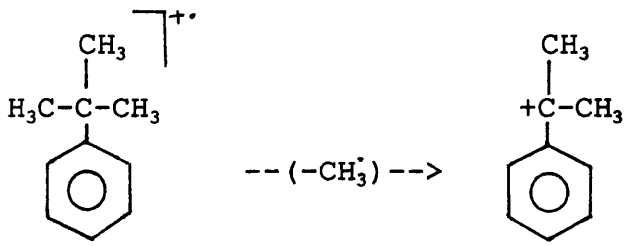

m/z 134 m/z 119

The loss of mass 28 from m/z 119 however is not so straightforward, neither in terms of the structure of the neutral (C_2H_4) but in the structure of the resultant $C_7H_7^+$ ion at m/z 91.

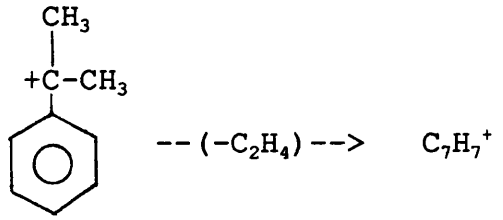

m/z 119 m/z 91

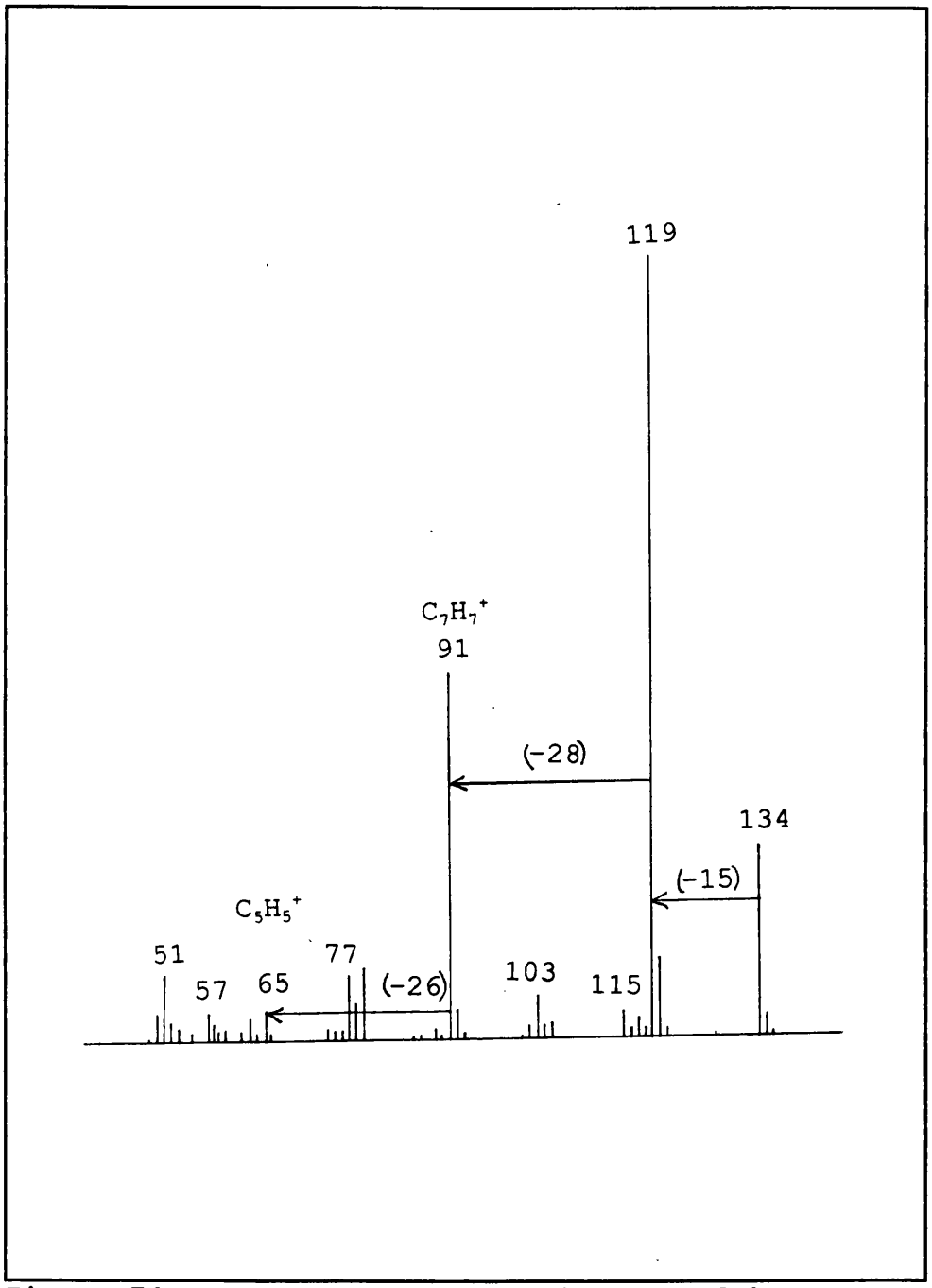

Figure 74 Mass spectrum of tertiary butyl benzene

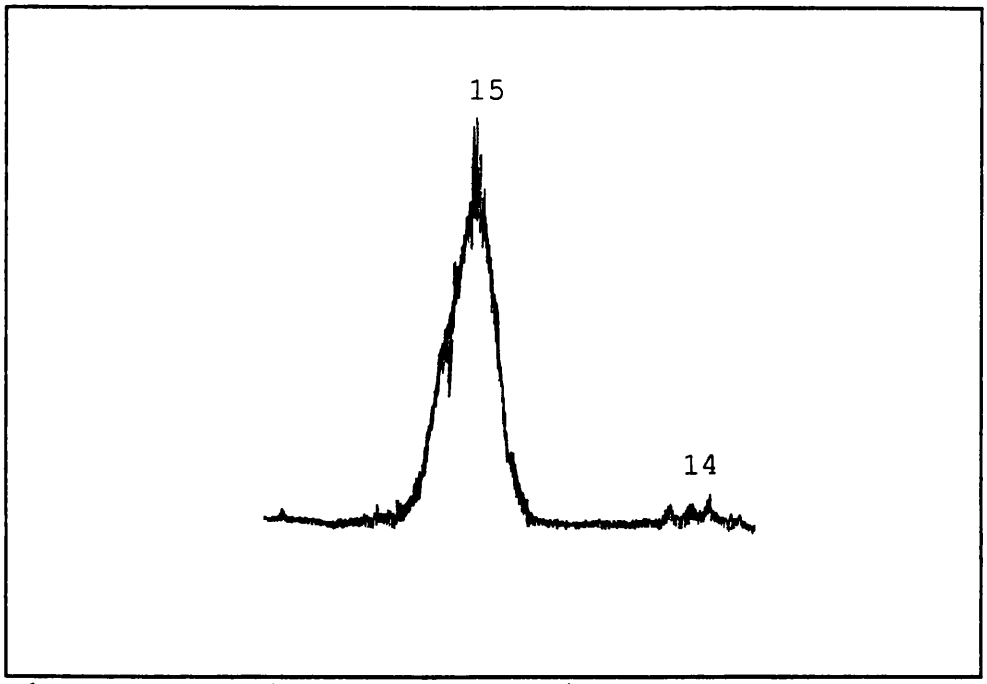

Figure 75 Partial NRMS ($Xe(10)/O_2(10)$) spectrum of the molecular ion of t-butylbenzene

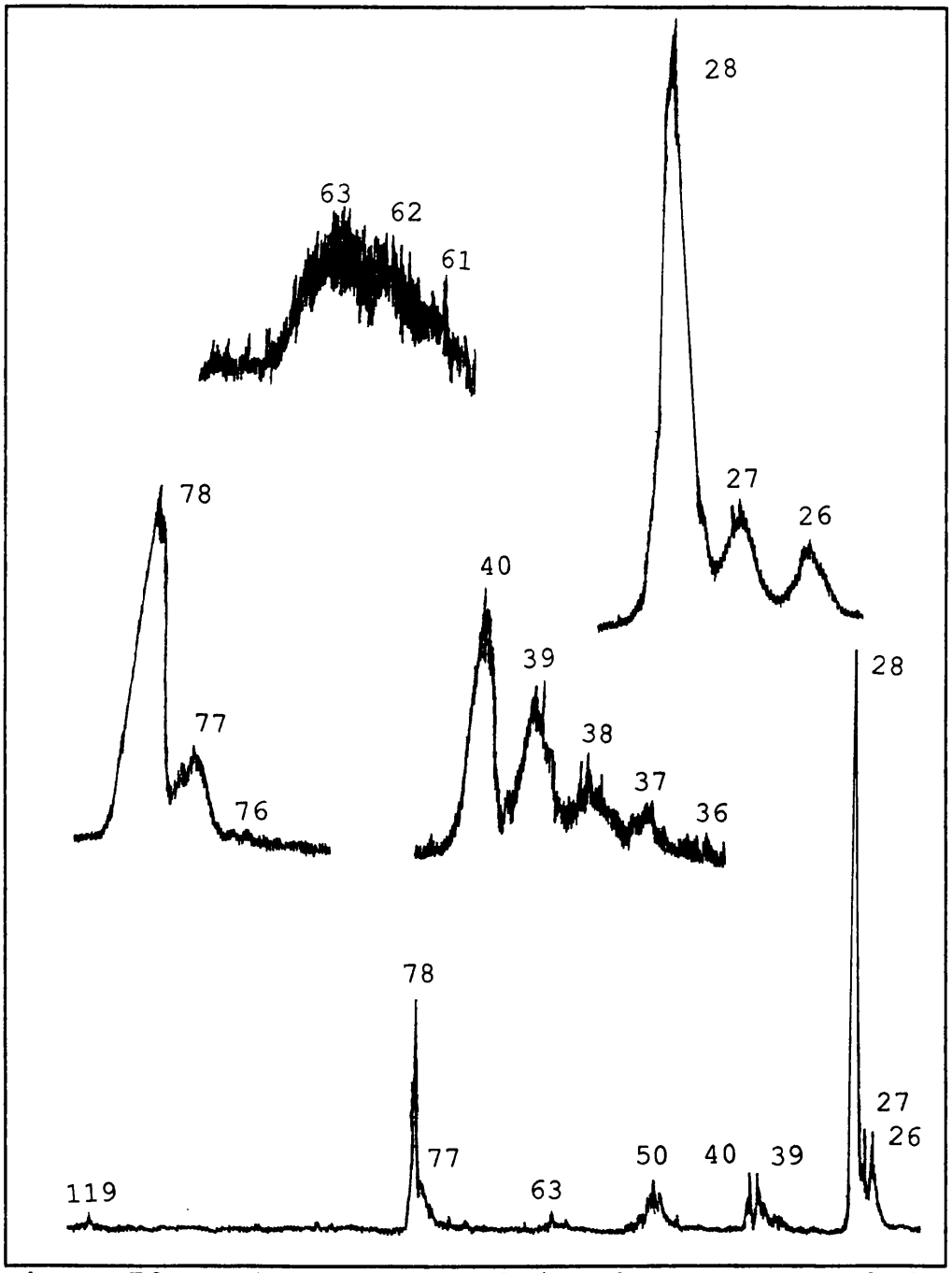

Figure 76 Partial NRMS ($Xe(10)/O_2(10)$) spectrum of the m/z 119 fragment ion from t-butylbenzene

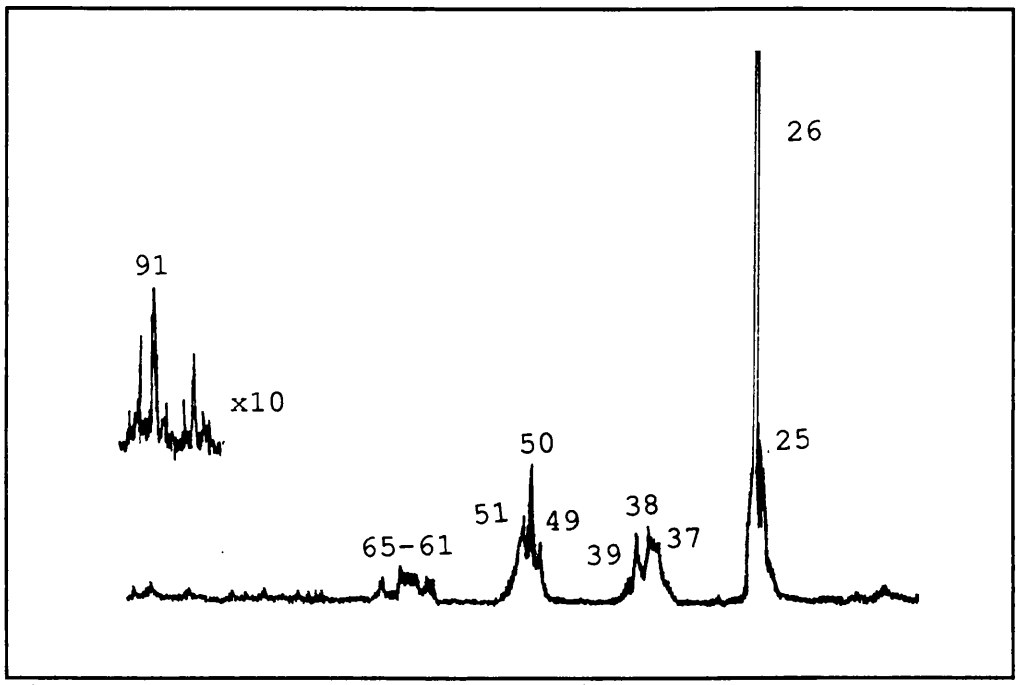

Figure 77 Partial NRMS ($Xe(10)/O_2(10)$) spectrum of the m/z 91 fragment ion from t-butylbenzene

4.3.3 Structure of the $C_7H_7^+$ Fragment

4.3.3.1 Introduction

The formation and structure of $C_7H_7^+$ ions (Fig 78) has long been of interest, and has been the subject of many studies [6-19]. Rylander et al [6] began by investigating alkylbenzenes and their derivatives, which had been assumed to decompose via a benzyl structure, the most logical given the structure of the parent. However, anomalies were found when comparing the actual stability of the $C_7H_7^+$ fragment ion of xylene from EI spectra at threshold energies to the expected stability of such an ion with the believed benzyl structure. The actual stability was much greater. Also, the $C_8H_9^+$ ion from trimethylbenzene, if it had the proposed tolyl structure, should have been appreciably more stable than the $C_7H_7^+$ ion, but experiment showed no significant increase in stability. Threshold EI spectra of deuterium labelled toluene gave evidence of extensive hydrogen scrambling suggesting the near equivalency of the hydrogen atoms. This lead to the proposition of a symmetrical structure for $C_7H_7^+$ - that of tropylium, (Fig 78) which is energetically more stable than the benzyl ion [16]. This explains the stability of the $C_7H_7^+$ ion from xylene (if a tropylium structure is proposed) and the lack of increased stability in the $C_8H_9^+$ ion from

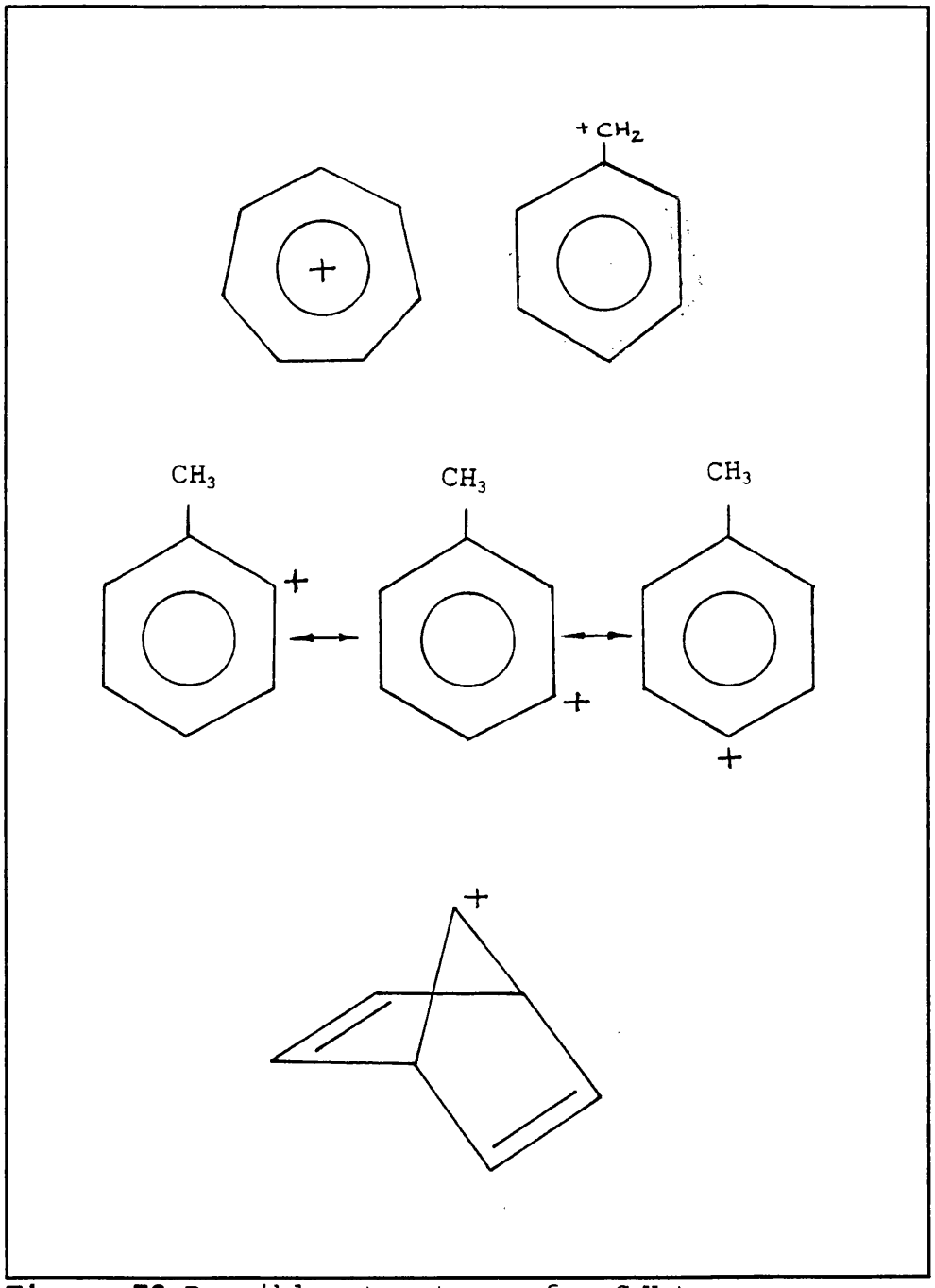

Figure 78 Possible structures for C_7H_7+

trimethylbenzene, which in the form of methyltropylium, will not be appreciably more stable than tropylium itself.

Appearance energy measurement [6,20] and heat of formation values [5] indicate that the unimolecular isomerisation of toluene and cycloheptatriene ions requires less energy than hydrogen atom loss. At threshold energies, cycloheptatriene cannot form benzyl ions but it may form the more stable tropylium, which is seen [5]. MINDO/3 calculations [18] have proposed two possible mechanisms for the rearrangement of toluene to cycloheptatriene: the Hoffman mechanism and the cyclohexadienyl ion mechanism.

At threshold energies, the structure of the $C_7H_7^+$ from a toluene precursor ion is believed to be exclusively or almost exclusively [5,10,15] that of tropylium. However, as the internal energy of the parent ion is increased above threshold, the picture is not so straightforward. EI [5,19] and photodissociation [14] spectra of toluene show more than one $C_7H_7^+$ ion present, and the proportion of each isomer present to be dependent upon the ionisation energy and the accelerating voltage [5,10,15,21]. In the case of toluene two $C_7H_7^+$ isomers were noted, the reactive isomer being identified as the benzyl ion, the non reactive isomer identified as the tropylium ion [14]. As the internal energy of the parent ion increases immediately above threshold (~1-2 eV above)

the production of benzyl ions increases rapidly as the production of benzyl and tropylium ions becomes more competitive [5]. At higher energies (~4.5 eV above threshold) C_2H_2 loss becomes competitive, and $C_5H_5^+$ ions are formed [5].

Though there are other $C_7H_7^+$ isomers, such as the tolyl ion (Fig 78), these are considerably less stable than the benzyl or tropylium ions [9]. Nevertheless, the tolyl ion has been identified in the CID spectrum of iodotoluene [7,9].

The percentage of each $C_7H_7^+$ isomer formed has also been found to be dependent upon the number of ring structures present in the precursor [6].

Conversely one study [10] has suggested a different relationship between benzyl ion production and internal energy of the precursor ion. As the ionisation energy is decreased, an increase in benzyl ion production is seen, said to be due to the direct formation of benzyl ions from toluene which have sufficient energy to rearrange to tropylium at very high energies, but not as the energy is lowered. Such a trend is seen in another study [5] however in this case no decrease in benzyl ion population is seen at low and threshold energies. The authors highlight the significance of artifact peaks (for instance, due to unimolecular decomposition in the magnet region) and their importance in low energy CID spectra. Also, their work on toluene-free cycloheptatriene

suggests that interconversion between toluene and cycloheptatriene takes place even at low energies, ensuring the presence of benzyl ions through hydrogen loss from toluene, at the lowest energy CID spectra.

The general method for determining the percentage composition of each $C_7H_7^+$ isomer relies upon the principle of 'linear superposition'; that is, where there are two or more components under analysis, The CID spectrum of that combination is simply the linear sum of the CID spectra for each component [5]. The proportion of each component is then found by 'subtracting' the 'pure' CID spectra for each of the other components. In principle this method is logical and in agreement with QET, but it has been criticised [22,23] for its assumptions; for instance that pure CID spectra for each of the components may be obtained and that certain CID peaks may be ignored where the unimolecular contribution is significant.

Following on from this, a way was sought to identify the structure of the $C_7H_7^+$ fragment ion from t-butyl benzene.

4.3.3.2 Experimental

The samples examined were tertiary butyl benzene, toluene and ethylbenzene, which were obtained from commercial sources and used without further purification.

In each case ~5µl of each sample was introduced through the heated septum inlet, ionised with 70eV electrons and the ions accelerated through 8 kV. The source temperature was maintained at approximately 200°C.

CID/MIKE spectra were obtained by admitting helium to the second of the collision cells in the 2FFR, at a pressure sufficient to attenuate the main beam intensity by 30%. The precursor ion was selected by the magnet and the ESA voltage scanned down from the value corresponding to the energy of the precursor (nominally 8keV).

The toluene used had not been purified to remove cycloheptatriene; such a step was believed unnecessary since the toluene ion would receive enough energy to isomerise to cycloheptatriene in the ionisation process.

4.3.3.3 Results and Discussion

Examination showed the spectra (Fig 79) to be identical except for the region m/z 74-79 in toluene which gave a relatively smaller intensity at m/z 77. It seems likely from the work already reported, that for each of the precursors the m/z 91 ions are a mixture of benzyl and tropylium ion forms. The similarity in the CID spectra for ethylbenzene and t-butylbenzene suggested that the proportions of the two parent structures were the same in each case. The unique CID spectrum for

toluene suggested a different ratio of benzyl to tropylium ions. Following the assertion that a prominent m/z 77 peak is indicative of the presence of the benzyl ion, the CID data suggested that in the case of toluene more ions of the tropylium structure were formed under these conditions. Since CID data does not reflect the energy of the parent ion prior to the collision the difference must lie in the relative proportions of the two structural forms of $C_7H_7^+$ which are present at the point of collision, hence the energetics of the formation of the m/z 91 ions.

Without a deeper analysis it is impossible to say which structures are present and in what proportions. This illustrates a problem when analysing CID data with little background information. Without knowing the possibility of isomeric structures being present, simply comparing the CID spectra of $C_7H_7^+$ from t-butylbenzene and toluene suggests different initial structures not necessarily different proportions of the same structures. Examination of the metastable
decomposition of m/z 119 gives an approximately gaussian metastable peak at m/z 91, not suggesting isomerism.

From this data the fragmentation pattern of t-butylbenzene is as follows:

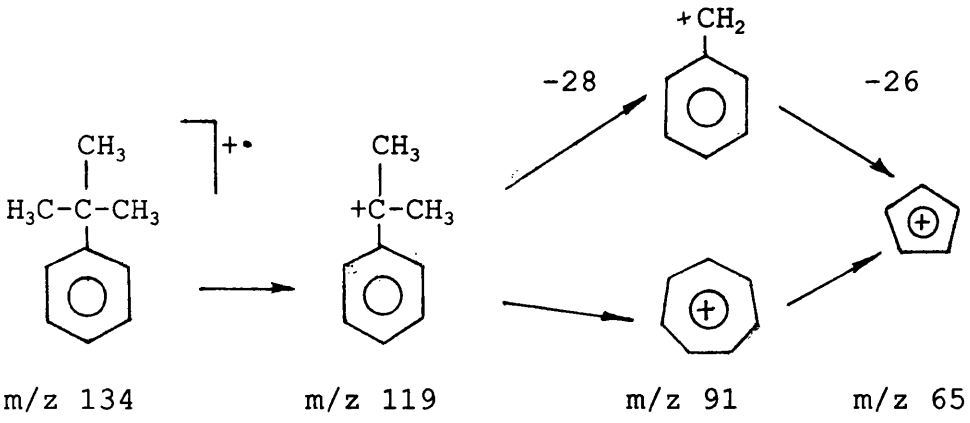

This still leaves the question of the C_2H_4 structure unresolved but it has been established that this is involved in a one-step loss from m/z 119 to m/z 91.

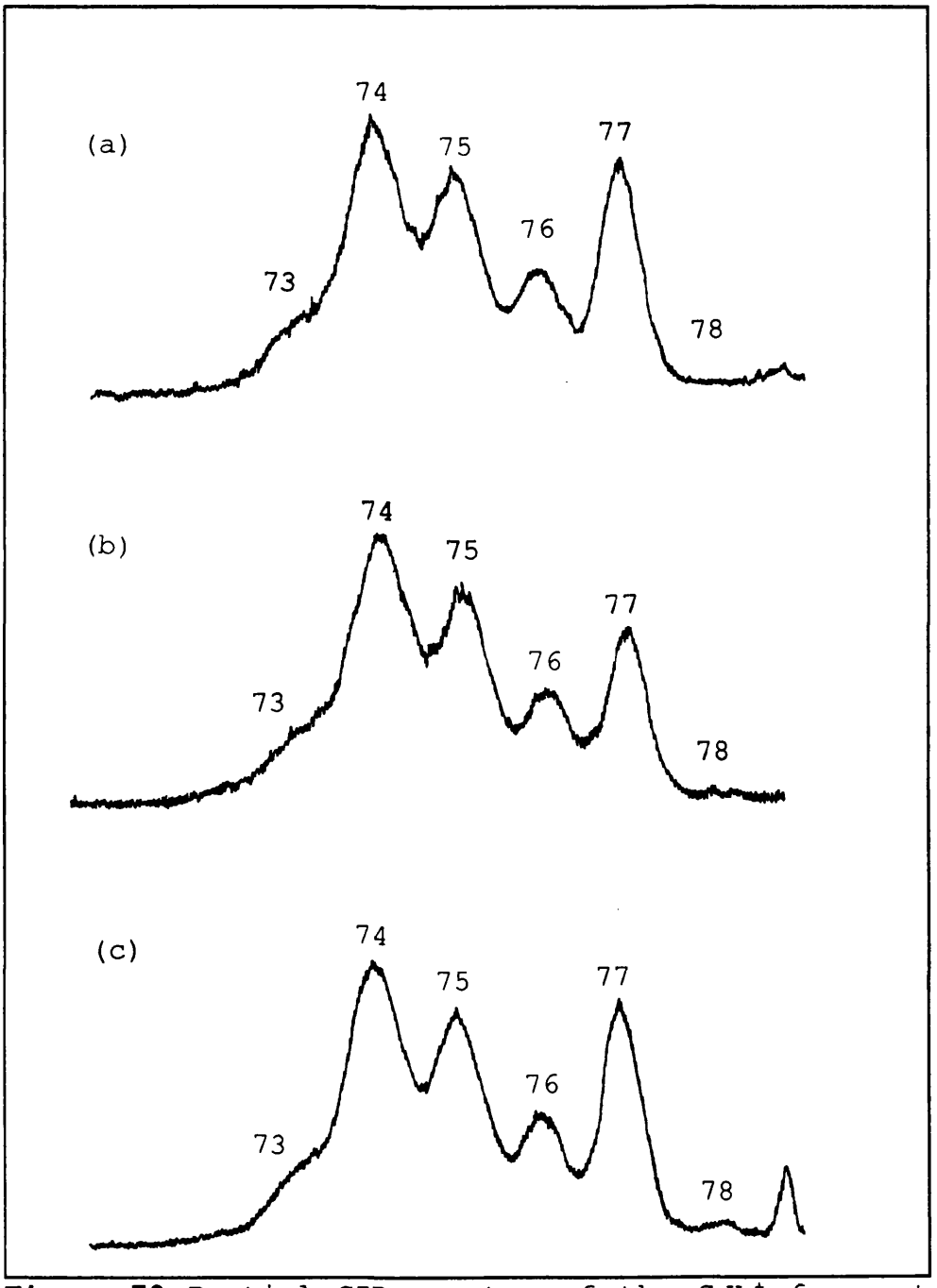

Figure 79 Partial CID spectra of the $C_7H_7^+$ fragment ions from (a) t-butylbenzene, (b) toluene and (c) ethylbenzene

4.4 $C_2H_5NO^{+\cdot}$ ISOMERS - STRUCTURAL INFORMATION FROM MS/MS

4.4.1 Introduction

As well as molecular weight information, mass spectrometry, in particular tandem mass spectrometry, can yield information on structure and can thus be used to differentiate between isomeric structures A study was undertaken to compare various tandem mass spectrometrical techniques in order to assess their utility in isomeric ion differentiation.

The isomers selected for this study were the molecular ion $M^{+\cdot}$ from acetamide (1), and the $[M-C_2H_4]^{+\cdot}$ ions from n-butyramide (2) and N-ethylacetamide (3), the latter two are both formed via a McLafferty rearrangement.

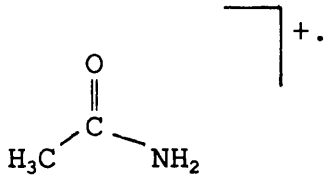

(1)

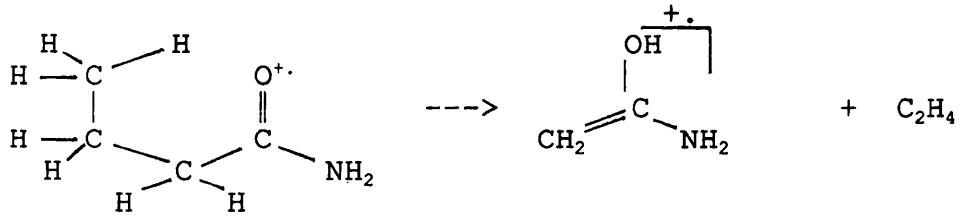

(2)

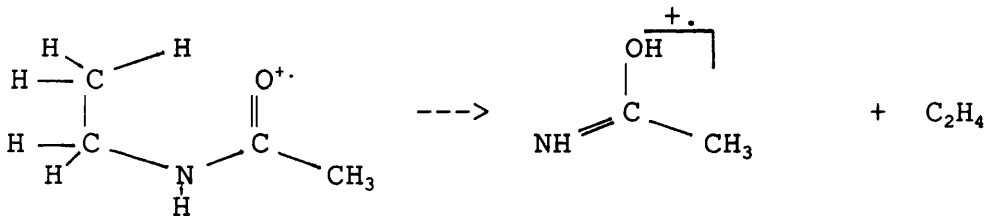

(3)

These three ions are structurally very similar, all having the formula $C_2H_5NO^{+\cdot}$.

The techniques selected for this comparison were unimolecular MIKE spectra, collision induced dissociation (CID)/MIKES, B/E linked scans and neutralisation-reionisation mass spectrometry (NRMS), all of which allowed the specific analysis of the $C_2H_5NO^{+\cdot}$ ion.

4.4.2 Experimental

The samples examined were

acetamide

n-butyramide

and N-ethyl acetamide

which were obtained from commercial sources and used without further purification. Acetamide and n-butyramide, were introduced via the solid probe which was water cooled throughout the experiment. N-ethyl acetamide, a volatile liquid, was introduced through the heated septum inlet. The samples were ionised with 70eV electrons and the ions accelerated through 8 kV. The source temperature was maintained at ~200°C.

All data except that for NRMS was acquired by the data system in multichannel analyser (MCA) mode and averaged over several scans. The NRMS data was acquired using the UV oscillograph over a single scan. Each spectrum was recorded several times to examine the reproducibility of the data.

4.4.2.1 Unimolecular MIKES

Unimolecular MIKE spectra were obtained by selecting the parent ion with the magnet, and then scanning the ESA voltage down from the value corresponding to the energy of the parent ion (nominally 8 keV). Since the resolution of the daughter ion fragment ions is determined by the resolution of the ESA alone, the mass

assignments were accurate to ±1 mass unit.

4.4.2.2 CID/MIKES

CID/MIKE spectra were obtained by admitting helium into the second of the collision cells in the 2FFR, at a pressure sufficient to attenuate the main beam intensity by 30%. The precursor ion was again selected by the magnet and the ESA voltage scanned in the same manner as for MIKES. To differentiate between fragment ions formed due to collisions between the precursor ion and helium and those formed through the unimolecular dissociation of the precursor, the collision cell was floated at V_c=1.2 kV with respect to ground. This actually differentiates between fragment ions formed in the collision cell and those formed elsewhere in the 2FFR. Where the unimolecular peak is small the majority of fragmentations that take place in the collision cell will be due to collisions with helium, so that the application of V_c will effectively separate the two sorts of fragments. However, if the unimolecular peak is of significant intensity the two processes cannot be effectively separated in this manner.

4.4.2.3 B/E linked scans

B/E linked scans gave daughter ion scans of a selected parent ion fragmentations in the 1FFR. Both the magnet and ESA were scanned together at a constant ratio under data system control.

4.4.2.4 NRMS

NRMS spectra were also obtained by scanning the instrument in the manner used for MIKES. The neutralisation gas Xe was admitted to the first cell in the 2FFR at a pressure sufficient to cause a 10% attenuation of the main beam intensity; the reionisation gas, oxygen, was admitted to the second cell in the 2FFR again at a pressure giving 10% attenuation of the main beam intensity. The deflector plate between the two gas cells was set at 1kV which had been found adequate to prevent any residual ions from the first cell entering the second collision cell.

4.4.3 Results and Discussion

4.4.3.1 Unimolecular MIKES

For each of the precursor ions the unimolecular MIKE spectra showed the same groups of daughter ion peaks but

with variations in their intensity (Figs 80-82). The $C_2H_5NO^{+\cdot}$ ions from N-ethylacetamide and acetamide gave similar spectra with a notable peak at m/z 31, loss of mass 28 (CO, C_2H_4 or CH_2N) whereas the spectrum for n-butyramide gave more intense peaks at m/z 42-44, loss of OH, NH_2 and CH_3 respectively. Although the three spectra were distinct, they were of limited utility in defining actual structural differences between the three precursor ions.

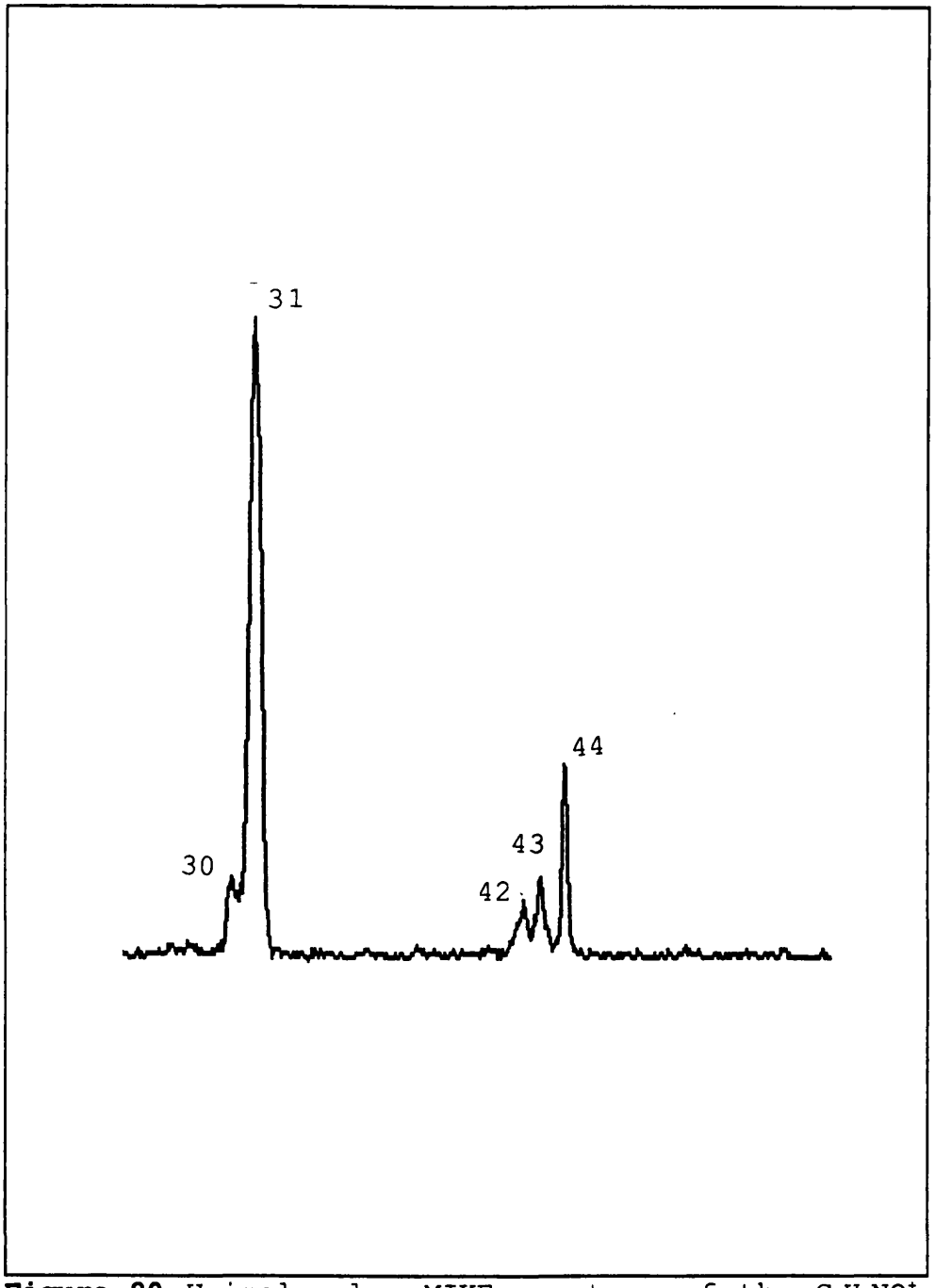

Figure 80 Unimolecular MIKE spectrum of the $C_2H_5NO^{+\cdot}$ ion from acetamide

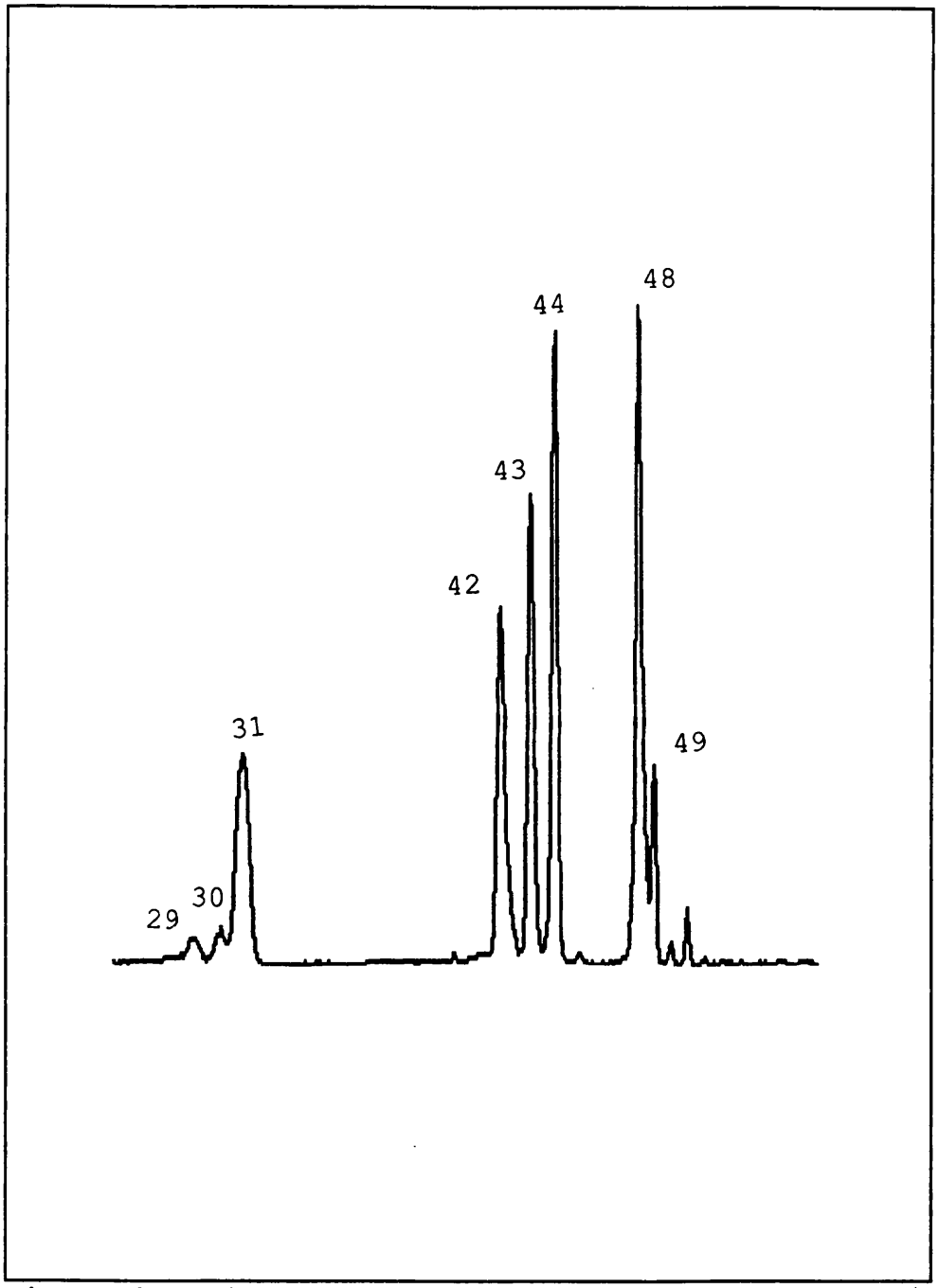

Figure 81 Unimolacular MIKE spectrum of the $C_2H_5NO^{+\cdot}$ ion from n-butyramide

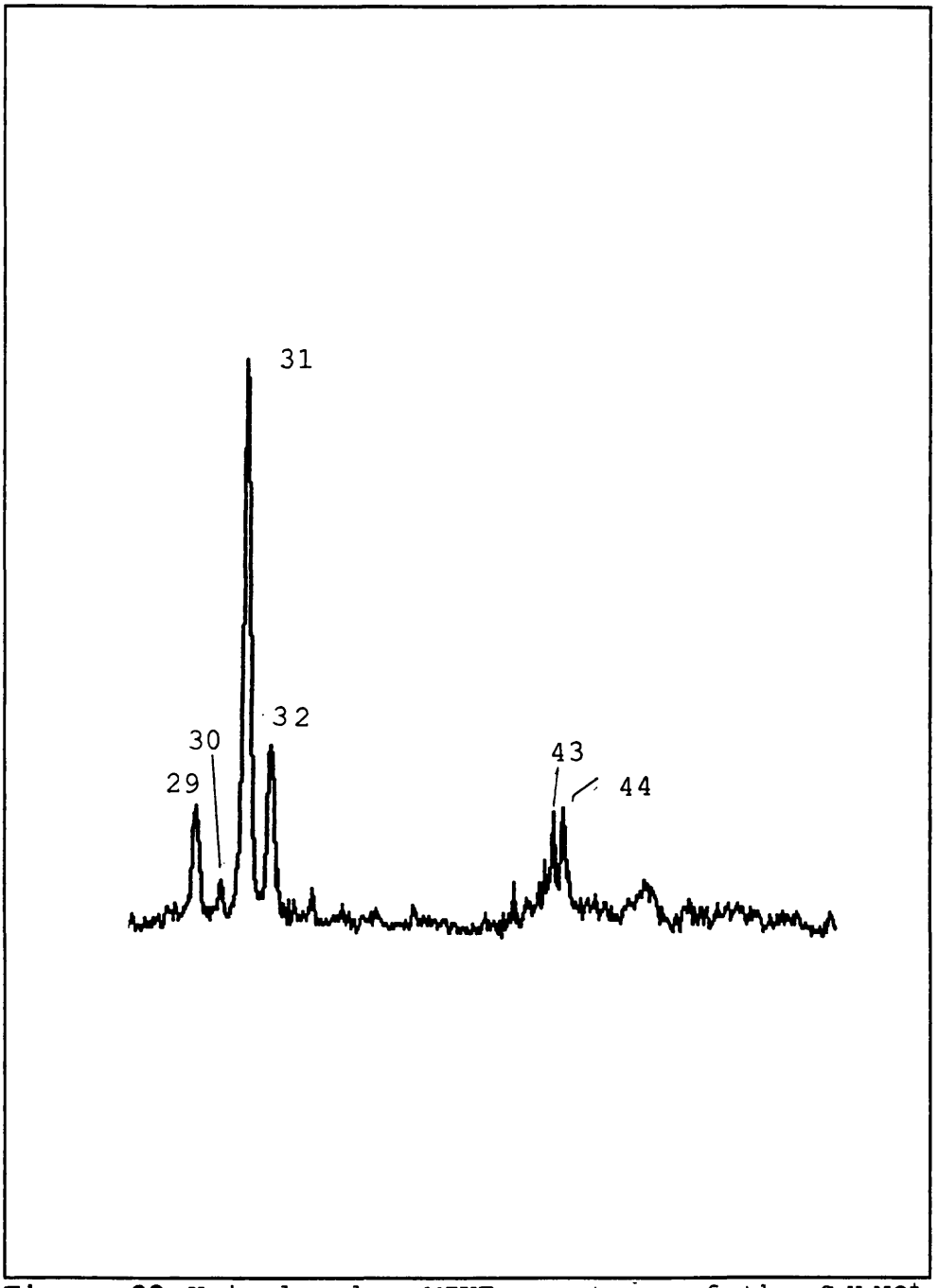

Figure 82 Unimolacular MIKE spectrum of the $C_2H_5NO^{+\cdot}$ ion from N-ethylacetamide

4.4.3.2 CID/MIKES

The CID/MIKES spectra (Figs 83-85) for each precursor ion showed three groups of daughter ion peaks : m/z 42-44, m/z 28-31 and m/z 13-18. In the case of n-butyramide and acetamide, the unimolecular peaks in the groups m/z 42-44 and m/z 28-31 were of significant intensity suggesting that the displaced peaks were a mixture of fragments from CID and unimolecular dissociations. For this reason, these regions of the spectra were disregarded. In the region m/z 13-18 only the portion m/z 13-17 could be used due to the influence of the intense m/z 18 peak due to unimolecular dissociations in the spectra for N-ethylacetamide and n-butyramide. The intensity of m/z 15 was notably smaller in the spectrum of $C_2H_5NO^{+\cdot}$ from n-butyramide probably because loss of CH_3 was more restricted from this ion due to the double bond between the carbon atoms. It was difficult to draw firm conclusions concerning the structures on the basis of the CID/MIKES spectra, however the fact that the spectra were different confirms that the isomers are structurally distinct.

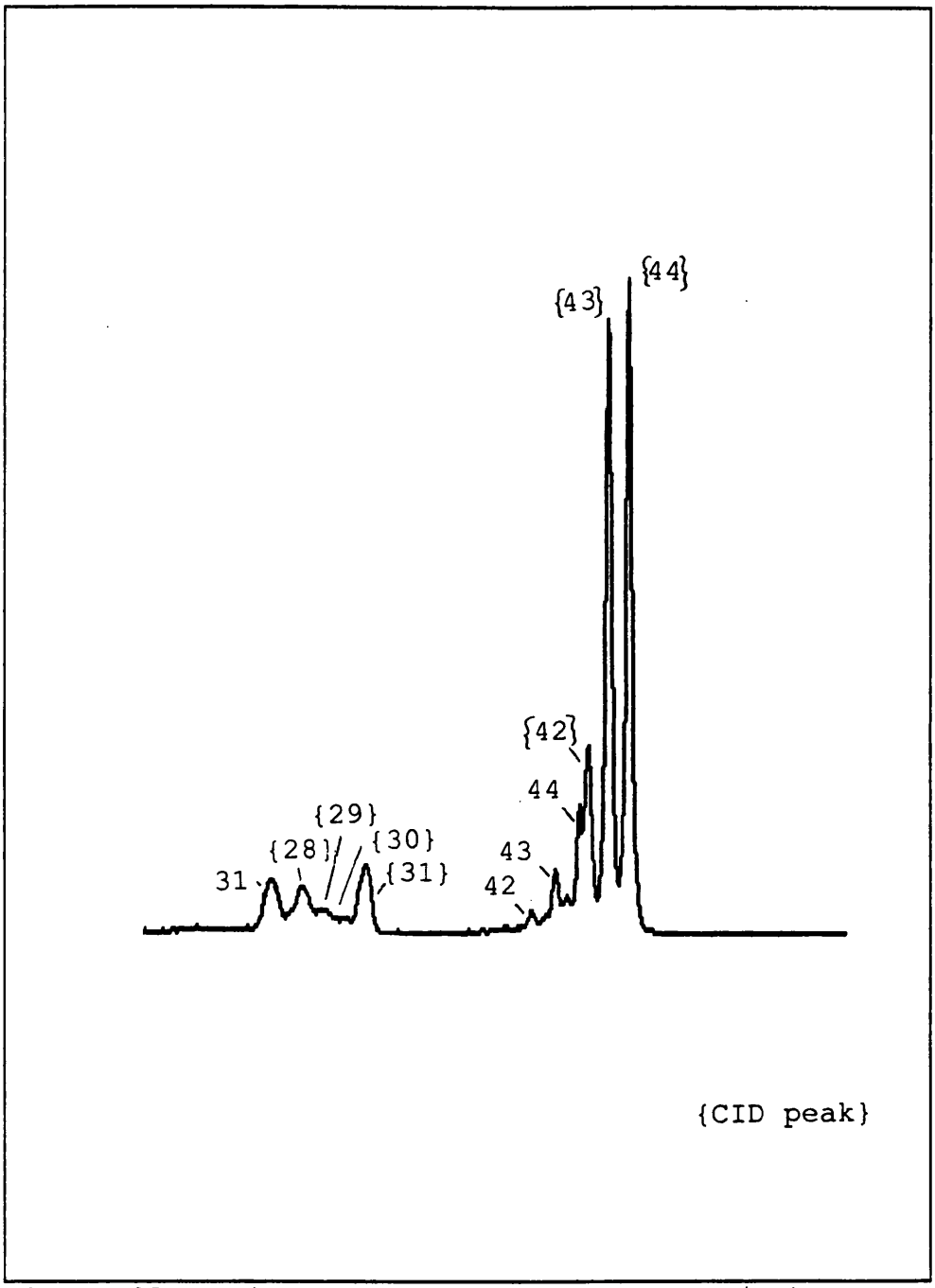

Figure 83 CID/MIKE spectrum of the $C_2H_5NO^{+\cdot}$ ion from acetamide

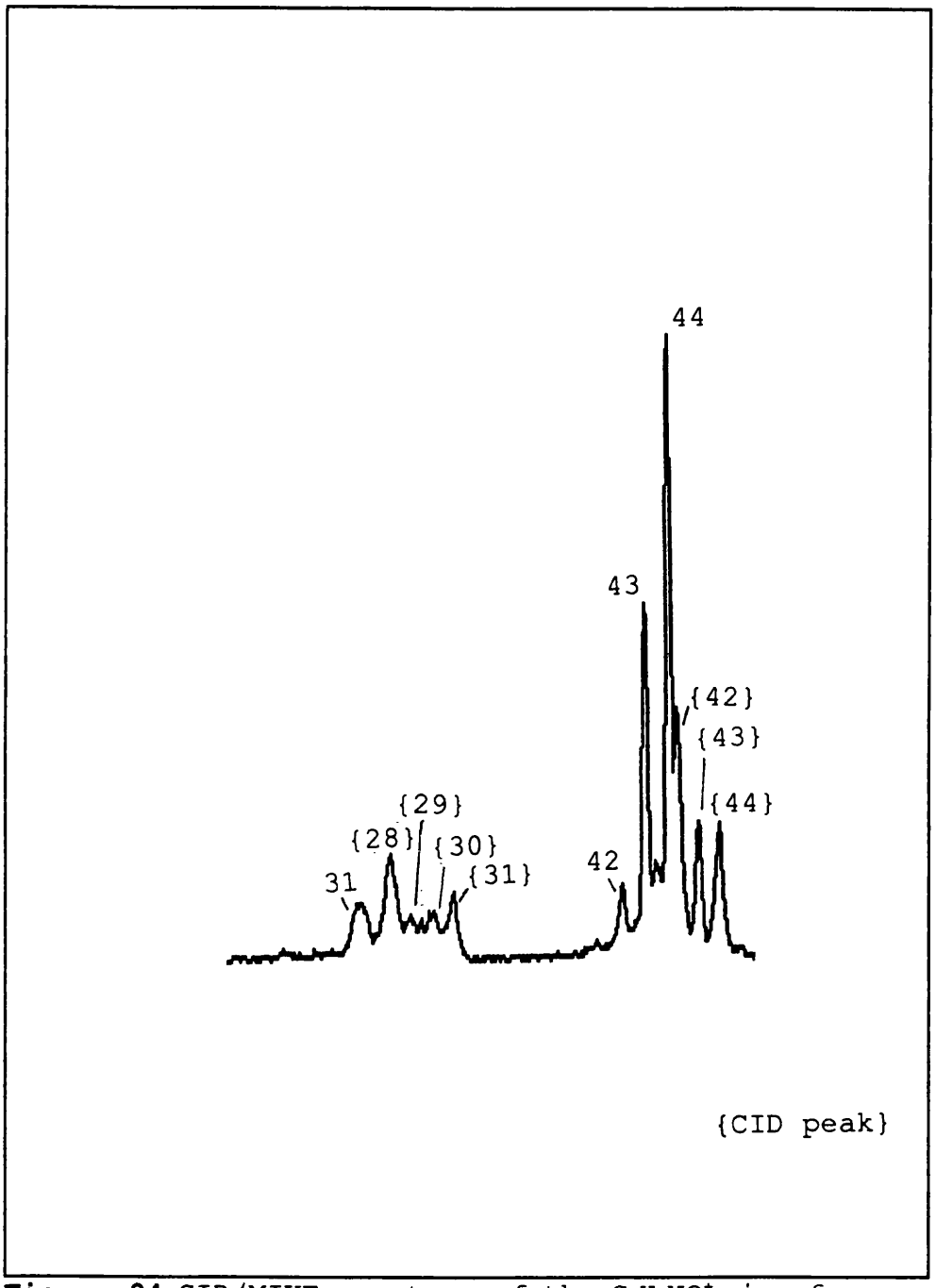

Figure 84 CID/MIKE spectrum of the $C_2H_5NO^{+\cdot}$ ion from n-butyramide

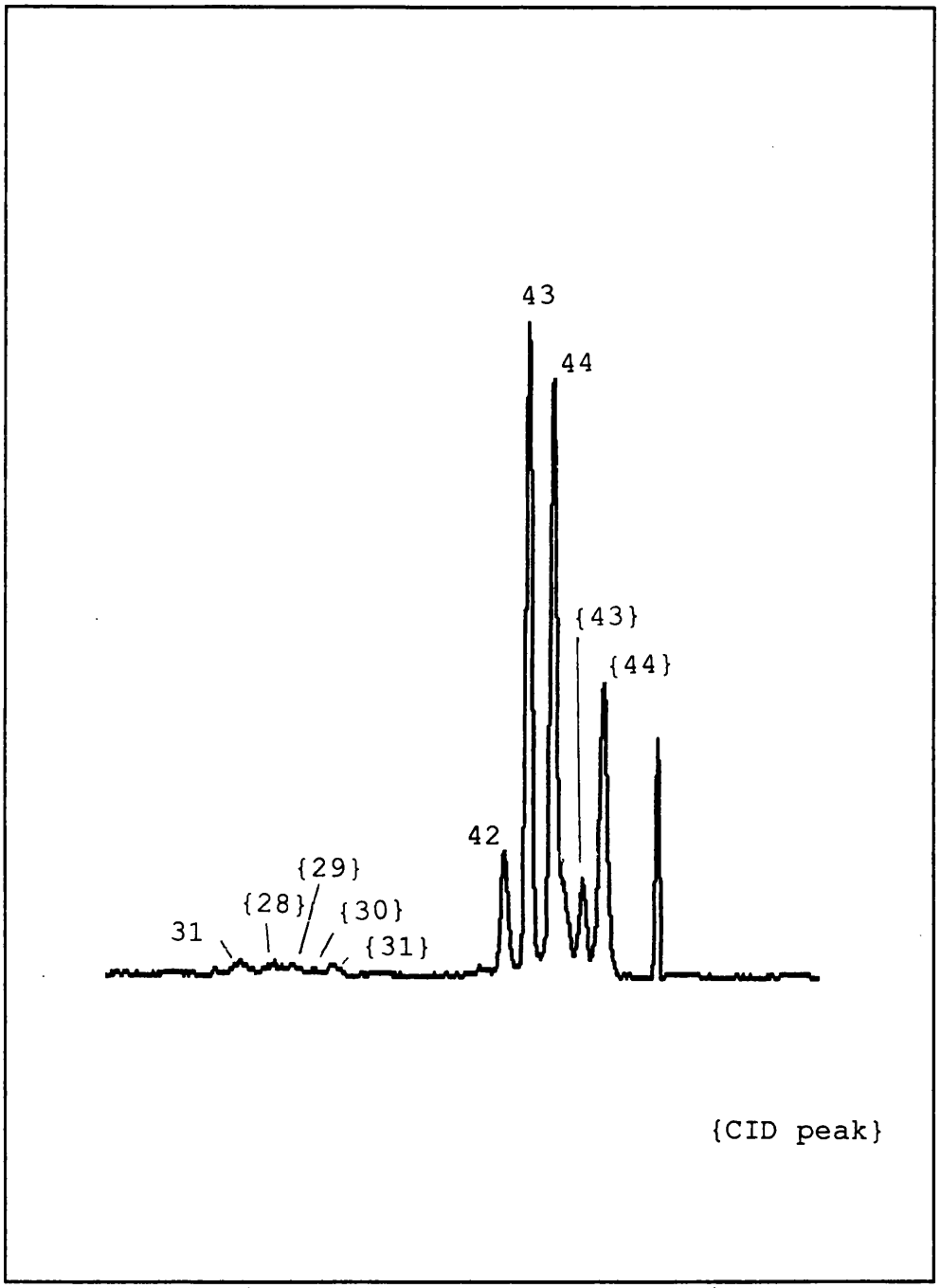

Figure 85 CID/MIKE spectrum of the $C_2H_5NO^{+\cdot}$ ion from N-ethylacetamide

4.4.3.3 B/E Linked Scans

From the B/E linked scans (Figs 86,87), the spectra for acetamide and n-butyramide showed some notable variations in relative intensities of the peaks in the group m/z 40-44, but again this yielded limited structural information. There was also some difficulty in calibrating down to a sufficiently low mass in order to examine all the daughter ion peaks. Consequently there may have been additional information in the low mass part of the spectrum which was not recorded.

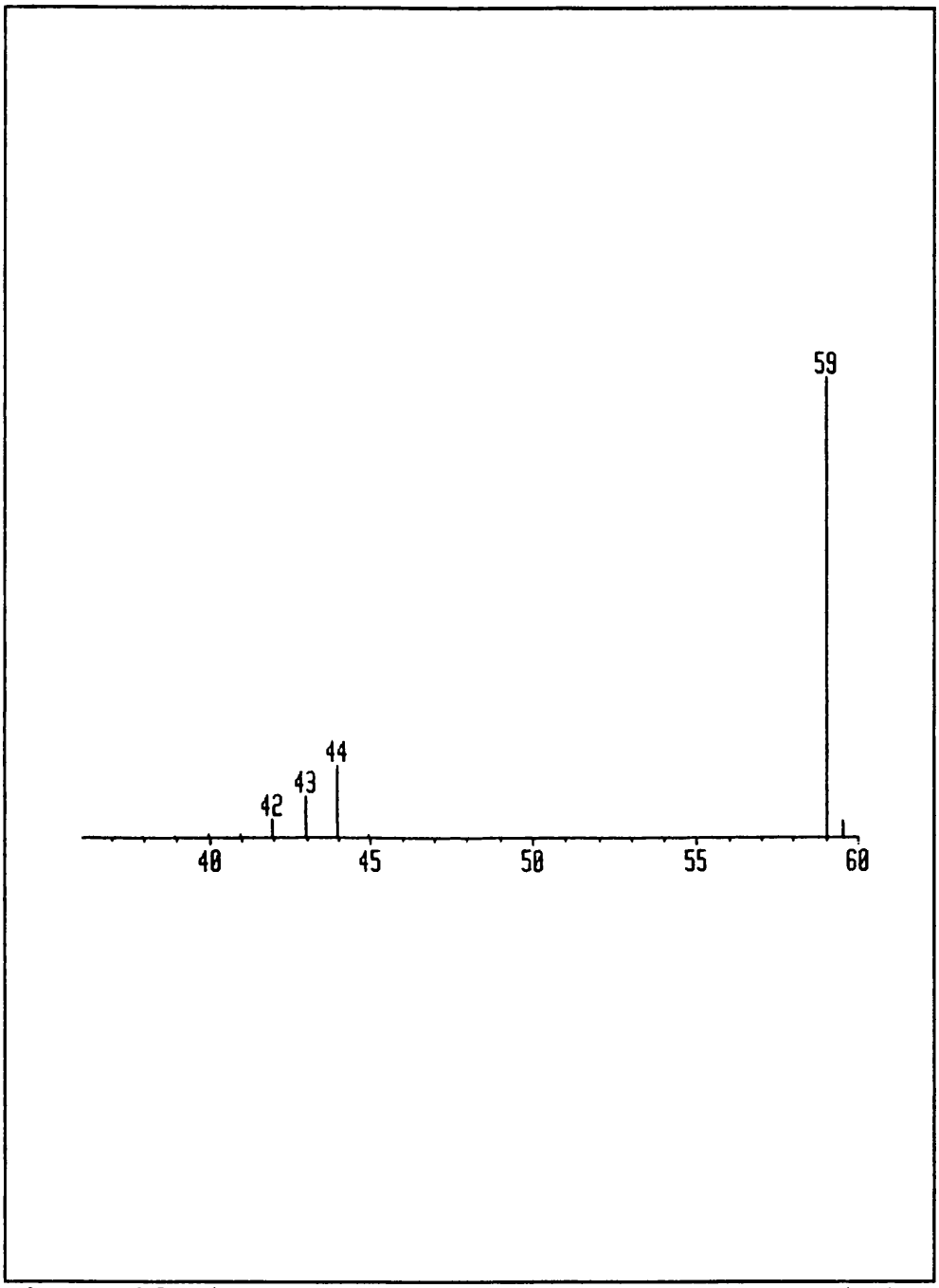

Figure 86 B/E linked scan spectrum of the $C_2H_5NO^{+\cdot}$ ion from acetamide

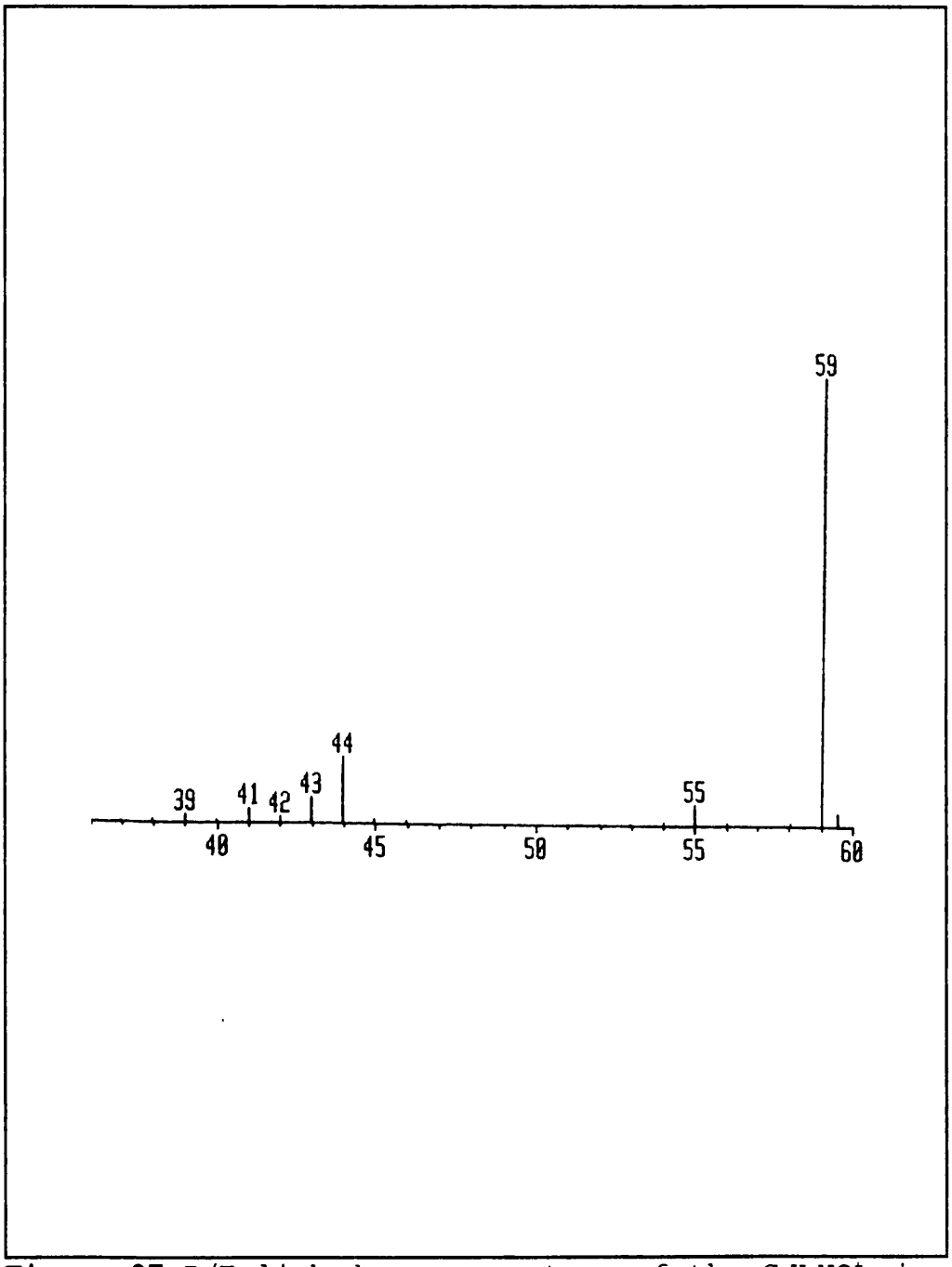

Figure 87 B/E linked scan spectrum of the $C_2H_5NO^{+\cdot}$ ion from n-butyramide

4.4.3.4 NRMS

The NRMS spectra (Figs 88-90) for the three isomeric ions showed the same groups of peaks: m/z 12-18, m/z 25-31 and m/z 40-44; however there were clear differences between the relative intensities of peaks within each group and between the groups themselves.

Of particular interest were the fragment ions from m/z 40-44 and m/z 12-18 which showed distinct differences for the three ion structures. The spectra for the $C_2H_5NO^{+\cdot}$ ion from acetamide exhibited intense peaks at m/z 44 and 45, due to loss of CH_3 and NH_3 respectively, which related to the proposed structure of this precursor. Also a relatively small m/z 17 could be related to the double bond between the carbon and oxygen atoms restricting the loss of an OH group. The spectrum of $C_2H_5NO^{+\cdot}$ from n-butyramide showed intense peaks at m/z 41 (loss of H_2O) and m/z 17 (OH) both confirming the presence of the OH group in the precursor ion. The NRMS spectrum of the $C_2H_5NO^{+\cdot}$ N-ethylacetamide shows an intense peak at m/z 41 and a relatively intense peak at m/z 44 due to loss of H_2O and CH_3 respectively, again giving confirmation of the proposed ion structure.

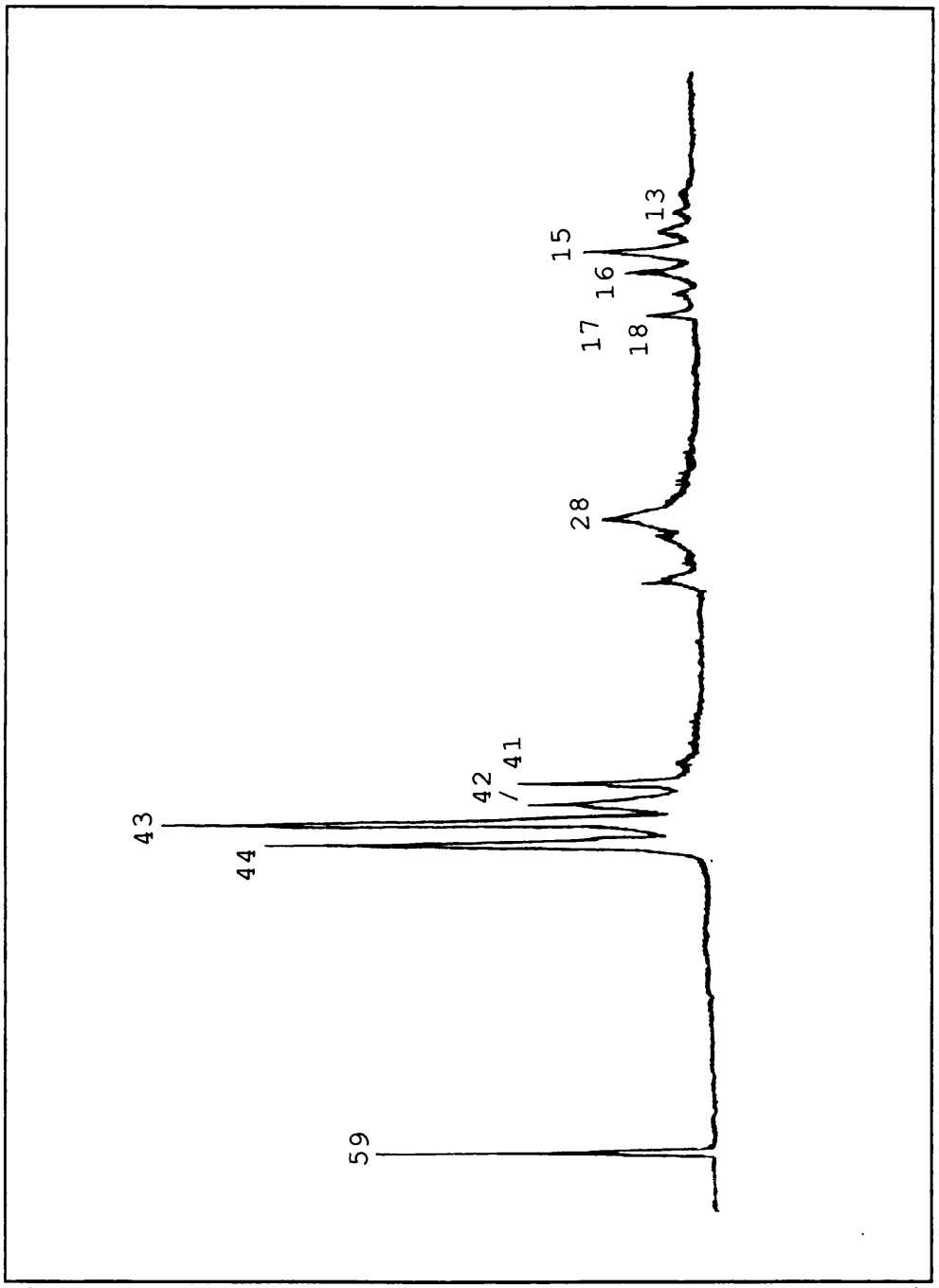

Figure 88 NRMS (Xe(10)/O_2(10)) spectrum of the $C_2H_5NO^{+\cdot}$ ion from acetamide

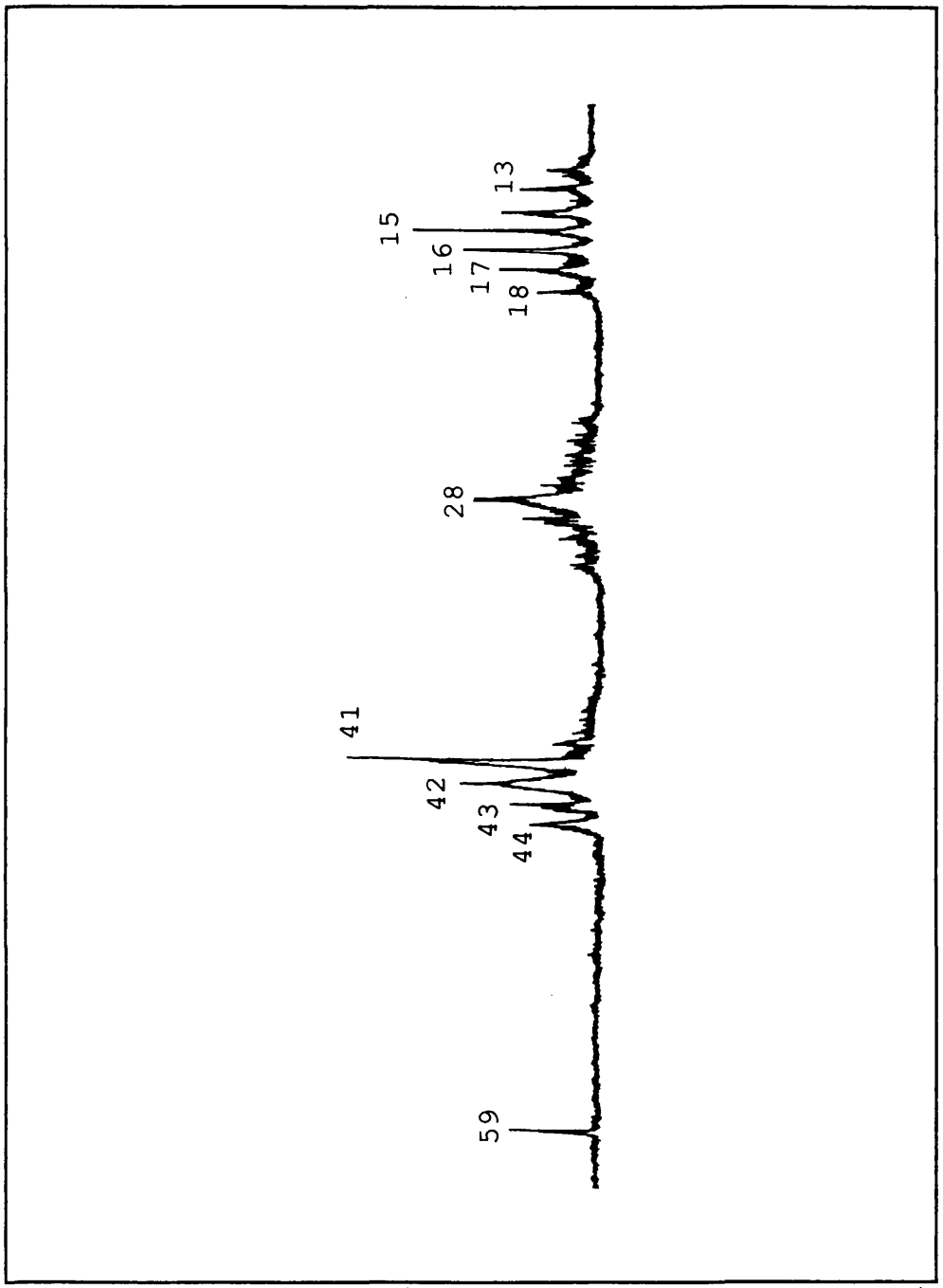

Figure 89 NRMS (Xe(10)/O_2(10)) spectrum of the $C_2H_5NO^{+\cdot}$ ion from n-butyramide

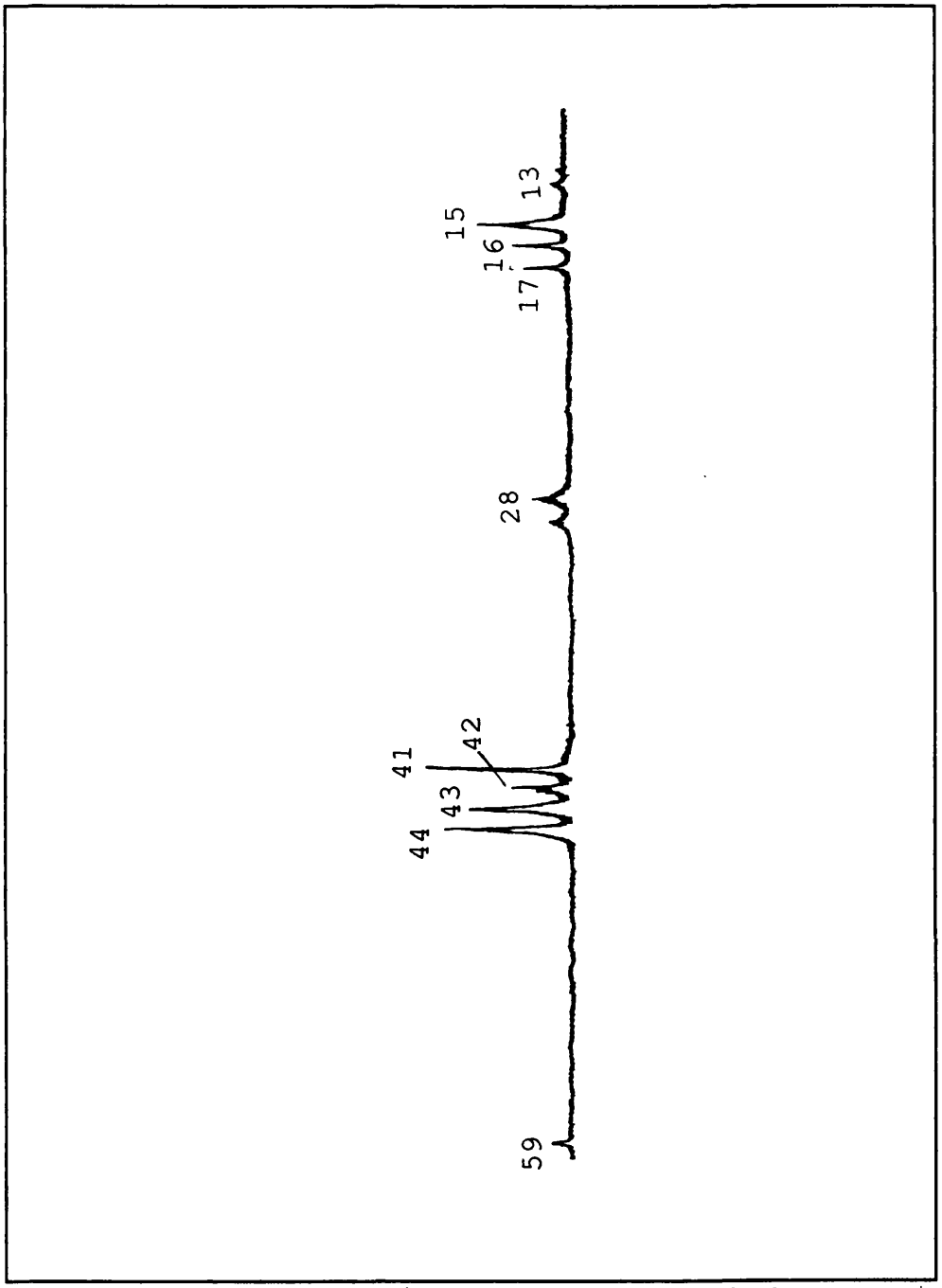

Figure 90 NRMS (Xe(10)/O_2(10)) spectrum of the $C_2H_5NO^{+\cdot}$ ion from N-ethylacetamide

The experiments performed have demonstrated that the three isomeric $C_2H_5NO^{+\cdot}$ ions do indeed have different structures as expected. Unimolecular MIKES spectra were limited in their usefulness by the small number of daughter ion peaks and their relatively low intensity; also this type of data is known to be dependent on the energy of the parent ion as well as its structure. B/E linked scans were hindered by the problems of calibration to a sufficiently low mass to observe all the daughter ion fragments. CID/MIKES technique, which could have yielded the most information was unfortunately found to be of limited utility in this case. NRMS was undoubtable the most successful technique used in this study, giving clear structural information. From this it would seem that NRMS may be of considerable use in identifying different isomeric ion structures, compared with other tandem techniques.

4.5 FACTORS AFFECTING IMMONIUM ION PRODUCTION IN THE HIGH ENERGY CID SPECTRA OF PEPTIDES

4.5.1 Introduction

Peptides and proteins [24,25] have a multitude of diverse functions; they appear as enzymes, hormones, vitamins and antibodies, catalyse many reactions in the cell and bind cells into tissue.

They are comprised almost solely of the same twenty three basic units (with a few others in low concentration) known as 'amino acids'. This is an abbreviation of 'α-aminocarboxylic acid', most of which have the general formula

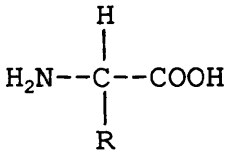

The side group R is the distinguishing factor between the amino acids and can be -H as in glycine, the simplest amino acid, or a much more complex group.

The nature of the side group determines the nature of the amino acid, for instance their hydrophobicity is determined by whether R is polar or non-polar

Hydrophilic (polar R) : Asp Glu Cys Lys Arg
Ser His Asn Gln Thr

Hydrophobic (non-polar R): Tyr Phe Pro Val Ala
Met Ile Gly

Since R is usually neutral the amino acid is also neutral. However when an ionic side group is present the amino acid is either acidic or basic

Acidic: Asp Glu

Basic: Lys Arg His Orn

The link between two amino acids is an amide bond known as a 'peptide bond'. It is formed by a condensation reaction resulting in the loss of a water molecule.

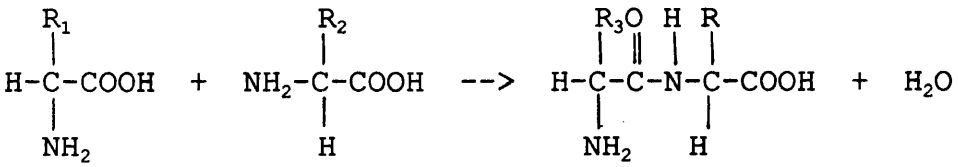

The peptide chain is built up in this way. The distinction between peptide and protein is somewhat arbitrary but the term protein is usually reserved for molecules over 10,000 daltons or those too large to dialyse through a cellophane membrane.

The unit

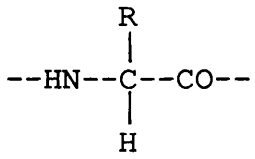

is known as an 'amino acid residue'. The first amino acid in the peptide has a free amino group and is termed the 'N-terminal residue'. The last amino acid in the peptide has a free carbonyl group as is termed the 'C-terminal residue'.

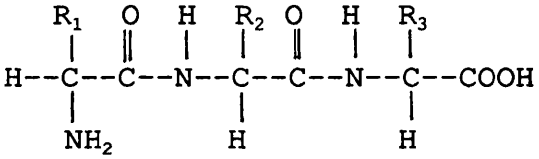

N-terminal C-terminal

By convention, peptide structures are written from left to right beginning at the N-terminus.

4.5.2 Peptide Analysis

Under the high energy CID conditions pertaining in sector tandem MS, protonated peptide ions formed by FAB or LSIMS give characteristic low mass fragment peaks corresponding to immonium ions and related species, some of which are listed in Table 11. These may differ significantly in intensity, e.g. histidine invariably

gives a very strong ion at m/z 110 whereas the aspartic and glutamic acid immonium ions at m/z 88 and 102 respectively are frequently weak or absent [26].

Because of the predictable nature of peptide fragmentation, computerised MS/MS spectral interpretation is now seen as an attainable goal. A recently reported method uses the presence or absence of peaks below mass 160 Da as a key indicator of the nature of the amino acids present [27], and another method also uses this data as an aid to interpretation [28]. This study has been made to examine factors influencing the relative intensities of these immonium ions.

Immonium ions are even-electron ions of general formula $H_2N^+=CHR$, formally corresponding to protonated neutral molecules. If the original site of protonation is the N-terminal NH_2, immonium ion formation requires two bond cleavages and a proton transfer to nitrogen for all but the N-terminal amino acid, which needs only one cleavage and a proton transfer away from nitrogen. In this latter case the ion formed is also the A_1 ion [29].

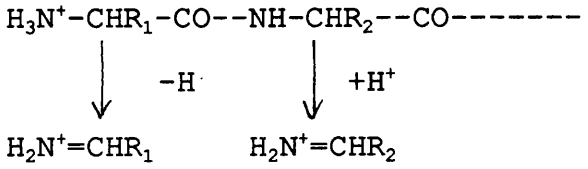

The amide nitrogens are energetically unfavourable sites for protonation, but some amino acids have basic side

chains such as arginine and lysine, and other nitrogen-containing side chains such as those of histidine and tryptophan may also act as sites for protonation [30]. Higher energy ions can also be formed with the proton located at other sites. The energetics of bond breaking and ion stability will also play an important role in determining ion intensities. Some amino acids such as arginine give other characteristic low mass peaks of greater abundance than the immonium ions, but it is not known whether these are formed by the breakdown of immonium ions or whether they are formed by alternative routes, possibly in competition with immonium ions. A basic amino acid that was the site for the initial protonation would give an ion isomeric with the immonium ion by two bond cleavages without proton transfer, but this would not necessarily possess the same stability to further fragmentation and might indeed give rise to alternative low mass ions.

The aim of this work was to investigate the various factors contributing to the production of immonium ions from small peptides, and in doing so establish whether or not there is a competitive effect involved, that is whether the production of immonium ions from one amino acid residue is affected by the presence and/or position of the other residues in the peptide.

Experiments were structured to examine the following:

a) the intensity of the immonium ion from the C-terminal residue relative to its intensity when the residue is elsewhere in the chain,

b) the intensity of the immonium ion from the N-terminal residue relative to its intensity when the residue is elsewhere in the chain,

c) the effect on other immonium ion intensities when one residue is exchanged for another,

d) immonium ion intensities from $[M+X]^+$ (where X=alkali metal) as opposed to $[M+H]^+$, and

e) the effect of an excess of protons at ionisation on immonium ion production.

In this study a series of enkephalin, morphiceptin, cytochrophin and casomorphin-related peptides from commercial sources were investigated, being mostly tetra- and pentapeptides. Most included the aromatic amino acids phenylalanine (**F**) and tyrosine (**Y**) giving immonium ions at m/z 120 and 136 respectively, and aliphatic hydrophobic amino acids such as glycine (**G**), alanine (**A**), leucine (**L**), norleucine (**Nle**), isoleucine (**I**), threonine (**T**), proline (**P**), hydroxyproline (**Hyp**) and methionine (**M**).

An earlier report by Russell et al on tripeptides based on $\mathbf{G_2,H}$ and **G,A,Y** suggested that immonium ions were of decreasing intensity in the order N-terminal>in-chain>C-terminal [30]. However, they quoted peak

intensities relative to the most intense fragment peak in each spectrum, rather than the parent peaks. This does not allow comparison between different spectra and no conclusions can be drawn concerning absolute ion intensities.

For most of the peptides studied the intensities of the immonium ions from both the **F** and **Y** ions were about 3% relative to the attenuated parent ion signals (at 50% transmission), whereas those of the aliphatics were 1% or less. There is no evidence for further breakdown of any of these immonium ions, no other lower mass peaks of significant intensity being observed. The aromatic side chains would be expected to confer stability on the immonium ions although the immonium double bond is not conjugated with the aromatic ring, but it is not obvious that this would affect protonation or proton transfer significantly.

Amino Acid Residue	Immonium Ion *i* (m/z)	Relative Intensity
W	159	v.strong
Y	136	v.strong
F	120	v.strong
M	104	weak
L	86	strong
I	86	strong
Nle	86	strong
Hyp	86	v.strong
T	74	weak
P	70	v.strong
A	44	weak
G	30	weak

Table 11: Masses of the immonium ions for some amino acids and their relative intensities

4.5.3 Experimental

A list of those peptides examined is given in Table 9. Most were obtained through commercial sources and used without further purification. Two of the peptides, YGFG-amide and GYFG-amide where synthesysised using an Applied Biosystems Peptide Sythesiser model 403A.

Standard solutions (10 $nmol.\mu l^{-1}$) were made by dissolving each of the peptides in a mixture of methanol and water (1:1), 4µl being added to the FAB probe tip along with 2µl of glycerol and dried in air. The 8keV protonated peptide ions were selected by the magnet and collided with He in the second field free region. The spectra were obtained by scanning the electric sector voltage (MIKES), and were accumulated by the data system in the multi-channel analyser mode. The intensity of the parent ion was kept on-scale to allow accurate recording of relative intensities. The resolving power and the accuracy of mass measurement of the MIKES technique were such as make the mass assignments reliable to only ±1 mass unit. However, the mass values quoted here are in agreement with expected values.

Sequence	
YGGFM	(acetate salt)
YWGFM	(acetate salt)
YAGFM	(acetate salt)
YGGFL	(acetate salt)
YAGFL	(acetate salt)
YAGFNle	(acetate salt)
YGGF	(acetate salt)
YAFAY	(amide)
YAFHypY	(amide)
YAFPY	(amide)
YAFP	(amide)
YPFP	(amide)
YGFG	(amide)
GYFG	(amide)
YPFT	(hydroxide)
YPVP	(amide)
YPFV	(hydroxide)
YAPTI	(hydroxide)
YGGFLK	(acetate salt)

Table 12: Sequence of those peptides examined for this study

4.5.4 Results and Discussion

4.5.4.1 C-terminal Effect

The intensity of i_y from **YGGF** to **YGGFL** ,**YGGF** to **YGGFM** and **YGGF** to **YGGFNle** increased approximately four-fold, four-fold and three-fold respectively (Figs 91,92), and the intensity of i_b increased approximately two-fold from the spectrum of **YAFP** to that of **YAFPY**. Also, the immonium ion for **T**, though not seen in the spectrum of **YAPT**, is just visible in the spectrum of **YAPTI** (Fig 93).

This data is represented in Table 13, and suggests that immonium ion formation is generally less favourable for the C-terminal amino acid.

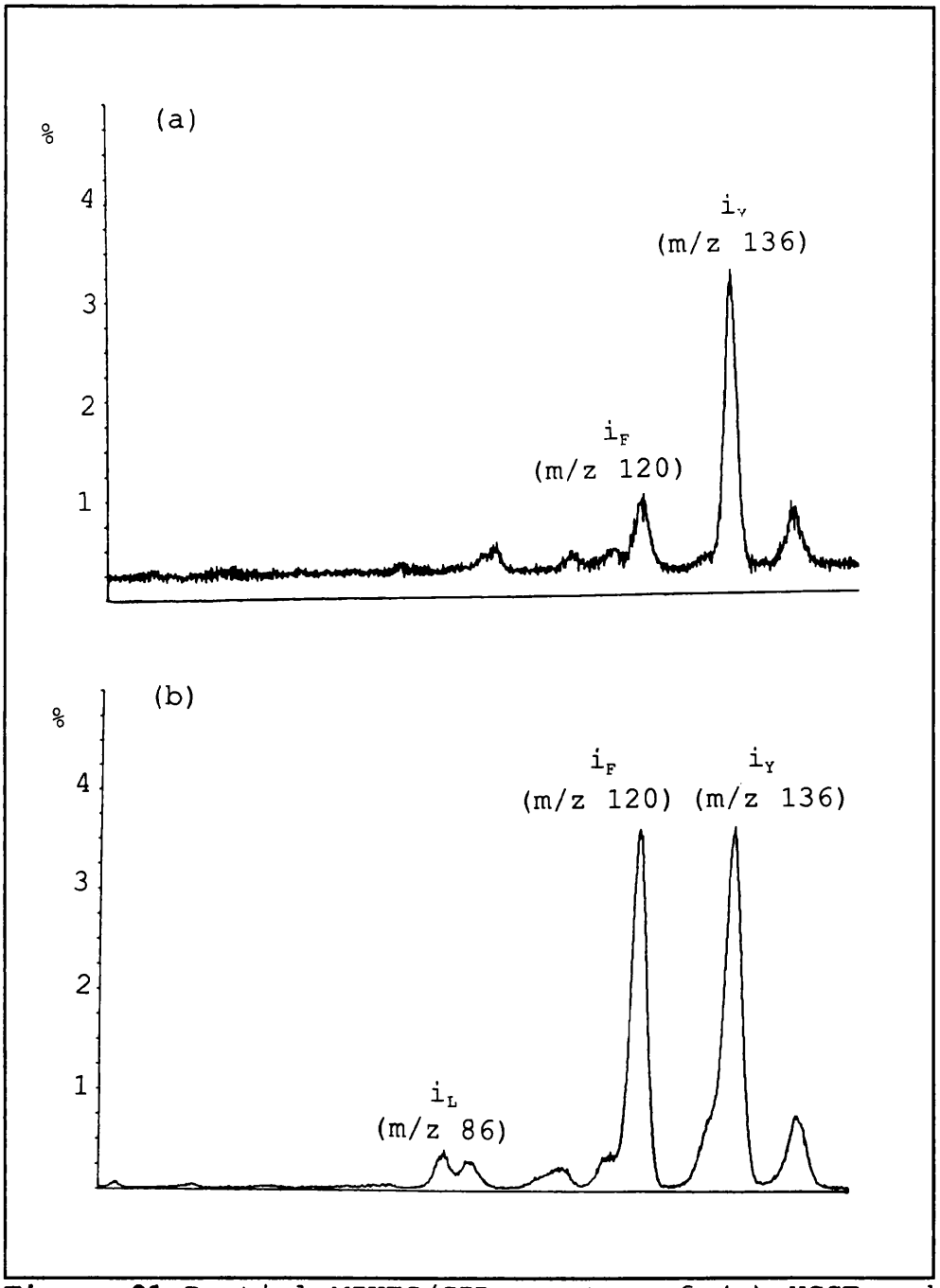

Figure 91 Partial MIKES/CID spectra of (a) YGGF and (b) YGGFL

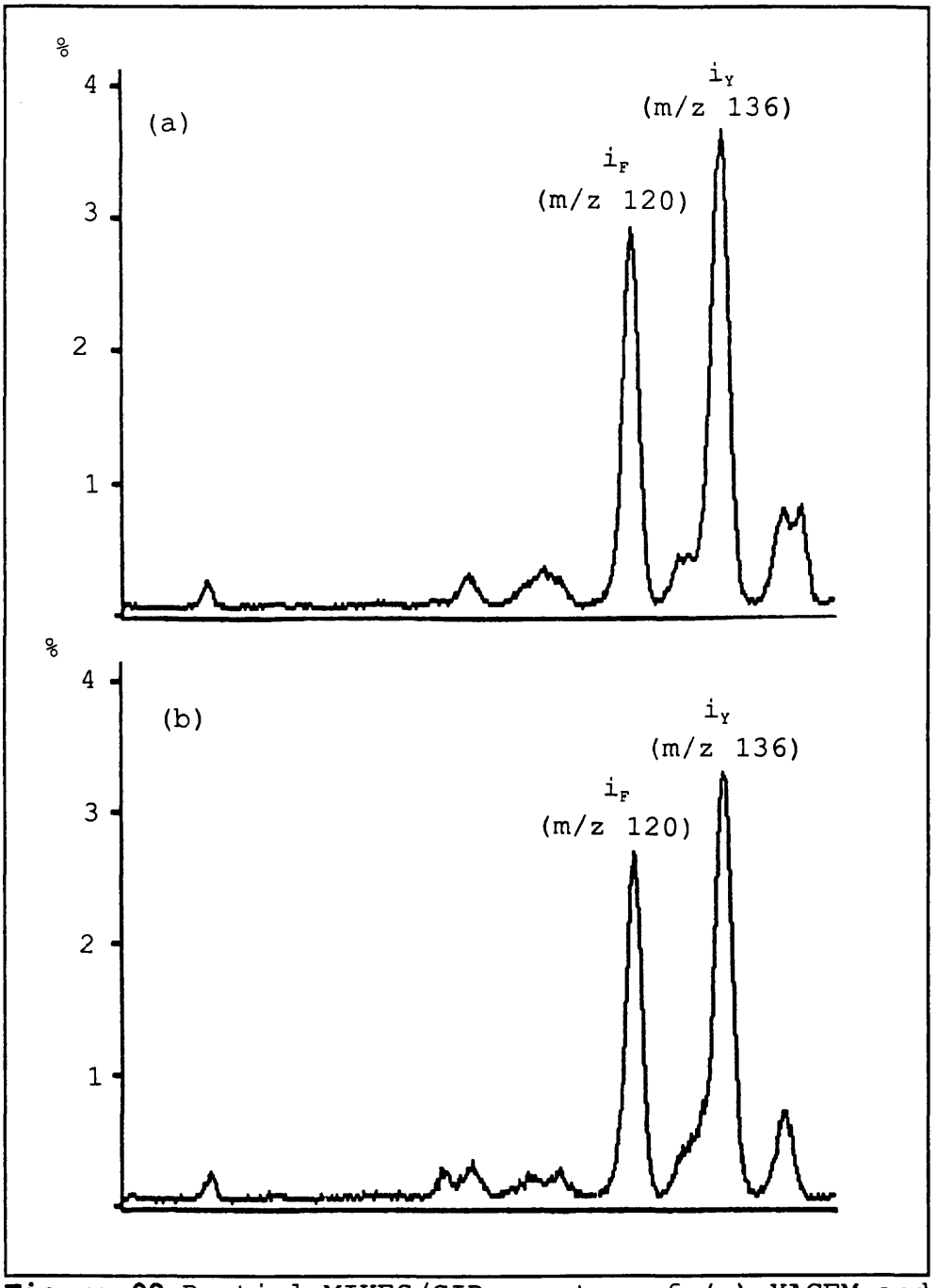

Figure 92 Partial MIKES/CID spectra of (a) YAGFM and (b) YAGFNle

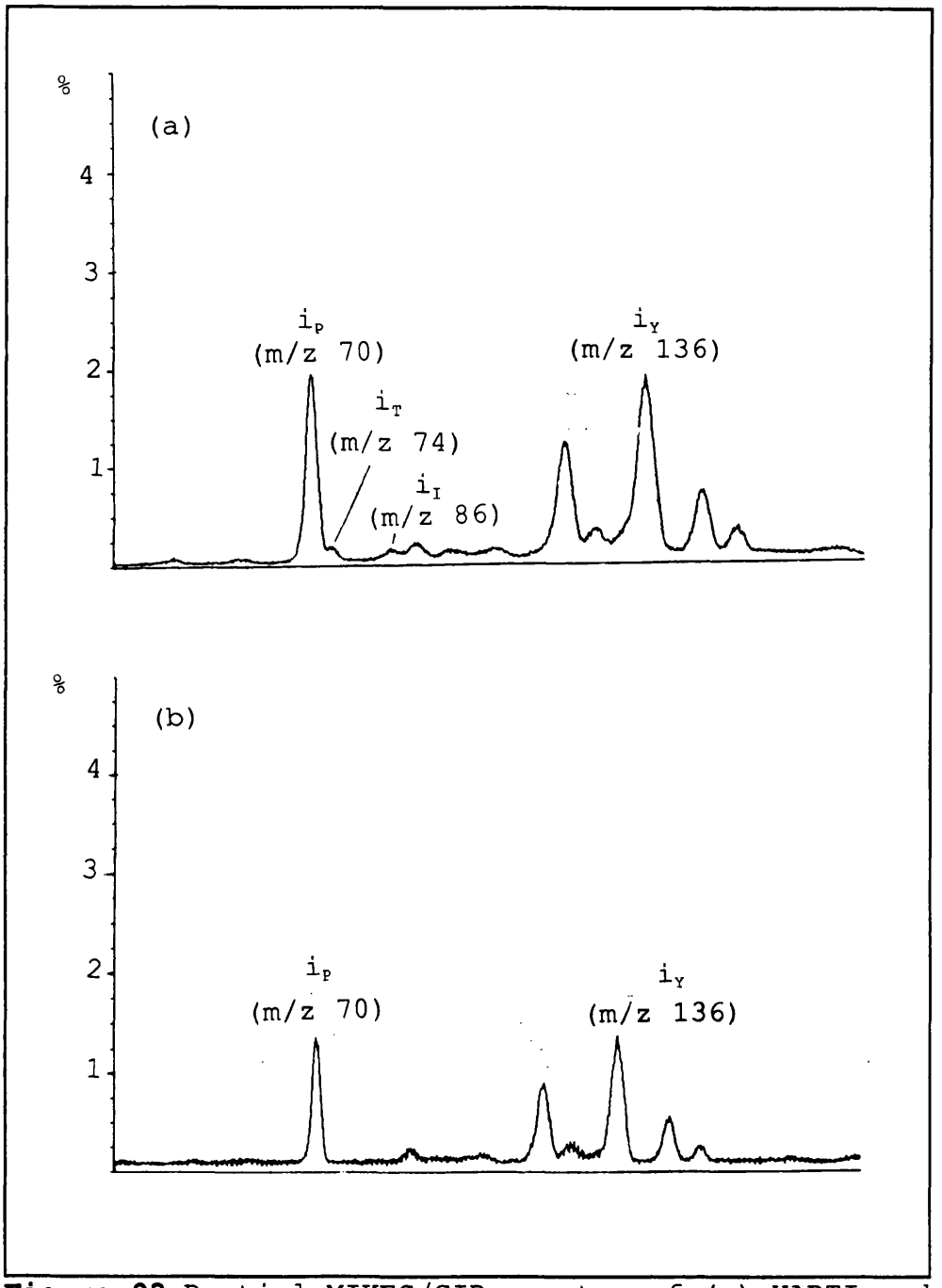

Figure 93 Partial MIKES/CID spectra of (a) YAPTI and (b) YAPT

4.5.4.2 N-terminal Effect

It can be seen from the case of **YGFG** and **GYFG** that the immonium ion from the N-terminal residue, i_Y in this case, is enhanced by virtue of its position (Fig 94).

This mass also corresponds to the A_1 fragment, and in the case of a peptide protonated at the N-terminus, (likely when **Y** is at this position) this is the easiest fragment to produce since it requires the breaking of only one bond, followed by deprotonation. These factors may well account for the favourable formation of this immonium ion.

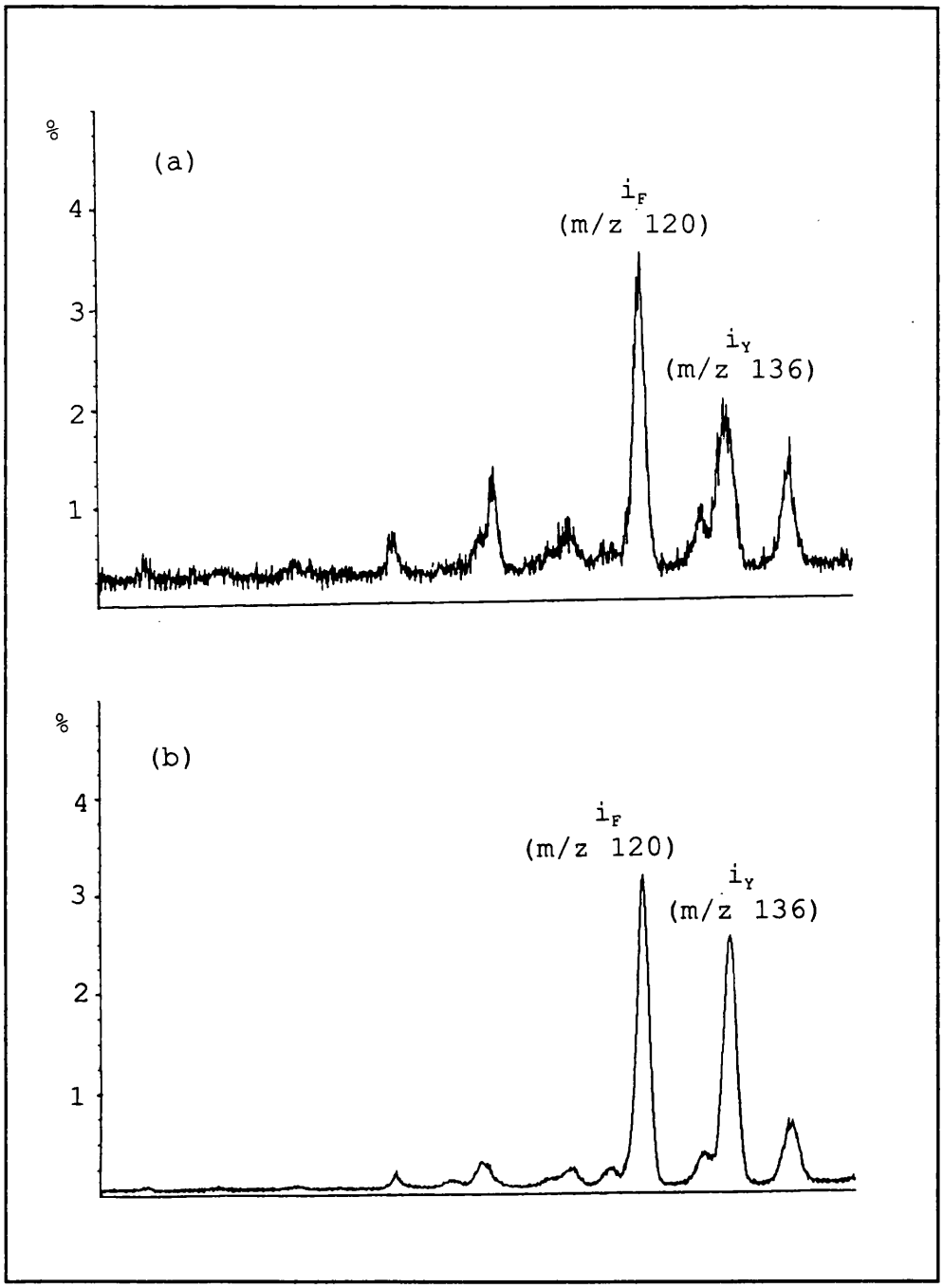

Figure 94 Partial MIKES/CID spectra of (a) GYFG and (b) YGFG

4.5.4.3 Substitution Of Single Residue

The effect that substituting one amino acid residue for another has on relative immonium ion intensity is very much dependent upon the particular amino acids involved. For peptides of the sequence **YAGF**- substituting the C-terminal residue for that of **M**, **L** or **Nle** has a minimal effect on the relative intensities of m/z 136 and m/z 120. Similarly, there is little effect when substituting the second residue of **Y-GFL** for that of **G** or **A**, or substituting the fourth residue of **YAF-Y** for that of **P** or **Hyp** (Fig 95). However, substituting the **A** of **YAFP** for **P** (Fig 95), or the **A** of **YAGFM** for **W** (Fig 96) results in a marked reduction in the intensity of both m/z 136 and m/z 120 in both cases (Table 13). It can be seen that the changes that have an effect on the other immonium ion intensities are those in which an amino acid residue that produces few immonium ions is substituted for one which produces many or vice versa, eg **P** (strong immonium ion signal) for **A** (very weak immonium ion signal) in **YAF-Y**. The substitutions that have little or no effect are those where the two amino acids that are exchanged give a similar number of immonium ions eg **P** and **Hyp** (both give relatively strong immonium ion signals) in **YAF-Y**.

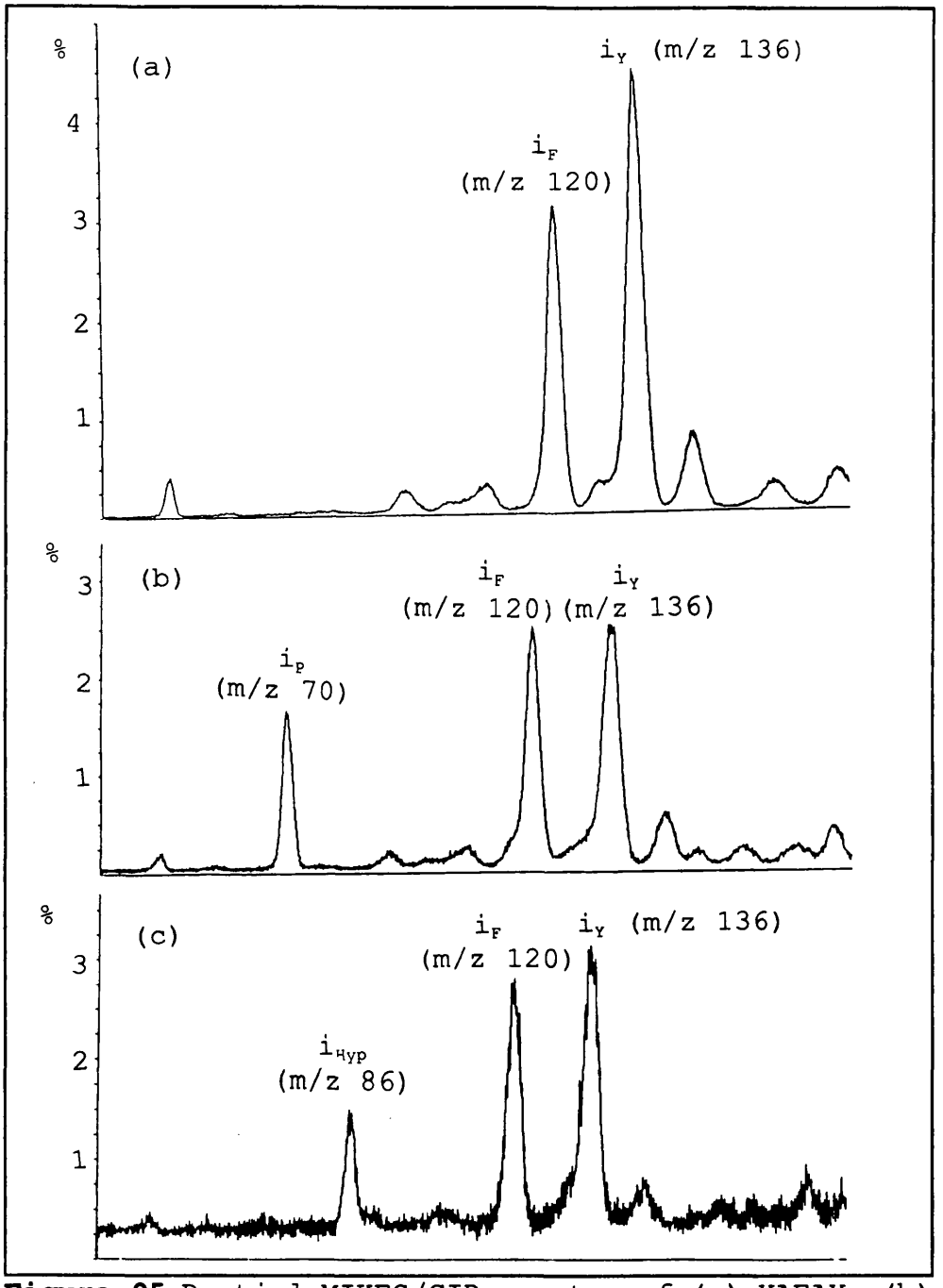

Figure 95 Partial MIKES/CID spectra of (a) YAFAY, (b) YAFHypY and (c) YAFPY

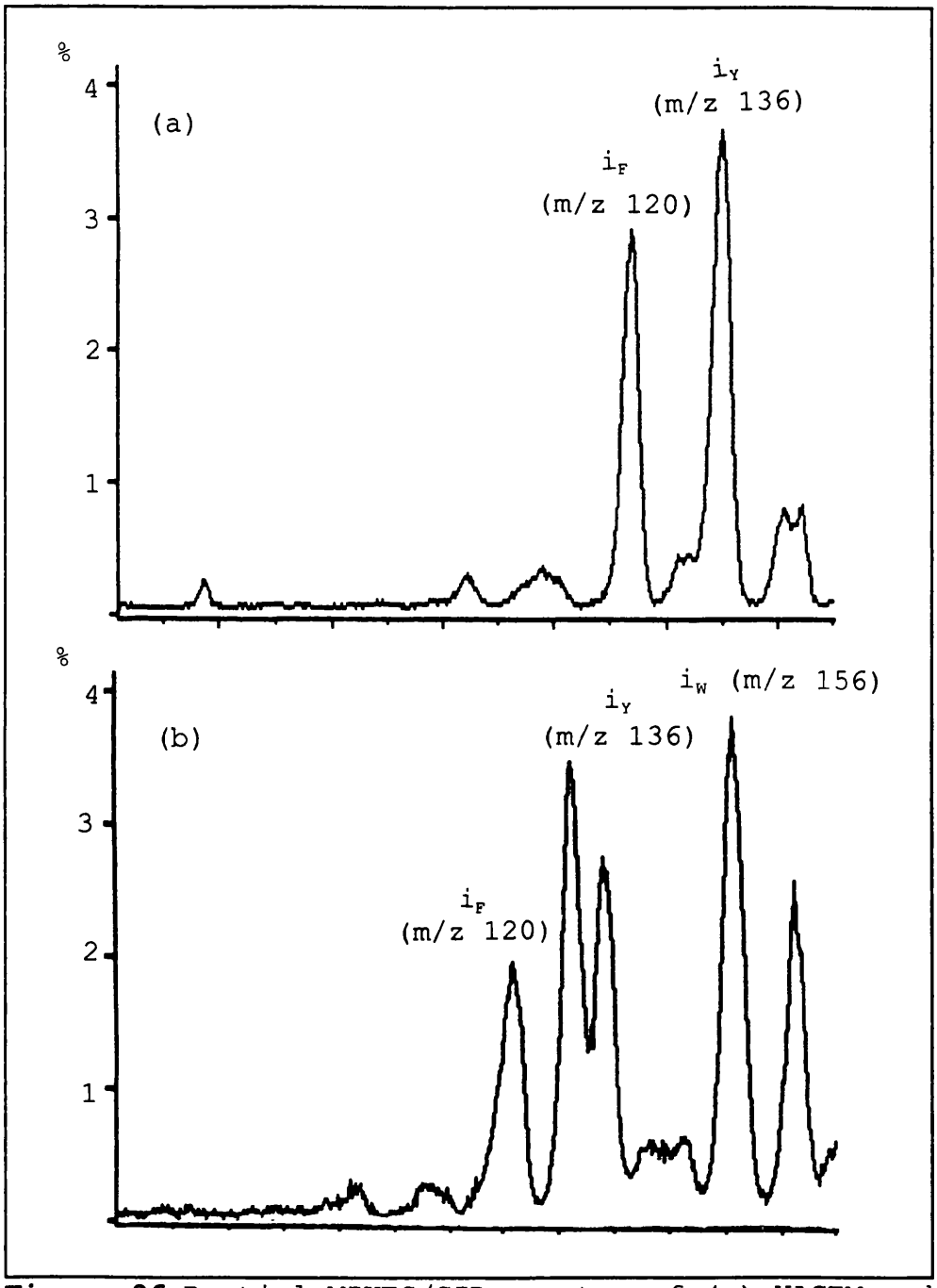

Figure 96 Partial MIKES/CID spectra of (a) YAGFM and (b) YWGFM

4.5.4.4 Immonium Ions from Cationated Species

By adding LiI or NaI to the probe tip along with the peptide and matrix, the ions $[M+Li]^+$ and $[M+Na]^+$ were formed. CID/MIKES spectra showed virtually no signals corresponding to the masses of the immonium ions or the corresponding cationated species eg $NaHN^+=CHR$ with either the lithium or sodium adduct (Fig 97). From this it was concluded that the proton gained in the ion source is necessary for the formation of the immonium ions; a proton was not or could not be donated from elsewhere in the peptide. That the cationated species were not formed is probably due to the relative immobility of the metal adduct compared with the proton.

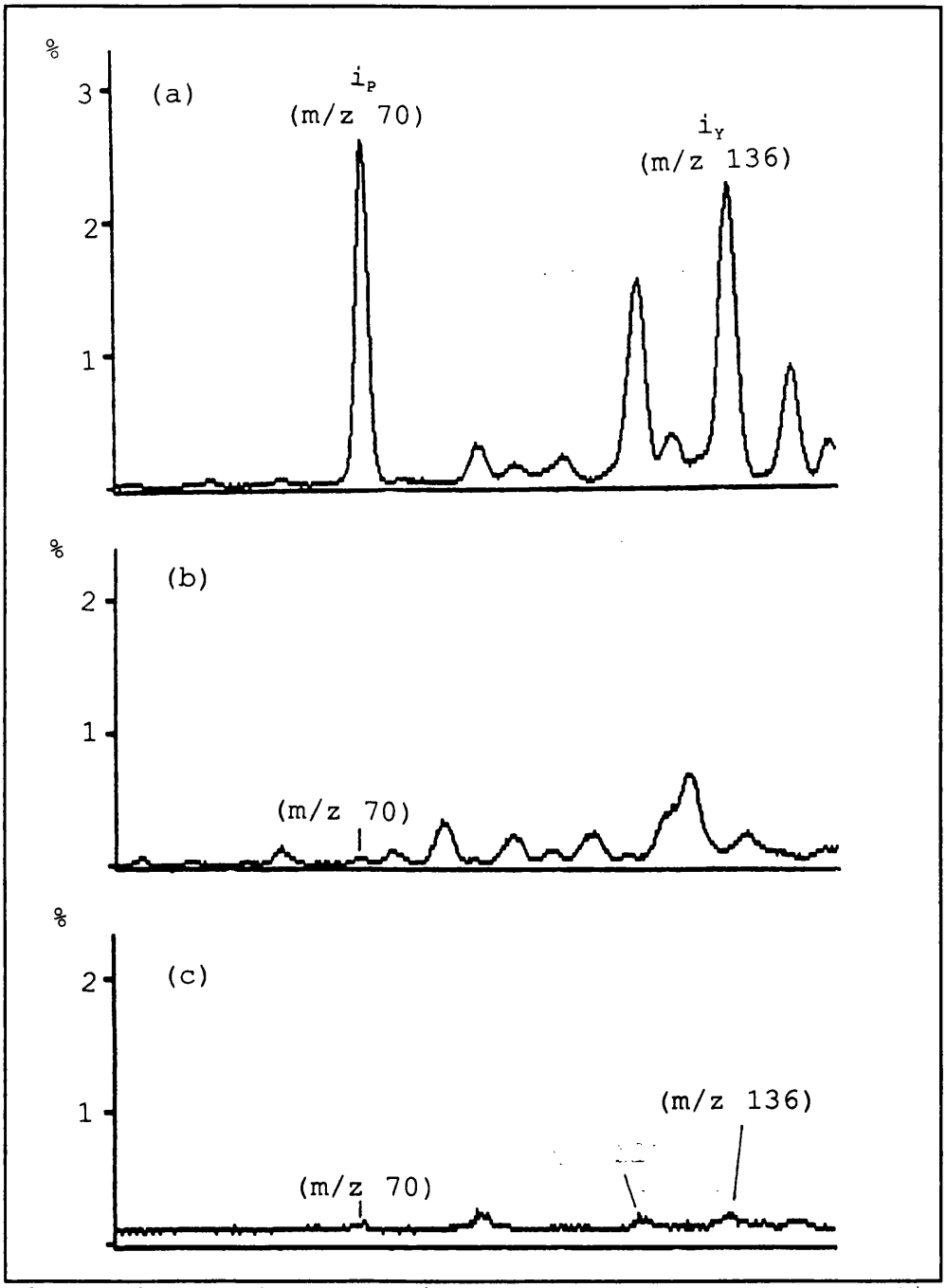

Figure 97 Partial MIKES/CID spectra of the (a) $[M+H]^+$, (b) $[M+Li]^+$ and (c) $[M+Na]^+$ ions from YPFV

4.5.4.5 Excess Protons At Ionisation

An excess of protons was achieved with the addition of oxalic acid to the sample and matrix on the FAB probe tip. Although this was found to increase the absolute intensity of the whole CID spectrum by increasing the number of free protons, it had no effect on the relative yields of the immonium ions (Fig 98). This illustrates that effects seen are not due to competition for a limited number of protons.

The absolute intensity of the $[M+H]^+$ ions for each group of peptides studied was compared, examples of which are shown in Table 14. It was found that when an amino acid is replaced by one which has a stronger immonium ion signal (eg the substitution of **W** for **G** in **YGGFM**) there is no corresponding increase in the number of protonated molecular ions (we have noted a small decrease): hence no increase in the total number of immonium ions. So for the substituted amino acid to produce more immonium ions than its predecessor it would have to be at the expense of the other amino acids in the peptide, their immonium ion intensities would then decrease (eg the decrease in m/z 136 from **YGGFM** to **YWGFM**). Substitutions of amino acids which give similar numbers of immonium ions also have no effect on the number of protonated molecular ions formed.

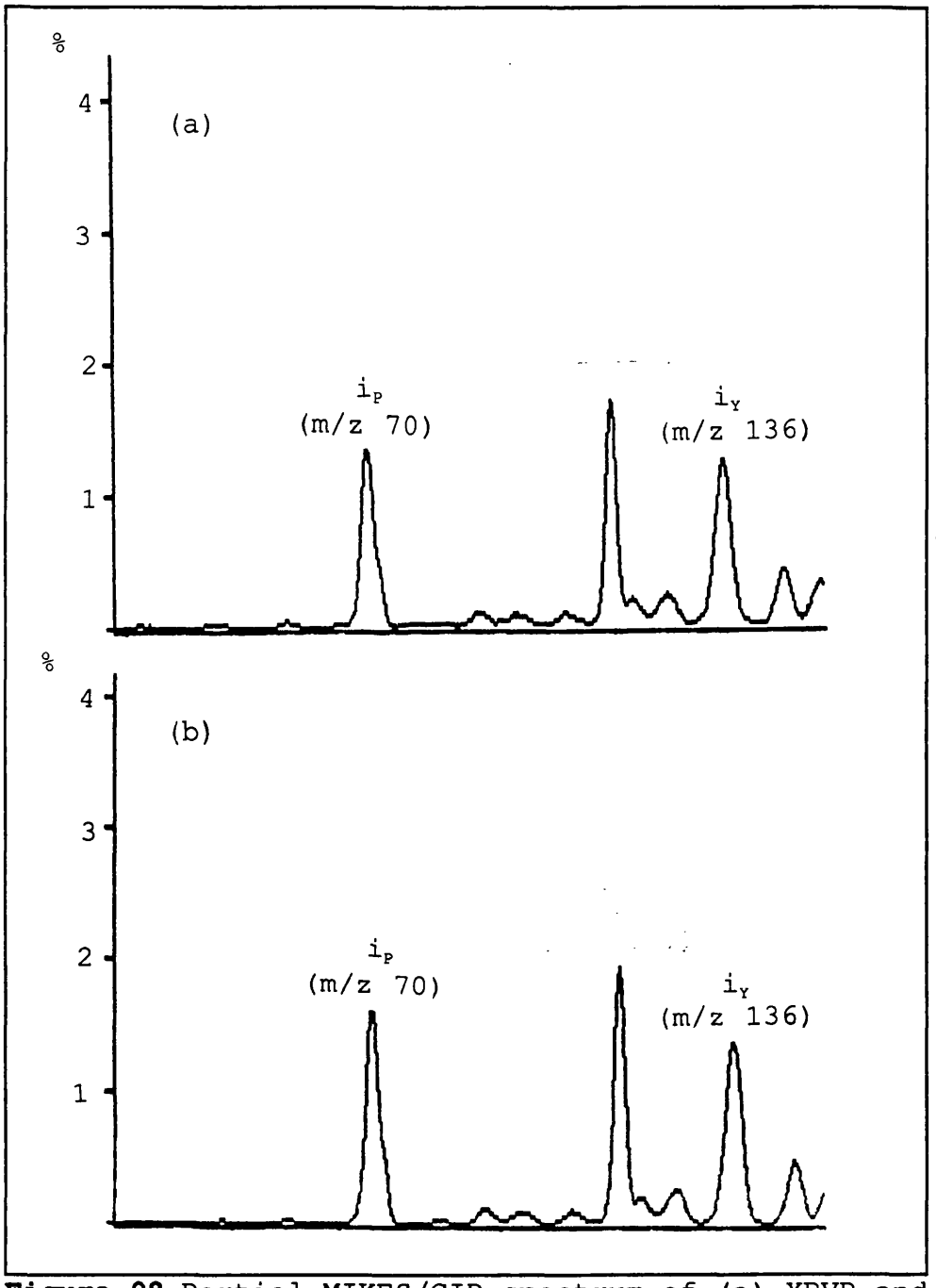

Figure 98 Partial MIKES/CID spectrum of (a) YPVP and (b) YPVP with oxalic acid added

4.5.4.6 Addition of a Basic Residue

It can be seen through comparing the spectra of **YGGFL** and **YGGFLK** (Fig 99) that the addition of the basic residue arginine **K** to the C-terminus has a marked effect on the relative intensity of the peak at m/z 136 but no effect on the relative intensities of the immonium ion peaks.

This can be said to be due to a change in the site of protonation in this case form the N-terminal residue **Y** in **YGGFL**, to the basic residue **K** in **YGGFLK**. The reduction in the signal at m/z 136 reflects the relative ease with which i_Y is formed from these two peptides.

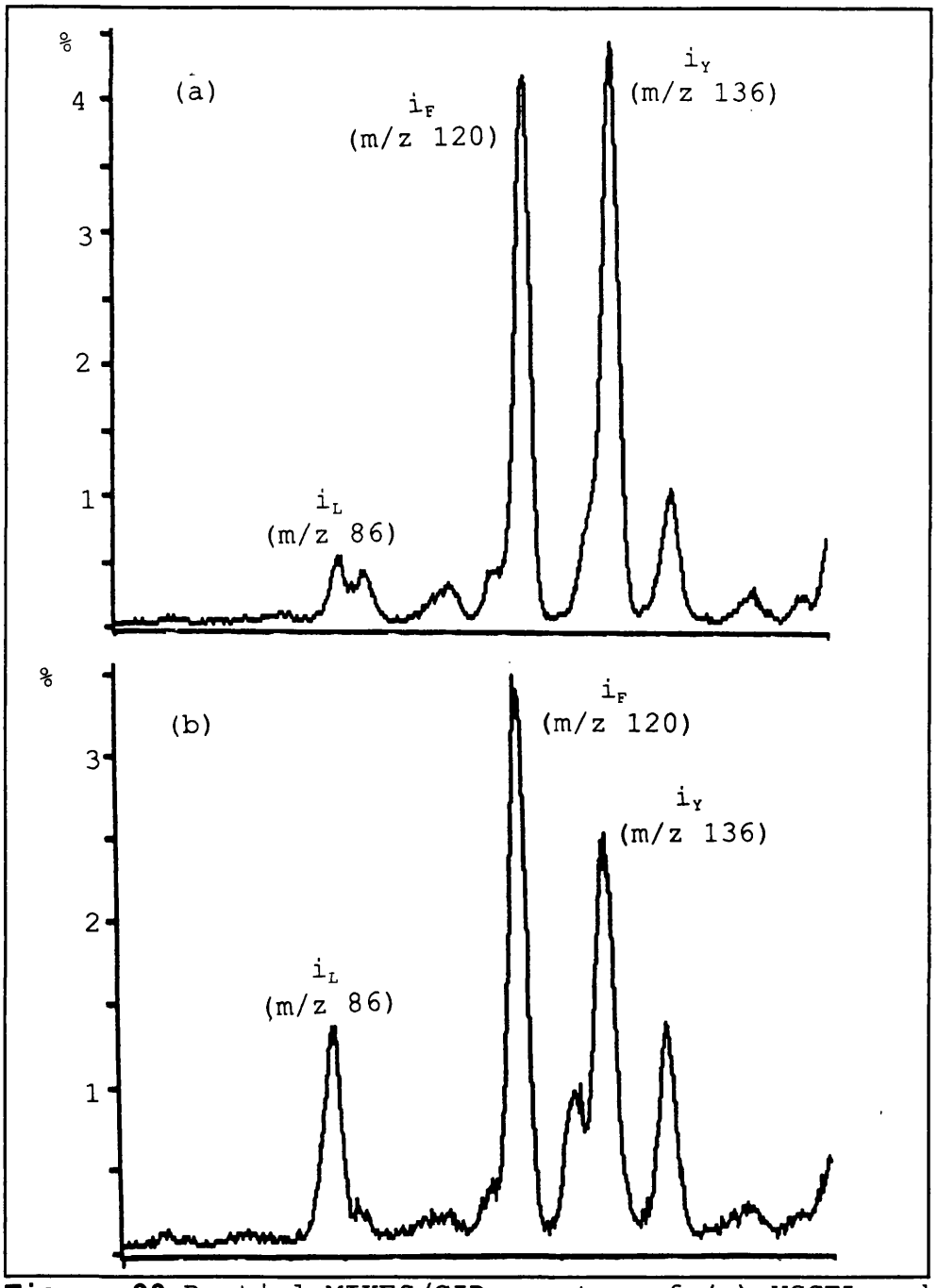

Figure 99 Partial MIKES/CID spectra of (a) YGGFL and (b) YGGFLK

Sequence	i_Y	i_F	i_P	i_{Hyp}
YWGFM	2.5±0.3	1.7±0.2		
YAGFM	3.6±0.3	2.8±0.2		
YGGFL	3.6±0.2	3.7±0.2		
YAGFL	3.9±0.5	3.2±0.4		
YAGFNle	3.2±0.2	2.6±0.2		
YGGF	3.0±0.2	0.8±0.03		
YAFAY	4.4±0.5	3.1±0.4		
YAFHypY	2.8±0.1	2.6±0.1		1.3±0.1
YAFPY	2.5±0.2	2.5±0.2	1.6±0.2	
YAFP	2.5±0.2	3.0±0.3	0.7±0.1	
YPFP	1.6±0.1	1.2±0.2	1.8±0.1	
YGFG	2.5±0.3	3.1±0.3		
GYFG	1.8±0.3	3.0±0.4		
YPFT	1.7±0.2	1.2	1.8±0.1	
YPFT	2.3±0.2	1.5±0.2	2.4±0.2	

Table 13: Intensities of the immonium ions given as percentages of the parent ion abundances after 50% attenuation by He. The mean values and standard deviations are from 2-9 separate measurements on a single occasion.

Sequence	Intensity of $[M+H]^+$
YAFAY	24±3
YAFPY	16±3
YAFHypY	19±2
YWGFM	8±1
YGGFM	16±6
YGGFL	19±4
YPVP	138±18
YPFP	84±11
YPFV	133±25

Table 14: Relative intensities of the protonated molecular ion (arbitrary units) for some of the peptides studied.

At this stage the data supports the theory of competition between amino acids for the production of immonium ions. The relative number of immonium ions produced depends not only on the other residues present but the position of the amino acid in the peptide chain, especially if it appears at the C- or N-terminus.

REFERENCES : Chapter 4 Experimental

1. M.A.Baldwin and G.J.Langley, J. Chem. Soc. Perkin Trans. II, 347-50, 1988
2. A.Kubo, S.-I.Sakai, S.Yamada, I.Yokoe and C.Kaneko, Chem. Pham. Bull., 16, 1533-1542, 1968
3. G.J. Langley, PhD Thesis, University of London, 1990
4. P.N.Rylander S.Meyerson and H.M.Grubb, J. Am. Chem. Soc., 79, 842-846, 1956
5. F.W.McLafferty and F.M.Bockhoff, *ibid*, 101, 1783-1786, 1979
6. L.J.Standley and R.A.Hites, Org. Mass Spectrom., 24, 767-772, 1989
7. S.Olesik, T.Baer, J.C.Morrow, J.J.Ridal, J.Buschek and J.L.Holmes, *ibid*, 24, 1008-1016, 1989
8. S.Meyerson, J. Am. Chem. Soc., 85, 3340-3344, 1963
9. F.W.McLafferty and F.M.Bockhoff, Org. Mass Spectrom., 14, 181-184, 1979
10. J.M.Buschek, J.J.Ridal and J.L.Holmes, *ibid*, 23, 543-549, 1988
11. K.L. Rinehart Jr., A.C. Buchholz, G.E. Van Lear and H.L. Cantrill, J. Am. Chem. Soc., 90 2983-2985, 1968
12. I. Howe and F.W. McLafferty, *ibid*, 93, 99-105, 1970
13. A. Siegal, *ibid*, 96, 1251-1252, 1974
14. R.C. Dunbar, *ibid*, 97, 1382-1384, 1975
15. F.W. McLafferty and J. Winkler, *ibid*, 96, 5182-5189, 1974

16. J.-L.M. Abboud, W.J. Hehre and R.W. Taft, *ibid*, 98, 6072-6073, 1976

17. C. Cone, M.J.S. Dewar and D. Landman, *ibid*, 99, 372-376, 1977

18. M.J.S. Dewar and D. Landman, *ibid*, 99, 2446-2453, 1977

19. J.-A.A. Jackson, S.G. Lias and P. Ausloos, *ibid*, 7515-7521, 1977

20. M.A. Baldwin, F.W. McLafferty and D.M. Jerina, *ibid*, 97, 6169-6174, 1975

21. F.W. McLafferty, P.F. Bente III, R. Kornfeld, S.-C. Tsai and I. Howe, *ibid*, 95 2120-2129,1973

22. C.J. Proctor and F.W. McLafferty, Org. Mass Spectrom., 18, 193-197, 1983

23. L.M. Bass and M.T. Bowers, *ibid*, 17, 229-239, 1982

24. R.T. Coutts and G.A. Small, 'Polysaccharides, Peptides and Proteins', Heinneman, 1983

25. R.D. Dyson, 'Cell Biology: A Molecular Approach (2nd ed.), Allyn and Bacon, 1978

26. A M Falick, unpublished data.

27. D Zidarov, P Thibault, M J Evans and M J Bertrand, Biomed. Mass Spectrom., 1990, 19, 13-26.

28. R S Johnson and K Biemann, *ibid*, 1989, 18, 945-957.

29. P Roepstorff and J Fohlman, *ibid*, 1984, 11, 601.

30. D H Russell, E S McGlohon and L M Mallis, Anal. Chem., 1988, 60, 1818-1824.

CHAPTER 5 : SUMMARY AND CONCLUSIONS

The principal aim of this thesis was to investigate the use of various tandem mass spectrometry techniques in structural and analytical studies. Results detailed here illustrate the successful application of such scanning techniques as unimolecular MIKES and linked scans, and collisional techniques including collision induced dissociation and neutralisation-reionisation mass spectrometry.

Tautomerism has been examined in hydroxy substituted bicyclic nitrogen containing compounds, through the comparison of their metastable peak shapes with those from compounds with known patterns of behaviour.

High energy CID spectra were used to investigate the structure of $[M-CO]^{+\cdot}$ ions from hydroxyquinoline isomers and $[M-CS]^{+\cdot}$ ions from mercaptoquinoline isomers. Deuterium labelling experiments on the subsequent breakdown of the $[M-CO]^{+\cdot}$ and $[M-CS]^{+\cdot}$ ions showed that the 2-isomers undergo unique fragmentations with little evidence of hydrogen scrambling.

Neutralisation-reionisation spectra were investigated as a means of differentiating between positional isomers of aromatic compounds.

The major fragmentation pathway for t-butyl benzene was established using linked scans to identify the major ionic fragments and NRMS to confirm the complementary

neutral fragments. The structure of the $C_7H_7^{+\cdot}$ ion was examined through a comparison of its high energy CID spectra with the spectra of $C_7H_7^{+\cdot}$ ions of known structure.

The structure of $C_2H_5NO^{+\cdot}$ isomers were examined using unimolecular MIKES, high energy CID spectra, linked scans and NRMS, as a comparison of their utility of these various methods for this kind of study.

High energy CID spectra were used to examine factors affecting the production of immonium ions from small peptides.

In all of this work, the common factor has been the complementary nature of many of the tandem mass spectrometrical techniques used. Where more than one technique was used to study one problem, they usually provided different kinds of information without conflicting.

It is obvious that certain techniques have their own strengths and weaknesses apart from how useful they prove to be in specific studies.

Unimolecular MIKES and CID/MIKES have the advantage of being very simple to carry out on this instrument in terms of setting up, scanning and data interpretation. Although the data system will display such data with a mass scale, without requiring a calibration file, the mass measurement is less accurate at low masses and mass assignment may need to verified manually. It has been

noted previously that scans that use the magnet and ESA of a double focusing instrument as separate analysers, can suffer from poor resolution, both mass resolution of the precursor ion and more specifically the energy resolution of the daughter ions. (This applies to all techniques based on the MIKES scan mode.) Attempting to improve the resolution by closing down any of the slit (source, intermediate or collector) may bring problems of reproducibility if slit positions cannot be reproduced exactly. A slight drift in magnet tuning is not usually a problem (except where data is being continuously averaged over several minutes or hours) and may be quickly rectified. Likewise the collision gas pressure should be stable once set but may be checked easily.

CID/MIKES spectra have a reputation for being useful in cases of establishing molecular structure. This technique has been used successfully here, particularly in the analysis of hydroxyquinoline and mercaptoquinoline isomers, and in the analysis of structurally significant fragments from small peptides.

Unimolecular MIKE scans have been used in the investigation into tautomerism in hydroxy substituted bicyclic nitrogen containing compounds, evidence for or against tautomerism being derived from the shapes of certain metastable peaks which are displayed in this type of spectrum.

Linked scans, B/E and B^2/E, can provide similar

information to unimolecular/MIKES and CID/MIKES spectra, the case of the latter only if there is a collision cell in the appropriate FFR. The advantage of using linked scans is the improvement in resolution of both the precursor and daughter ions. The disadvantage lies in the more complex nature of the scan. With the data system used here, a calibration file is required prior to linked scanned. The lowest mass in the calibration file is required to be notably lower than that of the lowest mass of interest in the sample. This is because, the 'apparent mass' m_A of any daughter ion m_D is given by

$$m_A = m_D^2/m_P$$

where m_P is the mass of the parent ion. For this reason it may not be possible to calibrate to a low enough mass to include all the peaks of interest in the spectrum. This was found to be the case when examining the fragmentation of $C_2H_5NO^{+\cdot}$ ions. Nevertheless linked scans, B/E and B^2/E, were used successfully to help establish the major fragmentation route of t-butyl benzene.

Although a considerable amount of work has appeared in the last ten years using NRMS as an analytical technique, it still remains a relatively little used technique compared with other tandem techniques and its use is largely confined to a handful of research laboratories interested in ion chemistry. One reason for

this may be the need for special instrumentation beyond the single collision cell that may already be present in one of the FFRs. From experience though it is felt that the main reason for its apparent lack of popularity lies in the technique itself. Even though NRMS has been used successfully in a number of studies detailed here - identifying neutral fragments in the fragmentation of t-butyl benzene, differentiating between positional isomers of cyclic compounds and structural analysis of $C_2H_5NO^{+\cdot}$ isomeric ions - its success has been somewhat overshadowed by problems of poor sensitivity. The efficiency of each collision stage, neutralisation and (re)ionisation, is only a few percent at best, thus the ion beam intensity is attenuated by approximately four orders of magnitude in the 2FFR. Because of this, the ion beam intensity before the magnet needs to be high for there to be any hope of showing a recovery signal at the detector. This naturally places limits on the kind of sample which can be analysed by NRMS, both in terms of its structure, in so far as it relates to stability, and molecular weight. Although there are applications for which NRMS is the most appropriate or only suitable technique, the problem of sensitivity will almost certainly limit its popularity as an analytical technique.

Appendix I : CALCULATING AN AVERAGE, WEIGHTED BY THE UNCERTAINTY IN INDIVIDUAL RESULTS [1]

N individual measurements are made of some parameter **x**

$$x_1 \pm y_1 \quad , \quad x_2 \pm y_2 \ldots . \ x_N \pm y_N$$

where x_i is the measure value and y_i its associated uncertainty or error.

The weighted average of these measurements is given by

$$x_{AVE} = \sum_{i=1}^{N} w_i x_i \Big/ \sum_{i=1}^{N} w_i$$

$$\text{where} \quad w_i = (y_i)^{-2}$$

The corresponding uncertainty in the average is given by

$$y_{AVE} = \left(\sum_{i=1}^{N} w_i \right)^{-\frac{1}{2}}$$

1. J.R. Taylor, 'An Introduction to Error Analysis, The study of Uncertainties in Physical Measurement', University Science Books, 1982